The Institute of Paper Chemistry

Appleton, Wisconsin

Doctor's Dissertation

Adsorptive Potential Distributions for Water-Dried Cellulose

Glendon W. Brown

June, 1972

ADSORPTIVE POTENTIAL DISTRIBUTIONS FOR WATER-DRIED CELLULOSE

A thesis submitted by

Glendon W. Brown

B.S. 1966, Miami University
M.S. 1968, Lawrence University

in partial fulfillment of the requirements
of The Institute of Paper Chemistry
for the degree of Doctor of Philosophy
from Lawrence University,
Appleton, Wisconsin

June, 1972

TABLE OF CONTENTS

SUMMARY

The objective of this study was to characterize the surface properties of water-dried celluloses with respect to Van der Waals type surface forces using gas adsorption techniques. The attractive surface forces can be conveniently divided into two broad categories: polar and nonpolar. The nonpolar forces are functional regardless of the solid and gas species interacting at the solid-gas interface. The magnitude of the polar forces depends upon the presence of an electrostatic field emanating from the solid surface. This field can interact with the permanent dipole moment of a polar molecule. Or, this field can polarize the electron cloud of a nonpolar molecule causing an induced dipole moment.

Three adsorbate gases, argon, nitrogen, and trichloromonofluoromethane, were used for adsorption measurements. Because of the differing physical properties of these polar and nonpolar gases, a comparison of the interaction of these gases with the same cellulosic substrate yielded an understanding of the relative importance of the polar and nonpolar surface forces.

A recording vacuum microbalance system using a Cahn electromagnetic balance was constructed for the collection of the necessary adsorption data. This gravimetric method was used because of the low surface area of the three adsorbents: a holocellulose, an alkali-extracted holocellulose, and an acid-hydrolyzed holocellulose.

Since adsorption data themselves cannot produce information but can only produce information in the light of a particular model, a physical adsorption model for multilayer adsorption on a patchwise heterogeneous surface was developed to aid in interpreting the adsorption data. This multilayer adsorption model is a significant improvement upon the presently used Ross and Olivier model which assumes only monolayer coverage. Nonlinear regression analysis techniques were used to fit the new model to the experimental gas adsorption data to obtain

estimates of the unknown model parameters. The model parameters characterize the surface in terms of a log-normal adsorptive potential distribution and the surface area. For the first time, confidence intervals were calculated for the parameters, thus enabling statistically valid comparisons to be made. The nonlinear regression analysis procedures can also be used to evaluate proposed adsorption experimental designs.

All three water-dried cellulosic adsorbents were found to be very heterogeneous surfaces with relatively low adsorptive potential energies. The adsorption data indicated that the untreated holocellulose and acid-hydrolyzed holocellulose have similar adsorptive potential distributions while the alkali-extracted holocellulose apparently has a lower and more uniform adsorptive potential distribution. Considering the results of the methods used in characterizing the adsorbents (e.g., electron-micrographs, carbohydrate analysis, and x-ray diffractometric procedures) the difference in the adsorptive potential distribution for the acid-hydrolyzed holocellulose and the alkali-extracted holocellulose appears to be due to physical effects and surface topology. However, the difference between the untreated holocellulose and the alkali-extracted holocellulose is probably due to chemical effects caused by the loss of hemicelluloses upon extraction. The apparent lack of a surface electric field resulted in an insignificant contribution of the classical electrostatic polar interactions to the adsorptive potential. Thus, the physical adsorption forces functioning at the cellulose solid-gas interface were predominately nonpolar dispersion forces.

INTRODUCTION

It is becoming increasingly apparent that the surface properties of cellulose play a dominant role in many industrial processes. Of particular importance are the surface forces that are present at the solid-gas interface of cellulose. These surface forces originate from the fields of force that hold a solid together. At the surface of a solid these fields of force cannot suddenly disappear, but will reach out into the space beyond; these forces can therefore attract the molecules of a liquid (as in wetting phenomena and adsorption from solution) or the molecules, atoms or ions of another solid (as in adhesion). These same surface forces also give rise to the phenomenon of gas adsorption that results in a greater concentration of gas molecules near the surface of a solid than in the surrounding gas phase.

The objective of this thesis is to characterize the surface properties of water-dried cellulose with respect to the functioning surface forces using gas adsorption techniques. Adsorption at the solid-gas interface can be visualized as a reaction scheme. This formulation emphasizes the basic concept of the experimental approach; that is, an investigation of the solid-gas complex can be used to characterize the solid (see Fig. 1).

$$X_{SOLID} + A_{GAS} \rightleftharpoons X \cdots A_{COMPLEX}$$

Figure 1. Solid-Gas Complex

It is apparent that a complete understanding of the solid-gas interface depends upon a knowledge of the mechanism of surface forces. Fundamentally, surface forces originate, as do all intermolecular forces, from the electromagnetic interactions

of the nuclei and the electrons comprising the system. The attractive surface forces can be conveniently divided into two broad categories: polar- and nonpolar-type adsorptive forces. The nonpolar-type forces are functional regardless of the solid and gas interacting at the solid-gas interface. The magnitude of the polar forces depends upon the presence of an electrostatic field emanating from the solid surface. A polar molecule with a permanent dipole moment can interact with this field by classical electrostatic interactions. Or, the electron cloud of a nonpolar molecule can be polarized by this field, creating an induced dipole moment which interacts with the field. The intent of this investigation is to characterize water-dried celluloses in terms of an adsorptive potential distribution and to determine the relative contribution of the polar and nonpolar surface forces to the adsorptive potential.

BACKGROUND OF THE THESIS PROBLEM

THE NATURE OF ADSORPTIVE FORCES IN PHYSICAL ADSORPTION

One of the first statements that must be made before discussing atomic forces and adsorption is that there are no special adsorption forces. The various forces that promote adsorption of gases have the same origin as all intermolecular forces (i.e., the electromagnetic interactions of the nuclei and electrons comprising the system) (1).

Adsorption is divided into two general categories: physical adsorption and chemisorption. Physical adsorption results from the action of Van der Waals forces which are considered to be made up of London dispersion forces and classical electrostatic forces. With these forces, there is no transfer or sharing of electrons between a molecule and the solid. As a molecule approaches the solid, the electrons may take up a new equilibrium distribution, but they maintain their respective associations in the interacting species. Chemisorption arises from the transfer or sharing of electrons between the adsorbate and adsorbent. The chemisorption bond has all the characteristics of a chemical bond (2). Physical adsorption is usually weaker than chemisorption. Experimentally determined heats of adsorption are often used to distinguish between the two types of adsorption.

The forces responsible for physical adsorption may be conveniently classified as those associated with:

(1) permanent dipole moments in the adsorbed molecule (orientation forces)

(2) polarization, i.e., distortion of the charge distribution within the adsorbed molecule (induction forces)

(3) dispersion effects

(4) short-range repulsive effects.

Since the dispersion and repulsive effects are invariably present, sometimes alone and sometimes in cooperation with other types of forces, they will be discussed first. The description of dispersion and repulsive forces which follows is essentially the development of Honig (3).

Fluctuating dipoles or multipoles are associated with the electron cloud configuration about the nuclei of any atoms or molecules. In the case of nonpolar gases these fluctuations are such that, on the average, the centers of positive and negative charge coincide. The transitory multipoles will induce similar asymmetries of charge on adjacent molecules. In addition, interactions occur with multipoles already present on neighboring partners. The assembly of multipoles just described, on the average, will remain in parallel orientation, since such a configuration leads to a maximum attractive interaction energy. Forces arising from this type of interaction are known as Van der Waals dispersion forces. In the case of a pair of atoms separated by distance r, the approximate attractive potential energy of interaction is

$$u_d(r) = -C_1/r^6 - C_2/r^8 - C_3/r^{10} \qquad (1)$$

where C_1, C_2, and C_3 are constants associated with instantaneous dipole-dipole, dipole-quadrupole, and quadrupole-quadrupole interactions, respectively.

Two molecules are also subject to a mutual force of repulsion that becomes prominent when appreciable interpenetration of their electron clouds occurs. Quantum mechanical calculations indicate that this repulsion potential is given by (54)

$$u_r(r) = Be^{-r/r'} \qquad (2)$$

where B and r' are appropriate constants. Frequently, an empirical expression of the form

$$u_r(r) = C_4/r^m \qquad (3)$$

is used in place of Equation (2). In this expression, the constant $\underline{m}$ is generally taken as 12.

The total interaction potential is given by a combination of dispersive terms (dipole-dipole and dipole-quadrupole only) with the repulsive terms

$$u(r) = -C_1/r^6 - C_2/r^8 + C_4/r^{12}. \qquad (4)$$

At a certain equilibrium distance $\underline{r} = \underline{r}_o$, the forces of attraction and repulsion just balance; thus, $(\partial \underline{u}/\partial \underline{r})_{\underline{r}=\underline{r}_o} = 0$. Using Equation (4) in this condition, one can write $\underline{C}_4$ in terms of $\underline{C}_1$ and $\underline{C}_2$ as

$$C_4 = {}^1/_2 C_1 r_o^6 + {}^2/_3 C_2 r_o^4 . \qquad (5)$$

Substituting Equation (5) into Equation (4) then yields

$$u(r) = -C_1/r^6 - C_2/r^8 + {}^1/_2 C_1 r_o^6/r^{12} + {}^2/_3 C_2 r_o^4/r^{12} \qquad (6)$$

so that

$$u_o = u(r_o) = -{}^1/_2 C_1/r_o^6 - {}^1/_3 C_2/r_o^8 . \qquad (7)$$

If the dipole-quadrupole term of Equation (7) is neglected ($\underline{C}_2 = 0$), then Equation (7) reduces to

$$u_o = -{}^1/_2 C_1/r_o^6. \qquad (7a)$$

Solving Equation (7a) for $\underline{C}_1$ and substituting $\underline{C}_1$, and $\underline{C}_2 = 0$, into Equation (6), one obtains finally

$$u(r) = u_o[2(r_o/r)^6 - (r_o/r)^{12}]. \qquad (8)$$

The dispersion and repulsion energies, in general, can be assumed to be additive; i.e., the total energy for a collection of the molecules can be expressed as a sum of pairwise interactions over all pairs of the configuration. The energy of attraction holding an adsorbed molecule to the surface of an idealized solid can thus be calculated once the interactions $u_d(r)$ and $u_r(r)$ between the adsorbate and a single lattice atom are known. It is necessary to sum Equation (8) over all distances r_i between the location of the adsorbed particle and lattice points of the idealized solid as illustrated in Fig. 2.

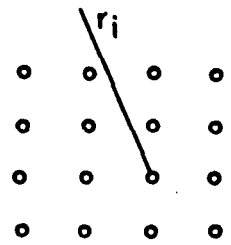

Figure 2. Adsorbate on an Ideal Lattice Bounded by a Smooth Surface (3)

This summation procedure can become quite tedious. Fortunately, it is possible to obtain qualitative information using an integration process. In this method, the real lattice is replaced by a semi-infinitive planar continuum. The density of this equivalent continuum must be adjustable to match the mass of the k lattice atoms per unit volume of the ideal solid; then ρ represents the number of "equivalent lattice points" per unit volume of the continuum.

Let z be the shortest distance between the location of the gas atom and the surface, and let the particle be located at the origin of coordinates. The total interaction energy between the adsorbate and the semi-infinitive planar solid is now

$$W(z) = \int_z^\infty \int_{-\infty}^{\infty} \int_{-\infty}^{\infty} u(r)\rho dx dy dz \qquad (9)$$

where x and y are orthogonal coordinates in the plane of the surface.

For simplicity, change to cylindrical coordinates, denoting by w the radial distance from the z axis to a point in the interior of the continuum, so that $r^2 = z^2 + w^2$ (see Fig. 3).

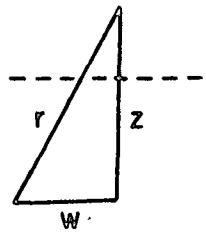

Figure 3. Adsorbate on Continuum-Bounded Plane Surface (3)

According to Equation (8), $u(r)$ has the form $\sum_{j=1}^{2} K_j r^{-n_j}$ where K_j is the coefficient of the jth term on the right-hand side of Equation (8), and where n_j assumes the values 6 and 12. Thus,

$$W(z) = \sum_{j=1}^{2} K_j \rho \int_z^\infty \int_{-\infty}^{\infty} \frac{2\pi w dw dz}{(z^2 + w^2)^{n_j/2}}$$

$$= \sum_{j=1}^{2} K_j \frac{\rho\pi}{n_j/2 - 1} \int_z^\infty \frac{dz}{z^{2(n_j/2 - 1)}}$$

$$= \sum_{j=1}^{2} K_j \left(\frac{\pi\rho}{(n_j - 3)(n_j/2 - 1)}\right)\left(\frac{1}{z^{2(n_j/2 - 1) - 1}}\right). \qquad (10)$$

For $\underline{j} = 1$, $\underline{n}_j = 6$, and for $\underline{j} = 2$, $\underline{n}_j = 12$. Substitution of these values into Equation (10) leads to

$$W(z) = \pi\rho r_o^3 u_o(q^3/3 - q^9/45) \qquad (11)$$

with $\underline{q} = \underline{r}_o/\underline{z}$. A plot of Equation (11) is given in Fig. 4 for the hypothetical case, $\underline{r}_o = 3.5$ A.

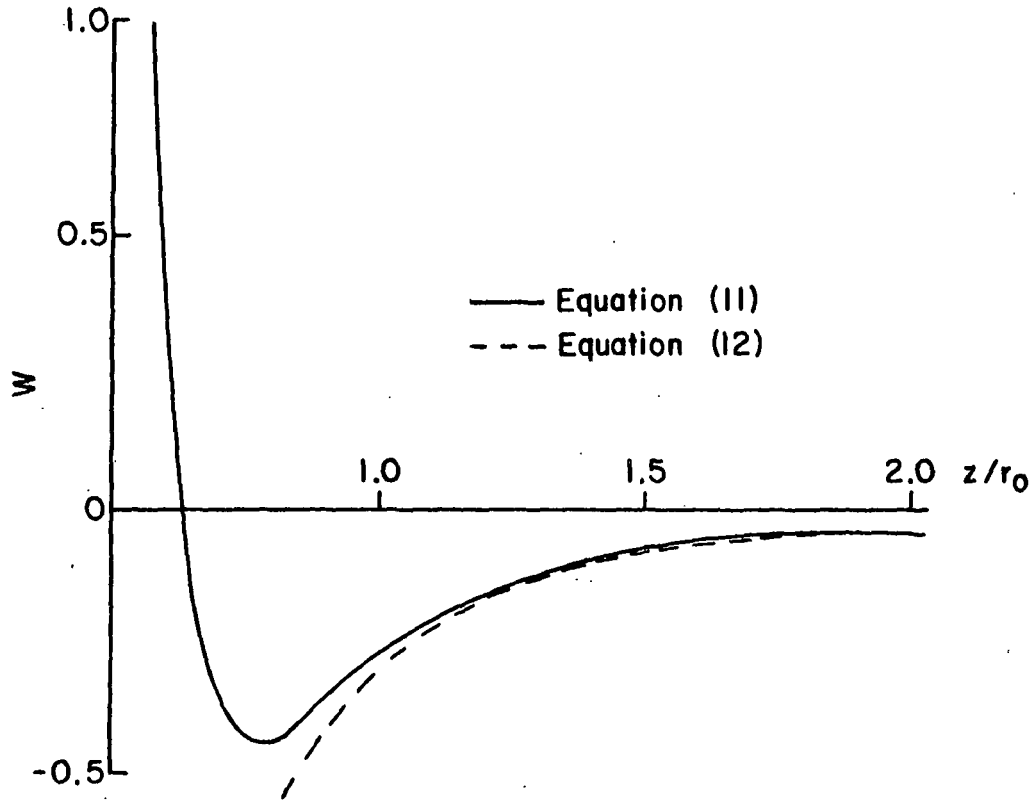

Figure 4. Van der Waals Dispersion Potentials for Interaction Between Adsorbate and Continuum Adsorbent (3)

The equilibrium distance $\underline{z}_o$ can be calculated by use of the condition $(\partial\underline{W}/\partial\underline{z})_{\underline{z}=\underline{z}_o} = 0$, which leads to a value $\underline{z}_o = 0.765\underline{r}_o$. The depth of the potential minimum is $\underline{W}_o = 0.497\underline{r}_o^3\pi\rho\underline{u}_o$. A final simplification can be effected by neglecting the repulsion potential (setting $\underline{C}_4 = 0$). Equation (11) now reduces to

$$W(z) = -\pi\rho C_1/6z^3. \qquad (12)$$

A plot of $\underline{W}$ versus $\underline{z}$ is shown in Fig. 4. Under the assumed conditions, it reproduces the more complex equations quite well in the range $\underline{z} \geq \underline{r}_o$ (4).

The quantity $-\underline{W}_o$ represents the energy required to remove the adsorbed atom back into the gas phase, and $\underline{z}_o$ is the equilibrium distance between the surface of the continuum and the adsorbate particle. One must consider another complicating factor in determining the adsorption potential. The center of mass of the molecule vibrates in the potential well of Fig. 4 along the $\underline{z}$ direction. Such vibrations are quantized and give rise to a set of discrete energy levels. The lowest vibration frequency was found by Hill (5) to be of the order of magnitude of $\nu_{\underline{z}} = 10^{12}$ sec.$^{-1}$. Thus, at 0°K, the adsorptive potential energy is given by $-(\underline{W}_o - \underline{h}\nu_{\underline{z}}/2)$.

In addition to these dispersion forces, an adsorbent may have an external classical electrical field described by an electric field intensity $\underline{E}$. This field will induce a dipole or higher order moment in the charge distribution of the adsorbed molecule (see Fig. 5). As a result, an adsorptive potential is developed. The contribution to the interaction energy arising from this cause at a distance $\underline{r}$ from the surface will be given by

$$u_{\xi}(r) = -E^2\xi/2 \qquad (13)$$

where ξ is the polarizability of the molecule.

If the adsorbed molecule possesses a permanent dipole, it will orient with the surface electric field producing an additional adsorptive potential. This energy of interaction is given by

$$u_{\mu}(r) = -E\mu \cos\Psi \qquad (14)$$

where μ is the dipole moment of the adsorbed molecule, $\underline{E}$ is the strength of the electric field, and Ψ is the angle between the axis of the dipole and the field (7).

Figure 5. (a) Unperturbed Atom Where Center of Positive and Negative Charges Coincide; (b) Induced Dipole $\underline{p}$ Resulting from an External Electric Field $\underline{E}$ ($\underline{6}$)

Up to this point, only the interactions between the adsorbate molecules and the adsorbent have been considered. However, two molecules adsorbed on the same surface will attract each other with Van der Waals forces. The contribution of these mutual attraction forces between adsorbed molecules may in some cases lead to an important increase in the total adsorption energy.

The general picture which emerges from this consideration of physical adsorption forces acting between a solid and a molecule of adsorbate is that the total interaction energy may consist of five principal components: $u_{\underline{d}}(\underline{r})$, the dispersion force contribution; $u_{\underline{\xi}}(\underline{r})$, the contribution due to the polarization of the adsorbate by the surface; $u_{\underline{\mu}}(\underline{r})$, the contribution arising from the interaction between a permanent dipole in the adsorbate and the electrical field of the adsorbent surface; $u_{\underline{int}}(\underline{r})$, the contribution arising from the interaction between adsorbate molecules; and $u_{\underline{r}}(\underline{r})$, the always-present repulsion term. Any physical adsorption phenomenon is a result of the cooperation of at least one of the attractive force

components and the repulsive force. Of the various attractive forces, the dispersion force component is always present and one or more of the other attractive forces may also be present.

ANALYSIS OF ADSORPTION DATA USING THE BET THEORY

Gas adsorption techniques can be used to characterize the surface properties of a solid with respect to functioning surface forces. Brunauer, et al. (8) classified adsorption isotherms according to five types. These are shown in Fig. 6. Type I is often referred to as the Langmuir type because it corresponds to experimental isotherms of monolayer adsorption. Type II is very common in the case of physical adsorption and corresponds to multilayer formation. Type III is relatively rare and seems to be characterized by a heat of adsorption less than or equal to the heat of liquefaction of the adsorbate. Types IV and V are considered to reflect capillary condensation phenomena in that they level off before the saturation pressure is reached and may show hysteresis effects.

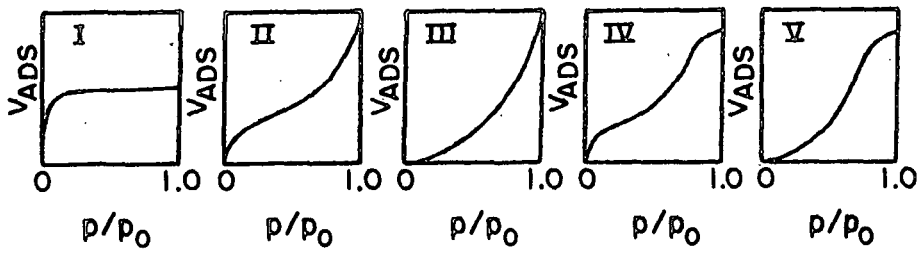

Figure 6. Five Types of Isotherms According to Brunauer, et al. (8)

The method that has gained the greatest prominence in analyzing gas adsorption data is the BET method. This very important theory of multilayer adsorption was developed by Brunauer, et al. (9). It is based on a localized model of adsorption

(i.e., the Langmuir isotherm). The BET equation was the first and still is the most used multilayer isotherm equation. The model from which the BET equation is obtained rests on the following assumptions (4):

(1) Equivalent sites are available for localized adsorption in the first layer.

(2) Each molecule adsorbed in the first layer is considered as a possible "site" for adsorption in a second layer; each molecule adsorbed in the second layer is considered as a possible "site" for adsorption in the third layer, etc.

(3) All molecules in the second and higher layers are assumed to have the same partition function as in the liquid state, which is different from the partition function of the first layer.

(4) Horizontal interactions between molecules are ignored for all layers.

Using the above assumptions and assuming an infinite number of adsorbate layers are possible, the following isotherm equation was derived for multilayer adsorption on a uniform surface.

$$p/[V(p_o - p)] = 1/(V_m c) + (c - 1)p/(V_m c p_o) \qquad (15)$$

where

V = volume adsorbed

p = pressure

p_o = vapor pressure of the gas at absolute temperature, T

V_m = monolayer volume

$c \cong \exp[(Q_1 - Q_L)/RT]$, and where

R = gas constant

Q_1 = the heat of adsorption of the gas in the first adsorbed layer

Q_L = the heat of vaporization of the liquid adsorbate.

If one plots the function $p/V(p_o - p)$ against p/p_o, one usually obtains a straight line between a p/p_o value of 0.05 and 0.3 whose slope and intercept give the values V_m and c.

With the possibility of evaluating the saturation capacity of a surface in terms of a monolayer volume, V_m, a practical application of the adsorption isotherm becomes obvious: the measurement of the relative degree of subdivision of a solid in terms of its specific surface area. The specific surface area of a solid adsorbent, Σ_{BET}, in $m.^2/g.$ then follows:

$$\Sigma_{BET} = (V_m/22400)N\sigma_o 10^{-20} \qquad (16)$$

where V_m is in cc. of adsorbate (measured at STP) per gram of adsorbent, N is Avogadro's number, and σ_o is the molecular cross-sectional area of the adsorbate in $A.^2$/molecule.

In spite of the crudity of the assumptions involved in its derivation, the BET equation is an extremely useful qualitative guide for experimental work, particularly as a method for determining surface areas. The use of this simple model has made possible great advances in both theoretical and practical studies of surface chemistry and physics.

One must not confuse the triumphs of the BET theory in this practical application with its claims as a model of the adsorption process. In this latter aspect it is far from satisfactory. Considering the assumptions on which the BET theory is based, one must conclude that a more satisfactory physical adsorption model is possible.

THE CONCEPT OF SURFACE HETEROGENEITY AND THE ROSS AND OLIVIER ADSORPTION THEORY

When considering adsorption on a real solid, one must question the assumption of a uniform adsorptive potential used in the BET theory. Various modifications must be considered for a realistic model for physical adsorption on real solids. Three complicating factors that must be taken into consideration are: (1) Real solids are finite in extent, so that a certain percentage of the constituent atoms are located on edges or corners of the lattice network. The higher surface energies attributable to the presence of such atoms are termed "edge effects." (2) The solid may be riddled with all types of imperfections, fissures, cracks, pores, elevations, and dislocations. (3) Impurities, consisting of foreign atoms or of ions with abnormal valencies may be present (3). All of the above imperfections may affect the adsorbent-adsorbate interaction energy. Thus, for any real solid, there is a distribution or spread of adsorptive potentials at the solid-gas interface. The surface is said to be heterogeneous or nonuniform.

Ross and Olivier (10) have written an entire monograph developing a more realistic physical adsorption model which attempts to correct for most of the criticisms of the BET theory model. Considerable attention was devoted to the concept of a heterogeneous surface.

The Ross and Olivier model of adsorption on a heterogeneous surface is based on the following postulates: (1) The surface is composed of very small patches (i.e., homotattic patches) of different energy that adsorb independently of each other. A homotattic surface is defined as the surface of a submicroscopic patch or region of a larger surface, which acts as if its structure were uniform and homogeneous. (2) On each homotattic patch the adsorbate behavior is described by a local adsorption isotherm equation. (3) The distribution of adsorption energies among these patches is represented by a continuous distribution function,

$$d\delta_i = \Phi(U)dU \tag{17}$$

where $d\delta_i$ is the incremental fraction of the total surface with potential energies between U and $U + dU$. (4) The relative coverage of the whole heterogeneous surface, Θ, is obtained by integrating θ_i, the coverage of the ith patch at any p and T, over all the patches. Thus,

$$\Theta(p,T) = \int_0^\infty \theta_i(p,T,U)\Phi(U)dU. \tag{18}$$

Since Θ can be determined experimentally, the two unknowns remaining are: the form of the local isotherm, θ_i, and the distribution function, $\Phi(U)$ (11, 12).

From these general considerations, Ross and Olivier proceeded by means of two assumptions: (1) On each homotattic patch the adsorbate adsorption is described by the Hill-deBoer adsorption isotherm equation:

$$p = k_i \frac{\theta}{1 - \theta} \exp\left[\frac{\theta}{1 - \theta} - \frac{2\alpha\theta}{RT\beta}\right] \tag{19}$$

where

k_i = a constant related to the adsorption energy of the substrate for the adsorbate

α = two-dimensional analog of the Van der Waals constant a

β = two-dimensional analog of the Van der Waals constant b

θ = the degree of coverage of the homotattic patch by a close-packed monolayer of adsorbate

T = absolute temperature.

The Hill-deBoer equation is derived from the two-dimensional analog of the Van der Waals equation using the Gibbs adsorption theorem to relate the equilibrium pressure, p, in the gas phase to the spreading pressure of the adsorbed film. Using this relationship, the adsorbed film is characterized as mobile, and the lateral interactions of the adsorbate molecules are taken into account. (2) The distribution

function, $\Phi(\underline{U})$, is assumed to be Gaussian

$$\Phi(U) = \frac{1}{f} \exp[-\gamma(U - U')^2] \qquad (20)$$

where

$\underline{U}'$ = the mean adsorptive potential at the maximum of the distribution curve

γ = the heterogeneity parameter which determines the width of the distribution

$\underline{f}$ = a normalizing factor, such that

$$\int_e^g d\delta_i = 1. \qquad (21)$$

For each distribution curve there are practical lower and upper limits of $\underline{U}$, which are designated $\underline{e}$ and $\underline{g}$, respectively, beyond which the density of the distribution function is insignificantly small (e.g., $\underline{U}$ values when the density is < 0.001).

As a result of the above assumptions, the adsorption isotherm equation now has the form

$$\Theta = \frac{1}{f} \int_e^g \theta_i \exp[-\gamma(u - U')^2]dU \qquad (22)$$

where θ_i is derived from the Hill-deBoer equation. Unfortunately, the above integral is intractable. However, with the aid of a computer, Ross and Olivier (10) prepared tables of model isotherm values using numerical techniques. The total range of $\underline{U}$ was divided into 50 (or occasionally 100) patches of different absorptive potential. To get the corresponding isotherm, each patch was treated as an individual uniform surface of energy $\underline{U_i}$, and its fractional coverage by the adsorbate was given by the Hill-deBoer equation.

The computed isotherms representing the total coverage at pressure $\underline{p}$ were then described by

$$\Theta = \sum_{i=1}^{50} \theta_i \Delta\delta_i \qquad (23)$$

where $\Delta\delta_i$ was the fraction of the surface having energies between U_i and $U_i + \Delta U$.

A typical family of computed isotherms, which were calculated from the above equation, is shown in Fig. 7. The same adsorbate was used with a number of substrates that vary only in their degree of heterogeneity, as measured by the parameter γ.

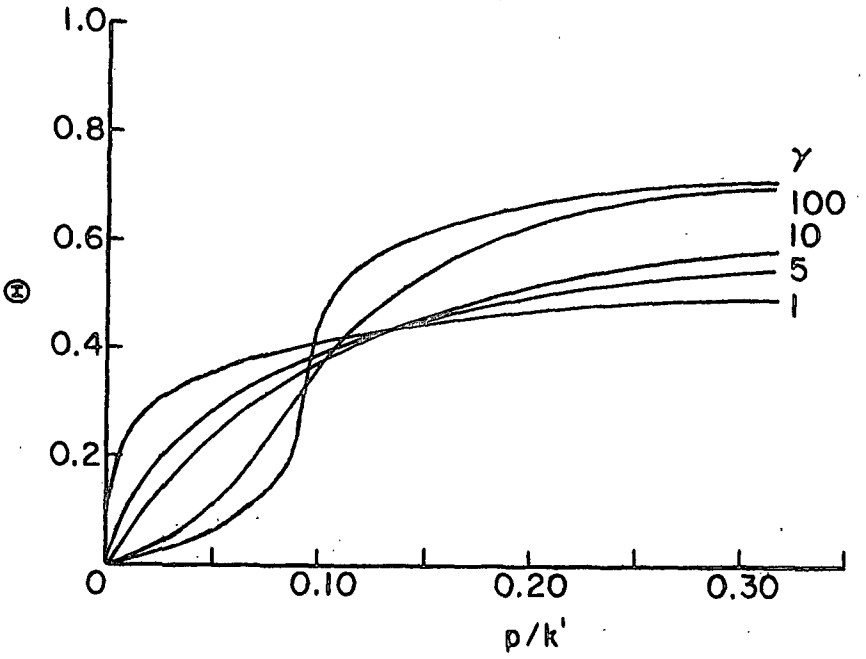

Figure 7. Computed Isotherms for Argon Adsorbed as a Mobile Film at 77.5°K on Substrates of Varying Heterogeneity

In the monograph by Ross and Olivier (10), tables are given listing Θ values for the different values of p/k'. The parameter k' is the particular value of k_i which corresponds to the mean U' of the Gaussian distribution.

To use the computed tables, the experimental isotherm is matched against computed isotherms until the best fit is obtained. This is done by plotting the theoretical isotherms in the form of $\ln \Theta$ against $\ln p/k'$ on a large sheet of paper. The experimental isotherm is plotted on tracing paper as $\ln V$ against $\ln p$ where V is the

quantity of adsorbate adsorbed at pressure p. The experimental isotherm is then slid along the axes until the theoretical isotherm which fits it most closely is found, as illustrated in Fig. 8.

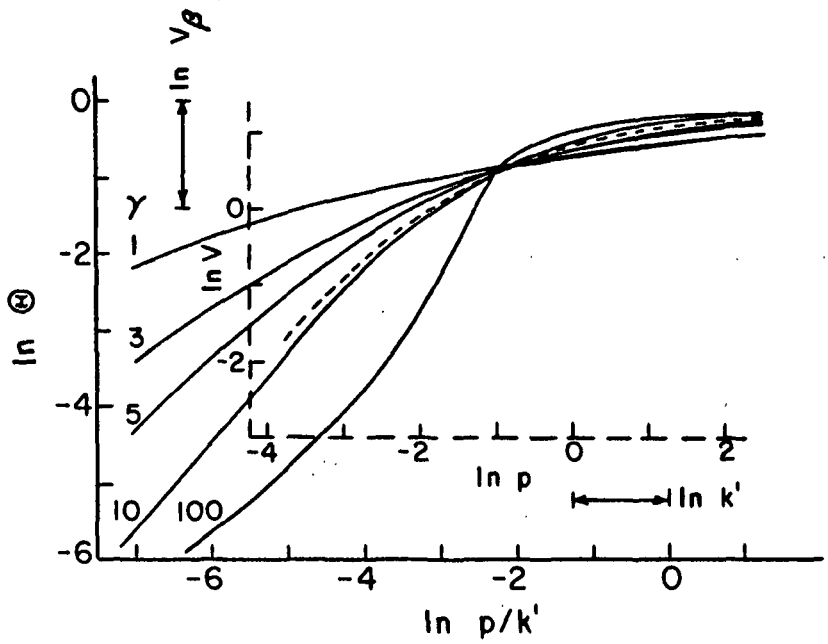

Figure 8. Theoretical Isotherms and Superposed Experimental Isotherm

The vertical displacement of the two scales is equal to $\ln(V_\beta)$ where V_β is the monolayer capacity. Since $\Theta = V/V_\beta$, then

$$\ln \Theta + \ln V_\beta = \ln V. \tag{24}$$

The horizontal displacement gives $\ln k'$ which is related to U' (the mean adsorptive potential) by the following relationship:

$$k' = \overset{\circ}{A} \exp(-U'/RT) \tag{25}$$

where $\overset{\circ}{A}$ is a temperature-dependent function defined by various standard changes of entropy and free energy that occur on adsorption.

For a mobile adsorbed film, $\ln \underline{\overset{\circ}{A}}$ is given by

$$\ln(\overset{\circ}{A}) = \frac{-\Delta S_s^{tr}}{R} - \frac{\Delta S^{rot}}{R} + \frac{{}_aF^{vib} - {}_aE_o^{vib}}{RT} + \frac{\Delta E^{kin}}{RT} - \ln\left(\frac{\theta_s}{1-\theta_s}\right) + \ln(760) \quad (26)$$

where

$\underline{\Delta S_s^{tr}}$ = the integral translational entropy change per mole of a gas in its standard state to a mobile adsorbed film in its standard state

$\underline{\Delta S^{rot}}$ = rotational entropy change upon adsorption

$\underline{{}_aF^{vib}}$ = additional Gibbs free energy of the adsorbed phase due to molecular vibrations with respect to the surface

$\underline{{}_aE_o^{vib}}$ = average vibrational energy of an adsorbed molecule at 0°K

$\underline{\Delta E^{kin}}$ = change in kinetic energy of translation and rotation upon adsorption

$\underline{\theta_s}$ = fraction of the surface covered at the standard state of the adsorbed phase.

The term $\ln \underline{\overset{\circ}{A}}$ describes in mathematical language the assumed character of the adsorbed film, taking into account a new vibration, peculiar to the adsorbed state of the molecule with respect to the substrate.

The adsorptive potential designated by $\underline{U}$ is defined as the potential energy difference between the lowest energy state of a molecule in the gas phase (i.e., infinitely removed from the surface) and its lowest energy state in the adsorbed phase (i.e., the zero point vibrational level, $\underline{{}_aE_o^{vib}}$), both at infinite dilution. A schematic description of $\underline{U}$ and its relation to other heats and energies of adsorption (i.e., isosteric, $\underline{q^{st}}$, and differential, $\underline{q^{diff}}$, heat of adsorption) are shown in Fig. 9. The $\underline{U}$ parameter, as defined above, is characteristic of the adsorbate-adsorbent system and is independent of temperature.

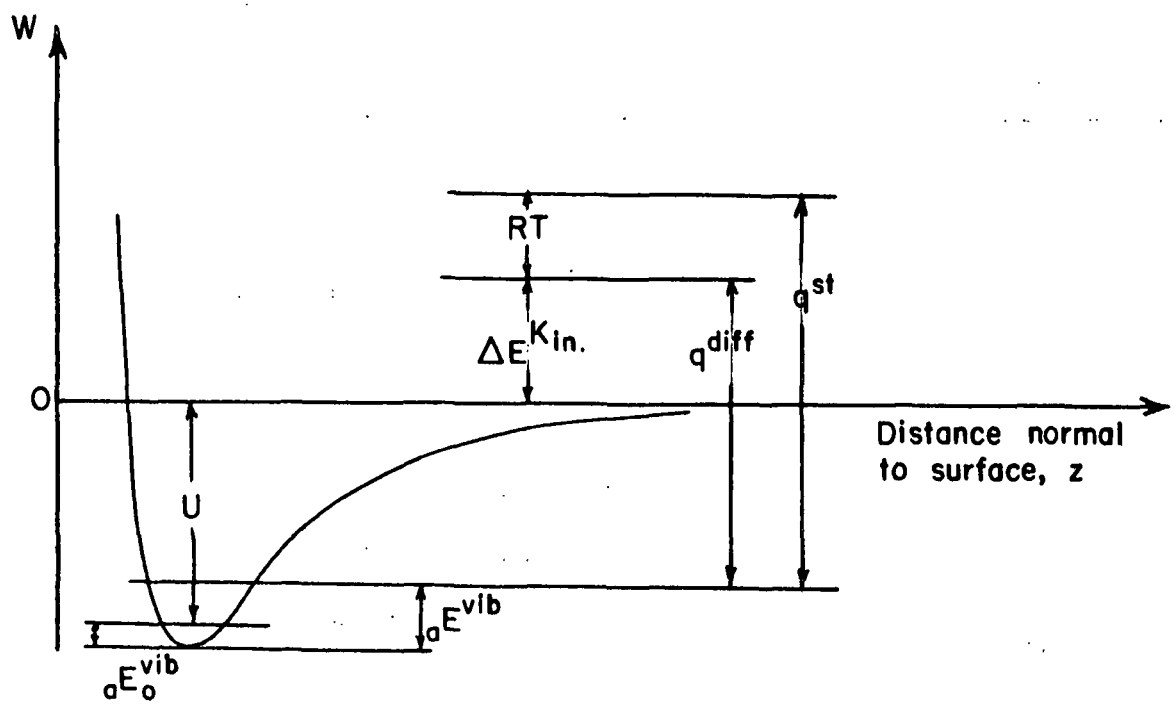

Figure 9. Energy Relations for an Adsorbate-Adsorbent System

In conclusion, Ross and Olivier have obtained a realistic model for physical adsorption of gases on real surfaces. They have been able to express the model with a workable mathematical set of equations in terms of the molecular properties of the adsorbed molecules and adsorbents.

PREVIOUS WORK IN GAS ADSORPTION ON CELLULOSE

The physical adsorption of gases on cellulose has been extensively investigated where the cellulose fiber specific surface area and pore size distribution were the experimental quantities obtained, as summarized by Stamm (13). In general, these investigations used the BET gas adsorption theory to determine the specific surface area. The Pierce method (14) was used to determine the pore size distribution.

A typical isotherm for the physical adsorption of a gas on cellulose is shown in Fig. 10. This particular isotherm was obtained by Haselton (15) for nitrogen

adsorption on a benzene-dried chlorite holocellulose at 77.5°K. The peculiar shape and the large hysteresis loop of the isotherm in Fig. 10 are indicative of the highly porous nature of solvent-dried cellulose adsorbents.

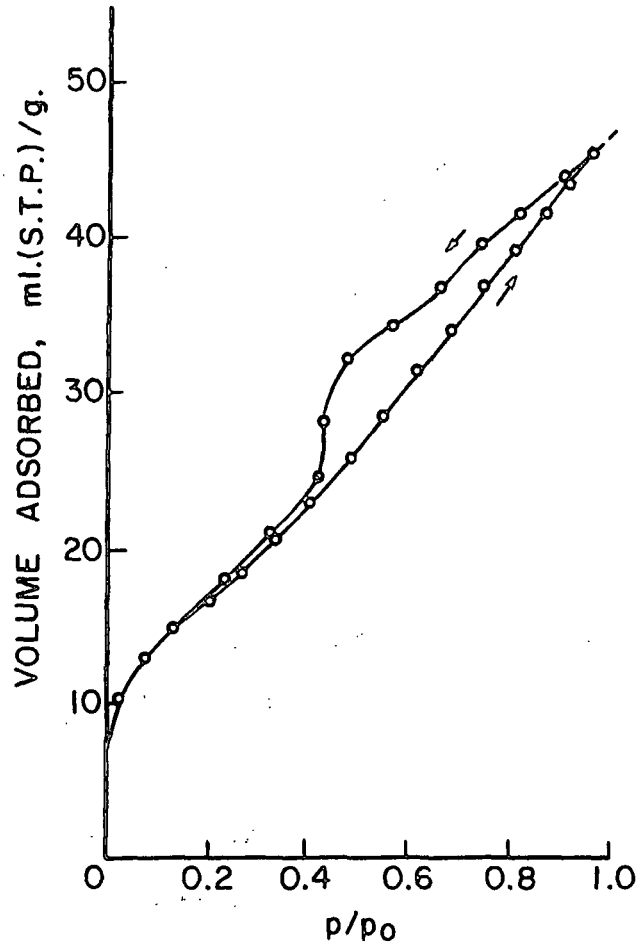

Figure 10. Nitrogen Adsorption on a Benzene-Dried Chlorite Holocellulose at 77.5°K (15)

More recently, Barber (16) concluded a study using the Rcss and Olivier theory to investigate the surface energy site distribution of cellulose fibers. Using the Ross and Olivier theory, three parameters were obtained to characterize the cellulose fiber surface. These parameters were the specific surface area, the mean adsorptive potential, and the surface heterogeneity factor, γ. An inert monoatomic adsorbate gas, argon, was used throughout the investigation. The possible adsorbate-adsorbent interactions were limited to nonpolar Van der Waals type interactions in

the data analyses by assuming that the interaction due to polarization of argon was negligible. A summary of the experimental results for water-dried fibers is presented in Table I.

TABLE I

EXPERIMENTAL RESULTS FOR WATER-DRIED FIBERS (16)

Adsorbent	Ross and Olivier Specific Surface Area, $m.^2/g.$	U', kcal./mole	γ
Water-dried cotton	1.41	1.26	4.0
Water-dried high-tenacity rayon	0.422	1.38	7.0
Water-dried hydroxyethylated cotton combers	1.36	1.17	3.0
Water-dried incense cedar chlorite holocellulose	0.52	1.10	5.0

Deitrich (17) continued this line of investigation by determining the energy site distribution of cotton cellulose fibers with a nitrogen gas adsorbate. All of the cellulose samples used in this investigation were prepared by WAN drying (i.e., solvent exchange from a water-swollen state). By using the diatomic adsorbate gas molecule, an additional type of adsorbate-adsorbent interaction was possible if the cellulose adsorbent had a surface electrostatic field to polarize the nitrogen molecule ($u_{\xi}(r) = -E^2\xi/2$).

In order to apply the Ross and Olivier theory to the nitrogen adsorption data, a separate estimate of the surface electrostatic field was required. Deitrich selected the technique of Chessick, et al. (18) for this determination.

Chessick, et al. (18) found that the heat of immersion of a solid in polar liquids was approximately a linear function of the dipole moment of the wetting liquid. This linear plot was explained on the basis that the additional energy

of interaction in the polar liquid was due to the added contribution of a polar Van der Waals adsorptive potential (i.e., $\underline{u}_{\mu}(\underline{r}) = -\underline{E}\mu \cos\Psi$). The slope of the plotted line gives an average strength of the electrostatic field $\underline{E}$ emanating from the solid at the position of the dipole. The intercept gives an average value of the dispersion energy.

Deitrich (17) found that the average electrostatic field strength of the cotton cellulose was 0.13×10^5 esu.cm.^{2} He concluded that this field was too weak to induce a significant induced dipole moment in the nitrogen molecule. Deitrich's results for cotton fibers are compared with the results for the other solids studied by Chessick, et al. in Fig. 11.

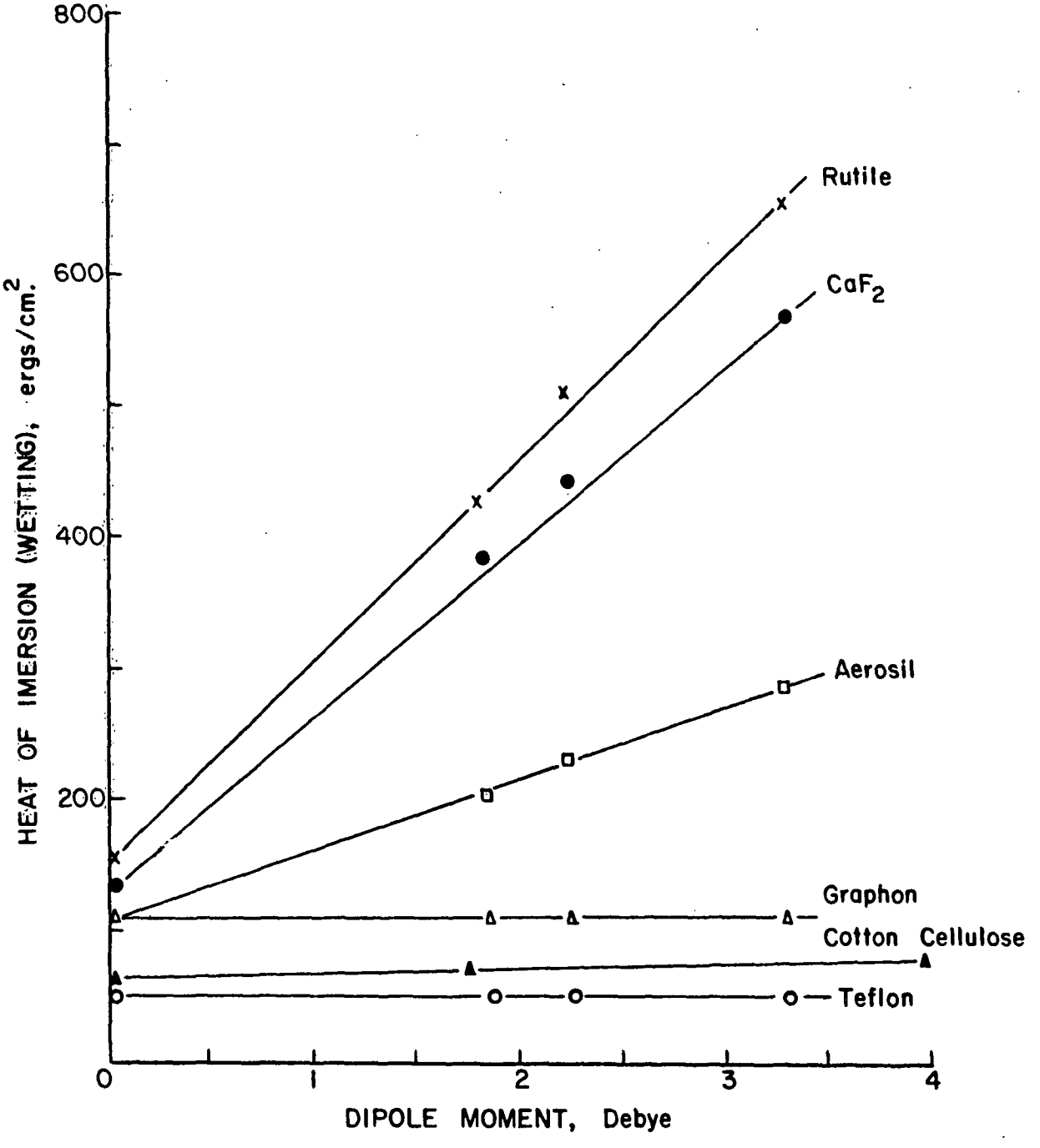

Figure 11. Heat of Immersion Versus Dipole Moment of Wetting Liquid

APPROACH TO THE THESIS PROBLEM

DEVELOPMENT OF A NEW MULTILAYER ADSORPTION MODEL

The Ross and Olivier model is difficult to apply to adsorbents of extreme heterogeneity. The adsorption isotherms of these adsorbents are nearly linear on a ln-ln plot. Therefore, the graphical solution methods suggested by Ross and Olivier (see Fig. 8) yield an ambiguous range of possible solutions. Because of this problem, the limitations to monolayer coverage on each homotattic patch in the Ross and Olivier model, a new adsorption model was developed. The new model retains the basic approach that Ross and Olivier used, but the model has been modified to permit multilayer adsorption on each homotattic patch. In addition, a more realistic distribution function for the adsorptive potentials was incorporated in the new model.

MULTILAYER ADSORPTION ON HOMOGENEOUS SURFACES

When adsorption takes place on a homogeneous surface, there are two-dimensional phase transitions resulting from the successive condensation of filled adsorbate layers. These transitions are very distinct if the isotherm temperature is below the two-dimensional critical temperature and if the adsorbent is extremely homogeneous. The results of Duval and Thomy (19) demonstrate this effect for the adsorption of krypton on an exfoliated graphite surface at 77.4°K. This homogeneous graphite surface was obtained by splitting graphite crystals by means of the thermal dissociation of its intercalation compound with ferric chloride. Five distinct transitions corresponding to the formation of five adsorbate layers are well defined in the adsorption isotherm (see Fig. 12). deBoer and Broekhoff (20) have shown that experimental adsorption data, such as shown in Fig. 12, can be explained theoretically as the independent and successive formation of mobile two-dimensional Van der Waals phases, one after another. That is, multilayer adsorption is interpreted as

the independent and successive formation of adsorbate monolayers, one on top of another. Each adsorbate layer is described by the Hill-deBoer equation [see Equation (19)] in the form

$$p = \overset{\circ}{A} \exp\left[\frac{-U_j}{RT}\right] \frac{\theta_j}{1 - \theta_j} \exp\left[\frac{\theta_j}{1 - \theta_j} - \frac{2\alpha\theta_j}{\beta RT}\right] \tag{27}$$

where the j index denotes the adsorbate layer and the other variables are used as defined on pages 17-21. The fractional coverage at each adsorbed layer, θ_j, can be expressed as a nonlinear function of the adsorptive potential, pressure, and temperature.

$$\theta_j = \theta_j(U_j, p, T). \tag{27a}$$

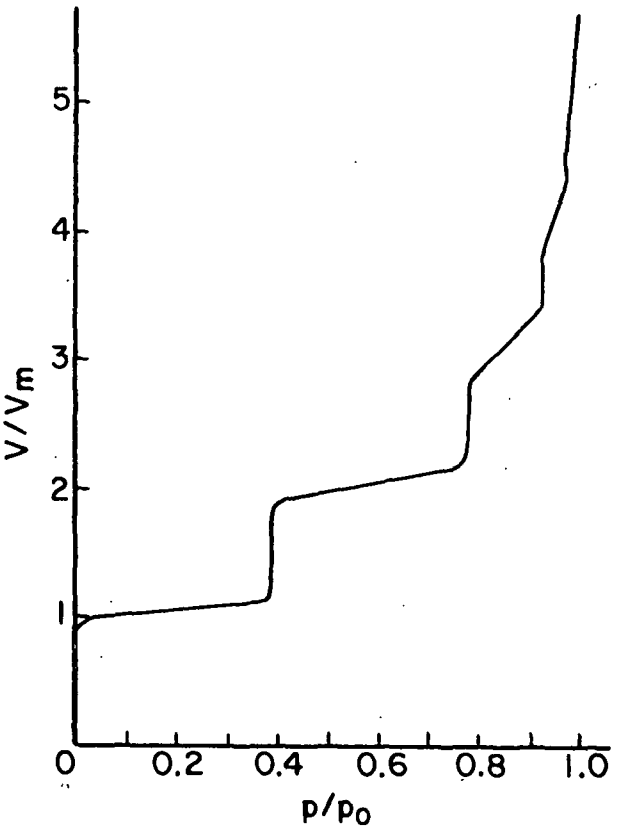

Figure 12. Krypton Adsorption on an Exfoliated Graphite at 77.4°K (19)

A relationship is needed to specify the adsorptive potential, U_j, at the jth adsorbate layer. Consider Equation (12) derived earlier, i.e.,

$$W(z) = -\pi\rho C_1/6z^3 \tag{28}$$

for the Van der Waals forces above a continuum surface. From Equation (28) it is evident that the adsorptive potential at the jth layer should be inversely proportional to the 3rd power of the distance of the jth adsorbate layer from the surface. If one assumes that the adsorbate layers are at equally spaced distances, r_o, above the surface, and that the surface adsorptive potential is U_1, then

$$\begin{aligned} U_2 &= U_1/2^3 \\ U_3 &= U_1/3^3 \\ U_4 &= U_1/4^3 \\ &\cdot \\ &\cdot \\ U_j &= U_1/j^3 \qquad j = 2,3,\ldots \end{aligned} \tag{29}$$

Equation (29) neglects the potential energy of interaction of the adsorbate molecules themselves. The adsorbate molecules in each layer below the adsorbate layer under consideration contribute an adsorptive potential proportional to $2\alpha/\beta$ where $2\alpha/\beta$ is the heat of condensation for a two-dimensional Van der Waals gas (10). Equation (29) can be modified to account for the adsorbate term as follows:

$$\begin{aligned} U_2 &= U_1/2^3 + (2\alpha\theta_1/\beta) \\ U_3 &= U_1/3^3 + (2\alpha\theta_1/\beta)/2^3 + (2\alpha\theta_2/\beta) \\ U_4 &= U_1/4^3 + (2\alpha\theta_1/\beta)/3^3 + (2\alpha\theta_2/\beta)/2^3 + 2\alpha\theta_3/\beta \\ &\cdot \\ &\cdot \\ U_j &= U_1/j^3 + (2\alpha\theta_1/\beta)/(j-1)^3 + (2\alpha\theta_2/\beta)/(j-2)^3 \\ &\quad + \ldots \qquad\qquad j = 2,3,\ldots \end{aligned} \tag{30}$$

Equation (30) can be written in a generalized form as

$$U_j = \frac{U_1}{j^3} + \frac{2\alpha}{\beta} \sum_{k=2}^{j} \frac{\theta_{(k-1)}}{(j - k + 1)^3} \qquad j \geq 2 \ . \tag{31}$$

The concepts used in deriving Equation (31) are consistent with the experimental observations of Beebe and Young (21). Their experimental data conform to a good approximation to the results predicted by Equation (31). Beebe and Young calorimetrically measured the heats of adsorption of argon on Spheron carbon blacks at 77.5°K as shown in Fig. 13.

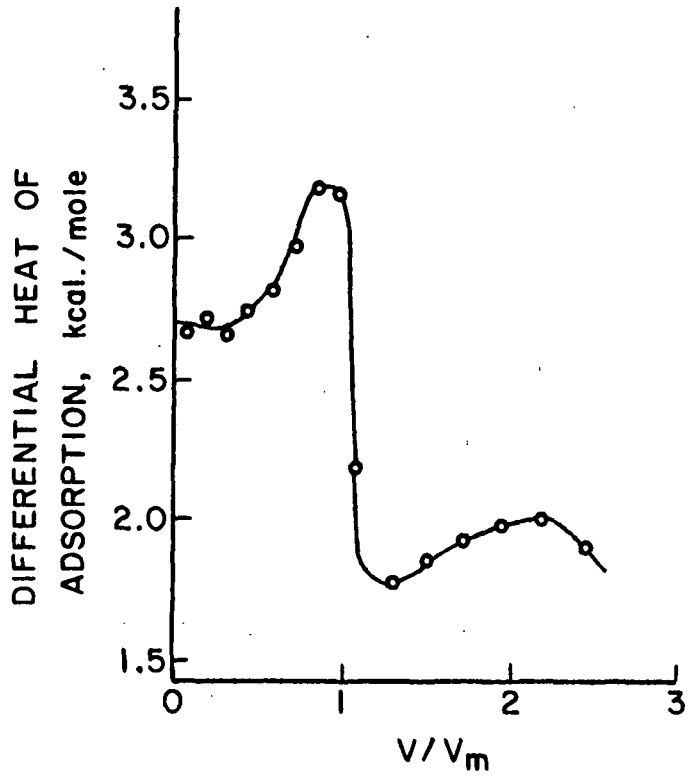

Figure 13. Calorimetrically Measured Heats of Adsorption of Argon on Spheron Carbon Blacks at 77.5°K (21)

Returning now to Equation (27a), the specific volume* of gas adsorbed at the jth layer is $V_\beta \theta_j$ where V_β is the volume of gas adsorbed per gram of adsorbent when

*Specific volume refers to volume per unit mass.

the area occupied by each adsorbate molecule is β. Therefore, the model for multilayer adsorption on a homogeneous surface is

$$V(p,T) = V_{\beta} \sum_{j} \theta_j(U_j,p,T) \tag{32}$$

where U_j is given in Equation (31).

MULTILAYER ADSORPTION ON HETEROGENEOUS SURFACES

Adsorptive Potential Distribution Function

A homogeneous surface was assumed to have a uniform adsorptive potential, U_1; however, a heterogeneous surface will have a distribution of adsorptive potentials, $\Psi(U_{i1})$ to describe the energetic heterogeneity of the surface.

A Gaussian probability function was selected by Ross and Olivier to describe the distribution of adsorptive potentials present on an adsorbent surface [see Equation (20)]. The Gaussian distribution function is presented in Equation (20a):

$$\Phi(U_{i1}) = \frac{1}{f} \exp\left[-\gamma(U_{i1} - U^{Mean})^2\right] \tag{20a}$$

where f is the normalizing factor and U^{Mean} is the mean value of the distribution. A schematic diagram of a Gaussian distribution is presented in Fig. 14 (22). Unfortunately, this distribution function has the disadvantage that at increasing degrees of heterogeneity, it assigns a negative value to the adsorptive potential U_{i1} for larger and larger fractions of the surface. One way to avoid negative values of U_{i1} is to truncate the Gaussian distribution at $U_{i1} = 0$, and to normalize the remaining part $U_{i1} \geq 0$ by dividing by the area under the distribution curve for $U_{i1} \geq 0$. However, the log-normal distribution avoids the difficulties of negative values of U_{i1} and truncation. Schematic diagrams of the truncated Gaussian and log-normal distributions are also presented in Fig. 14.

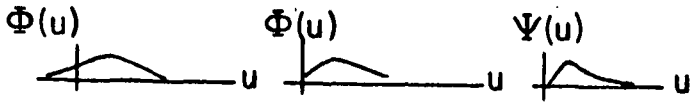

Complete Gaussian | Truncated Gaussian | Log-Normal

Figure 14. Distribution Functions

The log-normal distribution was selected for use in this multilayer adsorption model. The mathematical properties of this distribution function have been thoroughly discussed elsewhere (23). A plot of the distribution density for several degrees of heterogeneity is shown in Fig. 15. The log-normal distribution is skewed and is defined for only positive values of $\underline{U}_{i1}$.

The distribution density function, $\Psi(\underline{U}_{i1})$ is:

$$\Psi(U_{i1}) = \frac{1}{nU_{i1}} \exp\left[-\gamma(\ln U_{i1} - \ln U^{Median})^2\right] \qquad (33)$$

where γ is the heterogeneity parameter and $\underline{n}$ is the normalizing factor. $\underline{U}^{Median}$ is the median value for the distribution of $\underline{U}_{i1}$ given in Equation (33). The mean value, $\underline{U}^{Mean}$, and the most probable value, $\underline{U}^{Mode}$, are given by

$$U^{Mean} = \exp[\ln U^{Median} + (1/(4\gamma))] \qquad (34)$$

$$U^{Mode} = \exp[\ln U^{Median} - (1/(2\gamma))]. \qquad (35)$$

When γ is large, the log-normal distribution becomes very similar to the symmetrical Gaussian distribution (see Fig. 15).

The log-normal distribution of the surface adsorptive potentials

$$\Psi(U_{i1}) = \frac{1}{nU_{i1}} \exp\left[-\gamma(\ln U_{i1} - \ln U^{Median})^2\right] \qquad (36)$$

was normalized over the adsorptive potential range from $\underline{e}$ to $\underline{g}$ where

$$n = \int_{e}^{g} \frac{1}{U_{i1}} \exp[-\gamma(\ln U_{i1} - \ln U^{Median})^2] \qquad (37)$$

so that the total surface may be represented as unity, and therefore $\Psi(\underline{U}_{i1})$ is redefined as the partial number fraction of the surface with adsorptive potential $\underline{U}_{i1}$. The upper and lower limits of the integral in Equation (37) were determined so that the function in the integral had a value equal to 0.00001. Using these values for $\underline{e}$ and $\underline{g}$, values of $\underline{n}$ were calculated by Simpson's rule using a sufficiently large number of intervals to ensure an accurate estimate of the area under the distribution curve.

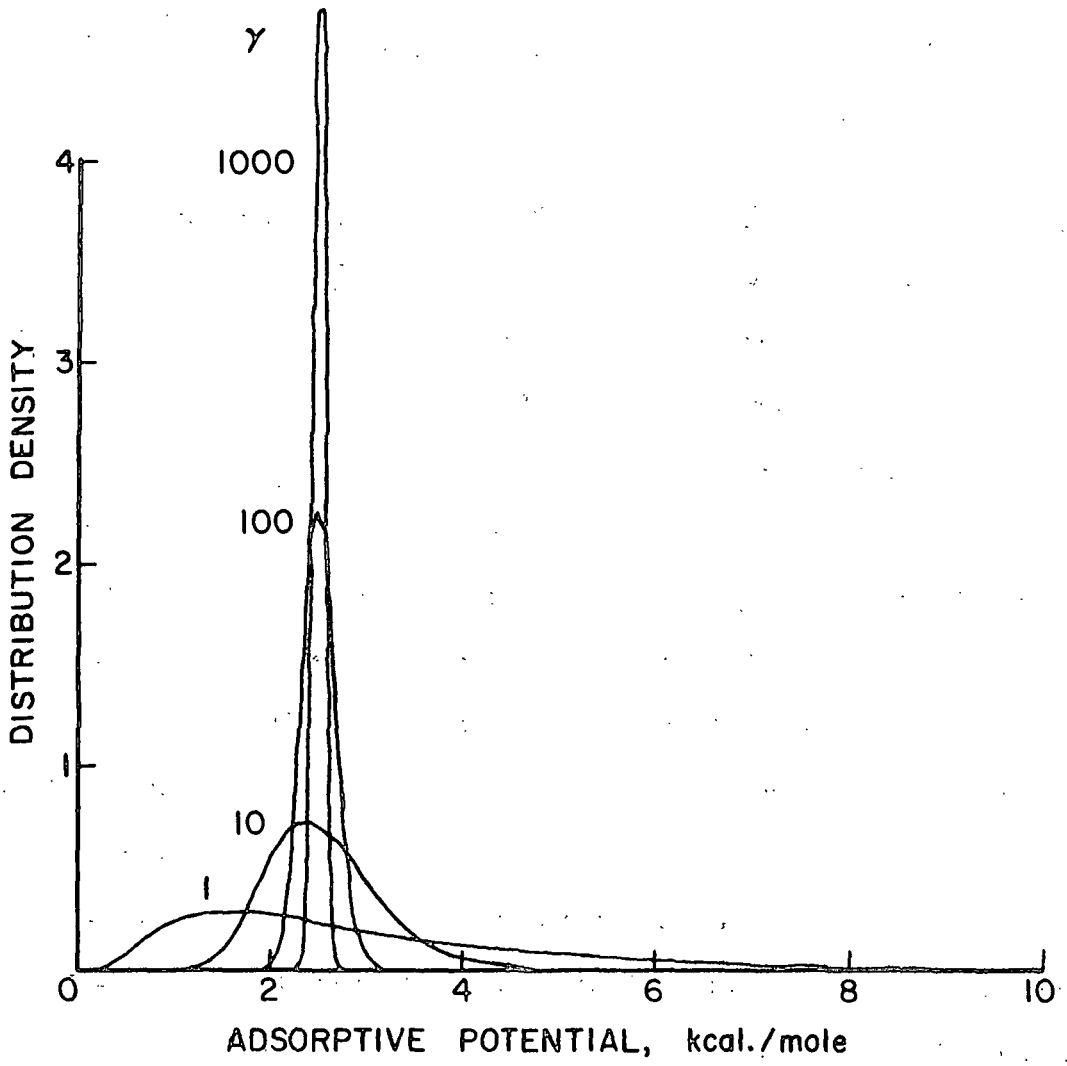

Figure 15. Log-Normal Distribution Function for Selected Values of the Heterogeneity Parameter at $\underline{U}^{Median}$ = 2.5 kcal./mole

Using the normalized log-normal distribution function to characterize the adsorptive potential in the first layer, $U_{i\,1}$, the adsorptive potential in the subsequent j layers was described by a relationship similar to Equation (31) which includes the adsorptive potential contribution due to the absorbate species already adsorbed:

$$U_{ij} = \frac{U_{i\,1}}{(j)^3} + \frac{2\alpha}{\beta} \sum_{k=2}^{j} \frac{\theta_{i(k-1)}}{(j - k + 1)^3} \qquad j \geq 2 \qquad (38)$$

where $2\alpha/\beta$ is the heat of condensation of a two-dimensional Van der Waals gas, i is the index denoting the surface adsorptive potential distribution, and j is the index denoting the adsorbate layer.

Adsorption on Each Homotattic Patch of the Heterogeneous Surface

A heterogeneous surface is one described by a distribution of adsorptive potentials. A region of a heterogeneous surface that acts as if its structure were uniform and homogeneous (i.e., energetically uniform) is defined as a homotattic patch. Each patch of surface characterized by a given potential becomes the seat of an adsorbed phase, so that a number of surface phases coexist at a given equilibrium pressure of the adsorbate gas. At equilibrium, the adsorbed species on each patch will have the same chemical potential, but the surface concentrations and spreading pressures will be different to achieve this equality. Implicit in this description of a heterogeneous surface is the assumption that the patches are sufficiently large so that they can be considered to act as mutually independent bits of surface area. Moreover, when the concentrations of adsorbed molecules are large enough that lateral molecular interactions are significant, then the patches must be large compared to the range of these interactions.

The equation used to describe the adsorption (i.e., fractional coverage) for the individual adsorbate layers on each homotattic patch of the heterogeneous surface

is the Hill-deBoer equation [see Equation (27)] written in the form:

$$p = \overset{\circ}{A} \exp[-U_{ij}/RT] \frac{\theta_{ij}}{1 - \theta_{ij}} \exp\left[\frac{\theta_{ij}}{1 - \theta_{ij}} - \frac{2\alpha\theta_{ij}}{\beta RT}\right] \tag{39}$$

where α is the two-dimensional Van der Waals constant corresponding to $\underline{a}$, β is the two-dimensional Van der Waals constant corresponding to $\underline{b}$, and $\underline{\overset{\circ}{A}}$ is a temperature-dependent function of various standard entropy and free energy changes that occur on adsorption. For a mobile physically adsorbed film, $\ln \underline{\overset{\circ}{A}}$ is given by

$$\ln \overset{\circ}{A} = - \frac{\Delta S_s^{tr}}{R} - \frac{\Delta S^{rot}}{R} + \frac{a^F{}^{vib} - a^F{}_o^{vib}}{RT} + \frac{\Delta E^{kin}}{RT} - \ln \frac{\theta_s}{1 - \theta_s} + \ln 760 \tag{40}$$

where the variables are used as defined on page 21.

Equation (32) which defined a model for multilayer adsorption on a homogeneous surface may be rewritten utilizing Equations (39) and (36) to describe multilayer adsorption on a heterogeneous surface.

$$V(p,T) = V_\beta \sum_i \Psi(U_{i1})\Delta U_{i1} \sum_j \theta_{ij}(p,U_{ij},T). \tag{41}$$

For computational purposes, the multilayer adsorption isotherm equation was approximated numerically using the relationship:

$$V(p,T) = V_\beta \sum_{i=1}^{100} \Psi(U_{i1})\Delta U_{i1} \sum_{j=1}^{5} \theta_{ij}(p,U_{ij},T) \tag{41a}$$

where the surface adsorptive potential range was divided into 100 intervals and up to 5 adsorbate layers were considered. The adsorptive potential range was divided into 100 intervals to obtain a smooth, continuous isotherm function. Only 5 adsorbate layers were considered because theoretical calculations indicated that only the first two layers reached significant coverage for the adsorbate-adsorbent systems used in this investigation.

ANALYSIS OF ADSORPTION DATA BY NONLINEAR REGRESSION TECHNIQUES

The mathematical model of a multilayer adsorption isotherm for a patchwise heterogeneous surface in its most general form is:

$$V = f(p;\ T,\ 2\alpha/\beta;\ U^{Median},\ \gamma,\ V_\beta,\ \nu) \qquad (42)$$

where

$\underline{p}$ = the independent variable, pressure

$\underline{T}$ = temperature, a known parameter

$2\alpha/\beta$ = two-dimensional Van der Waals constants corresponding to $\underline{a}$ and $\underline{b}$, respectively (α and β are known parameters)

$\underline{U}^{Median}$ = median adsorptive potential

γ = heterogeneity parameter

$\underline{V}_\beta$ = monolayer volume

ν = adsorbate vibrational frequency normal to the surface

$\underline{V}$ = the dependent variable, volume.

The variables $\underline{U}^{Median}$, γ, $\underline{V}_\beta$, and ν are unknown parameters in the equation. The function $\underline{f}$ is nonlinear in the parameters $\underline{U}^{Median}$, γ, and ν. The experimental adsorption isotherm data points are denoted as:

$$V_1,\ p_1,\ V_2,\ p_2,\ \ldots,\ V_i,\ p_i \qquad i = 1,2,\ \ldots,\ n.$$

The problem is to find the values of the unknown parameters in the model which will best fit the model to the experimental data. Because of the theoretical basis for the model, the unknown parameters have physical significance and can be used to characterize the nature of the surface.

As a result of the complexity of the adsorption model, the best possible method for estimating the unknown parameters in the model is nonlinear regression analysis (24). A rigorous description of the nonlinear regression method is presented in

Appendix I on pages 142-156. The nonlinear regression analysis can be simply described as an iterative search for the parameter values which permit the best fit of the model to the experimental data. A least-squares criterion is used to define the best fit, where the unknown parameters are adjusted until

$$S(\underset{\sim}{\varphi}) = \sum_{i=1}^{n} (V_i - \hat{V}_i)^2 \qquad (43)$$

is a minimum. $S(\underset{\sim}{\varphi})$ is the residual sum of squares where $\underset{\sim}{\varphi}$ is the unknown parameter vector, $\hat{V}_i$ is the value of the dependent variable volume predicted by the model, V_i is the experimental value of the volume, and n is the number of experimental data points.

The searching algorithm used in estimating the parameters was Marquardt's method (25, 26) described also in Appendix I. A Fortran program was written using a modified version of Marquardt's method to fit the multilayer adsorption model with the four unknown parameters to the experimental adsorption data. A flow chart and listing of the program are in Appendix II on pages 157-207. Also included in Appendix II is a sample data set and the printed output of results from the program.

At the completion of the search procedure, the estimated parameter values are listed along with their approximate 95% linear confidence intervals. An example result is listed in Table II. The confidence intervals were calculated as if the parameters were linear in the model and are valid only to the extent that the linearization provides a good approximation to the nonlinear model.

TABLE II

CONVERGED PARAMETER VALUES

Parameter	Mean Value	Approximate 95% Linear Confidence Interval
γ	7.4	± 0.8
U^{Median}	1.36 kcal./mole	± 0.02 kcal./mole
V_β	1.39 ml. (S.T.P.)/g.	± 0.07 ml. (S.T.P.)/g.
ν	2.3×10^{12} sec.$^{-1}$	± 0.6×10^{12} sec.$^{-1}$

When evaluating the parameters resulting from this nonlinear curve-fitting process, one must be cognizant of the fact that the parameters are all interdependent (i.e., correlated) to some extent. The variance of the estimated parameter value is the expected value of the squared deviations about its mean [i.e., $\underline{V}(\underline{b}_i)$]. The covariance of two interdependent estimated parameter values is analogous to a variance, but instead of the squared deviations of one variable it contains the product of the deviations of the two variables [i.e., $\underline{cov}(\underline{b}_i,\underline{b}_j)$]. The symmetric covariance matrix is composed of variance terms on the diagonal positions and covariance terms on the off-diagonal positions. The degree of correlation is indicated by the relative magnitude of the off-diagonal term in the covariance matrix in comparison to the corresponding diagonal terms {i.e., $\rho_{\underline{ij}} = \underline{cov}(\underline{b}_i,\underline{b}_j)/[\underline{V}(\underline{b}_i)\underline{V}(\underline{b}_j)]^{1/2}$}. The covariance matrix and correlation matrix that accompany the parameters in Table II are given in Table III. The degree of correlation between parameters determines the conditioning of the searching operation and the range of values to which the parameters can be constrained. It is obvious that if the parameters are highly correlated, the curve-fitting procedure cannot constrain the parameter values to a very narrow range of magnitude.

As a result of the correlation among the parameters, the joint confidence region of the parameters must be considered, not the individual confidence intervals. The joint approximate linear confidence region for the four parameters is a four-dimensional hyperellipsoid.

Individual confidence intervals for each parameter as given in Table II are very useful, but their individual use can often be misleading. To illustrate this point, Fig. 16 presents a possible situation that may arise when just two linear parameters (e.g., β_1 and β_2) are considered. The joint 95% confidence region for the parameters is a long, thin ellipse. The elliptical area encloses the parameter values which are jointly regarded as reasonable, taking into account the

TABLE III

PARAMETER COVARIANCE AND CORRELATION MATRICES

Parameter	γ	$\underline{U}^{Median}$	$\underline{V}_{\beta}$	ν
		Covariance Matrix		
γ	0.10466	--	--	--
$\underline{U}^{Median}$	0.00268	0.00009	--	--
$\underline{V}_{\beta}$	-0.00727	-0.00017	0.00084	--
ν	-0.02257	0.00020	0.00485	0.05330
		Correlation Matrix		
γ	1.0000	--	--	--
$\underline{U}^{Median}$	0.8554	1.0000	--	--
$\underline{V}_{\beta}$	-0.7776	-0.6013	1.0000	--
ν	-0.3022	0.0887	0.7276	1.0000

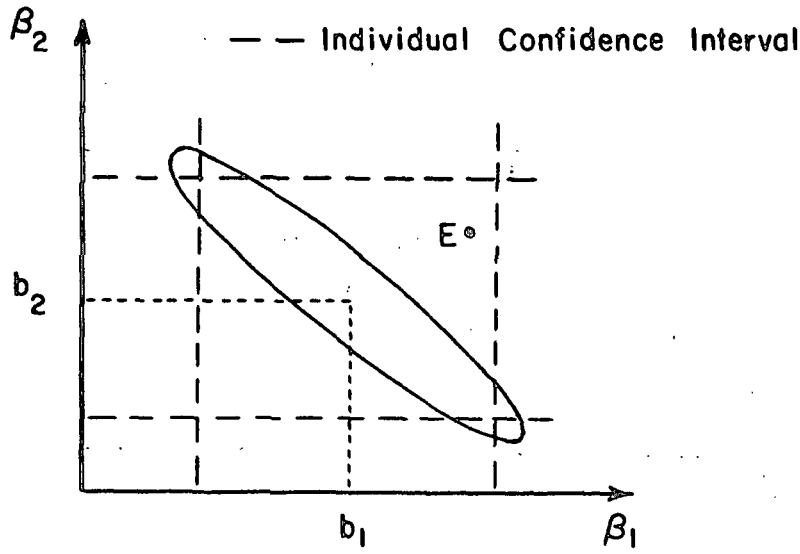

Figure 16. Comparison of Individual Confidence Limits and the Joint Confidence Region for Two Parameters (24)

correlation between the estimates of the parameter values $\underline{b}_1$ and $\underline{b}_2$. The individual 95% confidence intervals for $\underline{b}_1$ and $\underline{b}_2$ specify ranges for the individual parameters irrespective of the value of the other parameter. If an attempt is made to interpret these intervals simultaneously by using the rectangle which they define as a joint confidence region, it may be thought that the coordinates of the point $\underline{E}$ provide reasonable values for (β_1,β_2). The joint confidence region (i.e., the ellipse), however, clearly indicates that such a point is not reasonable for an estimate of β_1 and β_2. When only two parameters are involved, the construction of the confidence ellipse is not difficult, but when there are three or more parameters, the interpretation is much more difficult (see Fig. 17).

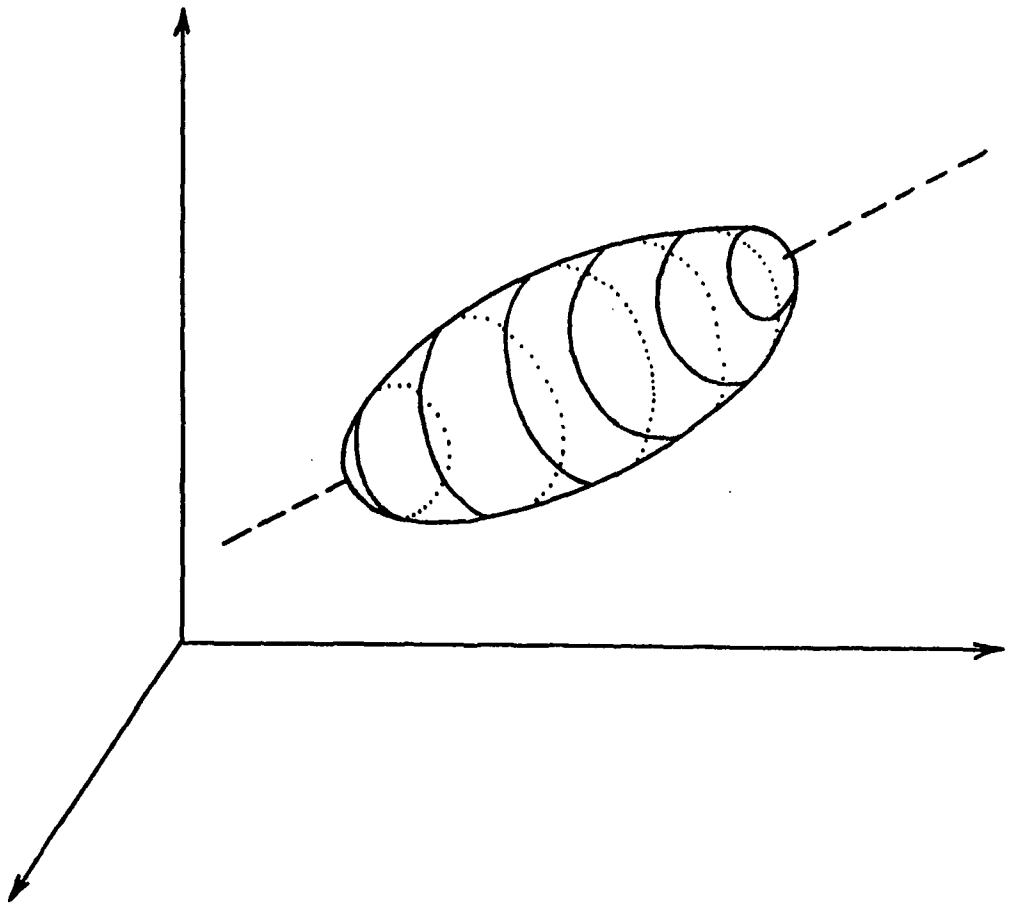

Figure 17. Joint Confidence Ellipsoid in a Three-Parameter Space

Therefore, the individual confidence intervals should be used with caution and attention should be paid to the variances and covariances of the individual parameters. This entire situation is complicated in the nonlinear case by the fact that the joint confidence region may often be a distorted ellipsoid (e.g., banana shaped).

APPLICATION OF CLUSTERING THEORY TO PHYSICAL ADSORPTION SYSTEMS

The general statistical mechanical theory of solutions developed with the aid of the theory of composition fluctuations (27-29) has been applied by Zimm (30, 31) to binary systems at adsorption equilibrium. A simplified derivation of the clustering theory for application in binary systems is included in Appendix III on pages 208-223. In this theory, a clustering function calculated from the activity concentration behavior of the adsorbate-adsorbent system gives a measure of the tendency for the adsorbate molecules to cluster. This theory does not compete with the multilayer adsorption model analysis of the gas adsorption data in that it does not predict isotherms, but it does serve to interpret the adsorbate interactions in molecular terms.

Zimm and Lundberg (31) were the first to apply clustering theory to the sorption of vapors by high polymers. Data from three systems, water-collagen, benzene-rubber, and toluene-polystyrene, were examined. A volume fraction activity coefficient, γ_x, was defined by the relationship

$$z_x = \gamma_x \varphi_x \tag{44}$$

where z_x is the activity and φ_x is the volume fraction. Component 1 was defined as the volatile material and Component 2 as the high polymer. A relation was derived between the activity coefficient, γ_1, and G_{11}, the clustering integral (see Appendix III)

$$G_{11}/v_1 = -\varphi_2 \left[\frac{\partial(z_1/\varphi_1)}{\partial z_1}\right] - 1 \qquad (45)$$

where $\varphi_2 = 1 - \varphi_1$ is the volume fraction of Component 2, and $\underline{v}_1$ is the partial molecular volume of Component 1. $\underline{v}_1$ is defined by the relationship $\underline{v}_1 = (\partial \underline{V}/\partial \underline{N}_1)_{\underline{p},\underline{T},\underline{N}_2}$ where $\underline{V}$ is the total volume and $\underline{N}_1$ and $\underline{N}_2$ are the number of molecules of Species 1 and 2, respectively. $\underline{p}$ and $\underline{T}$ are the pressure and temperature, respectively.

Referring to Equation (45), it is apparent that when the activity coefficient does not vary with concentration, as for example in the case of an ideal solution, $\underline{G}_{11}$ is minus one molecular volume. This means that a particular Type 1 molecule in such a system excludes its own volume to the other molecules but otherwise does not affect their distribution. This is what would be expected for an ideal solution.

When $\gamma_1 = \underline{z}_1/\varphi_1$ decreases with increasing φ_1, then $\underline{G}_{11}/\underline{v}_1$ is greater than -1 and may actually be positive. This means that the concentration of Type 1 molecules is higher than the ideal concentration in the neighborhood of a given Type 1 molecule, or, in other words, that the Type 1 molecules cluster together.

Scholz and his coworkers (32-34) used clustering functions in the interpretation of physical adsorption data for poly(methylmethacrylate), polystyrene, and polyvinyl chloride. The quantity $\varphi_1\underline{G}_{11}/\underline{v}_1$ was calculated from the adsorption data and interpreted in molecular terms as the average number in excess of a random expectation of Type 1 molecules in the neighborhood of a given Type 1 molecule. The relationship used in making the calculations

$$\frac{\varphi_1 G_{11}}{v_1} = \varphi_2\varphi_1 \left[\frac{\partial(z_1/\varphi_1)}{\partial z_1}\right]_{T,p} - \varphi_1 \qquad (46)$$

is derived in detail in Appendix III. From the molecular interpretation, it follows that positive values of $\varphi_1\underline{G}_{11}/\underline{v}_1$ indicate clustering of Type 1 molecules. Negative values of $\varphi_1\underline{G}_{11}/\underline{v}_1$ indicate that a given adsorbed molecule is less closely packed than a molecule in an ideal system where $\varphi_1\underline{G}_{11}/\underline{v}_1 = 0$.

From gas adsorption data, one obtains the adsorbate volume (Component 1) as a function of the adsorbate pressure and the adsorbent mass. To compute the clustering function, $\varphi_1 \underline{G}_{11}/\underline{v}_1$, one must know the activity and the volume fractions. The volume fractions can be calculated from the adsorbate volume and the adsorbent density and mass if one assumes additivity of volumes. The activity, $\underline{z}_1$, can be computed using the following relationship which is derived from the Berthelot equation:

$$z_1 = p + \frac{9T_c p^2}{128\ Tp_c}\left[1 - 6\,\frac{T_c^2}{T^2}\right] \qquad (47)$$

where

$\underline{p}$ = adsorbate pressure

$\underline{T_c}$ = adsorbate critical temperature

$\underline{p_c}$ = adsorbate critical pressure

$\underline{T}$ = adsorption isotherm temperature.

After evaluating the derivative $\partial(\underline{z}_1/\varphi_1)/\partial\underline{z}_1$ numerically, the clustering value in Equation (46) is easily evaluated using the appropriate volume fractions.

EXPERIMENTAL APPARATUS, PROCEDURES AND MATERIALS

VACUUM MICROBALANCE ADSORPTION APPARATUS

The gravimetric method of measuring gas adsorption was selected for use in this thesis because of the low surface area adsorbents being investigated. The gravimetric method is well suited to measure adsorption isotherms in the region where the alternative volumetric method is least accurate, namely, where the amount adsorbed is small compared to the amount unadsorbed. To gravimetrically determine the adsorption isotherm, the mass of the gas adsorbed is determined using a vacuum microbalance; the equilibrium pressure is measured by an independent method. The two measurements are independent, unlike the volumetric method where the measurement of the equilibrium pressure is also used for calculation of the volume of gas adsorbed. As a result, there is less chance of cumulative errors in the data obtained by the gravimetric method.

A recording vacuum microbalance system was constructed for the collection of the necessary adsorption data. The major components of the system which are shown in Fig. 18 are listed below:

(1) Cahn balance in a glass vacuum chamber

(2) Cahn balance control unit

(3) Recorder for the Cahn balance output signal

(4) Texas Instruments pressure gage

(5) Two-stage oil diffusion pump

(6) Ionization pressure gage

(7) Vacuum line and adsorbate gas addition system

(8) Ethylene glycol-water constant-temperature bath for controlling the adsorbent sample temperature environment.

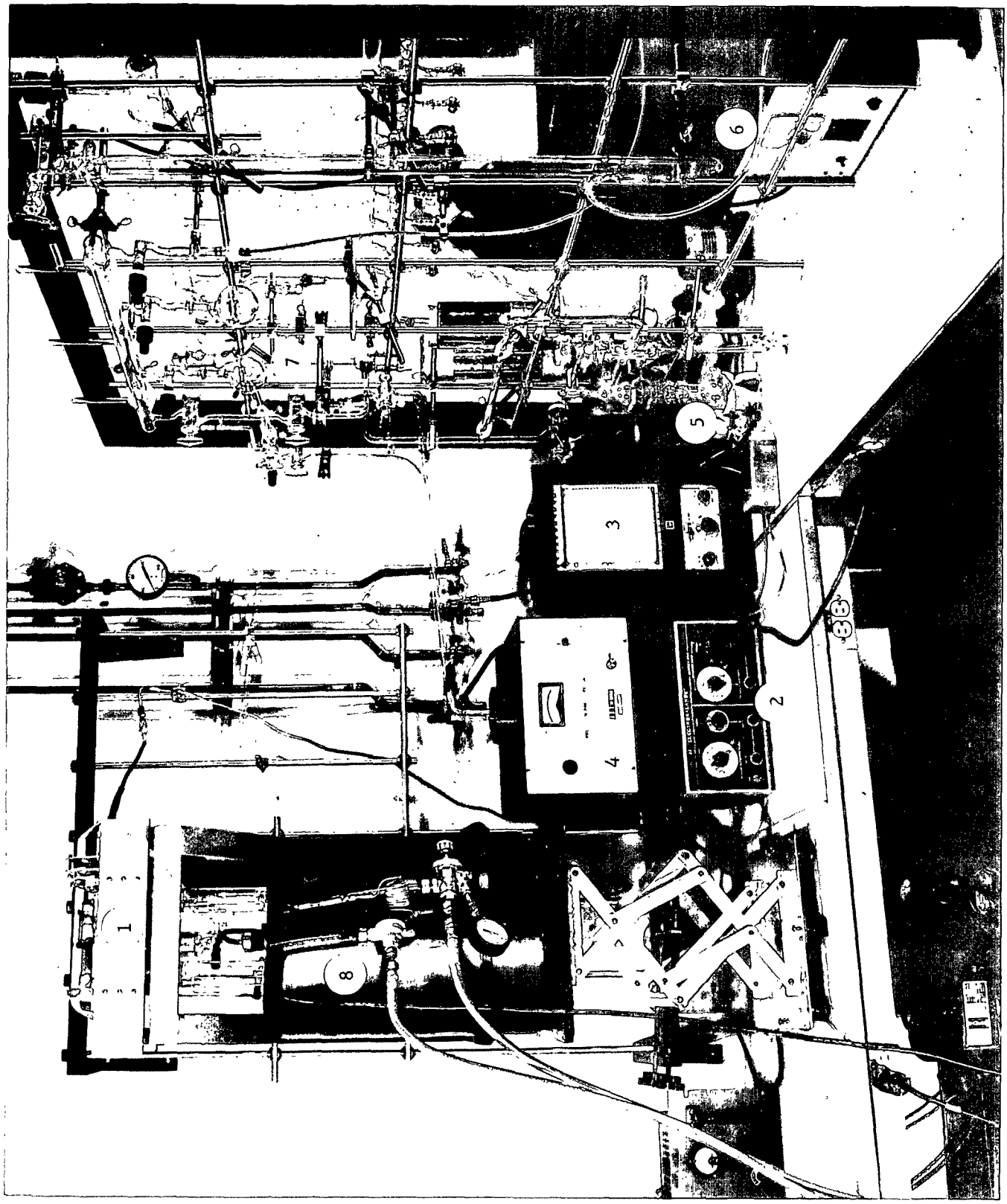

Figure 18. Recording Vacuum Microbalance Gas Adsorption Apparatus

CAHN ELECTROMAGNETIC BALANCE

The Cahn RG Electrobalance is a beam-type balance that works on the null principle. A schematic diagram of the balance system is presented in Fig. 19. The balance has two ranges of sensitivity for maximum sample weights of 1.0 and 2.5 grams. The range is determined by the choice of the sample loop (i.e., Loop A or B in Fig. 19) on the beam. For this investigation, the Outer Loop A with an ultimate sensitivity of 0.1 μg. was used. The balance beam is connected to a wire-wound coil which is suspended by a copper-beryllium ribbon between two permanent magnets. A sample is suspended from Sample Loop A and closely counterbalanced on the Counterweight Loop C. The electronic control unit of the balance system allows fine mass adjustments to compensate for mass changes. When the sample mass changes, the beam tends to deflect momentarily. The metal flag in front of the phototube moves with the balance beam, changing the amount of light to the phototube. The phototube current is amplified in a two-stage servo amplifier, and the amplified current is applied to the coil attached to the beam which is in a magnetic field. The current in the coil acts like a d.c. motor, exerting a force on the beam to restore it to the original null position. Thus, the change in electromagnetic force is equal to the change in the sample weight.

The voltage which develops across the coil is an extremely accurate measure of mass. No recorder made is accurate enough to display it to its full limits. In order to use a practical recorder, it is necessary to subtract and measure a part of the voltage with circuits inside the balance, and apply only the excess to the recorder.

Thus, a known, accurately calibrated voltage is subtracted from the voltage across the coil by means of a precision potentiometer. A dial on the potentiometer is calibrated directly in milligrams, corresponding to the amount of voltage being subtracted in the circuit. The excess of the coil voltage over the reference

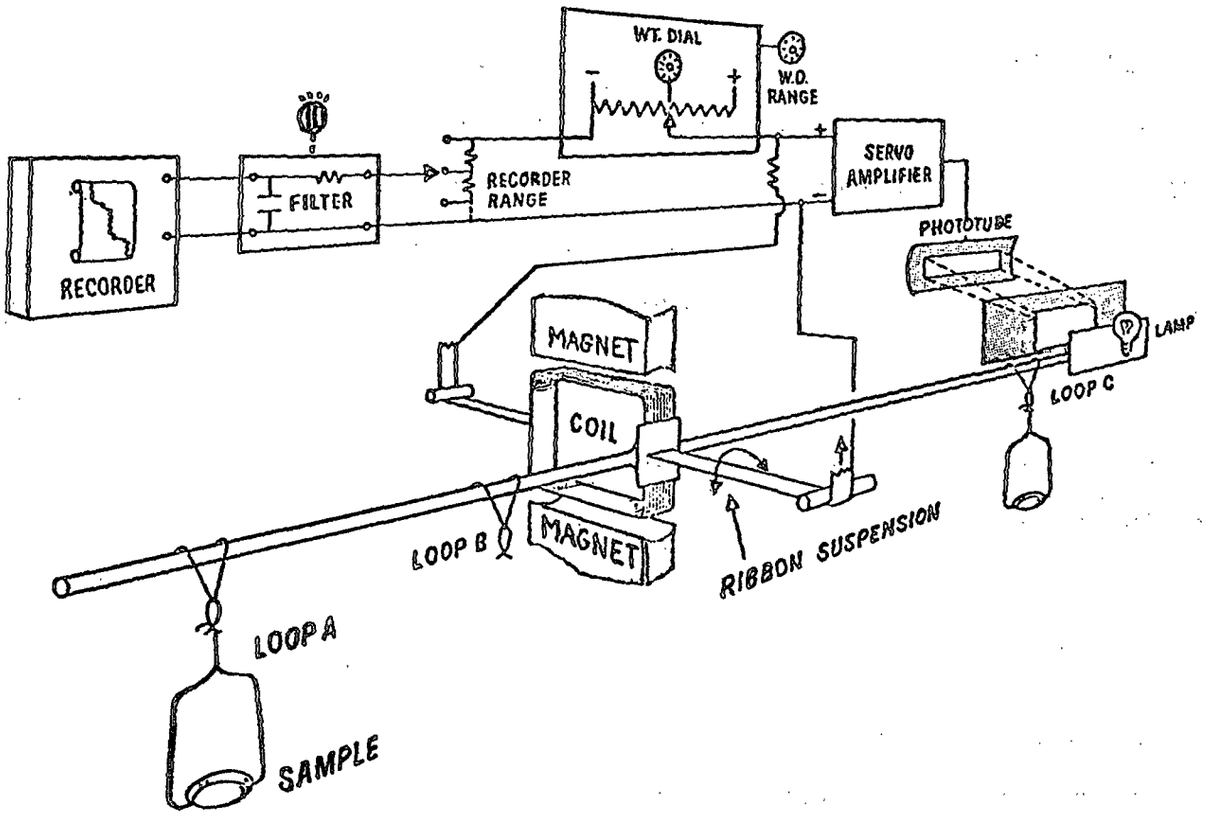

Figure 19. Schematic Diagram of Cahn RG Balance System

voltage is then available for the recorder. By attenuating this voltage by known ratios, various mass ranges can be displayed full scale on a fixed range recorder.

The balance beam and loops are mounted in a vacuum flask supplied by Cahn so that the sample and counterweight loops are centered over two standard taper joints in the flask. The beam unit is connected to the control unit of the balance by wires sealed through the glass flask.

Cylindrical fused quartz sample and counterweight pans are hung on long fused quartz fibers from their respective beam loops down through the ground joints into long pyrex tubes. The pyrex hangdown tubes are 500-mm. long with a 41-mm. inside diameter. The cylindrical quartz pans are 25 mm. in diameter and 20 mm. in height. The fused quartz hangdown fibers are 250 μm. in diameter.

Initial work with the balance system indicated that convection currents were present in the hangdown tubes when a large temperature gradient existed along the hangdown tubes. The instability in the balance operation resulting from these convection currents was most obvious when the hangdown tubes were placed in a liquid nitrogen bath.

A probable mechanism which explains the convection currents may be described as follows: As gas flows down into the hangdown tubes, it encounters the sides of the tubes cooled to 77.5°K. The cooled layers of gas that formed near the surface of the tube move down along the surface and are replaced by the upper warm layers of gas. The return flow is upward through the center of the tube past the sample pan and along the hangdown fiber. The fiber is at a warmer temperature than the sides of the tube because of thermal conductivity. When the gas flows past the sample pan, it creates two effects. First, the gas flow causes a noisy balance output signal at higher gas pressures. Second, the gas flow creates a low-density

region at the sample pan opening, removing gas from the inside of the pan and giving rise to a greater effective volume than the pan occupies. This aspirator effect results in anomalous buoyancy measurements (35).

Baffles in the hangdown tubes as shown in Fig. 20 provide a significant improvement by breaking up the flow along the sides of the hangdown tubes and localizing it into small compartments so that no strong convection currents are able to arise.

The mass potentiometer in the control unit was calibrated over a 10-mg. range. The signal output to the recorder was calibrated so that 1 mv. was equivalent to 0.1 mg.

RECORDER FOR CAHN BALANCE OUTPUT SIGNAL

The recorder used in conjunction with the balance was a Leeds and Northrup Speedomax H. A 1-mv. span was used for the adsorption work so that full-scale on the recorder was equivalent to 0.1 mg. Filtering circuits were added to the recorder and balance control unit system to reduce the amount of noise in the recorder trace due to vibration and pan swing. The Cahn balance was supplied with a filter circuit containing a capacitance of 10 μf. and resistances of 0, 9K, 20K, and 50K ohms depending upon the filter switch setting. By varying the resistance in the filter circuit, the amount of filtering was adjustable since the filter circuit time constant is equal to the product of the resistance and capacitance in the circuit.

Since the balance was being operated at the limits of its sensitivity, additional external filtering was added in the form of 40 μf. of capacitance across the output terminals. In Table IV, a summary is given of the new and original filtering time constants in the balance filter circuit.

Figure 20. Sample and Counterweight Hangdown Tubes with Baffles

TABLE IV

FILTERING CIRCUIT TIME CONSTANTS

Filter Switch Setting	Resistance, ohms	Filter Time Constant, sec.	
		10 μf. Capacitance	50 μf. Capacitance
0	0	no filtering	no filtering
1	9K	0.068	0.34
2	20K	0.17	0.85
3	50K	0.5	2.5

TEXAS INSTRUMENTS PRESSURE GAGE

The adsorbate gas pressure in the balance vacuum flask was measured using a Texas Instruments pressure gage Model 144. The precision pressure gage measures the adsorbate pressure by means of a differential fused quartz bourdon capsule. For absolute pressure measurements, the balance flask was connected to the pressure part of the bourdon capsule and the reference space surrounding the bourdon capsule was connected to the vacuum line. The bourdon capsule used in the adsorption data collection had a pressure range of 0 to 300 torr. with a sensitivity of 0.001 torr. over the entire range.

The bourdon capsule was maintained at a constant temperature of 44.1 ± 0.1°C. so that fluctuations in the room temperature would not affect the pressure readings. The calibration table for converting the pressure gage readings into units of torr. is in Appendix IV on p. 229.

TWO-STAGE OIL DIFFUSION PUMP

A Consolidated Vacuum Corp. Model GF-21 all-glass two-stage oil diffusion pump was used. The pumping fluid was Dow Corning no. 704 silicone oil. A Cenco Megavac rotary vacuum forepump was connected in series with the diffusion pump. The liquid

nitrogen trapped pumping system was capable of evacuating the vacuum system to dynamic pressures of 1×10^{-7} torr.

IONIZATION PRESSURE GAGE

A Phillips Model PHG-010A cold cathode ionization pressure gage was installed in the vacuum system to measure pressure below the sensitivity of the bourdon capsule pressure gage. The sensing range of the gage is 0.5 torr. to 1×10^{-7} torr. expanded over four scales. The calibration of the ionization gage was checked using a McLeod gage as a reference. The Phillips gage calibration was found to be satisfactory since the gage was used only to detect leaks and to monitor the pumping.

VACUUM LINE AND ADSORBATE GAS ADDITION SYSTEM

The glass vacuum system (Fig. 18) was custom built by Pope Scientific, Inc. of Menomonee Falls, Wisconsin. The vacuum system consists essentially of two manifolds. The larger manifold was connected to the diffusion pump by a liquid nitrogen trap. The smaller manifold was connected to the larger manifold via another trap and was used for storage of the purified adsorbate gases. The adsorbate gas stored in the small manifold was metered into the balance flask using a Teflon high-vacuum needle valve. All of the other valves in the system were high-vacuum quality. Apiezon N stopcock grease was used for all of the glass valves.

ADSORBENT TEMPERATURE CONTROL

The constant-temperature bath consisted of an Armaflex foam insulated glass battery jar of about 20-liter capacity. The bath liquid was a water-Prestone (ethylene glycol) mixture. Heat was continually removed from the bath by using an epoxy-coated steel cooling coil. The refrigerant gas used was Freon-12 which was condensed by a small compressor. The amount of refrigerant gas expansion in

the cooling coil was controlled by an expansion valve on the inlet side of the coil and a constant pressure valve on the outlet. A uniform temperature throughout the bath was maintained by the agitation provided by a submersible pump placed in the bottom of the bath.

Between the temperatures 25 and -15°C., a precision mercury thermoregulator and electronic relay controlled the flow of heat into the bath. Using this arrangement the temperature variation was less than ± 0.05°C.

The entire temperature control bath was mounted on a jack, thus permitting the placement of both the sample and counterweight hangdown tubes in the same temperature environment. The tubes were immersed to a depth of approximately 35 cm. in the bath liquid.

For the isotherm temperatures of 77.5°K and 90.1°K, liquid nitrogen and oxygen, respectively, were used at atmospheric pressure to provide thermostats. The boiling point temperature was checked before and after an adsorption isotherm determination using an oxygen gas thermometer. By mounting two dewar flasks side by side on a jack, both hangdown tubes were immersed to a depth of approximately 40 cm. in the liquefied gas. Contamination of the liquid oxygen and nitrogen was prevented by allowing the evolving gas from the boiling liquids in the dewar flasks to escape through a small orifice minimizing the back-diffusion of air.

EXPERIMENTAL PROCEDURES FOR ADSORPTION MEASUREMENTS

OPERATION OF VACUUM MICROBALANCE APPARATUS

The objective of an adsorption isotherm measurement is to determine the mass of gas adsorbed by an adsorbent sample as a function of the gas equilibrium pressure at a constant temperature.

Adsorbent Sample Preparations and Outgassing

The water-swollen cellulose adsorbents were frozen in liquid nitrogen and then freeze dried. The freeze drying operation was used to maximize the surface area of the samples and to minimize the interfiber bonding. The adsorbents were then stored in a controlled environment at 72°F. and 50% R.H.

The appropriate mass of the adsorbent was placed in the sample pan of the apparatus. Outgassing was done to remove the physically adsorbed air, water, and other contaminants from the surface of the adsorbent. The sample was evacuated over a 48-hour period until the balance flask pressure was less than 1×10^{-6} torr. and the sample maintained a constant mass. Then, the sample was heated in vacuo to a temperature of 40°C. for 12 hours. During all subsequent adsorption data collection, the sample was never exposed to a pressure greater than 1×10^{-5} torr. except for the adsorbate gases.

The sample was placed in the appropriate constant-temperature bath for a minimum period of 2 hours. Then the mass of the sample, free of adsorbed species, was determined. This value of the sample mass was used as a reference to calculate the mass changes of the sample due to adsorption or desorption.

Adsorbate Preparation

The purified $CFCl_3$ adsorbate was stored in a flask attached to the small manifold. The $CFCl_3$ was frozen in liquid nitrogen and degassed by exposing the frozen $CFCl_3$ to a vacuum for approximately 5 minutes before each adsorption isotherm determination.

For argon and nitrogen isotherms, the addition line from the pressurized cylinder to the small manifold was purged and filled with the gas to a pressure greater than one atmosphere. The small manifold was evacuated to a pressure less

than 1×10^{-5} torr. Then the small manifold was filled directly from the addition line with the gas to a pressure of approximately 1.5 atm. Throughout an adsorption run for either argon or nitrogen, the gas in the adsorbate manifold was exposed to a liquid nitrogen trap to minimize possible contamination from condensable vapors.

Adsorption Measurements

Adsorption data were collected by repeated dosing of the balance flask with the appropriate gas. Approximately 15 to 30 minutes was required for the sample to reach equilibrium after each dose. Then the pressure gage reading and the apparent mass of the sample were recorded. Desorption data were collected in a similar manner by removing doses of the gas from the balance system.

CALIBRATION OF THE BALANCE

The 0 to 10-mg. mass range of the balance was used. A mass measurement could be made to ± 0.001 mg. throughout the 0 to 10-mg. range. The balance and the recorder were calibrated in accordance with the Cahn instrument manual. The balance was calibrated with National Bureau of Standards (NBS) class S weights used as counterweights against a precision NBS class M 500-mg. weight, since all of the samples were approximately 0.5 g. The calibration was done with the pans and hang-down fibers in their appropriate positions.

Subsequently, the mass dial (i.e., the reference potentiometer) was calibrated to a 10-mg. range by a substitution procedure with a 5-mg. precision NBS class M weight. Upon completing this part of the calibration, the mass dial readout was directly in terms of milligrams over a 10-mg. range.

Finally, the recorder was adjusted so that the full scale was equivalent to 0.1 mg. using the mass dial. The balance was now ready to accept a sample. The final evacuated sample mass had to be within the limits of 0.505 ± 0.005 mg. to

be on the mass dial scale. Therefore, the moisture contents of the adsorbent samples had to be considered when placing a sample in the balance for evacuation.

BUOYANCY CORRECTIONS OF MASS DATA

According to Archimedes' Principle, any solid body immersed in a fluid is buoyed up by a force equal to the weight of the displaced fluid. As a result, a buoyancy effect develops in a balance due to the difference between the volumes and temperatures of the sample and the counterweight. Assuming an ideal gas, the buoyancy effect can be expressed as:

$$\Delta W = (M/RT)(V_c - V_B)p \qquad (48)$$

where

ΔW = the difference between the buoyancy force on the counterweight and on the sample

p = pressure

M = the molecular weight of the adsorbate

T = temperature

V_c = counterweight volume

V_B = sample volume

R = gas constant = 62,364 cm.^{3} torr. mol.$^{-1}$ $^oK^{-1}$.

The buoyancy effect can be measured by admitting a gas of negligible adsorption into the system at a series of pressures with the adsorbent *in situ*; the apparent mass change of the sample is determined as a function of the pressure. The buoyancy effect of the various cellulose samples was measured using argon gas at a controlled temperature in the 15-25°C. range. The apparent mass change was recorded as a function of the gas pressure (see Appendix IV). These data were used in a linear regression to compute $(V_c - V_B)$. The buoyancy effect of the adsorbate at a given pressure and temperature was calculated according to Equation (48). The buoyancy

effect of the balance system itself was measured in a similar manner so that this effect could be allowed for in the thermomolecular flow data (see Appendix IV).

CORRECTION OF PRESSURE MEASUREMENTS FOR THERMAL TRANSPIRATION

A correction may be necessary when a pressure reading is obtained from a pressure gage that is at a different temperature from that of the sample. The gas tends to pass from the cooler to the warmer region; a steady state is reached when the pressure difference between the two regions is sufficient to balance this thermal diffusion or transpiration (10). Since the adsorbent sample temperature was below the temperature of the pressure gage bourdon capsule (i.e., 44.1°C.), it was necessary to apply a correction to the measured pressures to obtain the equilibrium pressure at the sample temperature.

Using the thermal transpiration data of Liang (36), Bennett and Tompkins (37) have developed a semiempirical equation for correcting this effect:

$$\frac{p_1}{p_2} = \frac{\alpha_{He}(f\varphi_g x)^2 + \beta_{He}(f\varphi_g x) + R_m}{\alpha_{He}(f\varphi_g x)^2 + \beta_{He}(f\varphi_g x) + 1} \qquad (49)$$

where

p_1 = pressure at sample temperature T_1, torr.

p_2 = pressure at pressure gage temperature T_2, torr.

x = $p_2 d$, where d is the minimum inside diameter in millimeters of the tube connecting the sample and the pressure gage

R_m = $(T_1/T_2)^{1/2}$ where $R_m \leq 1$

f = 1.0 for tubes of diameter less than 1 cm.; = 1.22 for tubes of diameter greater than 1 cm.

α_{He} = constant

β_{He} = constant

φ_g = the pressure shifting factor which depends on the type of gas and is defined such that $\varphi_{He} = 1$.

For argon and nitrogen isotherms, the following relationships were used (37):

$$\alpha_{He} = 3.70 \times [1.70 - 2.6 \times 10^{-3} \times (\underline{T}_2 - \underline{T}_1)]^{-2}$$

$$\beta_{He} = 7.88 \times (1 - \underline{R}_{\underline{m}})$$

$$\varphi_{\underline{g}} = 2.70 \text{ for argon; } = 3.53 \text{ for nitrogen.}$$

For $CFCl_3$, a theoretical evaluation of the gas parameters was made from the relationships developed by Mason, et al. (38) such that:

$$\alpha_{He} = \underline{m}_{He}/(48\underline{k}\underline{T}\eta_{He}^2)$$

$$\beta_{He} = (1 + 2\pi/3) \times (3\alpha_{He}/4\pi)$$

$$\varphi_{\underline{g}} = (\eta_{He}/\eta_{\underline{g}}) \times (\underline{m}_{\underline{g}}/\underline{m}_{He})^{1/2}$$

where

$\underline{T}$ = average absolute temperature $(\underline{T}_1 + \underline{T}_2)/2$

$\underline{k}$ = Boltzmann's constant

η_{He} = viscosity of helium at $\underline{T}$

$\underline{m}_{He}$ = mass of helium atom

$\eta_{\underline{g}}$ = viscosity of $CFCl_3$ at $\underline{T}$

$\underline{m}_{\underline{g}}$ = molecular weight of $CFCl_3$.

The above relationship was used to correct for thermal transpiration effects where they were significant.

CORRECTION OF MASS DATA FOR THERMOMOLECULAR FLOW EFFECT

When a temperature gradient exists along the microbalance suspension fiber, sample, or counterweight, radiometric forces will be generated because of the thermomolecular flow (TMF) of gases at pressures which generally range from 10^{-3} to 20 torr. The gas molecules arriving at a unit surface from regions of different

temperatures, and hence with different momenta, produce a net force on the surface in the direction of decreasing temperature. The magnitude of the force depends upon the pressure, gas, temperature, temperature gradient, and the geometry of the system. The forces may be minimized by employing identical suspension fibers, hangdown tubes, and temperature gradients about identical samples and counterweight pans (39, 40).

The thermomolecular flow effect can be assessed directly by determining isotherms without the adsorbent samples present (41). For this reason, blank runs were made for all of the adsorbate gases and isotherm temperatures. The data are reported in Appendix IV. These blank runs were similar in all respects to the conditions used in collecting the adsorption data except that no sample adsorbent was present. The blank run not only measures the thermomolecular flow effect, but also the balance system buoyancy and adsorption. Therefore, the TMF correction to the raw adsorption data was calculated as the blank run data minus the balance system buoyancy effect.

CALCULATION OF THE CORRECTIONS TO THE ADSORPTION DATA

Typical mass adsorption data obtained for the adsorption of argon on acid-hydrolyzed holocellulose at 77.5°K are presented in Table V.

The pressure data in Table V have been corrected for the pressure gage calibration and thermal transpiration using the procedures outlined. The mass data in the second column are the raw adsorption data obtained directly from the Cahn balance. The third column contains data corrected for buoyancy. It should be noted that the buoyancy is a very significant correction at higher pressures. The final column contains the data corrected for both buoyancy and thermomolecular flow effects. The thermomolecular flow correction is most significant at low pressures.

TABLE V

ARGON — ACID-HYDROLYZED HOLOCELLULOSE ADSORPTION DATA AT 77.5°K

Pressure, torr.	Apparent Mass Change, μg.	Buoyancy Corrected Mass, μg.	Buoyancy and Thermomolecular Flow Corrected Mass, μg.
0.042	-2.0	-1.9	35.1
0.078	-1.0	-0.8	44.8
0.151	6.0	6.3	56.9
0.318	18.0	18.6	77.0
•	•	•	•
•	•	•	•
•	•	•	•
74.749	595.0	749.3	792.3
84.442	614.0	788.3	828.5
94.937	638.0	833.9	868.9

This method for correcting the mass data can be simply represented by:

$$M_{corr} = F(M_{raw}, M_{buoy}, M_{TMF}) \tag{50}$$

or more specifically,

$$M_{corr} = M_{raw} + M_{buoy} - M_{TMF} \tag{51}$$

where

$\underline{M}_{corr}$ = corrected mass adsorption data

$\underline{M}_{raw}$ = raw mass adsorption data

$\underline{M}_{buoy}$ = buoyancy correction

$\underline{M}_{TMF}$ = thermolecular flow effect correction.

The uncertainty in the corrected mass adsorption data, $\Delta\underline{M}_{corr}$, is related to the uncertainty in the other variables, $\Delta\underline{M}_{raw}$, $\Delta\underline{M}_{buoy}$, and $\Delta\underline{M}_{TMF}$, by:

$$\Delta M_{corr} = \frac{\partial F}{\partial M_{raw}} \Delta M_{raw} + \frac{\partial F}{\partial M_{buoy}} \Delta M_{buoy} + \frac{\partial F}{\partial M_{TMF}} \Delta M_{TMF}. \quad (52)$$

Squaring Equation (52) gives:

$$[\Delta M_{corr}]^2 = \left[\frac{\partial F}{\partial M_{raw}} \Delta M_{raw}\right]^2 + \left[\frac{\partial F}{\partial M_{buoy}} \Delta M_{buoy}\right]^2 + \left[\frac{\partial F}{\partial M_{TMF}} \Delta M_{TMF}\right]^2$$

$$+ \text{ cross product terms.} \quad (53)$$

Since the variables $\underline{M}_{raw}$, $\underline{M}_{buoy}$, and $\underline{M}_{TMF}$ are independent, they are said to be "uncorrelated" and the average value of the cross product terms approaches zero. Using this approximation, Equation (53) can be rewritten in the form:

$$\sigma^2_{M_{corr}} = \left[\frac{\partial F}{\partial M_{raw}}\right]^2 \sigma^2_{M_{raw}} + \left[\frac{\partial F}{\partial M_{buoy}}\right]^2 \sigma^2_{M_{buoy}} + \left[\frac{\partial F}{\partial M_{TMF}}\right]^2 \sigma^2_{M_{TMF}} \quad (54)$$

where $\sigma_{\underline{M}_{corr}}$, $\sigma_{\underline{M}_{raw}}$, $\sigma_{\underline{M}_{buoy}}$, and $\sigma_{\underline{M}_{TMF}}$ are the standard deviations of the various terms.

Since

$$\frac{\partial F}{\partial M_{raw}} = \frac{\partial F}{\partial M_{buoy}} = \frac{\partial F}{\partial M_{TMF}} = \pm 1, \quad (55)$$

Equation (54) reduces to the simple form of Equation (56):

$$\sigma^2_{M_{corr}} = \sigma^2_{M_{raw}} + \sigma^2_{M_{buoy}} + \sigma^2_{M_{TMF}}. \quad (56)$$

Using Equation (56), the uncertainty in the corrected mass adsorption data can be calculated from the estimated uncertainty in the independent variables of Equation (51). For example, if

$$\sigma_{M_{raw}} = \sigma_{M_{buoy}} = \sigma_{M_{TMF}} = 2 \text{ μg.}, \quad (57)$$

then

$$\sigma_{M_{corr}} = 3.5 \text{ μg.} \quad (58)$$

From this discussion, it should be obvious that the precision of the adsorption data is maintained in spite of the magnitude of the corrections used, since the standard deviation of the independent variables in Equation (51) is probably between 1 and 2 μg.

PREPARATION OF ADSORBENT SAMPLES

All of the cellulose samples were prepared from the same fiber source of black spruce (Picea mariana). The holocellulose fibers were prepared from chloroform-ethanol extracted chips by a modified chlorite method (42). The preparation procedure was essentially the same as that of Thompson and Kaustinen (43) except for the higher chlorite treatment temperature of 50°C.

The alkali-extracted holocellulose sample was prepared by a repeated extraction of the holocellulose with a 4% NaOH solution at ice bath temperatures. These conditions were selected to minimize the lattice transition of Cellulose I to Cellulose II, and to maximize the solution of the hemicellulose fraction present in the holocellulose (44).

The acid-hydrolyzed holocellulose was prepared by exposing the alkali-extracted holocellulose to a mild acid hydrolysis (2.5N HCl). When a sample of cellulose is hydrolyzed by acids, the attack is initially confined to the amorphous regions. The hydrolysis residue has a greater degree of crystallinity than the original material owing to the removal of the amorphous portion. A leveling-off of the degree of polymerization is observed as the hydrolysis slows down after removal of the amorphous material leaving only the more resistant crystalline cellulose material. Thus, the desired adsorbent sample was prepared by a controlled acid hydrolysis using the procedures developed by Battista (45, 46).

The adsorbent sample preparation procedures are described in greater detail in Appendix V on pages 230-231.

CHARACTERIZATION OF ADSORBENTS

ELECTRONMICROGRAPHS

Electronmicrographs of the adsorbent samples were prepared in order to observe their size, shape, and surface topography. Some of the same freeze-dried fibers used as gas adsorption samples were placed on aluminum specimen stubs which had been covered with an adhesive transfer tape. The fibers were then coated while rotating in a vacuum evaporator with about 100 A. of carbon followed by about 200 A. of a 60:40 gold:palladium coating. The fibers were then viewed in a Joel JSM-U3 scanning electron microscope equipped with a TV scan at an accelerating voltage of 10 to 25 kv. Selected images were recorded on a Polaroid camera using a P/N-55 type film.

CARBOHYDRATE ANALYSIS

A carbohydrate analysis was done on each of the adsorbent samples to determine the effect of the preparation methods on the sample chemical composition. The analysis of the monosaccharides present in the adsorbent samples was done by a gas chromatographic method (47). The monosaccharides present in the acid-hydrolyzed adsorbent samples were reduced to alditols with sodium borohydride. Following acetylation with acetic anhydride and sulfuric acid, the acetylated mixture was precipitated in ice water and extracted with methylene chloride for injection into the gas chromatograph. Using myo-inositol as an internal standard, the percentage compositions were calculated from the peak area measurements.

CUPRIETHYLENEDIAMINE VISCOSITY OF CELLULOSE SAMPLES

The relative degree of polymerization of the three adsorbent samples was assessed by determining the cupriethylenediamine disperse viscosity using a modified TAPPI T 230 su-66 method (48). The viscosity determination method was modified so that solution was accomplished by shaking in an atmosphere of nitrogen.

DETERMINATION OF THE STATE OF ORDER IN THE CELLULOSE ADSORBENTS BY AN X-RAY DIFFRACTOMETRIC PROCEDURE

The x-ray diffraction work was done to determine the relative crystallinity of the three cellulose adsorbents and to confirm that the Cellulose I crystal structure was retained by the alkali-extracted holocellulose and acid-hydrolyzed holocellulose samples.

The x-ray diffractograms were obtained for the three samples using the procedure outlined below. The cellulose samples were dried in a vacuum oven at 50°C., and then passed through a small Wiley mill fitted with a 40-mesh screen. A 0.500-g. portion was placed in a 1-in. diameter pellet mold, leveled, and pressed at 6000-lb. pressure for 15 sec. The resulting disk was pressed into a 1-in. diameter hole in the center of a brass mounting plate so that the surface of the disk was flush with the surface of the plate. The plate served to hold and align the sample in the goniometer of the x-ray diffraction apparatus.

The x-ray equipment used was a Norelco x-ray diffraction unit operating with parafocusing geometry. K_α radiation was obtained from a copper target and nickel filter at 35 kv. and 20 ma. The collimating beam was defined by a divergence slit of 0.5° angular aperture at the x-ray port. The diffracted beam was defined by a 0.006-in. receiving slit and by a 0.5° angular aperture scatter slit. The signal of the diffracted beam was received by a Geiger counter tube and recorded by a Brown recording potentiometer.

Diffraction pellets to be tested were placed in the holder and mounted in the goniometer. The diffraction intensity was measured from 2θ angles of 8° to 30°. In order to eliminate possible errors due to misalignment of the pellet in the holder, the pellet was removed, rotated 90°, and then retested.

PREPARATION OF ADSORBATES

The argon and nitrogen gases were a prepurified grade (99.997% and 99.998% minimum purity, respectively) obtained from Matheson Gas Products. The argon and nitrogen were used directly from the supplied cylinders.

The $CFCl_3$ was also obtained from Matheson (99.9% minimum purity). A gas chromatographic analysis indicated no detectable impurities. After placing the liquid $CFCl_3$ in an adsorbate flask attached to the small manifold, the $CFCl_3$ was degassed repeatedly by freezing in liquid nitrogen, evacuating, and allowing to thaw. Finally, the $CFCl_3$ was distilled *in vacuo* into another storage flask.

CHARACTERIZATION OF ADSORBATES

ADSORBATE CHARACTERISTIC PARAMETERS

A list of the characteristic parameters of the three adsorbate gases is presented in Table VI.

INFRARED INVESTIGATION OF $CFCl_3$ HYDROGEN BONDING PROPERTIES

A ternary solution containing ethanol (donor compound), $CFCl_3$ (acceptor compound), and carbon tetrachloride (solvent) was used to evaluate the hydrogen bonding properties of the $CFCl_3$. Five solutions as listed in Table VII were prepared containing 0.005M ethanol with $CFCl_3$ and carbon tetrachloride.

The infrared spectra were determined for the five solutions using a 1-cm. path cell in the vicinity of the free hydroxyl peak at 3640 $cm.^{-1}$

TABLE VI

ADSORBATE CHARACTERISTIC PARAMETERS[a]

Adsorbate	Molecular Diameter, A.	Ideal Two-Dimensional Van der Waals Constants		Principal Polarizabilities			Dipole Moment Debye	Comments
		α^{Id}, $\times 10^{30}$ ergs cm.^{2} / molecule^2	β^{Id}, A.^{2} / molecule	ξ_1	ξ_2	ξ_3		
				$\times 10^{24}$ cm.^{3}				
Argon	2.95	47.4	13.6	1.63	1.63	1.63	--	Sphere
Nitrogen	3.15	45.7	15.5	2.38	1.45	1.45	--	ξ_1 Symmetry axis
$CFCl_3$	6.30	343.0	31.2	7.60	8.57	8.57	0.45	ξ_1 Symmetry axis

[a]All data obtained from Reference (10) except for the $CFCl_3$ polarizabilities which were obtained from Reference (49).

TABLE VII

SOLUTION COMPOSITIONS

Solution Number	Ethanol Concentration, M	$CFCl_3$ Mole Fraction	CCl_4 Mole Fraction
1	0.005	0.00	1.00
2	0.005	0.05	0.95
3	0.005	0.10	0.90
4	0.005	0.20	0.80
5	0.005	1.00	0.00

DISCUSSION OF EXPERIMENTAL RESULTS

ADSORBENT SAMPLE CHARACTERIZATION

ELECTRONMICROGRAPHS

The size, shape, and surface topography of the three fibrous cellulose adsorbent samples are clearly illustrated in the electronmicrographs in Fig. 21-23. The holocellulose adsorbent shown in Fig. 21 is apparently composed of undamaged and unbonded tracheids. The surface topology is generally smooth except for shrinkage effects due to the drying operation. The alkali-extracted holocellulose adsorbent shown in Fig. 22 is very similar in physical appearance to the holocellulose. The only difference appears to be a slightly rougher surface. This rougher surface of the alkali-extracted holocellulose is probably due to greater shrinkage during drying of the alkali-swollen fibers. The acid-hydrolyzed holocellulose adsorbent shown in Fig. 23 is drastically different in physical appearance from the other two samples. The acid hydrolysis treatment had begun to destroy the fibrous nature of the sample. In addition, the surface of the fibers is much rougher, showing the effects of the hydrolysis.

In general, the electronmicrographs indicate that the acid-hydrolyzed holocellulose has the smallest fiber fragments and the most heterogeneous topography. The holocellulose and the alkali-extracted holocellulose have very similar physical appearance. If the electronmicrographs are used to rank the expected specific surface areas of the samples, the acid-hydrolyzed holocellulose would have the highest surface area. The alkali-extracted holocellulose would have a higher surface area than the untreated holocellulose due to the slightly rougher surface.

1300X Magnification
15 kv. Accelerating Voltage

600X Magnification
20 kv. Accelerating Voltage

600X Magnification
20 kv. Accelerating Voltage

120X Magnification
10 kv. Accelerating Voltage

Figure 21. Electronmicrographs of the Freeze-Dried Holocellulose Adsorbent

2200X Magnification
10 kv. Accelerating Voltage

1800X Magnification
10 kv. Accelerating Voltage

900X Magnification
10 kv. Accelerating Voltage

120X Magnification
10 kv. Accelerating Voltage

Figure 22. Electronmicrographs of the Freeze-Dried Alkali-Extracted Holocellulose Adsorbent

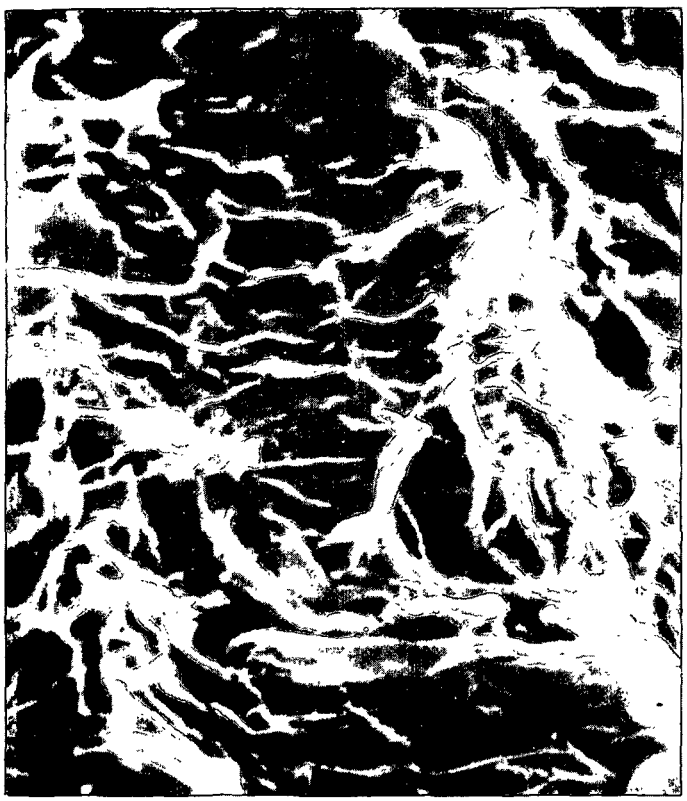

5000X Magnification
25 kv. Accelerating Voltage

2200X Magnification
25 kv. Accelerating Voltage

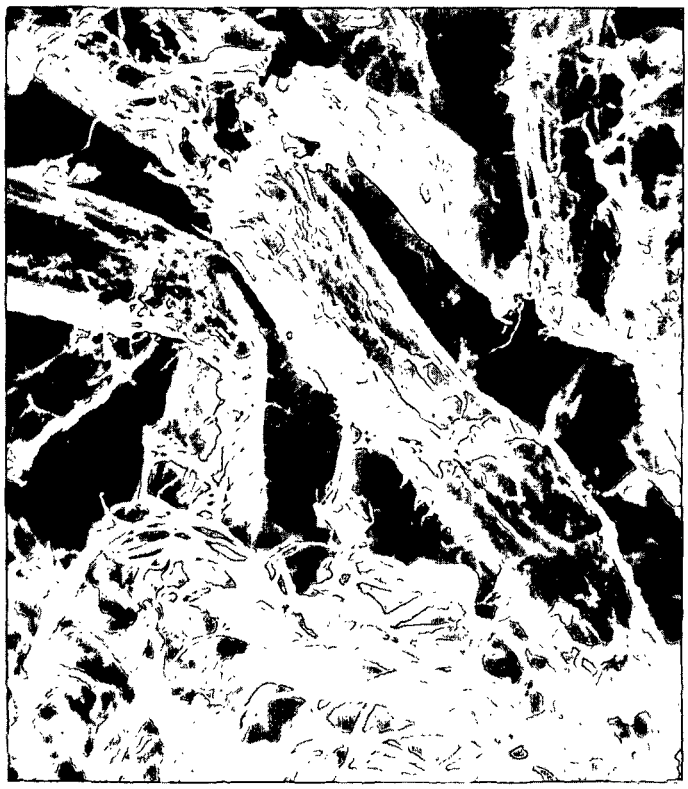

600X Magnification
10 kv. Accelerating Voltage

120X Magnification
10 kv. Accelerating Voltage

Figure 23. Electronmicrographs of the Freeze-Dried Acid-Hydrolyzed Holocellulose Adsorbent

CARBOHYDRATE ANALYSIS AND CUPRIETHYLENEDIAMINE VISCOSITY OF THE ADSORBENTS

In Table VIII the carbohydrate analysis data and the cupriethylenediamine solution viscosity data for the three adsorbent samples are presented. The predominant hemicellulose species removed from the holocellulose was the xylan fraction, leaving the more-difficult-to-remove glucomannan fractions in the alkali-extracted holocellulose. The increase in the viscosity of the alkali-extracted holocellulose, over the untreated holocellulose, was probably due to the removal of the low-molecular-weight hemicellulose fractions. The mild acid hydrolysis of the alkali-extracted holocellulose caused a significantly decreased average molecular weight of the acid-hydrolyzed holocellulose. A substantial fraction of the glucomannan hemicellulose component was retained even in the acid-hydrolyzed holocellulose sample.

TABLE VIII

CARBOHYDRATE ANALYSIS AND CUPRIETHYLENEDIAMINE VISCOSITY

	Adsorbent Sample Composition, %		
Monosaccharide	Holocellulose	Alkali-Extracted Holocellulose	Acid-Hydrolyzed Holocellulose
Araban	0.6	0.2	--
Xylan	5.8	1.3	0.5
Mannan	18.0	16.5	9.5
Galactan	1.8	1.4	0.7
Glucan	70.2	80.0	85.7

	Cupriethylenediamine Viscosity, centipoises		
Sample	Test 1	Test 2	Average
Holocellulose	36.32	35.61	35.96
Alkali-extracted holocellulose	43.70	44.19	43.96
Acid-hydrolyzed holocellulose	8.51	8.68	8.60

THE STATE OF ORDER IN THE CELLULOSE ADSORBENTS AS DETERMINED BY AN X-RAY DIFFRACTOMETRIC PROCEDURE

The x-ray diffraction work was done to determine the relative crystallinity of the three adsorbent samples and to confirm that the Cellulose I crystal structure was retained by the alkali-extracted holocellulose and acid-hydrolyzed holocellulose samples.

The x-ray powder method was used to obtain the diffraction data. In the Cellulose I structure, the strongest reflections are those corresponding to the (101), ($10\bar{1}$), and (002) lattice planes. The corresponding 2θ reflection angles for these planes are listed in Table IX. The x-ray diffractograms produced by the three adsorbents are presented in Fig. 24.

TABLE IX

EQUATORIAL REFLECTIONS OF CELLULOSE I

Lattice Plane	2θ Reflection Angle, degrees
101	14.6
$10\bar{1}$	16.2
002	22.6

The crystalline fraction of a partially ordered material is considered to produce the sharp diffraction patterns, whereas the amorphous fraction produces only a diffuse background. However, the contributions of the crystalline and amorphous fractions to the observed intensities in the diffractogram have not been clearly established. Several methods have been proposed to estimate the proportions of the crystalline and amorphous regions.

Segal, et al. (50) scanned the diffraction intensities from the Bragg angles of 12° to 24° to include the main diffraction maxima of the cellulose lattice

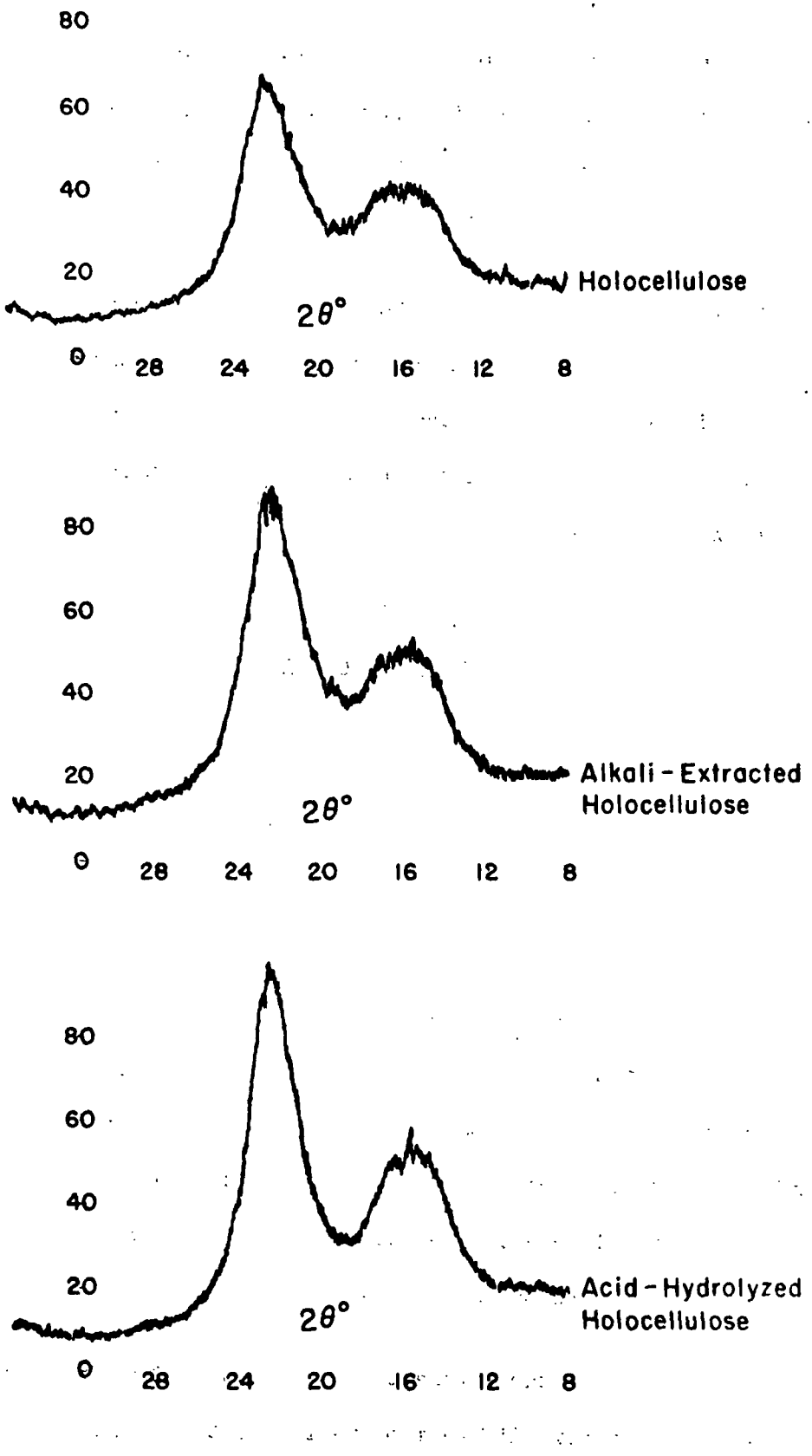

Figure 24. X-ray Diffractograms for the Cellulose I Adsorbent Samples

structure corresponding to the (101), (10$\bar{1}$), and (002) planes. They defined a percentage crystallinity index, CrI, by:

$$CrI = 100[(I_{002} - I_{am})/(I_{002})] \qquad (59)$$

where I_{002} is the intensity of the diffraction from the (002) plane at $2\theta = 22.6°$ and I_{am} is the intensity of the background scatter measured at $2\theta = 18°$. Using the Segal method, the relative crystallinity of the three cellulose adsorbents is summarized in Table X.

TABLE X

SEGAL CRYSTALLINITY DATA

Sample	I_{002} Trial 1	I_{002} Trial 2	I_{am} Trial 1	I_{am} Trial 2	CrI Trial 1	CrI Trial 2	Average CrI
Acid-hydrolyzed holocellulose	92.5	95.5	31.0	30.5	67.2	68.1	67.6
Alkali-extracted holocellulose	87.0	85.0	37.0	38.0	57.5	55.3	56.4
Holocellulose	67.0	70.5	29.5	32.5	55.9	53.9	54.9

Ant-Wuorinen and Visapää (51) proposed that x-ray methods do not determine the state of crystallinity or the percentage of crystalline cellulose in a sample, but only a general state of order. They define a quantity called the "index of order," IO. The index of order was calculated as follows: (1) The maximum height of the pattern between 22° and 23° 2θ was determined in arbitrary units and designated Th (total height). (2) The minimum height of the pattern between 18° and 19° 2θ was determined in the same arbitrary units and designated Ih (inordered height). (3) The ordered height, Oh, equals Th minus Ih, and

$$IO = \left[1 - \frac{Ih}{Oh}\right]100 = \left[1 - \frac{Ih}{(Th - Ih)}\right]100. \qquad (60)$$

The Ant-Wuorinen and Visapää calculated index-of-order values are presented in Table XI.

TABLE XI

ANT-WUORINEN AND VISAPÄÄ INDEX OF ORDER

Sample	Th		Ih		IO		Average IO
	Trial 1	Trial 2	Trial 1	Trial 2	Trial 1	Trial 2	
Acid-hydrolyzed holocellulose	94.5	95.5	31.0	30.5	51.2	53.1	52.2
Alkali-extracted holocellulose	87.0	85.0	37.0	38.0	26.0	19.3	22.6
Holocellulose	67.0	70.5	29.5	32.5	21.4	14.5	17.9

Both methods of calculating the relative crystallinity of the adsorbent samples ranked the samples in the same order. The acid-hydrolyzed holocellulose had the highest degree of order, and the holocellulose had the lowest degree of order. The diffractograms also confirmed that all of the adsorbents had a Cellulose I crystal structure.

ADSORPTION ISOTHERMS

The experimental adsorption data for argon, nitrogen, and $CFCl_3$ on each of the three adsorbents are presented in Fig. 25-30. Adsorption isotherms were determined for two temperatures, 77.5 and 90.1°K, for the argon while only one temperature, 77.5°K, was used for the nitrogen. Five isotherm temperatures ranging from 258.15 to 298.15°K were used for the $CFCl_3$ adsorption data. Five different isotherm temperatures for the $CFCl_3$ adsorbate were used because of the original intent in this thesis to use the Ross and Olivier adsorption model to analyze the adsorption data. A minimum of three different isotherm temperatures is required for a unique solution using the Ross and Olivier approach for polyatomic adsorbates.

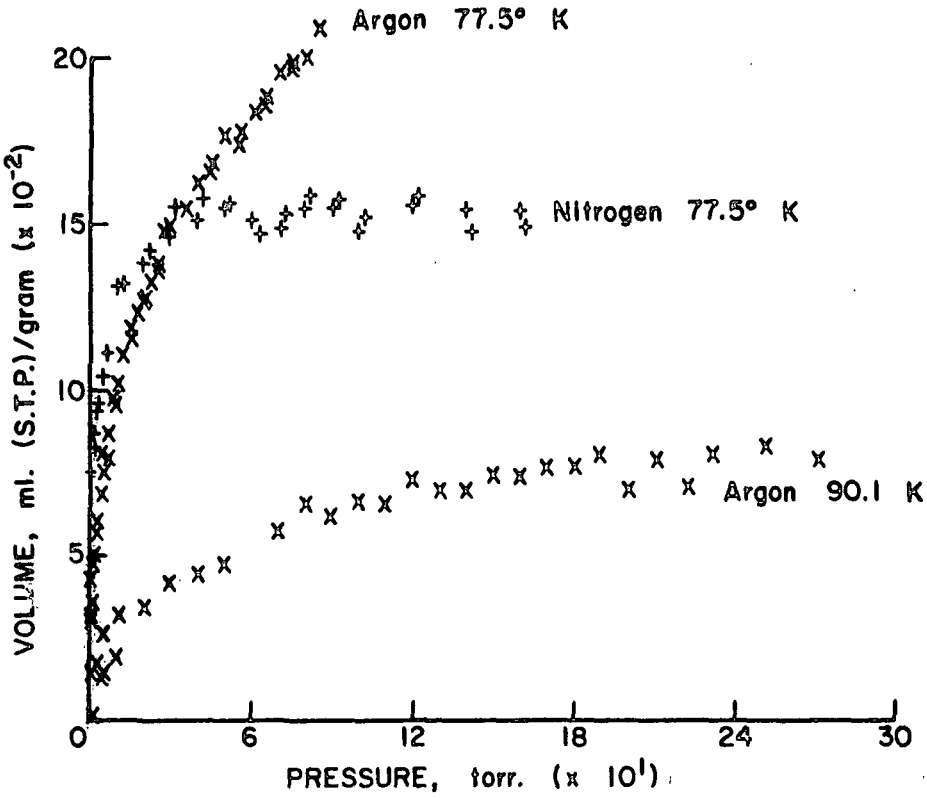

Figure 25. Argon and Nitrogen Adsorption on the Holocellulose Adsorbent

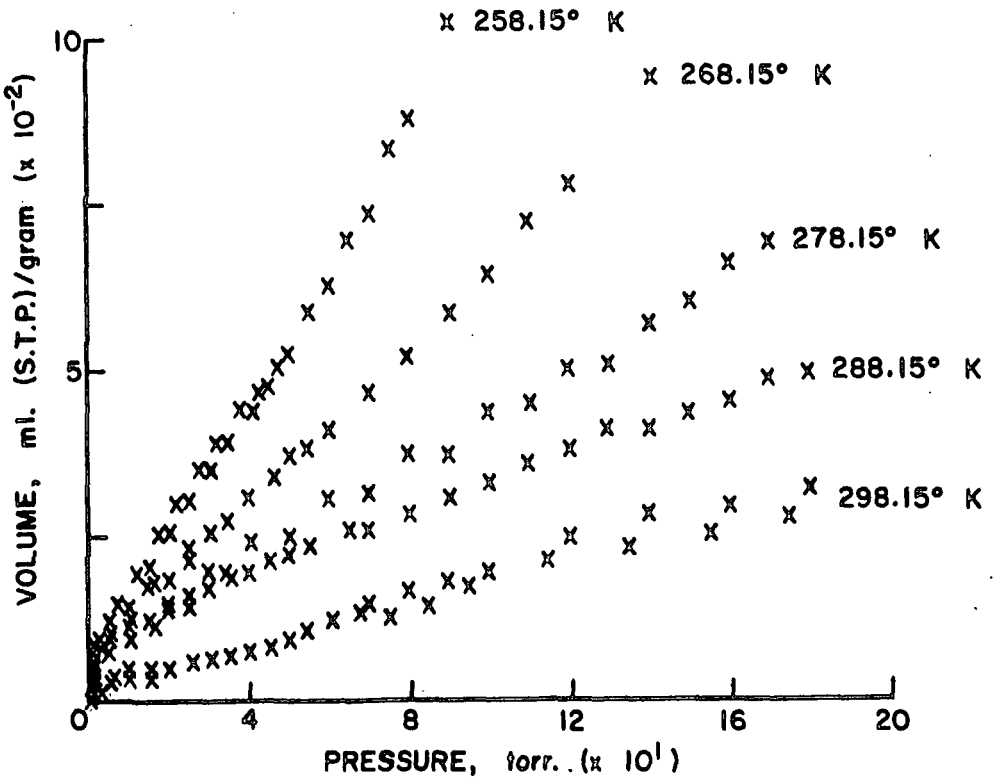

Figure 26. $CFCl_3$ Adsorption on the Holocellulose Adsorbent

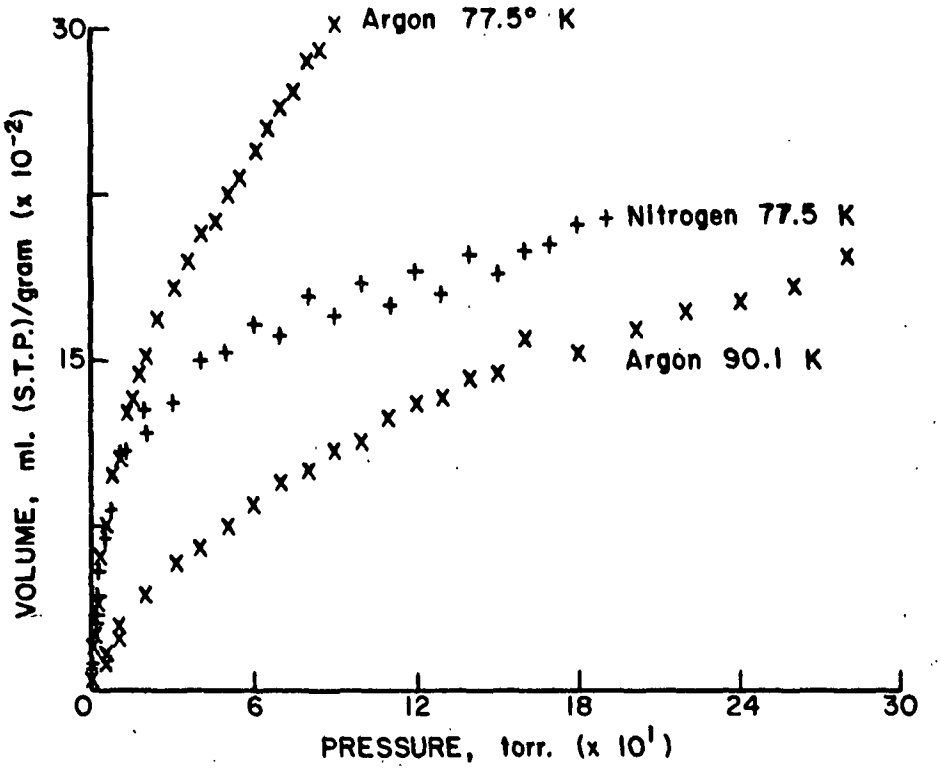

Figure 27. Argon and Nitrogen Adsorption on the Alkali-Extracted Holocellulose Adsorbent

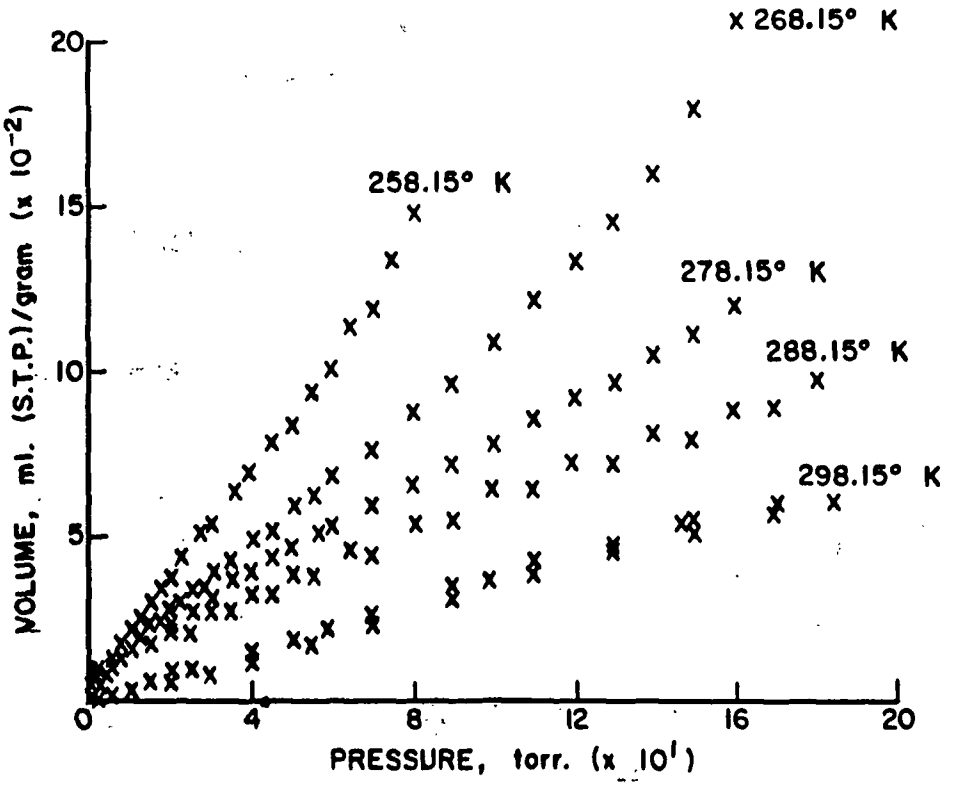

Figure 28. $CFCl_3$ Adsorption on the Alkali-Extracted Holocellulose Adsorbent

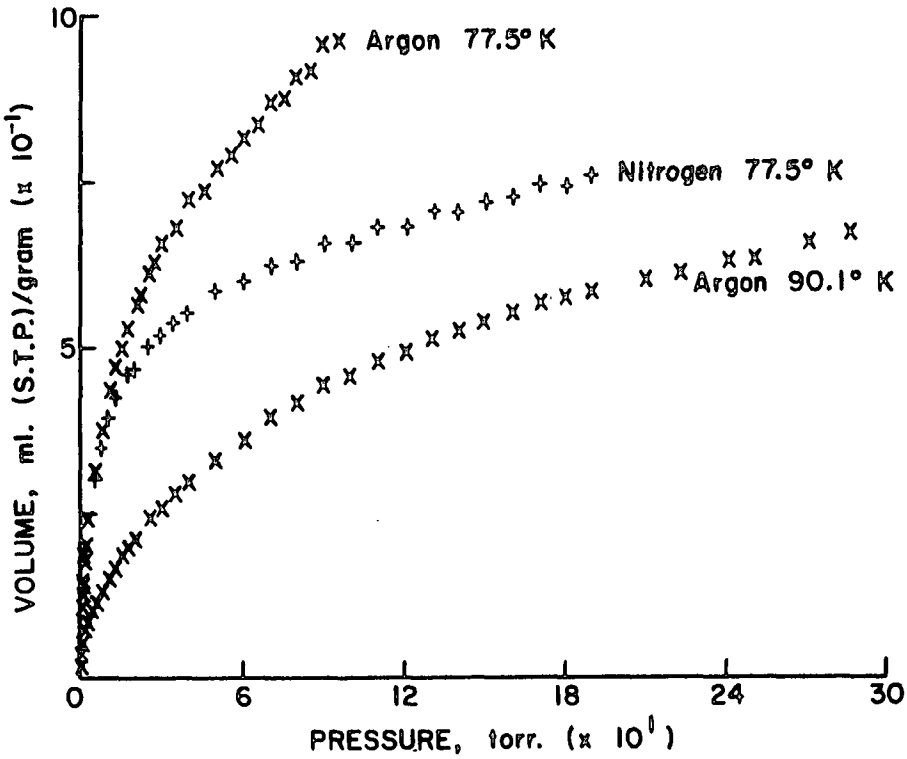

Figure 29. Argon and Nitrogen Adsorption on the Acid-Hydrolyzed Holocellulose Adsorbent

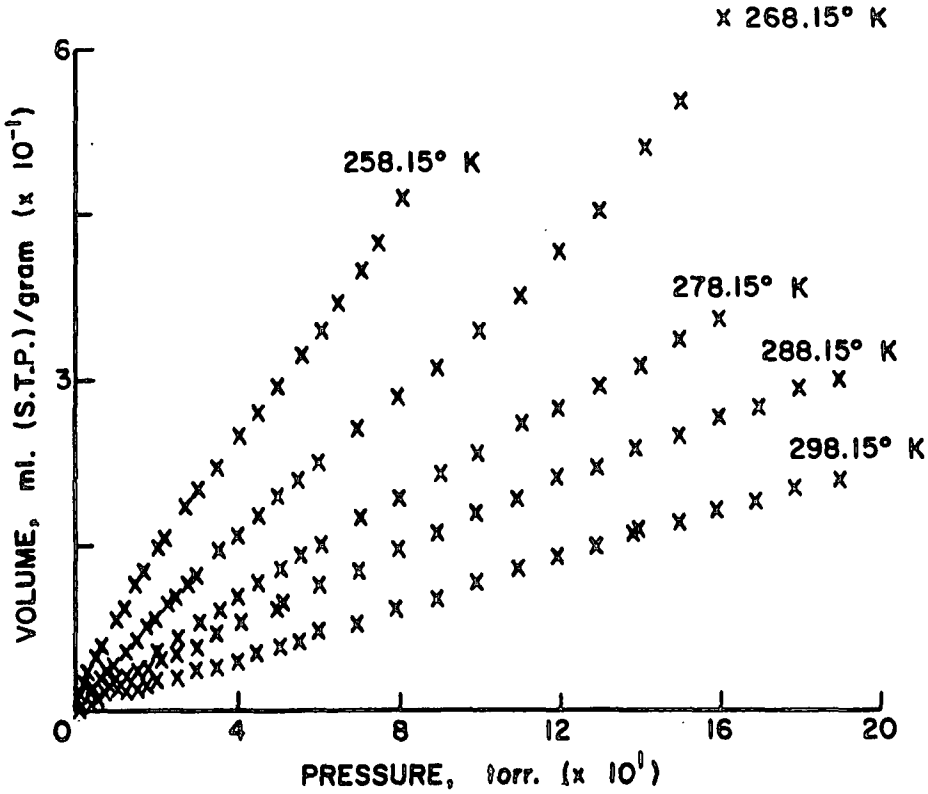

Figure 30. $CFCl_3$ Adsorption on the Acid-Hydrolyzed Holocellulose Adsorbent

The experimental data are reported as milliliters (STP) adsorbed gas per gram of adsorbate, as a function of the equilibrium pressure in torr. No measurements obtained above a relative pressure of 0.40 for the adsorbate gas were used in fitting the adsorption model, to avoid the possibility of capillary condensation contributing to the amount adsorbed.

The argon and nitrogen isotherms appeared to be Type II isotherms as classified by Brunauer, et al. (8), and the $CFCl_3$ isotherms appear to be the more unusual Type III isotherms.

BET THEORY ANALYSIS OF EXPERIMENTAL ADSORPTION DATA

Using the experimental adsorption data in the relative pressure range of 0.05 to 0.30, the monolayer volume, V_m, and the c parameter were obtained by a linear regression of $p/(V(p_o - p))$ versus p/p_o. The specific surface area, Σ_{BET}, in $m.^2/g.$ was then obtained using the relationship

$$\Sigma_{BET} = 0.269\ V_m\ \sigma_o. \tag{61}$$

The values of the molecular cross-sectional area, σ_o, used in calculating the BET specific surface area are listed below:

Argon	14.6 $A.^2$ at 77.5°K
	15.5 $A.^2$ at 90.1°K
Nitrogen	16.2 $A.^2$ at 77.5°K
$CFCl_3$	31.2 $A.^2$ at all isotherm temperatures.

For argon and nitrogen, the adsorbate was assumed to be a liquidlike, closely packed phase, so that σ_o was based on the liquid density following the suggestion of Emmett and Brunauer (52). The $CFCl_3$ molecular cross-sectional area was the two-dimensional Van der Waals constant, β.

Comparing the BET surface areas of the three adsorbates (see Table XII), the relative surface areas are reasonable considering the apparent particle size and surface roughness of the adsorbents in the electronmicrographs. Using the $\underline{c}$ parameter values and the relationship $\underline{c} \cong \exp[(\underline{Q}_1 - \underline{Q}_{\underline{L}})/\underline{RT}]$, the adsorbents can be ranked in terms of the heat of adsorption in the first adsorbate layer, $\underline{Q}_1$. For both the $CFCl_3$ and argon, the holocellulose has the highest $\underline{Q}_1$ value, followed by the acid-hydrolyzed holocellulose and the alkali-extracted holocellulose. The low $\underline{c}$ values for the polar $CFCl_3$ gas indicate that the adsorptive forces are not much greater in magnitude than the forces of interaction among the adsorbate molecules (i.e., $\underline{Q}_1 \cong \underline{Q}_{\underline{L}}$). The apparently weak interaction of the $CFCl_3$ gas with the three cellulosic adsorbents implies that the cellulose adsorbents are relatively nonpolar so that only dispersion-type adsorptive forces are functioning.

ANALYSIS OF THE ADSORPTION DATA USING THE MULTILAYER ADSORPTION MODEL

THE ARGON-CELLULOSE ADSORPTION SYSTEM

Evaluation of the $\underline{\mathring{A}}$ Parameter

Before the nonlinear curve-fitting procedures can be used to fit the multilayer adsorption model to the experimental argon adsorption data, an appropriate relationship must be developed to define $\underline{\mathring{A}}$ for the adsorption system. Inherent in the definition of $\underline{\mathring{A}}$ is a thermodynamic description of the adsorption system.

For a mobile, physically adsorbed film, $\underline{\mathring{A}}$ in its most general form is given by the relationship:

$$\ln \mathring{A} = - \frac{\Delta S_s^{tr}}{R} - \frac{\Delta S^{rot}}{R} + \frac{a^F{}^{vib} - a^E{}_o^{vib}}{RT} + \frac{\Delta E^{kin}}{RT} - \ln \frac{\theta_s}{1 - \theta_s} + \ln 760. \qquad (62)$$

The various terms in the above relationship are used as defined on page 21. To evaluate the thermodynamic functions in Equation (62), one must consider the degrees

TABLE XII

SUMMARY OF BET THEORY ANALYSIS RESULTS

Sample	Adsorbate Gas	Isotherm Temperature, °K	BET Surface Area, $m.^2/g.$	c Parameter
Acid-hydrolyzed holocellulose	argon	77.5	2.48 ± 0.02	38.9
"	argon	90.1	2.20 ± 0.01	
"	nitrogen	77.5	2.54 ± 0.01	
"	$CFCl_3$	258.15	2.39 ± 0.05	5.1
"	$CFCl_3$	268.15	2.70 ± 0.07	
"	$CFCl_3$	278.15	2.85 ± 0.07	
"	$CFCl_3$	288.15	2.65 ± 0.04	
"	$CFCl_3$	298.15	2.92 ± 0.05	
Alkali-extracted holocellulose	argon	77.5	0.76 ± 0.01	23.6
"	argon	90.1	0.68 ± 0.01	
"	nitrogen	77.5	0.71 ± 0.01	
"	$CFCl_3$	258.15	0.71 ± 0.04	4.3
"	$CFCl_3$	268.15	0.62 ± 0.02	
"	$CFCl_3$	278.15	0.69 ± 0.01	
"	$CFCl_3$	288.15	0.71 ± 0.03	
"	$CFCl_3$	298.15	0.90 ± 0.05	
Holocellulose	argon	77.5	0.55 ± 0.01	46.8
"	argon	90.1	0.25 ± 0.01	
"	nitrogen	77.5	0.50 ± 0.01	
"	$CFCl_3$	258.15	0.42 ± 0.04	5.7
"	$CFCl_3$	268.15	0.34 ± 0.03	
"	$CFCl_3$	278.15	0.35 ± 0.05	
"	$CFCl_3$	288.15	0.31 ± 0.01	
"	$CFCl_3$	298.15	0.40 ± 0.04	

of freedom of the argon atom in the gaseous and adsorbed states. The three translational degrees of freedom of the argon atom in the gas phase become two translational degrees parallel to the surface and one vibrational degree normal to the surface on physical adsorption. The spherical argon atom has no rotational degrees of freedom. The vibration terms in Equation (62) do not refer to internal vibrations of an adsorbed species which are not expected to be greatly affected by adsorption; they refer to the appearance of a new vibration of the adsorbed species as a whole with respect to the substrate. Recent investigations of the laser Raman spectra of adsorbed species (53) indicated no significant changes in the internal vibrations of a molecule upon physical adsorption.

The integral translational entropy change, ΔS_s^{tr}, per mole of gas from its standard state (760 torr., temperature = T) to a mobile adsorbed film in its standard state (θ_s, T) is calculated using a relationship (10) derived from the Sackur-Tetrode Equation (54) as shown below:

$$\Delta S_s^{tr} = -\frac{R}{2} \ln M + \frac{R}{2} \ln T + 2.30 \qquad (63)$$

where

R = gas constant, 1.9872 cal./mole °K

M = molecular weight of the adsorbate

T = absolute temperature.

Since the argon atom has no rotational degrees of freedom, the change in rotational entropy upon adsorption, ΔS^{rot}, is obviously zero.

The vibration of the adsorbed argon with respect to the surface contributes to the thermodynamic functions describing the adsorbate film. If one assumes the vibration to be that of a harmonic oscillator with one degree of freedom for which the frequency does not change with temperature, the vibrational term in Equation (62) equals:

$$ {}_{a}F^{vib} - {}_{a}E_{o}^{vib} = RT \ln(1 - \exp[-h\nu/kT]) \qquad (64) $$

where

${}_{a}F^{vib}$ = Gibbs free energy of the adsorbed phase due to molecular vibrations with respect to the surface

${}_{a}E_{o}^{vib}$ = average vibrational energy of the adsorbed species at 0°K

ν = vibration frequency of the adsorbed species

h = Planck's constant

k = Boltzmann's constant.

As a result of the loss of one degree of translational freedom for argon upon adsorption, the change in kinetic energy, ΔE^{kin}, is equal to $-{}^{1}/_{2}\,RT$.

The standard state of the gas is taken as 760 torr. at the temperature of the experiment. The standard state of the surface phase follows the convention selected by deBoer and Kruyer (55) so that at 0°C. the average distance between the adsorbed species in the two-dimensional state is the same as in the three-dimensional standard state (0°C., 760 torr.). This definition corresponds to a standard coverage defined as:

$$ \theta_s = \beta/(4.08T) \qquad (65) $$

where

θ_s = standard state coverage

β = two-dimensional Van der Waals constant corresponding to b.

Using the relationships outlined above, a subroutine ARGN in Appendix II was written for the nonlinear curve-fitting program which evaluates $\mathring{A}$ as a function of the unknown vibrational frequency for the argon adsorbate.

Results of Nonlinear Regression Analysis for the Argon Adsorption Data

An example of the experimental argon adsorption data and the fitted model multilayer isotherm resulting from the nonlinear regression analysis are shown

in Fig. 31. The adsorptive potential distribution function generated by the nonlinear curve-fitting procedure for the example isotherm is presented in Fig. 32, where the distribution frequency is plotted as a function of the adsorptive potential. The shape of this distribution function is determined by the two parameters $\underline{U}^{Median}$ and γ, determined in the regression analysis. The model parameter values and the thermodynamic data associated with the argon acid-hydrolyzed holocellulose data set are listed in Table XIII. The confidence intervals for the four unknown parameters evaluated in the nonlinear regression analysis are also listed in Table XIII. A similar set of figures and a table are in Appendix VI for each argon adsorption isotherm used for evaluation by the multilayer adsorption model.

A summary of the results from fitting the multilayer adsorption model to the argon adsorption data for the three sample adsorbents at the two isotherm temperatures is listed in Table XIV. Reviewing the results for the 77.5°K isotherms, the holocellulose and acid-hydrolyzed holocellulose have similar adsorptive potential distributions while the alkali-extracted holocellulose has a lower and more uniform (i.e., higher γ) adsorptive potential distribution. The specific surface areas, Σ_β, are ranked in the same order as the electronmicrographs suggest. The vibrational frequency, ν, of the argon adsorbate is of the same order of magnitude as theoretically predicted values (see p. 8 of text).

Precision of the Parameter Estimates

After inspecting the results for the 90.1°K isotherms, the immediate question that arises is: Why are the confidence intervals so much wider for the parameters derived from the 90.1°K isotherm data than for the 77.5°K isotherm data? Checking the plots of the fitted multilayer model isotherms for the 90.1°K argon experimental data in Appendix VI, one must conclude that the wider confidence limits cannot be explained in terms of additional data scatter at 90.1°K.

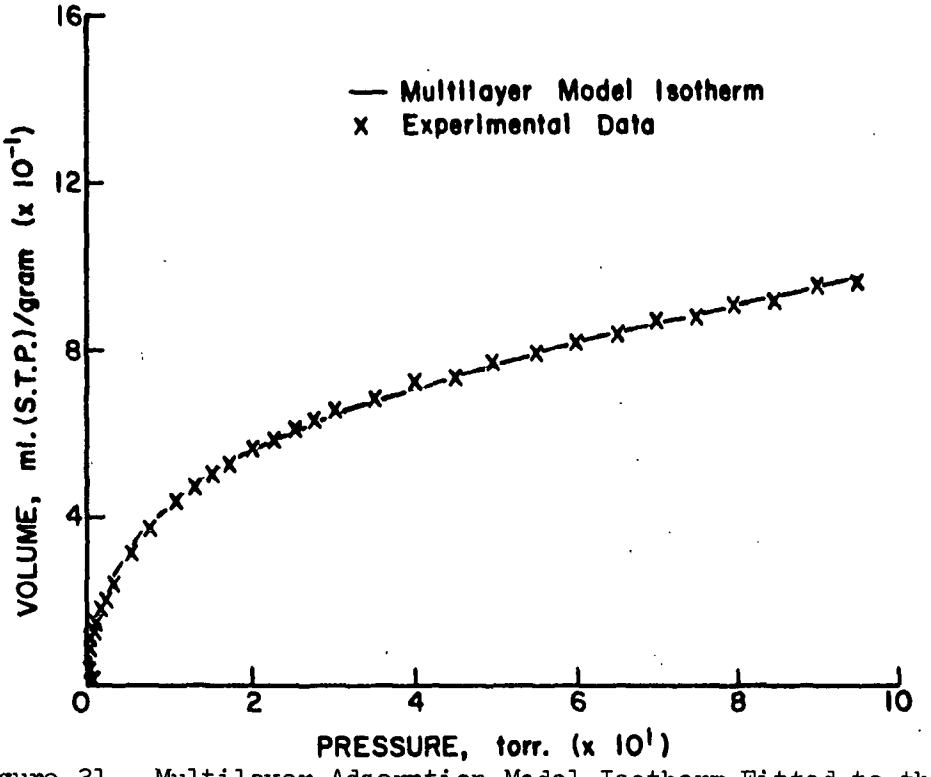

Figure 31. Multilayer Adsorption Model Isotherm Fitted to the Argon Acid-Hydrolyzed Holocellulose Adsorption Data at 77.5°K

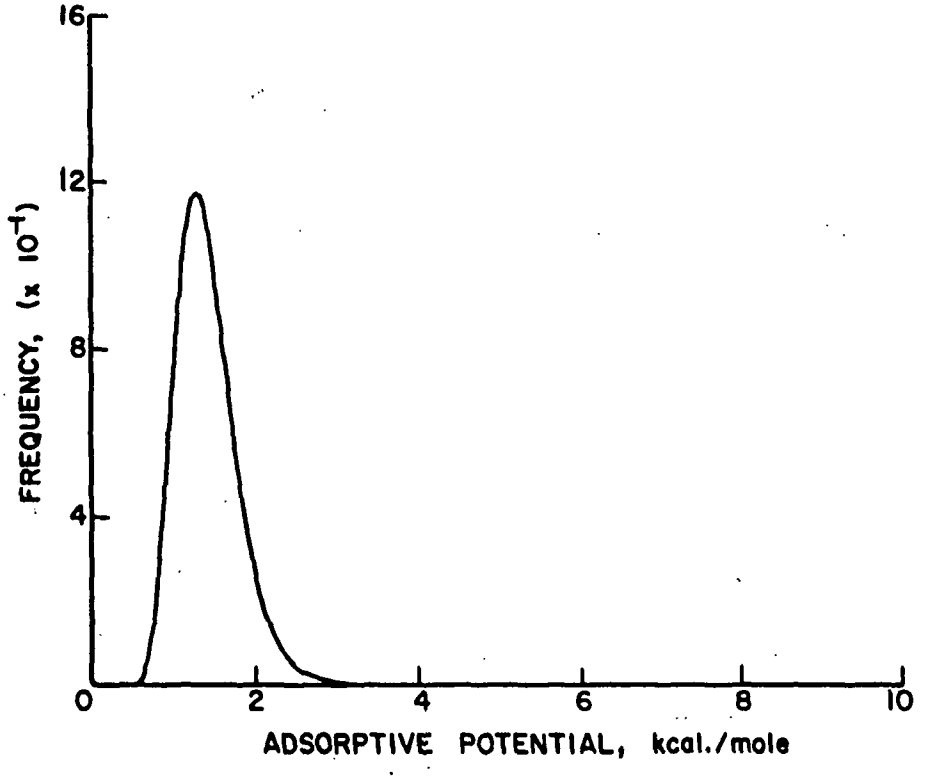

Figure 32. Adsorptive Potential Distribution for the Argon Acid-Hydrolyzed Holocellulose Adsorption Data at 77.5°K

TABLE XIII

RESULTS OF FITTING MULTILAYER ADSORPTION MODEL TO EXPERIMENTAL DATA

Adsorbent: Acid-hydrolyzed holocellulose
Adsorbate: Argon
Temperature: 77.5°K

Model Parameters

$\underline{U}^{Median} = 1.36 \pm 0.02^{a}$ kcal. mole^{-1}

$\underline{U}^{Mean} = 1.40$ kcal. mole^{-1}

$\underline{U}^{Mode} = 1.27$ kcal. mole^{-1}

$\gamma = 7.4 \pm 0.8$

$\underline{V}_{\beta} = 1.39 \pm 0.07$ ml. (STP) g.$^{-1}$

$\nu = 2.26 \pm 0.58 \times 10^{12}$ sec.$^{-1}$

$2\alpha/\beta$ (Ideal) $= 1.002$ kcal. mole^{-1}

$\alpha = 47.4 \times 10^{-30}$ erg cm.^{2} molecule^{-2}

$\beta = 13.6$ A.^{2} molecule^{-1}

Thermodynamic Data

$\Delta\underline{S}_{s}^{tr} = -0.0103$ kcal. mole^{-1} deg.$^{-1}$

$\Delta\underline{S}^{rot} = 0.0$ kcal. mole^{-1} deg.$^{-1}$

$\Delta\underline{S}^{vib} = 0.0015$ kcal. mole^{-1} deg.$^{-1}$

$\Delta\underline{E}^{kin} = -0.0770$ kcal. mole^{-1}

$\underline{A}^{o} = 0.13691 \times 10^{7}$

[a] Approximate 95% linear confidence limits.

TABLE XIV

RESULTS OF FITTING MULTILAYER ADSORPTION MODEL TO ARGON ADSORPTION DATA

	Holocellulose		Alkali-Extracted Holocellulose		Acid-Hydrolyzed Holocellulose	
Isotherm temperature, °K	77.5	90.1	77.5	90.1	77.5	90.1
$\underline{U}^{Median}$, kcal. mole^{-1}	1.36±0.06[a]	1.44±0.42	1.29±0.02	1.29±0.37	1.36±0.02	1.30±0.10
$\underline{U}^{Mean}$, kcal. mole^{-1}	1.43	1.50	1.31	1.32	1.40	1.36
$\underline{U}^{Mode}$, kcal. mole^{-1}	1.25	1.32	1.23	1.23	1.27	1.19
γ	5.5±1.3	5.8±10.4	12.1±2.3	10.4±4.1	7.4±0.8	5.5±2.1
$\underline{V}_\beta$, ml. (STP) g.	0.31±0.04	0.14±0.25	0.35±0.04	0.38±0.38	1.39±0.07	1.30±0.74
Σ_β, m.^{2} g.$^{-1}$[b]	1.13±0.15	0.51±0.91	1.28±0.15	1.39±1.39	5.09±0.26	4.76±2.71
$\nu \times 10^{12}$, sec.$^{-1}$	2.19±1.04	2.19±17.3	0.74±0.16	2.16±15.8	2.26±0.58	2.26±5.48
$\underset{\sim}{S}(\underset{\sim}{\varphi})$[c]	0.0005	0.00008	0.0002	0.0002	0.0025	0.0054
$\lvert \underset{\sim}{J}^T \underset{\sim}{J} \rvert$[d]	0.90×10^{-8}	0.36×10^{-12}	0.13×10^{-6}	0.65×10^{-12}	0.45×10^{-4}	0.64×10^{-7}

[a] Approximate 95% linear confidence limits.

[b] $\Sigma_\beta = 0.269\ \beta^{Id}\ \underline{V}_\beta$, specific surface area as determined by the multilayer adsorption model.

[c] $\underset{\sim}{S}(\underset{\sim}{\varphi})$ is the residual sum of squares.

[d] $\lvert \underset{\sim}{J}^T \underset{\sim}{J} \rvert$ is the determinant in Equation (66).

To understand the reason for the greater uncertainty in the estimated parameters for the 90.1°K argon isotherms, one must consider the volume of the joint confidence region hyperellipsoid in the four-dimensional parameter space (see Appendix I).

The boundary of the region in the parameter space with a confidence coefficient $1-\alpha$ is formed by the values of the parameters φ which satisfy the relationship

$$(\underset{\sim}{\varphi} - \underset{\sim}{\hat{\varphi}})^T \underset{\sim}{J}^T \underset{\sim}{J} (\underset{\sim}{\varphi} - \underset{\sim}{\hat{\varphi}}) = s^2 p F_{\alpha(p,n-p)} \qquad (66)$$

where

$\underset{\sim}{\hat{\varphi}}$ = least squares estimated parameter matrix

$\underset{\sim}{J}$ = $\underline{n} \times \underline{p}$ Jacobian matrix of partial derivatives

$\underline{s}^2$ = error variance which is related to the amount of data scatter

$\underline{F}_{\alpha(\underline{p},\underline{n}-\underline{p})}$ = α percentage point of the $\underline{F}$-distribution with $\underline{p}$ and $\underline{n}-\underline{p}$ degrees of freedom

$\underline{n}$ = number of adsorption data points

$\underline{p}$ = number of estimated parameters.

The $\sim$ subscript denotes matrix notation, and the $\underline{T}$ superscript denotes matrix transposition. The confidence region hyperellipsoid is described by Equation (66) with the volume proportional to the square root of the reciprocal of the determinant $|\underset{\sim}{J}^T\underset{\sim}{J}|$.

The eigenvalues of the $\underset{\sim}{J}^T\underset{\sim}{J}$ matrix indicate the conditioning of the confidence region hyperellipsoid or, equivalently, the state of correlation between the estimates of the unknown parameters. If the estimated parameters, φ, are completely uncorrelated, then each eigenvalue, ξ, is equal to unity. When the parameter estimates are correlated, one or more of the eigenvalues are small compared to the others. Since the determinant $|\underset{\sim}{J}^T\underset{\sim}{J}|$ is equal to the product of the eigenvalues

(i.e., $|\underline{J}^T\underline{J}| = \prod_{j=1}^{P} \xi_j$), the volume of the confidence region hyperellipsoid depends directly on the amount of correlation in the estimated parameters.

The determinant $|\underline{J}^T\underline{J}|$ for the argon acid-hydrolyzed holocellulose isotherm at 77.5°K is 0.45×10^{-4}, whereas for the 90.1°K isotherm the determinant is 0.64×10^{-7}. If it is assumed that the error variance (i.e., data scatter about the model isotherm) is the same for the two isotherms, then the greater correlation among the estimated parameters for the 90.1°K argon isotherm results in an increase in the confidence region hyperellipsoid volume by a factor of approximately 26.5. The increased correlation among the estimated parameters can be explained by the shape of the isotherm and by the fact that the 90.1°K isotherm data cover a smaller relative pressure range (i.e., 0.0 to 0.27 p/p_o). The higher degree of correlation reflects the fact that many different isotherm curves, having similar beginnings but with different endings, could be drawn through the experimental data points. In other words, the experimental data range sampled cannot constrain the estimated parameters to the same extent as the 77.5°K isotherm data which cover a larger relative pressure range (0.0 to 0.4 p/p_o).

If the 90.1°K isotherm data were extended up to a relative pressure of 0.40, the determinant $|\underline{J}^T\underline{J}|$ magnitude would increase to a value of 0.352×10^{-6} resulting in an accompanying decrease in the confidence region hyperellipsoid volume by a factor of 2.3. Even when the same relative pressure range is sampled for the two isotherms, the 90.1°K isotherm has a much larger confidence region ellipsoid volume. This is a consequence of the lower degree of curvature for the 90.1°K isotherm, so that the model parameters can be varied over wider ranges without perceptible changes in the resulting isotherm.

When the multilayer adsorption model is fitted simultaneously to the 77.5°K and 90.1°K argon isotherms for a given substrate, results as shown in Table XV are

obtained. The fitting operation is done by treating temperature as an independent variable in the multilayer adsorption model. Referring to Table XV, it is evident that the confidence limits for the unknown parameters are not improved when the model is fitted to the combined data set. This lack of improvement is to be expected since no additional data space (i.e., relative pressure range) is included in the combined data set. The addition of the 90.1°K isotherm data to the 77.5°K isotherm data adds only more data points within the same data space.

TABLE XV

RESULTS OF FITTING MULTILAYER MODEL TO ARGON ADSORPTION DATA

Adsorbent: Acid-Hydrolyzed Holocellulose

Isotherm temperature, °K	77.5	90.1	77.5 & 90.1
$\underline{U}^{Median}$, kcal. mole^{-1}	1.36 ± 0.02[a]	1.30 ± 0.10	1.34 ± 0.10
γ	7.4 ± 0.8	5.5 ± 2.1	7.5 ± 2.9
$\underline{V}_\beta$, ml. (STP) g.$^{-1}$	1.39 ± 0.07	1.30 ± 0.74	1.37 ± 0.32
$\nu \times 10^{12}$, sec.$^{-1}$	2.26 ± 0.58	2.26 ± 5.48	2.31 ± 1.89
$\underset{\sim}{S}(\underset{\sim}{\varphi})$	0.0025	0.0054	0.1094
$\lvert \underset{\sim}{J}^T \underset{\sim}{J} \rvert$	0.45×10^{-4}	0.64×10^{-7}	0.20×10^{-3}

[a] Approximate 95% linear confidence limits.

Elimination of the Vibrational Frequency as an Unknown Parameter

For a well-conditioned model, the confidence region contours defined by Equation (66) are well-rounded ellipsoids which result in rapid convergence for parameter estimation. When the joint confidence region ellipsoid is attenuated and contains long ridges, slow convergence of the iterative estimation procedure for the unknown parameters φ, is likely. In this case, the model needs to be reparameterized (e.g., one or more of the parameters combined or eliminated from the model) so that the confidence region is well conditioned.

Considering the values of the parameters of the multilayer adsorption model derived for the argon adsorption data (see Table XIV), the longest axis of the confidence region ellipsoid is associated with the vibrational frequency parameter, ν. The conditioning of the adsorption model should improve substantially if the vibrational parameter could be removed from the model or combined with another parameter.

Using a harmonic oscillator approximation, the frequency, ν, of the vibration of an adsorbed species normal to the surface is determined by the curvature of the interaction potential, $\underline{W}(\underline{z})$, at its minimum. Since the frequency of a one-dimensional harmonic oscillator is given by

$$\nu = (1/2\pi)\sqrt{f/m} \tag{67}$$

where $\underline{m}$ is the mass of the adsorbed species and $\underline{f}$ is the force constant [i.e., $(\partial \underline{W}(\underline{z})/\partial \underline{z}^2)$ at $\underline{z} = \underline{z}_o$], it can be shown that the vibrational frequency is proportional to the square root of the potential energy well depth (3). Therefore, the frequency is related to the adsorptive potential, $\underline{U}$, by

$$\nu^2 = \frac{\tau}{m}\left(U + {}_aE_o^{vib}\right) \tag{68}$$

where

$${}_aE_o^{vib} = {}^1/_2 Nh\nu \tag{69}$$

and where τ is a proportionality constant. Using the $\underline{U}^{Median}$ and ν values derived from the argon adsorption data at 77.5°K, an approximate value of the constant τ was calculated. Using the estimated constant τ, the vibrational frequency was calculated from the median adsorptive potential, $\underline{U}^{Median}$, by Equation (68) for the other temperatures and adsorbate gases. By using this relationship, the vibrational frequency was eliminated as an unknown parameter in the multilayer adsorption model. Results from using this approach in fitting the multilayer

adsorption model to argon 90.1°K isotherm data are shown in Table XVI. The elimination of the vibrational frequency as an unknown parameter in the multilayer adsorption model reduces the magnitude of the confidence intervals for the three remaining unknown parameters. In addition, the improved conditioning of the model accelerates the convergence of the iterative searching procedure.

TABLE XVI

RESULTS OF FITTING THE MULTILAYER MODEL TO ARGON ADSORPTION DATA WITH THE VIBRATIONAL FREQUENCY ELIMINATED AS AN UNKNOWN PARAMETER

	Holocellulose	Alkali-Extracted Holocellulose	Acid-Hydrolyzed Holocellulose
Isotherm temperature, °K	90.1	90.1	90.1
$\underline{U}^{Median}$, kcal. mole^{-1}	1.44 ± 0.34[a]	1.28 ± 0.09	1.30 ± 0.10
γ	5.8 ± 6.7	10.4 ± 4.4	5.6 ± 1.8
$\underline{V}_\beta$, ml. (STP) g.$^{-1}$	0.13 ± 0.07	0.36 ± 0.08	1.24 ± 0.22
$\nu \times 10^{12}$, sec.$^{-1}$ (calculated from $\underline{U}^{Median}$)	1.85	1.76	1.77
$\underline{S}(\underset{\sim}{\varphi})$	0.0008	0.0002	0.0058
$\lvert \underline{\underline{J}}^T \underline{\underline{J}} \rvert$	0.55×10^{-6}	0.20×10^{-5}	0.24×10^{-2}

[a]Approximate 95% linear confidence limits.

Polarization of the Argon Adsorbate by a Surface Electric Field

The ideal two-dimensional Van der Waals constants, α^{Id} and β^{Id}, were used in the multilayer adsorption model for the nonlinear regression analysis of the argon adsorption data. The ideal constants, α^{Id} and β^{Id}, can be calculated from the familiar three-dimensional constants, $\underline{a}$ and $\underline{b}$, as follows:

$$\alpha^{Id} = a \left(\frac{9\pi}{256b}\right)^{1/3} \tag{70}$$

$$\beta^{Id} = 2b \left(\frac{9\pi}{256b}\right)^{1/3} \tag{71}$$

or $\alpha^{Id}/\beta^{Id} = \underline{a}/2\underline{b}$. These ideal values apply when no orientation or polarization of the adsorbate due to the substrate is present.

Since the argon adsorbate is spherical, the orientation effects do not have to be considered. However, if a surface electric field is present at the adsorbent solid-gas interface, then an induced dipole moment may be created in the argon adsorbate. The induced dipole moment, μ^{ind}, is related to the electric field, $\underline{E}$, according to the following relation:

$$\mu^{ind} = E\xi \tag{72}$$

where ξ is the average polarizability for the freely rotating adsorbate species. deBoer (56) has derived an expression for the reduction of the two-dimensional Van der Waals constant α resulting from this effect:

$$\lambda = -(\mu^{ind})^2\pi/d \tag{73}$$

where λ is the change in α, and $\underline{d}$ is the diameter of the adsorbate species. Using this relation, an operative two-dimensional Van der Waals constant, α^{op}, can be calculated.

$$\alpha^{op} = \alpha^{Id} + \lambda. \tag{74}$$

Considering Equations (73) and (74), it is apparent that the α^{op} must be less than or equal to α^{Id}.

In order to check for the presence of a significant surface electric field in the three cellulose adsorbents, the α^{op} parameter was treated as an unknown parameter like the $\underline{U}^{Median}$, γ, $\underline{V}_\beta$, and ν parameters in the nonlinear regression analysis. However, unlike the other four unknown parameters, the α^{op} parameter was constrained so that the estimated α^{op} values could only take on values less

than or equal to α^{Id}. In this manner, an estimate of the surface electric field strength could be obtained directly from the estimated value of α^{op} and Equations (73) and (72).

For all three adsorbents, the estimated α^{op} value did not differ significantly from the α^{Id} value at the 95% confidence level. This result indicated that the three water-dried cellulosic adsorbents used in this investigation did not have a significant surface electric field. Deitrich (17) obtained similar results for cotton cellulose fibers using a heat of wetting technique to determine the surface electric field strength. Therefore, the α^{Id} value was used in subsequent calculations as a known parameter.

THE NITROGEN-CELLULOSE ADSORPTION SYSTEM

Evaluation of the Å Parameter

The three translational, two rotational, and one internal vibrational degrees of freedom of the symmetric diatomic nitrogen molecule become, on physical adsorption, two translational, two rotational, and one internal vibrational degrees of freedom with an additional center-of-mass vibrational degree of freedom perpendicular to the surface. The surface may introduce a potential barrier restricting the turning over of the molecule. The potential barrier may be high enough so that the two rotational degrees will become effectively one degree of planar rotation (rotation of the molecule about an axis perpendicular to the surface, the molecular axis being parallel to the surface) and one degree of vibration (rocking of the molecular axis out of a plane parallel to the surface).

Because of this orientation effect for the nitrogen adsorbate molecule, the fraction of the nitrogen molecules in either the flat (axis parallel to the surface) or perpendicular (axis perpendicular to the surface) position must be included in

the relationship defining $\underline{\overset{\circ}{A}}$. The superscript $||$ is used to denote an orientation with the molecular axis parallel to the surface, and the superscript $\perp$ denotes an orientation with the molecular axis perpendicular to the surface. If $\underline{x}$ equals the fraction of the nitrogen adsorbate molecules oriented in the flat position, the general relationship defining $\underline{\overset{\circ}{A}}$ is given by:

$$\ln \overset{\circ}{A} = \frac{-\Delta S^{tr}}{R} - x\,\frac{(\Delta S^{rot})^{||}}{R} - (1-x)\,\frac{(\Delta S^{rot})^{\perp}}{R} + x\,\frac{\left({}_aF^{vib} - {}_aE_o^{vib}\right)^{||}}{RT}$$

$$+ (1-x)\,\frac{\left({}_aF^{vib} - {}_aE_o^{vib}\right)^{\perp}}{RT} + x\,\frac{(\Delta E^{kin})^{||}}{RT} + (1-x)\,\frac{(\Delta E^{kin})^{\perp}}{RT} - \ln\frac{\theta_s}{1-\theta_s}$$

$$+ \ln 760. \qquad (75)$$

The integral translational entropy change, $\Delta\underline{S}_{\underline{s}}^{tr}$, is determined using the same formula as for the argon adsorption [i.e., Equation (63)]. The rotational entropy change upon adsorption, $\Delta\underline{S}^{rot}$, can be evaluated using the rotational partition function. The rotational partition function, $\underline{Q}^{rot}$, for a molecule free to rotate in $\underline{n}$ independent ways is given by (10):

$$Q^{rot} = \frac{1}{\pi\sigma}\left[\frac{8\pi^3(I_A I_B I_C)^{1/n}kT}{h^2}\right]^{n/2} \qquad (76)$$

where

$$n \leq 3 \qquad (77)$$

and $\underline{I}_{\underline{A}}$, $\underline{I}_{\underline{B}}$, and $\underline{I}_{\underline{C}}$ are the moments of inertia and σ is the symmetry factor which equals 2 for nitrogen. Since the rotational entropy, $\underline{S}^{rot}$, equals

$$S^{rot} = R[\ln Q^{rot} + T\,\partial(\ln Q^{rot})/\partial T] \qquad (78)$$

the rotational entropy change upon adsorption, $\Delta\underline{S}^{rot}$, is calculated as:

$$\Delta S^{rot} = S_a^{rot} - S_g^{rot} \qquad (79)$$

where the $\underline{S}_{\underline{a}}^{rot}$ and $\underline{S}_{\underline{g}}^{rot}$ are the rotational entropies of the adsorbate and gas phase, respectively.

For the orientation of the nitrogen molecule perpendicular to the surface, the rotational degrees of freedom do not change, so that $(\Delta\underline{S}^{rot})^{\perp} = 0$. However, the adsorbed nitrogen molecule oriented parallel to the surface has lost one rotational degree of freedom, so that using Equations (76), (78), and (79)

$$(\Delta S^{rot})^{||} = -R\left[\ln\left(\frac{8\pi^3 IkT}{h^2}\right)^{1/2} + \frac{1}{2}\right] \tag{80}$$

where $\underline{I}$ is the moment of inertia for the nitrogen molecule.

When the nitrogen adsorbate molecule is in the perpendicular orientation, the adsorbate molecule has one external vibrational mode normal to the surface so that $(\underline{a}F^{vib} - \underline{a}E_o^{vib})^{\perp}$ is defined by the identical relationship used for argon [see Equation (64)].

$$({}_aF^{vib} - {}_aE_o^{vib})^{\perp} = RT \ln(1 - \exp[-h\nu/kT)]. \tag{81}$$

For the parallel orientation, an additional rocking vibrational mode is present.

Coupling is likely to exist between the two external vibrational modes in this situation. The assumption is made that the two vibrational frequencies are equal. Therefore,

$$({}_aF^{vib} - {}_aE_o^{vib})^{||} = 2RT \ln(1 - \exp[-h\nu/kT]). \tag{82}$$

Since only one degree of translational freedom is lost upon adsorption for the perpendicular orientation of nitrogen, the kinetic energy change, $(\Delta\underline{E}^{kin})^{\perp}$, upon adsorption is equal to $-\frac{1}{2}\underline{RT}$. In the parallel orientation, a translational plus an additional rotational degree of freedom is lost, so that $(\Delta\underline{E}^{kin})^{||} = -\underline{RT}$.

The standard state coverage, θ_s, was calculated using the relationship:

$$\theta_s = [x\beta^{||} + (1 - x)\beta^{\perp}]/4.08T \qquad (83)$$

where

$\beta^{||}$ = the two-dimensional Van der Waals constant corresponding to b for the parallel orientation

$\beta^{\perp}$ = the two-dimensional Van der Waals constant corresponding to b for the perpendicular orientation.

Using the relationship described in this section, a subroutine NITR in Appendix II was written for the nonlinear curve-fitting program to evaluate $\underline{A}$ as a function of the vibrational frequency, ν, and the fraction of nitrogen adsorbate molecules in the flat position, x, oriented parallel to the surface.

Results of Nonlinear Regression Analysis for the Nitrogen Adsorption Data

Because of the added complexity of orientation for the nitrogen adsorbate molecule, an additional unknown parameter, x, the fraction of adsorbed molecules in a flat position, must be introduced. Therefore, a range of the two-dimensional constants, α and β, is possible depending upon the orientation (56). For the flat position with the long axis of the nitrogen molecule parallel to the surface,

$$\alpha^{||} = 45.0 \times 10^{-30} \text{ erg cm.}^2 \text{ molecule}^{-2}$$

$$\beta^{||} = 17.1 \text{ A.}^2 \text{ molecule}^{-1}.$$

When the long axis of the nitrogen molecule is perpendicular to the surface,

$$\alpha^{\perp} = 52.5 \times 10^{-30} \text{ erg cm.}^2 \text{ molecule}^{-2}$$

$$\beta^{\perp} = 12.3 \text{ A.}^2 \text{ molecule}^{-1}.$$

The nonlinear regression analysis for the nitrogen adsorption data was done with five unknown parameters, γ, $\underline{U}^{Median}$, $\underline{V}_{\beta}$, ν, and α^{op}. The operative value of the two-dimensional Van der Waals constant, α^{op}, was constrained to have values between $\alpha^{||}$ and $\alpha^{\perp}$. The fraction of nitrogen molecules adsorbed in the flat position, $\underline{x}$, was calculated from the α^{op} value using the relationship:

$$x = (\alpha^{op} - \alpha^{\perp})/(\alpha^{||} - \alpha^{\perp}) \tag{84}$$

and β^{op} was calculated as follows:

$$\beta^{op} = x\beta^{||} + (1 - x)\beta^{\perp} . \tag{85}$$

An example of the experimental nitrogen adsorption data and the fitted multilayer model isotherm resulting from the nonlinear regression analysis are shown in Fig. 33. The adsorptive potential distribution function generated by the nonlinear curve-fitting procedure for the nitrogen acid-hydrolyzed holocellulose data at 77.5°K is presented in Fig. 34. The model parameter values and the thermodynamic data for this example nitrogen isotherm are listed in Table XVII. A similar set of figures and a table are in Appendix VI for each of the nitrogen isotherms.

A summary of the results from fitting the multilayer adsorption model to the nitrogen isotherms for each of the three adsorbents is listed in Table XVIII. The results of the nitrogen isotherm analysis ranks the adsorptive potential distribution and the specific surface area of the three cellulose adsorbents in the same order as the argon isotherms. The specific surface areas from the argon and nitrogen isotherms for the same adsorbent were approximately equal as would be expected. For all three adsorbents, the nitrogen molecules were all adsorbed essentially in the flat position. The adsorptive potential was higher for the nitrogen molecule than for the argon adsorbate for several reasons. Because the nitrogen was adsorbed in the flat position, the additive effect of the two atoms was involved in the

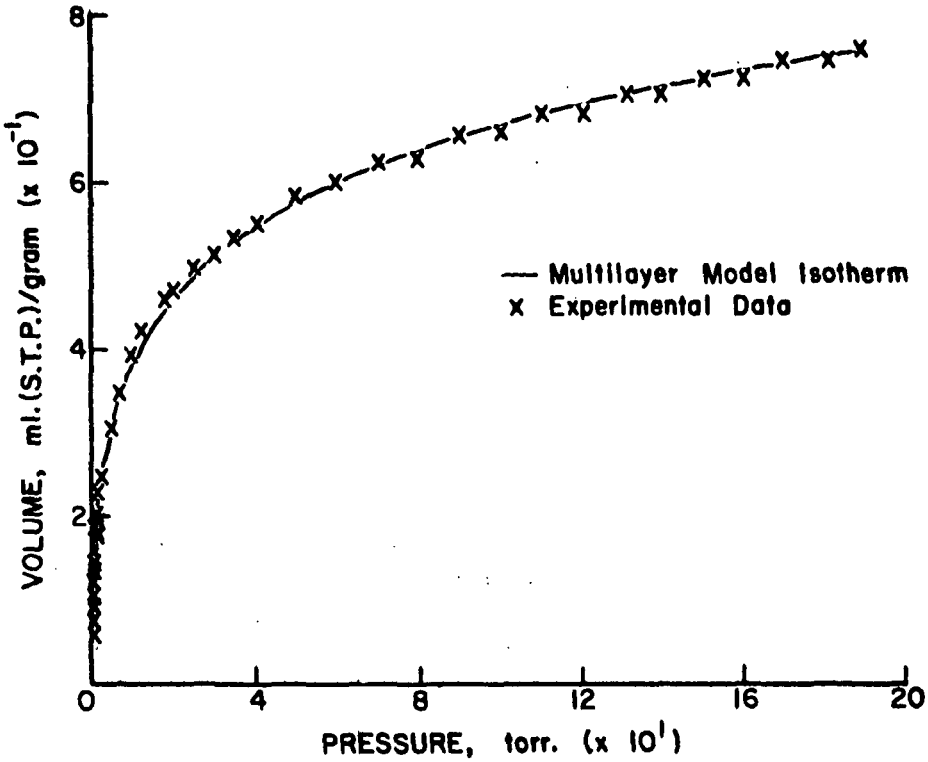

Figure 33. Multilayer Adsorption Model Isotherm Fitted to the Nitrogen Acid-Hydrolyzed Holocellulose Adsorption Data at 77.5°K

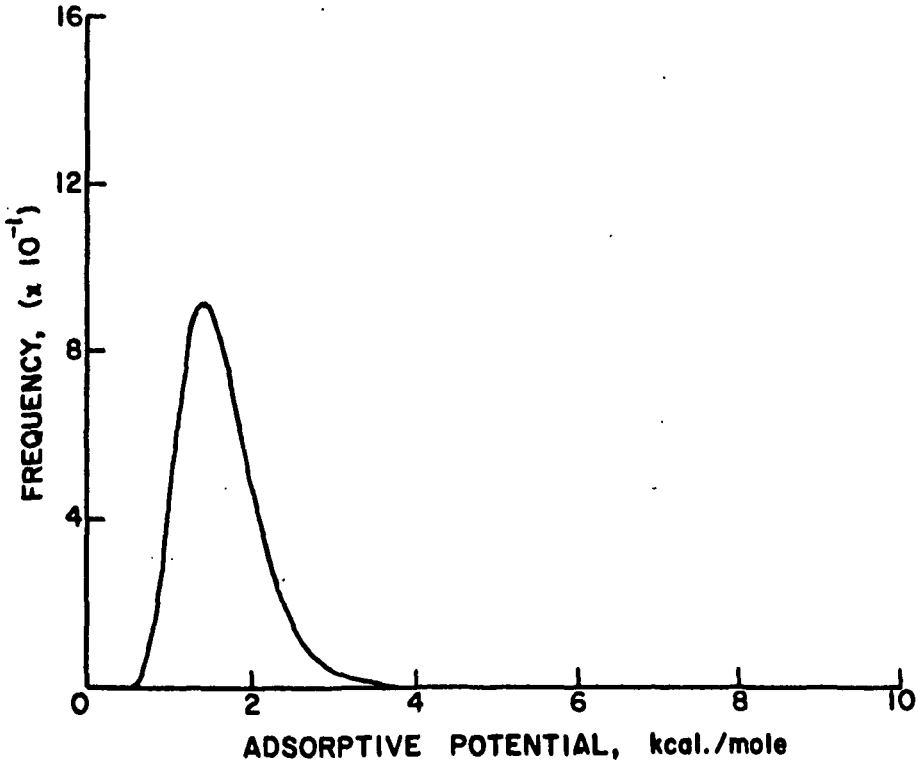

Figure 34. Adsorptive Potential Distribution for the Nitrogen Acid-Hydrolyzed Holocellulose Adsorption Data at 77.5°K

TABLE XVII

RESULTS OF FITTING MULTILAYER ADSORPTION MODEL TO EXPERIMENTAL DATA

Adsorbent: Acid-hydrolyzed holocellulose
Adsorbate: Nitrogen
Temperature: 77.5°K

Model parameters:

$\underline{U}^{Median} = 1.56 \pm 0.41^{a}$ kcal. mole^{-1}

$\underline{U}^{Mean} = 1.62$ kcal. mole^{-1}

$\underline{U}^{Mode} = 1.43$ kcal. mole^{-1}

$\gamma = 5.8 \pm 1.73$

$\underline{V}_{\beta} = 1.18 \pm 0.38$ ml. (STP) g.$^{-1}$

$\nu = 1.19 \pm 3.26 \times 10^{12}$ sec.$^{-1}$

$2\alpha/\beta$ (Ideal) $= 0.849$ kcal. mole^{-1}

$\alpha = 45.0 \times 10^{-30}$ erg cm.^{2} molecule^{-2}

$\beta = 17.1$ A.^{2} molecule^{-1}

Fraction of nitrogen molecule in flat position = 1.0

Thermodynamic data:

$\Delta\underline{S}_{\underline{s}}^{tr} = -0.0099$ kcal. mole^{-1} deg.$^{-1}$

$\Delta\underline{S}^{rot} = -0.0054$ kcal. mole^{-1} deg.$^{-1}$

$\Delta\underline{S}^{vib} = 0.0053$ kcal. mole^{-1} deg.$^{-1}$

$\Delta\underline{E}^{kin} = 0.1540$ kcal. mole^{-1}

$\underline{A}^{o} = 0.29937 \times 10^{7}$

---

[a] Approximate 95% linear confidence limits.

TABLE XVIII

RESULTS OF FITTING MULTILAYER ADSORPTION MODEL TO NITROGEN ADSORPTION DATA

	Holocellulose	Alkali-Extracted Holocellulose	Acid-Hydrolyzed Holocellulose
Isotherm temperature, °K	77.5	77.5	77.5
$\underline{U}^{Median}$, kcal. mole^{-1}	1.81 ± 19.1[a]	1.40 ± 0.34	1.56 ± 0.41
$\underline{U}^{Mean}$, kcal. mole^{-1}	1.94	1.46	1.62
$\underline{U}^{Mode}$, kcal. mole^{-1}	1.57	1.28	1.43
γ	3.5 ± 54.1	5.7 ± 2.6	5.8 ± 1.73
$\underline{V}_\beta$, ml. (STP) g.$^{-1}$	0.25 ± 0.37	0.33 ± 0.24	1.18 ± 0.38
Σ_β, m.^{2}g.$^{-1}$[b]	1.15 ± 1.70	1.50 ± 1.09	5.43 ± 1.75
$\nu \times 10^{12}$, sec.$^{-1}$	1.38 ± 340.17	0.78 ± 2.35	1.19 ± 3.26
Percentage of nitrogen molecules in flat position, %	100	96.7	100
$\underline{S}(\underset{\sim}{\varphi})$	0.0048	0.0012	0.0033
$\lvert \underline{J}^T \underline{J} \rvert$	0.25 × 10^{-9}	0.20 × 10^{-8}	0.74 × 10^{-6}

[a] Approximate 95% linear confidence limits.

[b] $\Sigma_\beta = 0.269\ \beta^{op}\ \underline{V}_\beta$, specific surface area as determined by the multilayer adsorption model.

interaction with the adsorbent surface. In addition, the adsorbent surface interacts more favorably with the linear diatomic nitrogen molecule than with the spherical electron cloud of the argon atom.

Precision of the Parameter Estimates

The wider confidence intervals for the model parameters derived from the nitrogen adsorption isotherms can be attributed to two sources. First, there is more data scatter in the nitrogen adsorption data due to the smaller molecular weight of the nitrogen adsorbate molecule relative to the argon adsorbate. Thus, the mass measurements were of smaller magnitude in the nitrogen adsorption determinations, resulting in a larger error variance, $\underline{s}^2$, in Equation (66). Secondly, the volume of the confidence region ellipsoid could be decreased significantly if the range of the data sampled were extended to higher relative pressures. The nitrogen adsorption data used in determining the parameter values in Table XVIII were for relative pressures of nitrogen up to 0.25 which resulted in a determinant $|\underline{J}^T\underline{J}|$ value of 0.74×10^{-6} for the nitrogen acid-hydrolyzed holocellulose data. If adsorption data had been experimentally determined up to a relative pressure of 0.40, the corresponding determinant value would have been 0.27×10^{-5}. This increased range of sampled data would have decreased the confidence region ellipsoid volume by a factor of 1.9.

As with the argon adsorption data, the model parameter values derived from the nitrogen adsorption data could have been constrained with greater precision if a greater range of adsorption data had been sampled.

Elimination of the Vibrational Frequency as an Unknown Parameter

Using Equation (68) and the constant τ derived from the argon adsorption data, the vibrational frequency of the nitrogen adsorbate was calculated from the median

adsorptive potential, $\underline{U}^{Median}$. The results of fitting the multilayer adsorption model to the nitrogen adsorption data when using this relationship are presented in Table XIX.

TABLE XIX

RESULTS OF FITTING THE MULTILAYER MODEL TO NITROGEN ADSORPTION DATA WITH THE VIBRATIONAL FREQUENCY ELIMINATED AS AN UNKNOWN PARAMETER

	Holocellulose	Alkali-Extracted Holocellulose	Acid-Hydrolyzed Holocellulose
Isotherm temperature, °K	77.5	77.5	77.5
$\underline{U}^{Median}$, kcal. mole^{-1}	1.81 ± 0.81[a]	1.55 ± 0.03	1.65 ± 0.03
γ	3.5 ± 6.9	9.4 ± 0.2	7.4 ± 0.7
V_β, ml. (STP) g.$^{-1}$	0.25 ± 0.19	0.25 ± 0.02	1.02 ± 0.03
$\nu \times 10^{12}$, sec.$^{-1}$ (calculated from $\underline{U}^{Median}$)	2.56	2.38	2.45
Percentage of nitrogen molecules in flat position, %	100	43	69
$\underline{S}(\underset{\sim}{\varphi})$	0.0087	0.0008	0.0015
$\lvert \underline{\underline{J}}^T \underline{\underline{J}} \rvert$	0.12×10^{-4}	0.74×10^{-3}	0.14×10^{-1}

[a] Approximate 95% linear confidence limits.

The elimination of the vibrational frequency as an unknown parameter permits an improved estimate of the fraction of adsorbed nitrogen molecules in the flat position, $\underline{x}$, because of the improved search conditioning.

THE $CFCl_3$-CELLULOSE ADSORPTION SYSTEM

Evaluation of the $\underline{A}^{\circ}$ Parameter

The three translational, three rotational, and nine internal vibrational degrees of freedom of the asymmetric top type $CFCl_3$ molecule in the gaseous phase change upon

physical adsorption depending on the mode of adsorption. Assuming that no significant surface electric field exists at the cellulose solid-gas interface, two possible models for the molecules in the adsorbate phase seem possible: (1) a free rotational model where the adsorbed molecule has the same freedom to rotate as in the gas phase, and (2) an oriented model, where the adsorbed molecule is oriented with the symmetry axis of the molecule normal to the surface because the dispersion force type interactions are at a maximum in this orientation when the chlorine atoms of the $CFCl_3$ molecule are closest to the surface.

For the free rotation model, the adsorbed phase has two translational, three rotational, and nine internal vibrational degrees of freedom, and one external molecular vibrational degree of freedom normal to the surface. Since there are no rotational degrees of freedom lost upon adsorption, the free rotational model $\underset{\circ}{A}$ can be calculated using the same formulas used for the argon adsorption system. A subroutine $CFCl_3$ in Appendix II was written for the nonlinear curve-fitting program for the $CFCl_3$ adsorbate molecule with no preferential orientation.

For the oriented model, the adsorbed phase has two translational, one rotational, and nine internal vibrational, and three external molecular vibrational degrees of freedom. In this orientation, the freedom to rotate about the two principal axes that are parallel to the surface is restricted to oscillations of frequency, ν_1 and ν_2; in addition, the center of mass of the molecule vibrates with respect to the surface, with a frequency of ν_3. The vibrational frequencies ν_1 and ν_2 are clearly equal to each other by virtue of symmetry. It would seem likely that some coupling exists between the three vibrations so that one could reasonably assume that all three vibrational frequencies are equal. Using this assumption, the vibrational term in the general relation for $\underset{\circ}{A}$ is:

$$({}_aF^{vib} - {}_aE_o^{vib}) = 3RT \ln(1 - \exp[-h\nu/kT]). \qquad (86)$$

The rotational entropy change upon adsorption, ΔS^{rot}, can be evaluated using Equations (78) and (79).

$$\Delta S^{rot} = -R\left[\ln\left(\frac{8\pi^3 kT(I_A I_B)^{1/2}}{h^2}\right) + 1\right] \qquad (87)$$

where I_A and I_B are the moments of inertia lost on adsorption. Since one degree of translational freedom and two rotational degrees of freedom are lost upon adsorption, the kinetic energy change upon adsorption, ΔE^{kin}, is equal to $-{}^3/_2 RT$.

For both the free rotation and oriented model, the standard state coverage, θ_s, was calculated using the relationship:

$$\theta_s = \beta^{Id}/4.08T \qquad (88)$$

where β(oriented) is assumed equal to β^{Id} since the $CFCl_3$ molecule is almost symmetrical.

Results of Nonlinear Regression Analysis for the $CFCl_3$ Adsorption Data

For the free rotation model for $CFCl_3$ adsorption, the ideal values of the two-dimensional Van der Waals constants, α^{Id} and β^{Id}, were used. However, the oriented model required a correction of the α^{Id} value for the alignment of the permanent dipole and the anisotropy of the polarizability. The $CFCl_3$ molecule was assumed to orient itself in response to the dispersion force interaction, with the three chlorine atoms closest to the surface and the permanent dipole of the molecule normal to the surface. The operative two-dimensional constant, α^{op}, is determined using the relationship (10)

$$\alpha^{op} = \omega\alpha^{Id} + \lambda. \qquad (89)$$

The alignment of the permanent dipole would reduce α^{Id} by introducing a mutual repulsion term, λ; the lateral polarizability of the oriented molecule is greater

than the average polarizability of the freely rotating molecule. This would have the effect of increasing α^{Id} (i.e., ω is greater than unity). The orientation factor, ω, is defined as:

$$\omega = (d^4/\xi^2)^{Id}(\xi^2/d^4)^{op} \tag{90}$$

where $\underline{d}$ and ξ are the molecular diameter and polarizability, respectively. For a freely rotating molecule, the time-average polarizability is independent of direction and is related to the polarizability along the three principal axes of the molecule by the expression:

$$\xi^{Id} = (\xi_1 + \xi_2 + \xi_3)/3. \tag{91}$$

The oriented molecule has a polarizability in the plane parallel to the surface given by:

$$\xi^{op} = (\xi_2 + \xi_3)/2. \tag{92}$$

Assuming the molecular diameter to be unchanged on orientation and using the principal polarizabilities from Table VI, the ω factor was calculated to be equal to 1.079 for this orientation of $CFCl_3$. The repulsion term, λ, due to the alignment of the permanent dipole in $CFCl_3$ is defined by the expression:

$$\lambda = -\bar{\mu}^2(\pi/d) \tag{93}$$

where $\bar{\mu}$ is the permanent dipole moment. Using 0.45 Debye as the permanent dipole moment of $CFCl_3$, the λ correction factor is equal to -14.3×10^{-30} erg cm.^{2} molecule^{-2}. Substitution of the λ and ω values into Equation (89) yields $\alpha^{op} = 355.7 \times 10^{-30}$ erg cm.^{2} molecule^{-2} which is slightly greater than $\alpha^{Id} = 343.0 \times 10^{-30}$ erg cm.^{2} molecule^{-2}.

The free rotational model was selected for the analysis of the adsorption data because it was felt that the cellulose surface does not have strong enough dispersion forces to overcome the repulsion of the oriented molecular dipoles and to hinder the molecular thermal motion in the oriented position.

An example of the experimental $CFCl_3$ adsorption data and the fitted multilayer model isotherm resulting from the nonlinear regression analysis are shown in Fig. 35. The adsorptive potential distribution function generated by the nonlinear curve-fitting procedure for the $CFCl_3$ acid-hydrolyzed holocellulose data at 258.15°K is presented in Fig. 36. The model parameter values and the thermodynamic data for this $CFCl_3$ isotherm are listed in Table XX. A similar set of figures and a table have been placed in Appendix VI for each of the $CFCl_3$ isotherms at 258.15°K.

A summary of the results from fitting the multilayer adsorption model to the $CFCl_3$ isotherms at 258.15°K for each of the three adsorbents is listed in Table XXI.

Precision of the Parameter Estimates

In spite of the ability of the model to fit the experimental isotherms, the unknown model parameter values could not be constrained to a narrow enough range for interpretative use. The isotherm data covered a relative pressure range of 0.0 to 0.40, but this portion of the isotherm was not unique enough in nature to constrain the model parameters. Because of the almost linear nature of the Type III adsorption isotherms, many possible combinations of the four unknown parameters would fit the data. The determinant value $|\underline{J}^T\underline{J}|$ was 0.121×10^{-13} indicating a very high degree of correlation among the four unknown parameters. This high correlation could not have been improved by extending the range of the adsorption data. At higher relative pressures, the added complexity of capillary condensation may be encountered, but the adsorption model does not apply to capillary condensation.

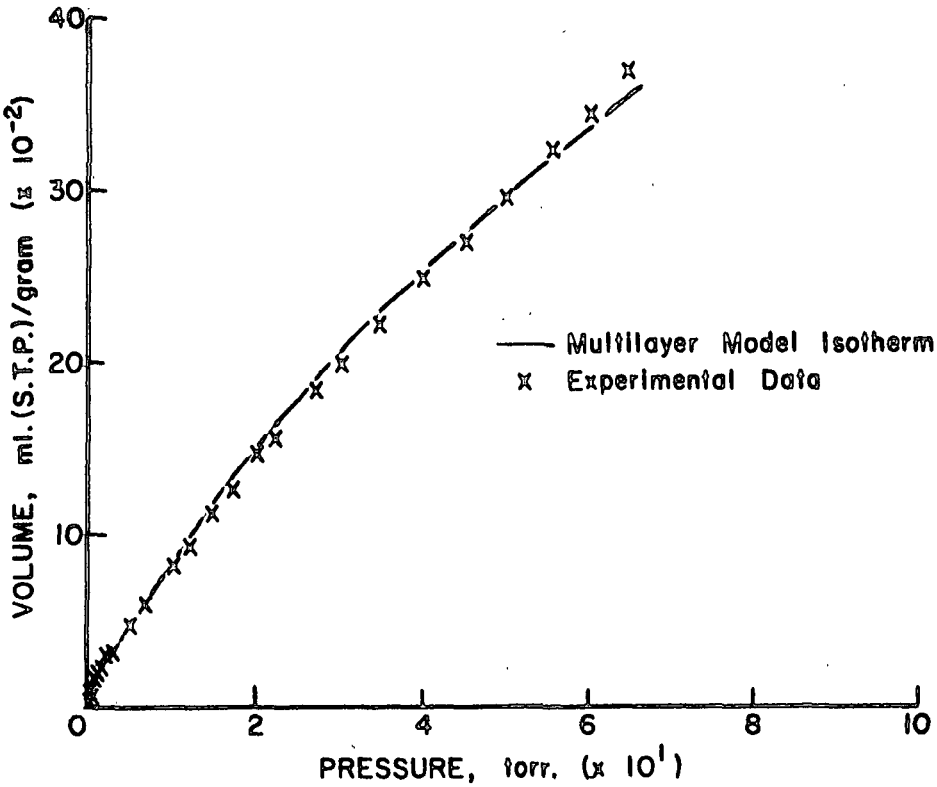

Figure 35. Multilayer Adsorption Model Fitted to the $CFCl_3$ Acid-Hydrolyzed Holocellulose Adsorption Data at 258.15°K

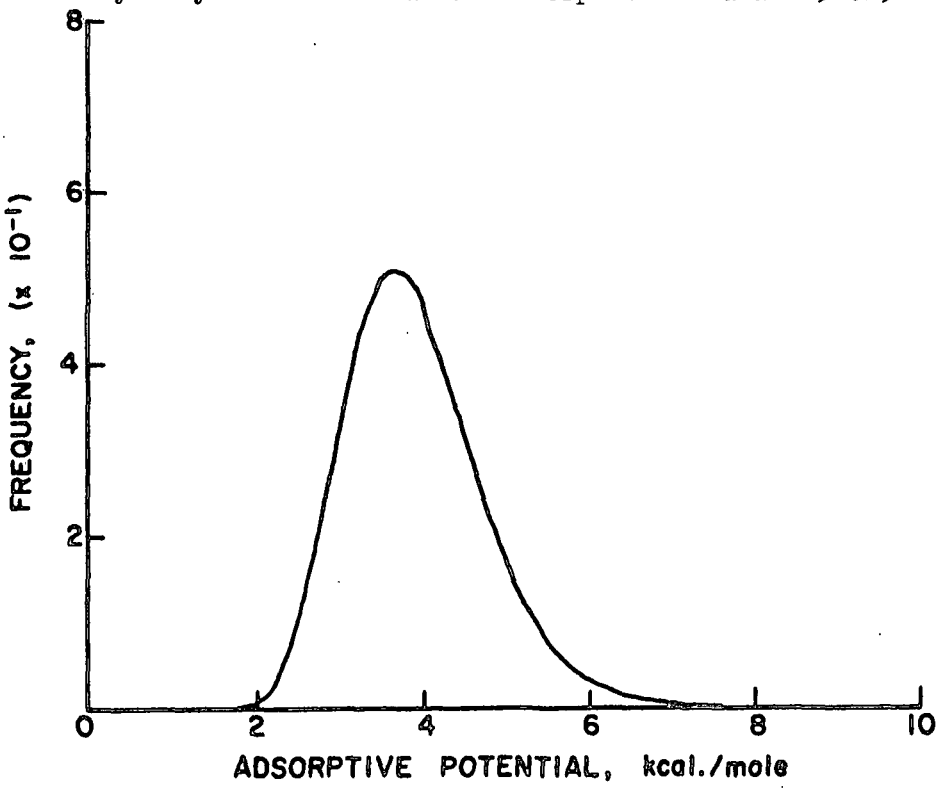

Figure 36. Adsorptive Potential Distribution for the $CFCl_3$ Acid-Hydrolyzed Holocellulose Adsorption Data at 258.15°K

TABLE XX

RESULTS OF FITTING MULTILAYER ADSORPTION MODEL TO EXPERIMENTAL DATA

Adsorbent: Acid-hydrolyzed holocellulose
Adsorbate: $CFCl_3$
Temperature: 258.15°K

Model Parameters

$\underline{U}^{Median} = 3.80 \pm 4.10^{a}$ kcal. mole^{-1}

$\underline{U}^{Mean} = 3.89$ kcal. mole^{-1}

$\underline{U}^{Mode} = 3.64$ kcal. mole^{-1}

$\gamma = 11.2 \pm 20.9$

$\underline{V}_{\beta} = 1.90 \pm 3.38$ ml. (STP) g.$^{-1}$

$\nu = 2.59 \pm 29.62 \times 10^{12}$ sec.$^{-1}$

$2\alpha/\beta$ (Ideal) $= 3.16$ kcal. mole^{-1}

$\alpha = 343.0 \times 10^{-30}$ erg cm.^{2} molecule^{-2}

$\beta = 31.2$ A.^{2} molecule^{-2}

Thermodynamic Data:

$\Delta\underline{S}^{tr} = -0.0127$ kcal. mole^{-1} deg.$^{-1}$

$\Delta\underline{S}^{rot} = 0.0$ kcal. mole^{-1} deg.$^{-1}$

$\Delta\underline{S}^{vib} = 0.0034$ kcal. mole^{-1} deg.$^{-1}$

$\Delta\underline{E}^{kin} = 0.2565$ kcal. mole^{-1}

$\underline{A}^{\circ} = 0.34708 \times 10^{7}$

---

[a] Approximate 95% linear confidence limits.

TABLE XXI

RESULTS OF FITTING MULTILAYER ADSORPTION MODEL TO $CFCl_3$ ADSORPTION DATA

	Holocellulose	Alkali-Extracted Holocellulose	Acid-Hydrolyzed Holocellulose
Isotherm temperature, °K	258.15	258.15	258.15
$\underline{U}^{Median}$, kcal. mole^{-1}	3.21 ± 9.71[a]	3.03 ± 9.60	3.80 ± 4.10
$\underline{U}^{Mean}$, kcal. mole^{-1}	3.33	3.13	3.89
$\underline{U}^{Mode}$, kcal. mole^{-1}	2.98	2.85	3.64
γ	6.7 ± 32.5	8.1 ± 41.6	11.2 ± 20.9
$\underline{V}_\beta$, ml. (STP) g.$^{-1}$	0.82 ± 3.07	1.80 ± 9.35	1.90 ± 3.38
Σ_β, m.^{2} g.$^{-1}$[b]	6.88 ±25.77	15.11 ±78.47	15.95 ±28.37
$\nu \times 10^{12}$, sec.$^{-1}$	4.27 ±99.81	2.49 ±45.36	2.59 ±29.62
$\underset{\sim}{S}(\varphi)$	0.0002	0.0002	0.0016
$\lvert \underset{\sim}{J}^T \underset{\sim}{J} \rvert$	0.21×10^{-18}	0.38×10^{-18}	0.12×10^{-13}

[a] Approximate 95% linear confidence limits.

[b] $\Sigma_\beta = 0.269\ \beta^{Id} \underline{V}_\beta$, specific surface area as determined by the multilayer adsorption model.

The reason for this unfortunate situation was the lack of a significant surface electric field for the three cellulosic sample substrates so that only nonpolar adsorptive forces were functioning. With only nonpolar adsorptive forces functioning, the $CFCl_3$ adsorbate clustered in multilayers only on the higher energy patches since the interaction energy was higher for adsorbate-adsorbate interactions than the adsorbate-surface interactions. This concept is illustrated best by considering Equation (30) again:

$$U_j = U_1/j^3 + (2\alpha\theta_1/\beta)/(j-1)^3 + (2\alpha\theta_2/\beta)/(j-2)^3 + \ldots \quad j = 2,3,\ldots \quad (30)$$

For the polar $CFCl_3$ gas, the adsorbate-adsorbate interactions are strong enough (i.e., $2\alpha/\beta$ = 3.16 kcal./mole) so that once significant coverage ($\theta_1 \rightarrow 1$) is reached on the higher energy patches, the adsorptive potential for the second layer, $\underline{U}_2$, of a high energy patch is greater than the surface adsorptive potential, $\underline{U}_1$, for the remaining lower energy portions of the surface. Thus, only the initial knee in the adsorption isotherm (see Fig. 36) was influenced by the surface. The remaining portion of the adsorption isotherm was due to multilayer formation on the higher energy patches which is essentially a condensation phenomenon. Since the surface properties have little influence on the isotherm shape in this case, the model parameters describing the surface could not be constrained to a very narrow range.

It seems that the only possible means for obtaining better parameter estimates would be to select a different polar gas. For better results, the adsorbate gas should have a lower heat of condensation (e.g., carbon monoxide with $2\alpha/\beta$ = 0.890 kcal./mole) which would result in a Type II isotherm. The greater curvature and more distinct shape of the Type II isotherm should permit constraining the model parameters to a greater extent.

Similar parameter estimates and confidence intervals were obtained when the oriented model for the $CFCl_3$ adsorbate was used in the multilayer adsorption model for the nonlinear regression analysis. The multilayer adsorption model was not fitted to the isotherms for temperatures above 258.15°K since this operation would be fruitless because of the very wide confidence intervals determined for the fitted parameters at the 258.15°K isotherm temperature.

Elimination of the Vibrational Frequency as an Unknown Parameter

The results from the elimination of the vibrational frequency of the $CFCl_3$ adsorbate as an unknown parameter in the multilayer adsorption model are given in Table XXII. The removal of the one additional unknown parameter does not reduce the magnitude of the confidence intervals sufficiently for the model parameters to be useful for characterizing the surface.

TABLE XXII

RESULTS OF FITTING THE MULTILAYER MODEL TO $CFCl_3$ ADSORPTION DATA WITH THE VIBRATIONAL FREQUENCY ELIMINATED AS AN UNKNOWN PARAMETER

Adsorbent: Acid-hydrolyzed holocellulose

Isotherm temperature, °K	258.15
$\underline{U}^{Median}$, kcal. mole^{-1}	3.08 ± 1.41[a]
γ	7.3 ± 7.4
$\underline{V}_\beta$, ml. (STP) g.$^{-1}$	3.57 ± 6.02
$\nu \times 10^{12}$, sec.$^{-1}$ (calculated from $\underline{U}^{Median}$)	1.48
$\underline{S}(\underset{\sim}{\varphi})$	0.0012
$\lvert \underline{J}^T \underline{J} \rvert$	0.12 × 10^{-8}

[a]Approximate 95% linear confidence limits.

Elimination of Both the Vibrational Frequency and the Monolayer Volume as Unknown Parameters

In an effort to further reduce the magnitude of the confidence intervals for the unknown parameters in the adsorption model, an attempt was made to remove both the monolayer volume, $\underline{V}_\beta$, and the adsorbate vibrational frequency, ν, as unknown parameters. By assuming that the argon adsorbate was accessible to the same surface area as the $CFCl_3$ adsorbate, a monolayer volume for the $CFCl_3$ adsorbate

was calculated (i.e., $[\underline{V}_\beta\ \beta^{Id}]^{CFCl_3} = [\underline{V}_\beta\ \beta^{Id}]^{argon}$). The results from fitting the multilayer adsorption model with two unknown parameters to the $CFCl_3$ adsorption data are presented in Table XXIII. This approach was unsatisfactory for several reasons. The adsorption model with only two unknown parameters does not have enough degrees of freedom to adequately fit the adsorption data as indicated by the large increase in the $\underline{S}(\underset{\sim}{\varphi})$ value. The restriction of the $\underline{V}_\beta$ and ν parameters to fixed values does not allow for the parameter correlations present even in the best-conditioned data sets (e.g., argon-acid hydrolyzed holocellulose at 77.5°K).

TABLE XXIII

RESULTS OF FITTING THE MULTILAYER MODEL TO $CFCl_3$ ADSORPTION DATA WITH BOTH THE VIBRATIONAL FREQUENCY AND MONOLAYER VOLUME ELIMINATED AS UNKNOWN PARAMETERS

Adsorbent: Acid-hydrolyzed holocellulose

Isotherm temperature, °K	258.15
$\underline{U}^{Median}$, kcal. mole^{-1}	4.65 ± 0.07[a]
γ	43.3 ± 22.0
$\underline{V}_\beta$, ml. (STP) g.$^{-1}$	0.606
$\nu \times 10^{12}$, sec.$^{-1}$	1.82
$S(\underset{\sim}{\varphi})$	0.0053
$\lvert \underline{\underline{J}}^T \underline{\underline{J}} \rvert$	0.50×10^{-5}

[a] Approximate 95% linear confidence limits.

The above unsuccessful attempts to improve the adsorption model conditioning by removing unknown parameters indicate that the effort for improvement should be on the cause, not the effect, of the ill-conditioning. The real cause of the model ill-conditioning is the lack of influence of the surface properties on the

$CFCl_3$ adsorption isotherms when the substrate is a nonpolar and relatively low-energy surface.

Infrared Investigation of $CFCl_3$ Hydrogen Bonding Properties

This investigation was undertaken to determine if the $CFCl_3$ adsorbate could possibly hydrogen bond with the cellulosic adsorbent substrates. Hydrogen bonding can occur in any system containing a proton donor group (X-H) and a proton acceptor (Y) if the s-orbital of the proton can effectively overlap the p- or π-orbital of the acceptor group. Atoms X and Y are electronegative with Y possessing lone pair electrons. The common proton donor groups in organic molecules are carboxyl, hydroxyl, amine, or amide groups. Common proton acceptor atoms are oxygen, nitrogen, and the halogens.

The strength of the hydrogen bond is at a maximum when the proton donor group and the axis of the lone pair orbital are collinear. The strength of the bond is inversely proportional to the distance between X and Y.

Hydrogen bonding alters the force constant of both groups so that the frequencies of both stretching and bending vibrations are altered. The X-H stretching bonds move to longer wavelengths (lower frequencies) usually with increased intensity and band widening. The stretching frequency of the acceptor group, e.g., C-F, is also reduced, but to a lesser degree than the proton donor group. The change in frequency between the "free" OH adsorption and bonded OH adsorption is a measure of the strength of the hydrogen bond. These effects are illustrated in Table XXIV for the stretching frequencies of hydroxyl groups (57).

A ternary solution of ethanol (donor compound), $CFCl_3$ (acceptor compound), and carbon tetrachloride (solvent) was used to evaluate the intramolecular hydrogen bonding properties of the $CFCl_3$. When hydrogen bonding is present, both the free

and associated hydroxyl bands are observable in the I.R. spectra. Increasing the concentration of the acceptor increases the intensity of the associated band and decreases the intensity of the free band (58).

TABLE XXIV

EFFECT OF HYDROGEN BONDING ON THE FREE STRETCHING FREQUENCY OF HYDROXYL GROUPS

X-H...Y Strength	Frequency Reduction from the Free to Associate Band, νOH, $cm.^{-1}$
Weak	300
Strong	500

The free hydroxyl peak was observed at 3640 $cm.^{-1}$, but no associated hydroxyl peak was observed for any of the prepared solutions. These results indicate that $CFCl_3$ does not effectively form hydrogen bonds with hydroxyl groups. From these observations, it was concluded that only Van der Waals-type forces functioned in the adsorption of $CFCl_3$ on cellulose and that no hydrogen bonding forces were operative. The lack of hydrogen bonding between $CFCl_3$ and hydroxyl groups is further confirmed by the insolubility of $CFCl_3$ in hydroxyl-containing compounds like ethylene glycol and glycerol.

ANALYSIS OF ADSORPTION DATA USING CLUSTERING FUNCTIONS

In the notation of Zimm and Lundberg (31), the clustering function is given by $\varphi_1 \underline{G}_{11}/\underline{v}_1$ in which φ_1 and $\underline{v}_1$ are the volume fraction and partial molecular volume of the adsorbate and $\underline{G}_{11}$ is a cluster integral. The clustering function is defined equal to the mean number of adsorbate molecules in the vicinity of a given adsorbate molecule in excess of random expectation. Thus, a negative clustering value indicates that a given adsorbate molecule is less closely packed than a

molecule in an ideal system. A positive clustering value is interpreted as indicative of a clustering of the adsorbed phase.

The clustering function versus the volume of argon adsorbed on acid-hydrolyzed holocellulose at 77.5°K is presented in Fig. 37. As the adsorbed volume increases there is an increasing availability of energetically favorable adsorption sites. As the molecules are adsorbed on successively lower and lower energy, unoccupied, homotattic patches of the heterogeneous surface, the molecular packing density decreases. This decreasing clustering value with increased volume adsorbed is evident in Fig. 37.

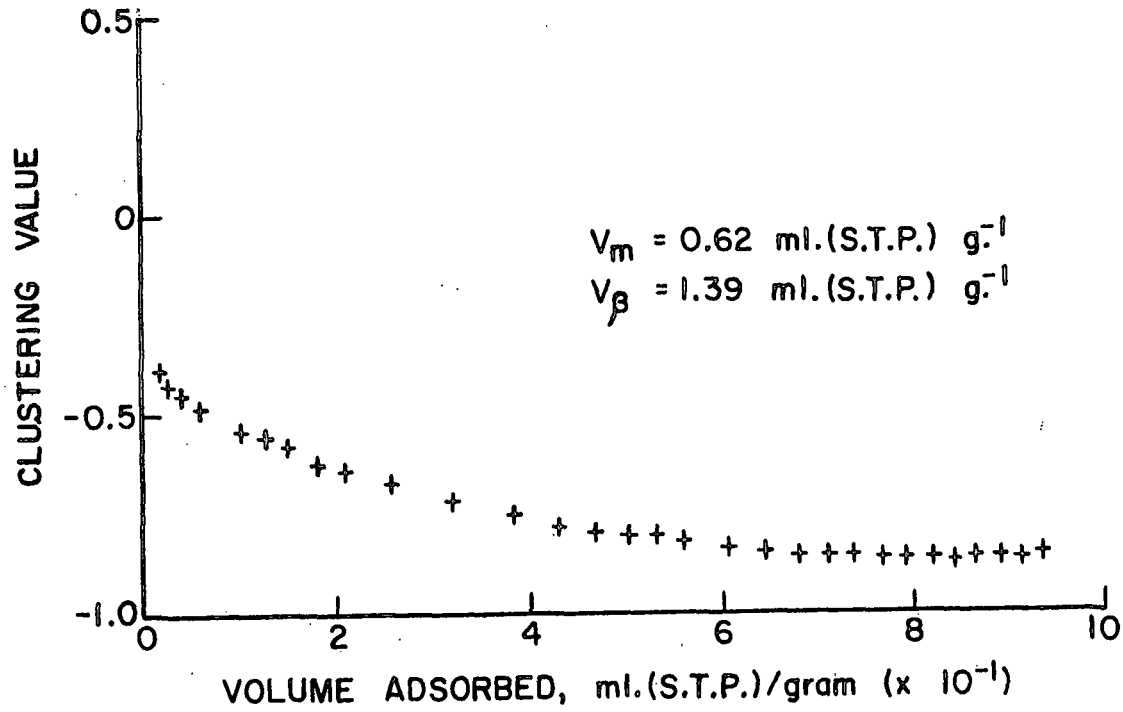

Figure 37. Clustering Function $\varphi_1 \underline{G}_{11}/\underline{v}_1$ for Argon Adsorbed on Acid-Hydrolyzed Holocellulose at 77.5°K

With further increases in the adsorbed volume, the molecular packing density will begin to increase as the adsorbate molecules fill up or cluster on the higher energy patches (i.e., a positive slope of the clustering value curve). The curve

will have a broad minimum due to the heterogeneity of the surface. This minimum is expected to be near the monolayer volume. Examining Fig. 37, a minimum does not exist at the monolayer volume, $\underline{V}_{\underline{m}}$, defined by the BET theory. In fact, the clustering function continues to decrease beyond the $\underline{V}_{\underline{m}}$ value. The volume range of the adsorption data does not include the monolayer volume, $\underline{V}_{\beta}$, defined by the multilayer adsorption model. It is anticipated that the clustering function values would begin to increase beyond the $\underline{V}_{\beta}$ value.

Very similar results were obtained for the nitrogen data. The clustering function *versus* the volume of nitrogen adsorbed on acid-hydrolyzed holocellulose at 77.5°K is presented in Fig. 38.

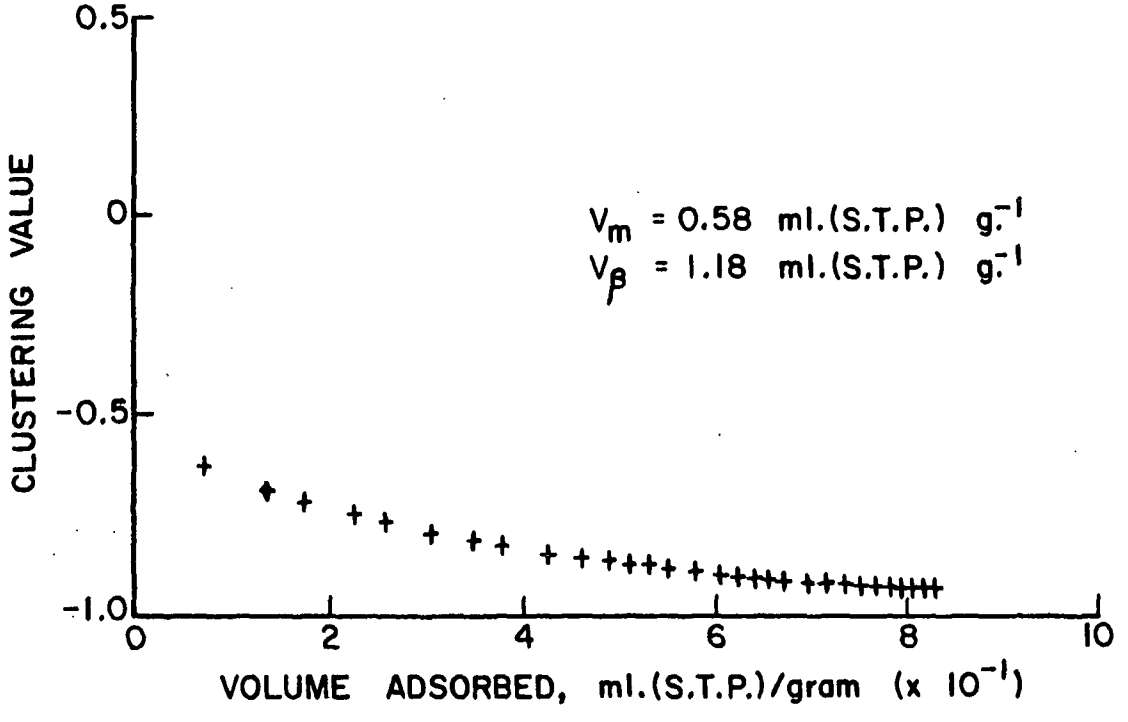

Figure 38. Clustering Function $\varphi_1 \underline{G}_{11}/\underline{v}_1$ for Nitrogen Adsorbed on Acid-Hydrolyzed Holocellulose at 77.5°K

The clustering function *versus* the volume of $CFCl_3$ adsorbed on acid-hydrolyzed holocellulose at 258.15°K is presented in Fig. 39. The clustering functions for the $CFCl_3$-cellulose system require a different interpretation.

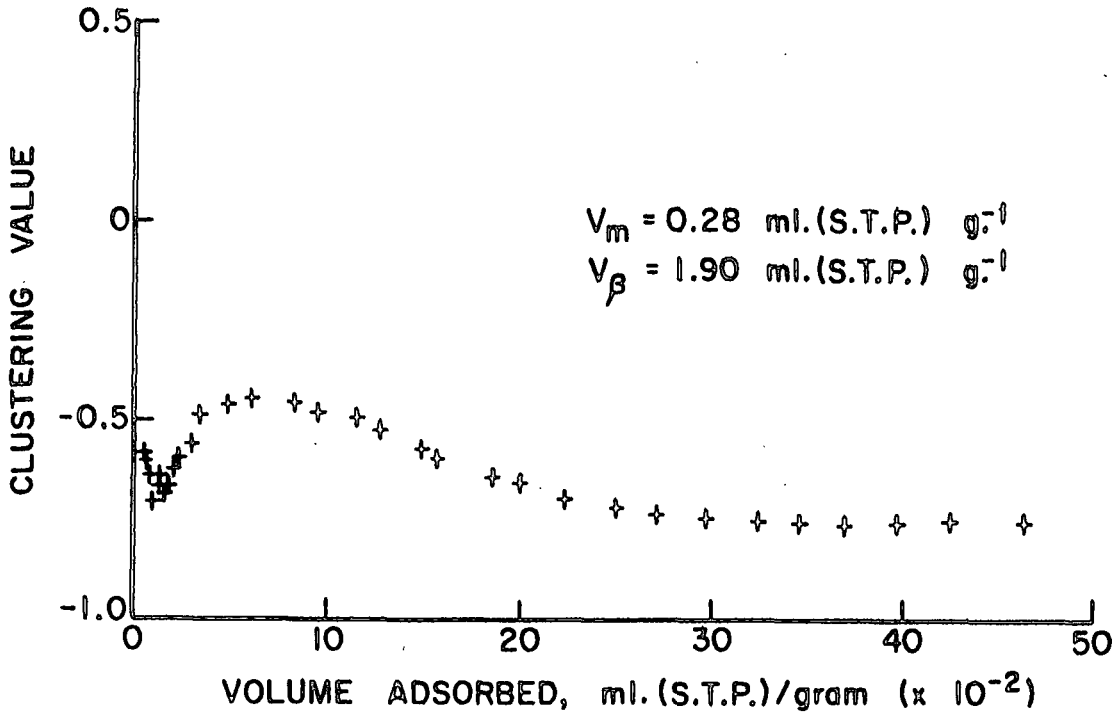

Figure 39. Clustering Function $\varphi_1 \underline{G}_{11}/\underline{v}_1$ for $CFCl_3$ Adsorbed on Acid-Hydrolyzed Holocellulose at 258.15°K

The initial negative slope can be explained in the same manner as for the argon data. However, at low coverage, as the volume adsorbed increases there is a short region of positive slope. This positive slope is due to the preferential adsorption of molecules on the higher energy homotattic patches. The clustering or preferential adsorption on these patches is due to the greater energy of interaction among the adsorbate molecules themselves (i.e., $2\alpha/\beta$ = 3.16 kcal./mole) than the adsorptive potential of a substantial portion of the surface homotattic patches. Only after a multilayer adsorbed phase is present on the higher energy patches do the lower energy patches begin to fill with adsorbate molecules. The filling of the lower energy unoccupied patches results in the negative slope of the clustering function curve after the local minimum. From this point on, the interpretation of the clustering function curve is similar to the argon and nitrogen data. In this

case, again, the BET theory predicts a monolayer volume, $\underline{V}_m$, at a volume where the clustering function is still decreasing.

These results seem to indicate that the BET theory does not yield an accurate estimate of the monolayer volume for the total accessible surface. For all three adsorbates, the monolayer volume estimate derived from the BET theory appears to be too low.

DISCREPANCIES BETWEEN MONOLAYER VOLUMES DETERMINED BY THE MULTILAYER ADSORPTION MODEL AND THE BET THEORY

The multilayer adsorption model was used to generate theoretical adsorption data for argon adsorbed on surfaces where the heterogeneity parameter, γ, and the median adsorptive potential, $\underline{U}^{Median}$, were varied. The other parameters in the multilayer adsorption model were fixed [$\underline{V}_\beta$ = 1.0 ml. (STP)/g. and $\nu = 1 \times 10^{12}$ sec.$^{-1}$]. The BET equation was applied to the model isotherms over the relative pressure range from 0.05 to 0.30 to determine the monolayer volume, $\underline{V}_m$, predicted by the BET theory. The results of these model calculations for the various median adsorptive potentials and different heterogeneity parameters are shown in Fig. 40 where $\underline{V}_\beta/\underline{V}_m$ is plotted as a function of γ and $\underline{U}^{Median}$. It is clear from this figure that the monolayer volume predicted from the BET equation is dependent on the median adsorptive potential as well as the width of the adsorptive potential distribution function as determined by the heterogeneity parameter. The discrepancies between the two monolayer volumes are especially magnified at the lower median adsorptive potentials. For median adsorptive potentials less than 1.25 kcal./mole, the monolayer volume, $\underline{V}_m$, predicted by the BET theory may be either greater than or less than the model monolayer volume, $\underline{V}_\beta$, depending upon the width of the adsorptive potential distribution.

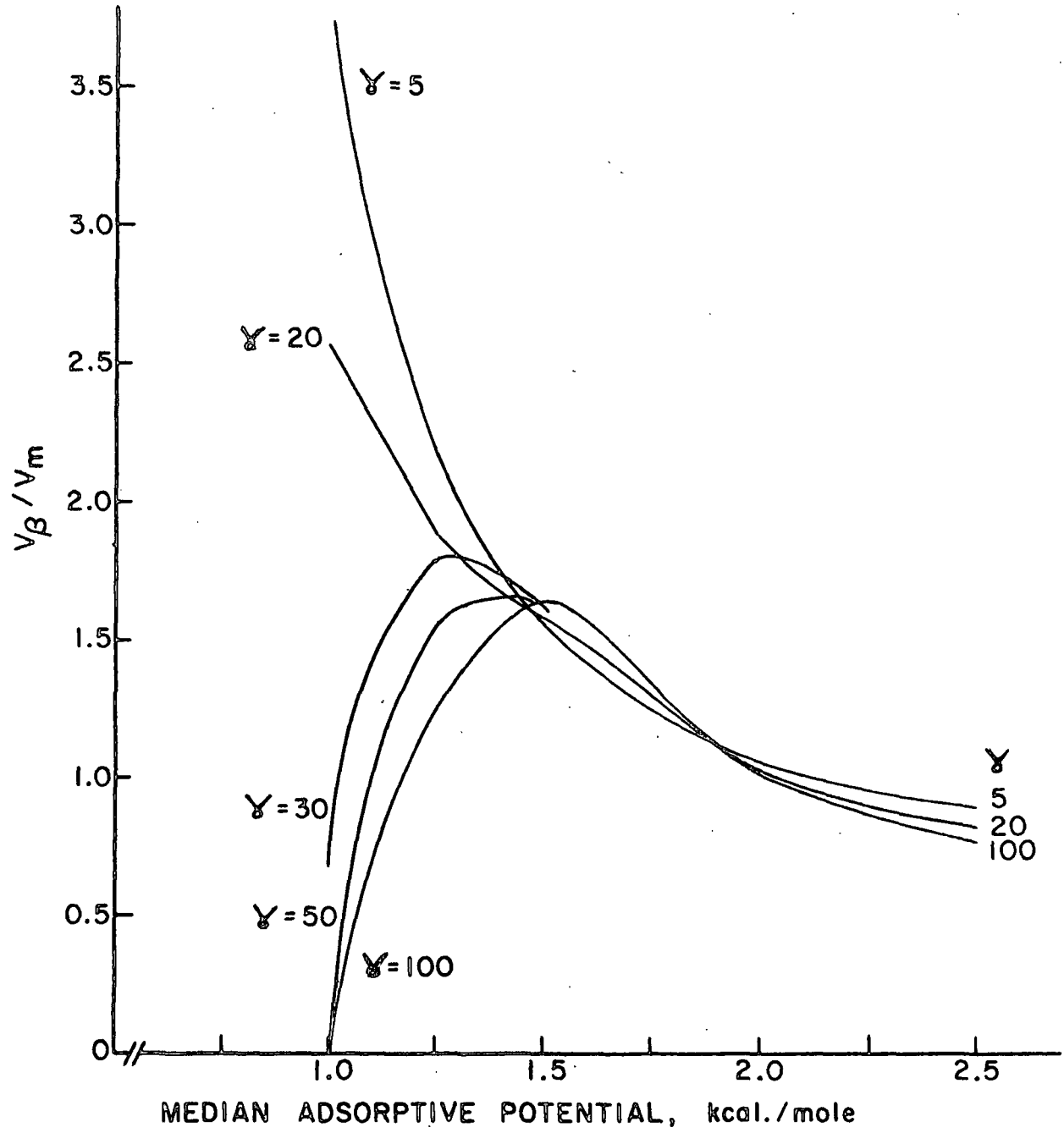

Figure 40. Variation of the Ratio $\underline{V}_\beta/\underline{V}_m$ with the Median Adsorptive Potential and the Heterogeneity Parameter

It is not pretended that the model isotherms calculated in this section are the ultimate in exact images of real adsorption isotherms. But the results in Fig. 40 may be taken as an indication that the accuracy of the results of the BET equation may be influenced by the adsorptive potential distribution median and width. Even when the BET theory is used to calculate relative surface areas of samples, one must be cognizant of the fact that the comparisons are accurate only when the adsorptive potential distribution is unchanged for the samples.

For the cellulosic samples investigated in this work, the BET monolayer volume, $\underline{V}_m$, is lower than the multilayer adsorption model monolayer volume, $\underline{V}_\beta$, by a factor of 1.5 or greater. Ross and Olivier (10) have suggested that the values of Σ_{BET} derived from $\underline{V}_m$ are only estimates of the surface area having an adsorptive potential greater than that of the adsorbate film (e.g., $2\alpha/\beta$ = 1.002 kcal./mole for argon). Considering the low and broad adsorptive potential distributions for the cellulosic substrates, it is obvious that the BET surface area estimates only a fraction of the total accessible surface area.

DESIGN OF GAS ADSORPTION EXPERIMENTS FOR USE WITH THE MULTILAYER ADSORPTION MODEL

In this section, the problem of designing experiments for generation of data to evaluate the parameters in the model will be considered. Since the form of the theoretical adsorption model is now known, the problem which confronts the experimenter is to constrain the unknown parameters of the model.

If experiments are not carefully planned, the experimental data may be so situated in the space of the variables that the estimates which can be obtained for the parameters $\underline{\varphi}$ are not only imprecise but also highly correlated. Once the data are collected, a statistical analysis, no matter how elaborate, can do nothing to remedy this unfortunate situation. However, by selecting a suitable experimental

design in advance, these shortcomings can often be avoided. Although the problem of designing experiments in nonlinear situations has received comparatively little attention by statisticians, some possible approaches have been suggested (59-61).

All of the approaches attempt to choose a design, $\underset{\sim}{D}$*, in such a manner that the volume of the approximate confidence region for $\underset{\sim}{\varphi}$ is minimized. If the experimental errors are approximately normally distributed and the model is approximately linear in the vicinity of the least-squares estimated parameters $\hat{\underset{\sim}{\varphi}}$, then the volume of the confidence region is proportional to the square root of the reciprocal of the determinant $|\underset{\sim}{J}^T\underset{\sim}{J}|$.

Unfortunately, since one does not know the values of the parameters $\hat{\underset{\sim}{\varphi}}$ (indeed, to obtain these estimates is the object of carrying out the experiment), one does not know the derivatives in $\underset{\sim}{J}$ on which the design is to be evaluated. In most cases, some knowledge of the size of the $\underset{\sim}{\varphi}$'s in the model will be available. It is suggested that preliminary guesses $\underset{\sim}{\varphi}^\circ$ should be made, and that the derivatives should be determined at these values $\underset{\sim}{\varphi}^\circ$ instead of $\underset{\sim}{\varphi}$. The resulting determinant $|\underset{\sim}{J}^{\circ T}\underset{\sim}{J}^\circ|$ is then an explicit function of the values of the independent variables in the model. It is therefore possible to find numerically those values for the independent variables in the model which maximize the determinant $|\underset{\sim}{J}^{\circ T}\underset{\sim}{J}^\circ|$. Thus, the optimum design, $\underset{\sim}{D}$, is chosen so as to maximize the determinant.

The need for some preliminary knowledge of the parameters is not peculiar to this method of experimental design. It is an example of the more general fact that, if nothing is known about the experimental situation, then, properly speaking, no experiment can be designed. The experimental design is thus efficient depending on whether the experimenter turns out to be nearly right on the parameter preliminary

*$\underset{\sim}{D}$ denotes the design matrix.

guesses $\underset{\sim}{\varphi}^{o}$. The statistical design of experiments is the art of determining on current evidence what additional experiments will furnish the most knowledge of the situation.

From the above discussion, it is obvious that the process of experimental investigation is an iterative one. Experimentation involves the steps of conjecture, design, experiment, and analysis continually repeated as illustrated in Fig. 41. Experimentation is thus essentially a dynamic process. Design leads to analysis via experiment, and analysis leads to new design via conjecture.

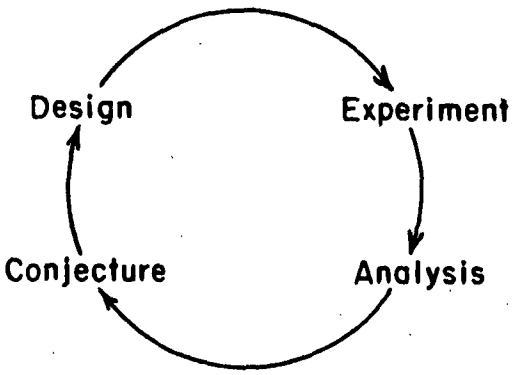

Figure 41. Experimentation

Of the two, design and analysis, the former is undoubtedly of greater importance. The damage of poor design is irreparable, no matter how ingenious the analysis; little information can be salvaged from poorly planned experimental data.

It is hoped that the multilayer adsorption model and nonlinear regression techniques developed in this thesis will be used by future workers, not only in analysis of gas adsorption data but also in the design of gas adsorption experiments so that the model parameters can be constrained within significant bounds.

CONCLUSIONS

The physical adsorption model for multilayer adsorption on a patchwise heterogeneous surface, which was developed in this thesis, offers a more realistic model for adsorption on extremely heterogeneous surfaces. Multilayer adsorption is likely to take place on the higher energy patches of heterogeneous surfaces before a significant monolayer coverage occurs on the lower energy patches. Since the Ross and Olivier model considers only monolayer coverage, the multilayer model is a significant improvement. Using the new adsorption model in combination with nonlinear regression analysis techniques, confidence intervals for the model parameters can be obtained for the first time. It was demonstrated that the nonlinear regression analysis procedures can be used not only to determine the precision of model parameter estimates but also to evaluate proposed adsorption experimental designs.

When the multilayer adsorption model and the nonlinear regression analysis techniques were applied to the argon adsorption data, the holocellulose and acid-hydrolyzed holocellulose had similar adsorptive potential distributions while the alkali-extracted holocellulose apparently had a lower and more uniform (i.e., higher γ) adsorptive potential distribution. The specific surface areas, Σ_β, were ranked in the same order as indicated by the electronmicrographs. Considering the results of the various methods used in characterizing the adsorbent samples (e.g., electronmicrographs, carbohydrate analysis, x-ray diffractometric procedures, etc.), one can speculate that the difference between the adsorptive potential distributions for the acid-hydrolyzed holocellulose and the alkali-extracted holocellulose was due to physical effects (i.e., surface imperfections, fissures, cracks, pores, etc.) or surface topology. However, the difference between the holocellulose and the alkali-extracted holocellulose was probably due to chemical effects (i.e., loss of hemicellulose components upon extraction).

Considering the results in Table XXV from fitting the multilayer adsorption model to the argon adsorption data at 77.4°K obtained by Deitrich (17) for the Stoneville-2B cotton, the model parameters indicated that the purified cotton was probably a lower energy surface than the three wood-derived cellulosic samples which were investigated in this thesis.

TABLE XXV

RESULTS OF FITTING MULTILAYER ADSORPTION MODEL TO ARGON ADSORPTION DATA FOR COTTON (17)

	SV-2B-3 Sample
$\underline{U}^{Median}$, kcal. mole^{-1}	1.10 ± 0.24
γ	4.23 ± 2.68
$\underline{V}_{\beta}$, ml. (STP) g.$^{-1}$	23.5 ± 12.3
$\nu \times 10^{12}$, sec.$^{-1}$	1.19 ± 0.40

For all three adsorbents, the estimated value of the operative two-dimensional Van der Waals constant, α^{op}, for argon did not differ significantly from the α^{Id} value at the 95% confidence level. This result indicated that the three cellulose adsorbents did not have a significant surface electric field, in agreement with the results of Deitrich (17) for cotton. The lack of a significant surface electric field confirmed the absence of surface dipoles for cellulosic substrates, indicating that the surface hydroxyl groups of the water-dried celluloses were internally involved in hydrogen bonding within the cellulose structure. Therefore, there was an insignificant contribution of the classical electrostatic interactions to the adsorptive potential.

The results of the nitrogen isotherm analysis ranked the adsorptive potential distribution and the specific surface area of the three cellulose adsorbents in the same order as the argon isotherms. The specific surface areas from the argon

and nitrogen isotherms for the same adsorbents were approximately equal as would be expected.

The almost linear Type III isotherms, instead of the curved Type II isotherms, obtained for the polar $CFCl_3$ adsorbate, confirmed the conclusion from the argon adsorption data that apparently no surface dipoles were present on the water-dried cellulose surfaces investigated. Only nonpolar adsorptive forces were functioning due to the lack of a significant surface electric field. The polar $CFCl_3$ adsorbate clustered in multilayers on the higher energy patches of the surface. The interaction energy was higher for the adsorbate-adsorbate interactions than adsorbate-surface interactions for the remaining lower energy patches of the surface. Thus, only the initial portion of the $CFCl_3$ adsorption isotherm was influenced by the surface, but the remaining portion of the isotherms was due to the multilayer formation on the higher energy patches, which is essentially a condensation phenomenon. Since the surface properties had little influence on the isotherm shape in the Type III case, the model parameters describing the surface were highly correlated and could not be constrained to a narrow enough range for comparative conclusions.

The application of clustering function theory to the adsorption data provides a molecular level interpretation of the physical adsorption process. For all three adsorbates, the clustering theory interpretation was compatible with the multilayer adsorption model analysis.

The BET theory analysis of the adsorption data ranked the adsorbent samples in terms of specific surface area and adsorptive potential (i.e., $\underline{c}$-parameter value) in the same order as the multilayer adsorption model analysis. However, the BET monolayer volume, $\underline{V}_m$, was lower than the multilayer adsorption model volume, $\underline{V}_\beta$, by a factor of 1.5 or greater for all the cellulosic samples. These

results confirmed that the monolayer volume predicted from the BET equation is dependent on the median adsorptive potential as well as the width of the adsorptive potential distribution.

In conclusion, it should be emphasized that the results obtained from this study apply only to the interaction of species with the cellulosic surfaces where hydrogen bonding is not involved.

SUGGESTIONS FOR FUTURE RESEARCH

A model for multilayer adsorption on heterogeneous surfaces has been sufficiently developed to be used as a research technique in characterizing the surface properties of solids. The next logical step in studying the surface chemistry of the cellulosic substrates should be an attempt to correlate other surface phenomena (e.g., interfiber bonding, adhesion, adsorption, wetting, etc.) with the adsorptive potential distribution and surface area derived from the model.

In particular, it is hoped that future workers will make use of the mathematical model and the nonlinear regression analysis techniques to design proposed gas adsorption experiments to constrain the model parameters adequately for interpretative use. For almost any conceivable adsorption substrate, enough information is available so that the feasibility of a proposed experimental design can be adequately tested.

Moreover, every effort should be made by future workers to use rigorous statistical methods in analyzing adsorption data, so that valid statistically sound conclusions can be made.

NOMENCLATURE

$\underline{a}$ = Van der Waals constant of a nonideal gas

$\underline{A}_o$ = temperature-dependent function of various changes of free energy and entropy which occur on adsorption

$\underline{b}$ = Van der Waals constant of a nonideal gas

$\underline{b}_1$, $\underline{b}_2$ = estimated values of the parameters β_1 and β_2

$\underline{B}$ = constant in Equation (2)

$\underline{c}$ = defined on page 14

cos = cosine function

$\underline{cov}(\underline{b}_i, \underline{b}_j)$ = covariance of parameters $\underline{b}_i$ and $\underline{b}_j$

$\underline{CrI}$ = percentage crystallinity index

$\underline{C}_1$-$\underline{C}_3$ = coefficients of terms in potential energy function

$\underline{C}_4$ = empirical constant in repulsive potential equation

$\underline{d}$ = diameter of the adsorbate molecule; minimum inside diameter of tube in millimeters

$\underline{\underline{D}}$ = design matrix

e = 2.7183; integration limit

exp[ ] = $e^{[\ ]}$

$\underline{E}$ = surface electric field intensity

$\underline{a}\underline{E}_o^{vib}$ = average vibrational energy of an adsorbed molecule at 0°K

$\underline{f}$ = normalizing factor for $\Phi(\underline{U})$ function; factor for diameter of the hangdown tubes; vibrational force constant

$\underline{f}(\ )$ = generalized model multilayer adsorption function

$\underline{a}\underline{F}^{vib}$ = additional Gibbs free energy of the absorbed phase due to molecular vibrations with respect to the surface

$\underline{F}_{\alpha(\underline{p},\underline{n}-\underline{p})}$ = α percentage point of the $\underline{F}$-distribution with $\underline{p}$ and $\underline{n}-\underline{p}$ degrees of freedom

$\underline{g}$ = integration limit

$\underline{G}_{11}$ = clustering integral

h = Planck's constant

i = index denoting the experimental set of data; index denoting the surface adsorptive potential distribution

I = moment of inertia of nitrogen molecule

IO = index of order

I_{am} = intensity of background scatter at $2\theta = 18°$

Ih = inordered height or minimum height of the diffraction pattern between 18 and 19° 2θ

I_A, I_B = moment of inertia about axis A, B, and C

I_{002} = intensity of the diffraction from the (002) plane at $2\theta = 22.6°$

j = index denoting the adsorbate layer

$\underset{\sim}{J}$ = $n \times p$ Jacobian matrix of partial derivatives

k = Boltzmann constant; number of lattice atoms per unit volume; summation index

k_i = defined in text on page 17

k' = value of k_i which corresponds to U' of the Gaussian distribution function k_i

K_j = defined in text on page 9

K_α = x-ray radiation wavelength line

ln = natural logarithm function

m = empirical constant in Equation (3); mass of the specified atom or molecule

M = molecular weight of the adsorbate; molarity

M_{buoy} = buoyancy correction to mass adsorption data

M_{corr} = corrected mass adsorption data

M_{raw} = raw or uncorrected mass adsorption data

M_{TMF} = thermomolecular flow effect correction to the mass adsorption data

n = normalizing factor for the log-normal distribution $\Psi(U_{i_1})$; number of experimental data points; degrees of rotational freedom

n_j = defined in text on page 9

N = Avogadro's number; normality

Oh = ordered height = $Th - Ih$

p = pressure; number of unknown parameters

p_c = adsorbate critical pressure

p_o = saturation vapor pressure

p_1 = pressure at sample temperature T_1

p_2 = pressure at gage temperature T_2

q = r_o/z

q^{diff} = differential heat of adsorption

q^{st} = isostericheat of adsorption

Q_L = heat of vaporization of the liquid adsorbate

Q^{rot} = rotational partition function

Q_1 = heat of adsorption of gas in first adsorbate layer

r = distance of separation of two atoms

r_i = distance between an adsorbed particle and lattice points of idealized solid

r' = constant in Equation (2)

r_o = equilibrium distance where $\partial u/\partial r = 0$

R = gas constant

R_m = defined in text on page 57

s^2 = error variance

S^{rot} = rotational entropy

T = absolute temperature; adsorption isotherm temperature; superscript denoting matrix transposition

T_c = adsorbate critical temperature

Th = total height of diffraction pattern between 22 and 23° 2θ

$u(r)$ = total interaction potential

$u_d(r)$ = dispersion interaction potential

$\underline{u}_{int}(\underline{r})$ = interaction potential due to interaction between adsorbed molecules

$\underline{u}_{r}(\underline{r})$ = repulsive interaction potential

$\underline{u}_{\mu}(\underline{r})$ = interaction potential due to the interaction between a permanent dipole in the adsorbate and the electric field of the adsorbent surface

$\underline{u}_{\xi}(\underline{r})$ = interaction potential due to polarization of the adsorbate by the surface

$\underline{u}_{o}$ = equilibrium interaction potential at $\underline{r} = \underline{r}_{o}$

$\underline{U}$ = adsorptive potential energy

$\underline{U}'$ = mean adsorptive potential at the maximum of the Gaussian distribution function

$\underline{U}_{\underline{i}}$ = surface adsorptive potential for monolayer adsorption on a heterogeneous surface

$\underline{U}_{\underline{i}1}$ = surface adsorptive potential for multilayer adsorption on a heterogeneous surface

$\underline{U}_{\underline{i}\underline{j}}$ = adsorptive potential for multilayer adsorption on a heterogeneous surface, where $\underline{i}$ denotes the surface adsorptive potential distribution, and $\underline{j}$ denotes the adsorbate layer

$\underline{U}_{\underline{j}}$ = adsorptive potential at the $\underline{j}$th adsorbate layer on a homogeneous surface

$\underline{U}_{1}$ = uniform surface adsorptive potential for a homogeneous surface

$\underline{U}^{Mean}$ = mean or average adsorptive potential

$\underline{U}^{Median}$ = median adsorptive potential

$\underline{U}^{Mode}$ = most probable adsorptive potential

$\underline{v}_{1}$ = partial molecular volume of Component 1

$\underline{V}$ = volume adsorbed

$\underline{V}(\underline{b}_{\underline{i}})$ = variance of parameter $\underline{b}_{\underline{i}}$

$\underline{V}_{ADS}$ = volume adsorbed

$\underline{V}_{\underline{B}}$ = sample volume

$\underline{V}_{\underline{c}}$ = counterweight volume

$\underline{V}_{\underline{m}}$ = monolayer volume defined by the BET equation

$\underline{V}_{\beta}$ = monolayer volume defined by the Ross and Olivier or multilayer adsorption model

$\underline{V}$ = value of the dependent variable, volume, predicted by the model

$\underline{w}$ = radial distance from the $\underline{z}$ axis to a point in the interior of the continuum

$\underline{W}(\underline{z})$ = total energy of interaction between the adsorbate and the semi-infinite continuum solid

$\underline{W}_o$ = depth of potential energy minimum

$\underline{x}$ = orthogonal coordinate in the plane of the surface; $\underline{p}_2\underline{d}$, as defined in text on page 57; fraction of nitrogen adsorbate molecules in the flat position

$\underline{y}$ = orthogonal coordinate in the plane of the surface

$\underline{z}$ = shortest distance from gas atom or molecule to the surface

$\underline{z}_o$ = equilibrium distance between the surface of a continuum and an adsorbate molecule

$\underline{z}_{\underline{x}}$ = activity of species $\underline{x}$

α = two-dimensional analog of Van der Waals constant $\underline{a}$

α^{Id} = ideal value of α

α^{op} = operative value of α

α_{He} = constant defined in text on page 57

$2\alpha/\beta$ = heat of condensation for a two-dimensional Van der Waals gas

β = two-dimensional analog of Van der Waals constant $\underline{b}$

β^{Id} = ideal value of β

β^{op} = operative value of β

β_{He} = constant defined in text on page 57

β_1, β_2 = parameters used in illustration on page 39

γ = heterogeneity parameter for the log-normal distribution

$\gamma_{\underline{x}}$ = volume fraction activity coefficient of species $\underline{x}$

$d\delta_{\underline{i}}$ = fraction of surface having energies between $\underline{U}$ and $\underline{U} + d\underline{U}$

$\Delta\underline{E}^{kin}$ = change in kinetic energy of translation and rotation upon adsorption

$\Delta\underline{S}^{rot}$ = rotational entropy change upon adsorption

ΔS_s^{tr} = integral translational entropy change upon adsorption

ΔS^{vib} = vibrational entropy change upon adsorption

Δw = difference between the buoyancy force on the counterweight and on the sample

$\Delta \delta_i$ = incremental fraction of surface with energies between U and $U + dU$

η = viscosity of the gas

θ = Bragg angle of diffraction; degree of coverage of a homotattic patch by a closely packed monolayer of adsorbate

θ_i = fractional coverage of the ith homotattic patch for monolayer adsorption on a heterogeneous surface

θ_{ij} = fractional coverage of the jth adsorbate layer and the ith homotattic patch for multilayer adsorption on a heterogeneous surface

θ_j = fractional coverage of the jth adsorbate layer on a homogeneous surface

θ_s = fractional coverage of the surface at the standard state of the adsorbed phase

Θ = fractional coverage of the total surface

λ = polarization factor in Equation (70)

μ = dipole moment

$\bar{\mu}$ = permanent dipole moment

μ^{ind} = induced dipole moment

ν = adsorbate vibrational frequency normal to the surface

ν_z = lowest vibrational frequency of molecule in the potential well

ξ = polarizability of a molecule; eigenvalue of a matrix

π = 3.14159

Π = product notation

ρ = number of "equivalent lattice points" per unit volume

ρ_{ij} = correlation coefficient

σ = symmetry factor

σ_o = molecular cross-sectional area of the adsorbate

$\sigma_{\underline{M}}$ = standard deviation of the adsorption data terms

$\sum$ = summation notation

Σ_β = specific surface area of the adsorbent calculated from $\underline{V}_\beta$

Σ_{BET} = specific surface area of the adsorbent calculated from $\underline{V}_{\underline{m}}$

τ = constant in Equation (92)

φ = parameter matrix

φ^o = initial guess parameter matrix

$\hat{\underset{\sim}{\varphi}}$ = least squares estimated parameter matrix

$\varphi_{\underline{g}}$ = pressure shifting factor

$\varphi_{\underline{x}}$ = volume fraction of species $\underline{x}$

$\Phi(\underline{U})$ = Gaussian distribution of potential energy $\underline{U}$

Ψ = angle between the axis of the dipole and the surface electric field

$\Psi(\underline{U}_{\underline{i}\,l})$ = log-normal distribution of the potential energy $\underline{U}_{\underline{i}\,l}$

ω = orientation factor

$\int$ = integral

∞ = infinity

$\sim$ = subscript denoting matrix notation

$|\ |$ = determinant

$||$ = superscript denoting an orientation of the molecular axis parallel to the surface

$\perp$ = superscript denoting an orientation of the molecular axis perpendicular to the surface

ACKNOWLEDGMENTS

Many people have contributed directly or indirectly to the successful completion of this thesis. The author is indebted to each one for his or her assistance.

The guidance, support, and criticism of Mr. John W. Swanson, Chairman of my Advisory Committee, and other members of the Committee, Dr. Rajai H. Atalla and Dr. Robert Holm, during this thesis are greatly appreciated.

The discussions with Dr. Richard Nelson on nonlinear regression analysis in this study are also acknowledged with appreciation.

Finally, I would like to express my most sincere gratitude to Ms. Marilyn Kinsey, whose faith, patience, encouragement, and assistance made possible the completion of this work.

LITERATURE CITED

1. deBoer, J. H. Advances in colloid Science. Vol. 3. New York, Interscience, 1950. 384 p.

2. Crowell, A. D. Surface forces. In The solid-gas interface. E. A. Flood, Ed. I. p. 175-99. New York, Marcel Dekker, Inc., 1967.

3. Honig, J. M., Ann. N.Y. Acad. Sci. 58:741(1954).

4. Clark, A. The theory of adsorption and catalysis. New York, Academic Press, 1970. 418 p.

5. Hill, T. L., J. Chem. Phys. 16:181(1948).

6. Halliday, D., and Resnick, R. Physics for students of science and engineering. New York, John Wiley and Sons Inc., 1963. 1122 p.

7. Gregg, S. J., and Sing, K. S. W. Adsorption, surface area, and porosity. New York, Academic Press, 1967. 371 p.

8. Brunauer, S., Deming, L. S., Deming, W. E., and Teller, E. J., J. Am. Chem. Soc. 62:1723(1940).

9. Brunauer, S., Emmett, P. H., and Teller, E. J., J. Am. Chem. Soc. 66:309(1938).

10. Ross, S., and Olivier, J. P. On physical adsorption. New York, Interscience, 1964. 401 p.

11. Ross, S. The homotattic surface. In The solid-gas interface. E. A. Flood, Ed. I. p. 491-501. New York, Marcel Dekker, Inc., 1967.

12. Ross, S. The heterogeneity of solid substrates. In Burke, Reed, and Weiss's Surfaces and interfaces. I. p. 169-96. Syracuse, New York, Syracuse University Press, 1967.

13. Stamm, A. J. Wood and cellulose science. New York, Ronald Press, 1964. 549 p.

14. Pierce, C. J., J. Phys. Chem. 57:149(1953).

15. Haselton, W. R. An investigation of the adsorption of gases by wood and its components and of gas adsorption techniques as a means of studying the area and structure of pulp and paper. Doctor's Dissertation. Appleton, Wis., The Institute of Paper Chemistry, 1953. 172 p.

16. Barber, H. A. The determination of the energy site distribution of the surface of cellulose fibers by gas adsorption method. Doctor's Dissertation. Appleton, Wis., The Institute of Paper Chemistry, 1968. 107 p.

17. Deitrich, W. H. A comparison of adsorptive potential energies for argon and nitrogen adsorption on the surface of cellulose fibers. Doctor's Dissertation. Appleton, Wis., The Institute of Paper Chemistry, 1970. 181 p.

18. Chessick, J. J., Zettlemoyer, A. C., Healey, F. H., and Young, G. J., Can. J. Chem. 33:251(1955).

19. Duval, X., and Thomy, A., C. R. Acad. Sci., Paris 259:4007(1964).

20. deBoer, J. H., and Broekhoff, J. C. P., (a) Proc. Kon. Ned. Ak. v. Wet. B70: 317(1967); (b) B70:326(1967); (c) B70:333(1967); (d) B70:342(1967); and (e) B70:354(1967).

21. Beebe, R. A., and Young, D. M., J. Phys. Chem. 58:93(1954).

22. Hoory, S. E. Adsorption of gases on homogeneous and heterogeneous surfaces. Doctor's Dissertation. Berkeley, Calif., University of California, Berkeley, 1966.

23. Aitchison, J., and Brown, J. A. C. The log-normal distribution. Cambridge, Cambridge University Press, 1957. 176 p.

24. Draper, N. R., and Smith, H. Applied regression analysis. p. 407. New York, John Wiley and Sons, Inc., 1966.

25. Marquardt, D. W., J. Soc. Ind. Appl. Math. 11:431(1963).

26. Smith, F. B., Jr., and Shanno, D. F., Technometrics 13:63(1971).

27. Mayer, J. E., and Mayer, M. G. Statistical mechanics. p. 494. New York, John Wiley and Sons, 1940.

28. McMillan, W. G., and Mayer, J. E., J. Chem. Phys. 13:276(1945).

29. Kirkwood, J. G., and Buff, F. P., J. Chem. Phys. 19:774(1951).

30. Zimm, B. H., J. Chem. Phys. 14:164(1946).

31. Zimm, B. H., and Lundberg, J. L., J. Phys. Chem. 60:425(1956).

32. Lohr, J. E., and Scholz, J. J., J. Colloid Sci. 20:846(1965).

33. Hoburg, R. F., Handler, G. S., and Scholz, J. J., J. Colloid Interfacial Sci. 28:443(1968).

34. Braught, D. C., Bruning, D. D., and Scholz, J. J., J. Colloid Interfacial Sci. 31:263(1969).

35. Ferchak, J. D., Rev. Sci. Instr. 38:273(1967).

36. Liang, S. C., J. Appl. Phys. 22:1581(1951); J. Phys. Chem. 53:811(1949).

37. Bennett, M. J., and Tompkins, F. C., Trans. Faraday Soc. 53:185(1957).

38. Mason, E. A., Evans, R. B., and Watson, G. W., J. Chem. Phys. 38:1808(1963).

39. Thomas, J. M., and Poulis, J. A., Vac. Microbalance Tech. 3:15(1963).

40. Poulis, J. A., and Thomas, J. M., J. Sci. Instr. 40:95(1963).

41. Wolsky, S. P., and Zdanuk, E. J. Ultra micro weight determinations in controlled environments. New York, Interscience, 1969. 511 p.

42. Browning, B. L. Methods of wood chemistry. Vol. II. New York, Interscience, 1967. 882 p.

43. Thompson, N. S., and Kaustinen, O. A., Tappi 47:157(1964).

44. Ranby, B. G. Doctor's Dissertation. Uppsala, 1952. (Source: Browning, B. L., The chemistry of wood. New York, Interscience, 1963. 689 p.)

45. Battista, O. A., Ind. Eng. Chem. 42:502(1950).

46. Battista, O. A., U.S. pat. 2,978,446(April 4, 1961).

47. Borchardt, L. G., and Piper, C. V., Tappi 53:257(1970).

48. TAPPI Suggested Method T 230 su-66.

49. LeFevre, J. W., and Ritchie, G. L. D., J. Chem. Soc. 1965:3520.

50. Segal, L., Creely, J. J., Martin, A. E., Jr., and Conrad, C. M., Text. Res. J. 29:786(1959).

51. Ant-Wuorinen, O., and Visapää, A., Paperi Puu 47:311(1965).

52. Emmett, P. H., and Brunauer, S., J. Am. Chem. Soc. 59:1953(1937).

53. Hendra, P. J., and Loader, E. J., Trans. Faraday Soc. 67:828(1971).

54. Glasstone, S. Theoretical chemistry. New York, D. Van Nostrand Co., Inc., 1944. 513 p.

55. deBoer, J. H., and Kruyer, S., Koninkl. Ned. Akad. Wetenshap. Proc. 55B:451 (1952).

56. deBoer, J. H. The dynamical character of adsorption. p. 240. Oxford, Clarendon Press, 1968.

57. Silverstein, R. M., and Bassler, G. C. Spectrometric identification of organic compounds. New York, John Wiley and Sons, Inc., 1963.

58. Mitra, S., J. Chem. Phys. 36:3286(1962).

59. Box, G. E. P., Ann. N.Y. Acad. Sci. 86:792(1960).

60. Box, G. E. P., and Hunter, W. G., Technometrics 4:301(1962).

61. Box, G. E. P., and Hunter, W. G., Technometrics 7:23(1965).

62. Hartley, H. O., Technometrics 3:269(1961).

63. Dennis, J. E., Jr., Proc. Assocn. Computing Machinery 1971:446.

64. Marquardt, D. W., Technometrics 12:591-612(1970).

65. Hoerl, A. E., and Kennard, R. W., Technometrics 12:55-67(1970).

66. Atkinson, A. C., and Hunter, W. G., Technometrics 10:271-89(1968).

67. Morrison, D. F. Multivariate statistical methods. p. 338. New York, McGraw-Hill Book Co., Inc., 1967.

68. Guttman, I., and Meeter, D. A., Technometrics 7:623-37(1965).

69. Hill, T. L. An introduction to statistical thermodynamics. Reading, Mass., Addison-Wesley Publishing Co., Inc., 1960. 508 p.

70. Hill, T. L. Statistical mechanics. New York, McGraw-Hill Book Co., Inc., 1956. 432 p.

71. Friedman, H. L. Ionic solution theory. New York, Interscience, 1962. 265 p.

72. Eyring, H., Henderson, D., and Jost, W. Physical chemistry an advanced treatise. Vol. II. New York, Academic Press, 1967. 561 p.

APPENDIX I

NONLINEAR REGRESSION ANALYSIS

INTRODUCTION

The experimental scientist is frequently faced with the task of fitting a model in the form of a functional relationship between a response variable, $\underline{Y}$, and a number of input variables, $\underline{x}_1$, $\underline{x}_2$, ..., $\underline{x}_k$, that have been collected during a controlled experiment. Often a mathematical relationship is assumed and is written in the form of a regression function

$$Y = f(x_1, x_2, \ldots, x_k; \phi_1, \phi_2, \ldots, \phi_p) + \varepsilon. \qquad (94)$$

The explicit regression function, f, is referred to as linear or nonlinear in the unknown parameters ϕ_1, ϕ_2, ..., ϕ_p. The residual, ε, is the difference between the observed response, $\underline{Y}$, and the response calculated from the regression function.

The sum of squares of the residuals,

$$S(\underset{\sim}{\phi}) = \Sigma\underset{\sim}{\varepsilon}^2 = \Sigma(\underset{\sim}{Y}-\underset{\sim}{f})^2 \qquad (95)^*$$

is a $\underline{p}$-variable function of the parameters ϕ_1, ϕ_2, ..., ϕ_p. The method most frequently employed to estimate the values of the unknown parameters is the Method of Least Squares which minimizes the sum of squares of the residuals as a function of the unknown parameters.

When the regression function f is linear in the parameters, the $\underline{p}$ equations resulting from setting $\partial\underline{S}(\underset{\sim}{\phi})/\partial\phi_{\underline{j}} = 0$ for $\underline{j} = 1,2,\ldots,\underline{p}$, are linear in the $\phi_{\underline{j}}$ and they are known as the normal equations in multiple regression estimation. When the regression function is nonlinear in the parameters, both the theory and the practice of the estimation procedure is considerably more difficult (24).

*The subscript $\sim$ denotes matrix notation.

FORMULATION OF THE NONLINEAR REGRESSION PROBLEM

Consider the following nonlinear least squares problem: Given n sets of experimental observations

$$(Y_i, x_{1i}, x_{2i}, \ldots, x_{ki}) \qquad i = 1,2,\ldots, n \tag{96}$$

fit the regression equation

$$\underset{\sim}{Y} = f(\underset{\sim}{x}, \underset{\sim}{\phi}) \tag{97}$$

where

$$\underset{\sim}{x} = (x_1, x_2, \ldots, x_k)^T \tag{98}*$$

and

$$\underset{\sim}{\phi} = (\phi_1, \phi_2, \ldots, \phi_p)^T \tag{99}$$

to the data (62). The problem is to estimate the parameter values which will minimize

$$S(\underset{\sim}{\phi}) = \sum_{i=1}^{n} [Y_i - f_i(\underset{\sim}{x}, \underset{\sim}{\phi})]^2. \tag{100}$$

ESTIMATING THE PARAMETERS OF A NONLINEAR SYSTEM

An iterative procedure is used to estimate the parameter values which will minimize $S(\underset{\sim}{\phi})$. An initial informed guess of the parameter values, $\underset{\sim}{\phi}^0$, must be supplied. The algebraic form of the iterative procedure is

$$\underset{\sim}{\phi}^{s+1} = \underset{\sim}{\phi}^s + \underset{\sim}{\delta}^s \tag{101}$$

where the superscripts indicate the iteration index, and $\underset{\sim}{\delta}^s$ is the increment vector computed at $\underset{\sim}{\phi}^s$. There are several methods available to compute the increment vector: (1) linearization, (2) steepest descent, and (3) Marquardt's compromise.

*The superscript T denotes matrix transposition.

LINEARIZATION

The Gauss-Newton method uses a linearization of the function by a Taylor series to compute successive linear least square estimates of the parameters.

$$f(x_i, \underset{\sim}{\phi} + \underset{\sim}{\delta}_t) = f(x_i, \underset{\sim}{\phi}) + \sum_{j=1}^{p} \left(\frac{\partial f_i}{\partial \phi_j}\right)(\underset{\sim}{\delta}_t)_j \tag{102}$$

or

$$\underset{\sim}{f} = \underset{\sim}{f}^{\circ} + \underset{\sim}{J}\underset{\sim}{\delta}_t. \tag{103}$$

The vector $\underset{\sim}{\delta}_t$ is a small correction to $\underset{\sim}{\phi}$, with the subscript t used to designate $\underset{\sim}{\delta}$ as calculated by this Taylor series method. $\underset{\sim}{J}$ is the n by p Jacobian matrix of partial derivatives $\partial f_i/\partial \phi_j$. The matrix $\underset{\sim}{J}$ is obtained by finite difference quotients, and therefore is a discrete approximation to a matrix of first-order partial derivatives (63). The ratios are computed as

$$[f(\underset{\sim}{x}, \underset{\sim}{\phi} + h_j) - f(\underset{\sim}{x}, \underset{\sim}{\phi})]/h_j \qquad j = 1,2,\ldots, p \tag{104}$$

where h_j is a small increment. Equation (104) is an approximation to the expression

$$\left[\frac{\partial f(\underset{\sim}{x}, \underset{\sim}{\phi})}{\partial \phi_j}\right]_{\underset{\sim}{\phi}=\phi_j} \tag{105}$$

since by definition, the limit of Equation (104) as $h_j \to 0$ is Equation (105).

Since δ_t appears linearly in Equation (102), δ_t can therefore be found by the standard least squares method of setting $S(\underset{\sim}{\phi})/\partial\phi_j = 0$ for all j. Thus, δ_t is found by solving

$$\underset{\sim}{A}\,\underset{\sim}{\delta}_t = g \tag{106}$$

where

$$\underset{\sim}{A}^{(P\times P)} = \underset{\sim}{J}^T\underset{\sim}{J} \tag{107}$$

$$\underset{\sim}{J}^{(n\times P)} = \partial f_i/\partial\phi_j \qquad i = 1,2,\ldots, n \quad j = 1,2,\ldots, p \tag{108}$$

$$\underset{\sim}{g}^{(p\times 1)} = \sum_{i=1}^{n} (Y_i - f_i)(\partial f_i/\partial \phi_j) \qquad j = 1,2,\ldots, p$$

$$= \underset{\sim}{J}^T(\underset{\sim}{Y} - \underset{\sim}{f}). \tag{109}$$

The Gauss-Newton vector is therefore,

$$\underset{\sim}{\delta}_t = (\underset{\sim}{J}^T\underset{\sim}{J})^{-1}\ \underset{\sim}{J}^T\ (\underset{\sim}{Y} - \underset{\sim}{f}) \tag{110}$$

or

$$\underset{\sim}{\delta}_t = (\underset{\sim}{A})^{-1}\ \underset{\sim}{g}. \tag{111}$$

A linear function can be solved by this method in just one iteration.

STEEPEST DESCENT

The steepest descent or gradient method steps off from the current trial value in the direction of the negative gradient. The gradient of $\underline{S}(\phi)$ is the vector with components $\underline{S}(\underset{\sim}{\phi})/\partial\phi_{\underline{j}}$, $\underline{j} = 1,2,\ldots,\underline{p}$ more conveniently written in the matrix form as $\nabla\underline{S}(\underset{\sim}{\phi}) = -2\underset{\simeq}{g}$.

The gradient search method attempts to locate a point where $\nabla\underline{S}(\underset{\sim}{\phi}) = 0$ with $\underline{S}(\underset{\sim}{\phi})$ approximated locally as a first-order Taylor series. Search methods using the gradient are called steepest descent methods where the gradient search vector, $\underset{\sim}{\delta}_{\underline{g}}$, equals $\underset{\simeq}{g}$. Although a steepest descent strategy has been found to be good initially, especially when the starting point is some distance from the minimum, the Gauss-Newton search has better convergence properties. Despite this advantage, the strict use of the Gauss-Newton search in nonlinear least squares problems has very real computational difficulties. Inverting the matrix $\underset{\simeq}{J}^T\underset{\simeq}{J}$ requires considerable care because of the near singular conditions which may occur. Always lurking as a subtle danger is the nearly singular situation where a vector, $\underset{\sim}{\delta}_{\underline{t}}$, of considerable length is determined, relocating the search to some remote region of space

incompatible with the initial estimates. In addition, an ill-conditioned $\underset{\sim}{J}^T\underset{\sim}{J}$ matrix may occur by chance at any stage of the search if the partial derivatives with respect to one parameter should become much smaller than derivatives with respect to another parameter.

MARQUARDT'S COMPROMISE

Marquardt's compromise reduces this difficulty by searching with a more general gradient, the Newton-Raphson vector

$$\underset{\sim}{\delta}_n = (\underset{\sim}{J}^T\underset{\sim}{J} + \underset{\sim}{C})^{-1}\,\underset{\sim}{g}. \tag{112}$$

Here an arbitrary square matrix $\underset{\sim}{C}$ is defined to accelerate convergence and avoid singularities. Marquardt noted that the properties of the gradient (25, 64) methods are not scale invariant. It is necessary to scale the parameter space in some convenient manner. He chose to scale the parameter space in units of standard deviations of the derivatives $\partial f_i/\partial\phi_j$ taken over the sample points $i = 1,2,\ldots,n$. This choice of scale causes the $\underset{\sim}{A}$ matrix to be transformed into the matrix of simple correlation coefficients among the $\partial f_i/\partial\phi_j$. Furthermore, this choice of scaling is widely used in linear least squares methods for improving the numerical aspects of the computing procedures. The scaled matrices $\underset{\simeq}{A}^*$ and $\underset{\simeq}{g}^*$ are defined as

$$\underset{\sim}{A}^* = A^*_{jj'} = A_{jj'}/(\sqrt{A_{jj}}\,\sqrt{A_{j'j'}}) \tag{113}$$

$$\underset{\sim}{g}^* = g^*_j = g_j/\sqrt{A_{jj}}\,. \tag{114}$$

The Gauss-Newton vector, $\underset{\sim}{\delta}_t$, is solved, using $\underset{\simeq}{A}^*\underset{\sim}{\delta}^*_t = \underset{\simeq}{g}^*$ where

$$\underset{\sim}{\delta}_t = \underset{\sim}{\delta}^*_t/\sqrt{A_{jj}}. \tag{115}$$

Marquardt then worked with the vector

$$\underset{\sim}{\delta}_M^* = (\underset{\sim}{A}^* + \lambda \underset{\sim}{I})^{-1} \underset{\sim}{g}^* \tag{116}$$

the Newton-Raphson vector with $\underset{\sim}{C} = \lambda \underset{\sim}{I}$, where λ is a finite non-negative scalar and $\underset{\sim}{I}$ is the identity matrix. For $\lambda = 0$, $\underset{\sim}{\delta}_M = \underset{\sim}{\delta}_t$ the Gauss-Newton vector; as $\lambda \to \infty$, the orientation of $\underset{\sim}{\delta}_M$ approaches $\underset{\sim}{\delta}_g$, the gradient vector. Thus, Marquardt's vector, $\underset{\sim}{\delta}_M$, combines the better features of both the steepest descent and the Gauss-Newton search methods through a single blending parameter λ. The vector $\underset{\sim}{\delta}_M$ decreases monotonically in length as λ increases.

Figure 42 illustrates a system of contours representing constant values of $\underline{S}(\underset{\sim}{\phi})$ in a two parameter space. The minimum value of $\underline{S}(\underset{\sim}{\phi})$ is at $\hat{\underset{\sim}{\phi}}$. $\underset{\sim}{\phi}^\circ$ represents the base location of the search vector initially or at a given iteration. The local contours at $\underset{\sim}{\phi}^\circ$ are linearly approximated by an ellipse which is indicated with a dashed line. The steepest descent vector, $\underset{\sim}{\delta}_g$, is normal to this ellipse; the Gauss-Newton vector, $\underset{\sim}{\delta}_t$, is directed toward the center of the ellipse. The locus of the Marquardt search vector, $\underset{\sim}{\delta}_M$, is the twisted dotted curve segment $\underset{\sim}{\Gamma}$. The appropriate selection of λ will orient the $\underset{\sim}{\delta}_M$ vector to penetrate the $\underline{S}(\underset{\sim}{\phi})$ contours toward the true minimum $\hat{\underset{\sim}{\phi}}$, more deeply than either the $\underset{\sim}{\delta}_g$ or $\underset{\sim}{\delta}_t$ vectors.

The broad outline of the algorithm to estimate the nonlinear parameters is clear. At the sth iteration, the equation

$$(\underset{\sim}{A}^{*s} + \lambda^s \underset{\sim}{I})\, \underset{\sim}{\delta}_M^{*s} = \underset{\sim}{g}^{*s} \tag{117}$$

is constructed. This equation is then solved for $\underset{\sim}{\delta}_M^{*s}$. Then Equation (115) is used to obtain $\underset{\sim}{\delta}_M^s$. The new trial vector $\underset{\sim}{\phi}^{s+1} = \underset{\sim}{\phi}^s + \underset{\sim}{\delta}_M^s$ will lead to a new sum of squares $\underline{S}(\underset{\sim}{\phi})^{s+1}$.

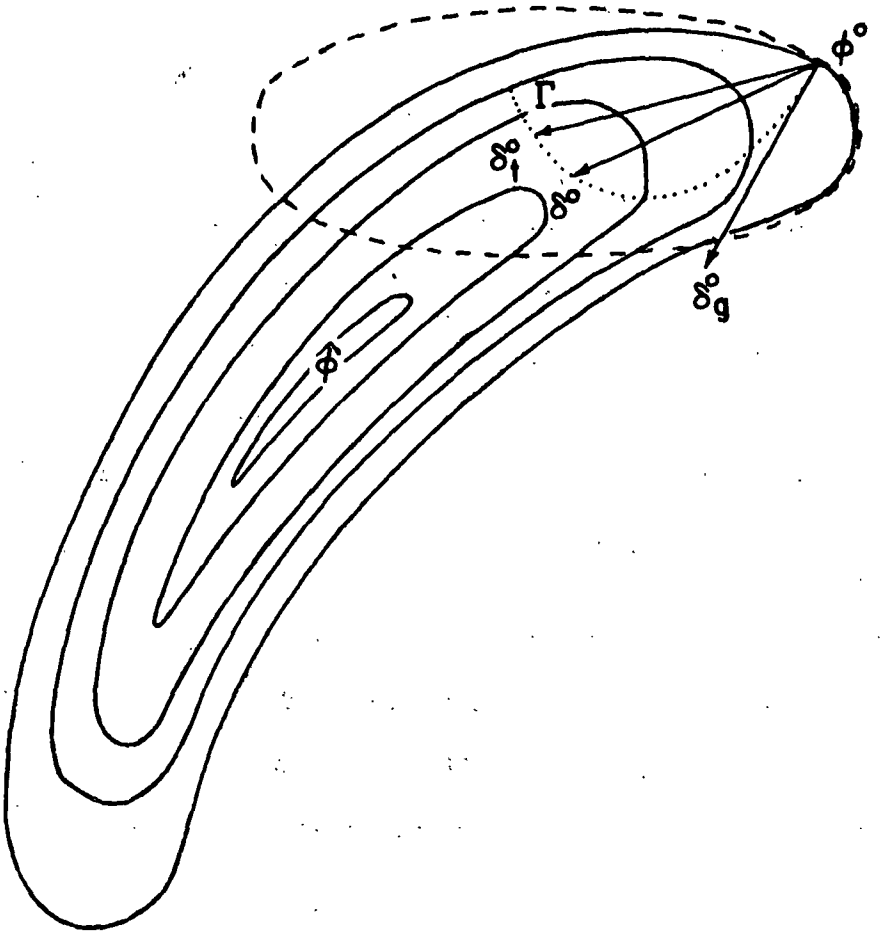

Figure 42. $S(\underset{\sim}{\phi})$ Contours in a Hypothetical Two-Parameter Space (26)

It is essential to select $\underline{\lambda}^s$ such that

$$S(\underset{\sim}{\phi})^{s+1} < S(\underset{\sim}{\phi})^s \tag{118}$$

It should be clear from the foregoing theory that a sufficiently large $\underline{\lambda}^s$ always exists such that Equation (118) will be satisfied unless $\underset{\sim}{\phi}^s$ is already at a minimum of $S(\underset{\sim}{\phi})$.

OPTIMIZING THE SCALING FACTOR

The strategy for choosing λ must seek to use as small a value of λ, i.e., as large a step δ_M, as possible to accelerate the convergence. This is especially pertinent in the later stages of the search procedure when the guesses are in the immediate vicinity of the minimum, where the contours of $S(\phi)$ are asymptotically elliptical, and where the linear expansion of the model needs to be a good approximation over only a very small region. Under this condition the unmodified Taylor series method will converge nicely.

A technique has been developed for estimating a value of λ for substitution into Equation (117) such that $S(\phi)$ is locally minimal along the arc Γ of Fig. 42. The analytic determination of λ used in this thesis is similar to the method suggested by Smith and Shanno (26). Selection of a search procedure for λ is largely a matter of personal preference, but a requisite for any search should be a control to keep λ away from its danger zone near zero when $J^T J$ is nearly singular.

In formulating an initial guess for λ_1 for each iteration, the condition number, μ, for the matrix $J^T J$ was used as a control. It is defined as $\mu = \xi_1/\xi_p$, where ξ_1 and ξ_p are the largest and smallest eigenvalues of $J^T J$, respectively. Indicating the iteration number by a superscript, and the sub-iteration number by a subscript, the initial guess $\lambda_1^s = 10^{-8}\,\mu^s$, is near zero when $(J^T J)^s$ is well conditioned and one wants to move in the Gauss-Newton direction. But for $(J^T J)^s$ ill-conditioned, the initial guess of λ_1^s is pulled away from zero.

Using this initial guess a search is performed to obtain the locally optimum choice of the scaling factor at the sth iteration. This search simply involves stepping in increments from the initial guess λ_1^s in the direction that decreases the value of $S(\phi)$. After computing two additional values of $S(\phi)^s$ besides the

$\underset{\sim}{S}(\underset{\sim}{\phi})^{s}_{1}$ for the initial guess, the $\lambda^{s}_{\underline{\ell}}$ and $\underset{\sim}{S}(\underset{\sim}{\phi})^{s}_{\underline{\ell}}$ values for $\underline{\ell} = 1,2,3$ are used in a quadratic function to estimate the local minimum value of $\underset{\sim}{S}(\underset{\sim}{\phi})$ and the corresponding value of the scaling factor. Using the parameters, $\underset{\sim}{\phi}$, which gave the minimum value of $\underset{\sim}{S}(\underset{\sim}{\phi})$ for this iteration, a new iteration is begun by evaluating a new $\underline{\underline{J}}$ matrix at this new base point.

The only restriction imposed on the value of λ is that $\lambda > -\xi_{\underline{p}}$. Hence, for a nonsingular $\underline{\underline{J}}^{T}\underline{\underline{J}}$ matrix, one will allow a negative λ if it will help find a low value of $\underset{\sim}{S}(\underset{\sim}{\phi})$ and can safely do so since $(\underline{\underline{J}}^{T}\underline{\underline{J}} + \lambda\underline{\underline{I}})$ is nonsingular in this range.

Practical considerations dictate special handling where λ is indicated to be large. Without some corrective measures, the steepest descent direction is approached but with a vector length nearly zero. One can interpret a large λ as indicative that the steepest descent direction is the best path to follow for this particular iterative step. If λ is such as to bring $\underset{\sim}{\delta}_{\underline{M}}$ within an angle of $\pi/6$ of $\underset{\sim}{\delta}_{\underline{g}}$, then a vector

$$\underset{\sim}{\delta}_{R} = [\underset{\sim}{g}^{T}\underset{\sim}{g}/\underset{\sim}{g}^{T}(\underset{\sim}{J}^{T}\underset{\sim}{J})\underset{\sim}{g}]\,\underset{\sim}{g} \qquad (119)$$

is used instead. Since $\underset{\sim}{\delta}_{\underline{g}} = \underline{\underline{g}}$, the search vector $\underset{\sim}{\delta}_{\underline{R}}$ is recognized as a scaled gradient vector. The scaling factor is the reciprocal of the Rayleigh quotient. The determination of $\underset{\sim}{\delta}_{\underline{R}}$ is followed by a one-sided binary search of its path if the sum of squared value does not decrease from the previous iteration. The binary search is done by looking at fractional multiples of $\underset{\sim}{\delta}_{\underline{R}}$ for a better $\underset{\sim}{S}(\underset{\sim}{\phi})$ value.

Two other circumstances lead to the use of the steepest descent direction as an alternative to using the Marquardt vector on a given iteration. One is where the condition number μ is quite large, say 10^{9} or greater, indicating an ill-conditioned $\underline{\underline{J}}^{T}\underline{\underline{J}}$ matrix. The other is where the $\underset{\sim}{S}(\underset{\sim}{\phi})$ for λ is greater than the $\underset{\sim}{S}(\underset{\sim}{\phi})$ of the base point. This is interpreted as a danger signal; either $\underset{\sim}{S}(\underset{\sim}{\phi})$ is a local

maximum, or perhaps a local minimum for a different neighborhood. Both are possibilities unless the contours of constant $\underset{\sim}{S}(\underset{\sim}{\phi})$ are globally convex. In either case, the steepest descent direction is a safe way to move until the inequality reverses.

SEARCH CONVERGENCE

The search is converged when in successive iterations s, $s+1$,

$$(\phi_j^{s+1} - \phi_j^s)/\phi_j^s < X \qquad j = 1,2,\ldots,p \tag{120}$$

where X is some prespecified amount, e.g., 10^{-4}. The converged values of $\underset{\sim}{\phi}$ are termed the least square estimates of $\hat{\underset{\sim}{\phi}}$. The progress of the search can be monitored at each iteration by computing the estimated squared distance from $\underset{\sim}{\phi}$ to $\hat{\underset{\sim}{\phi}}$. If the eigenvalues of $\underset{\sim}{J}^T\underset{\sim}{J}$ are denoted by

$$\xi_{max} = \xi_1 \geq \xi_2 \geq \ldots \geq \xi_p = \xi_{min} > 0 \tag{121}$$

then the average value of the squared distance from $\underset{\sim}{\phi}$ to $\hat{\underset{\sim}{\phi}}$ according to linear least square theory is given by

$$E[L_1^2] = \sigma^2 \sum_{j=1}^{p} (1/\xi_j). \tag{122}$$

The variance of the estimated distance when the error is normally distributed is given by

$$VAR[L_1^2] = 2\sigma^4 \sum_{j=1}^{p} (1/\xi_j)^2 \tag{123}$$

where (65)

$$\sigma^2 = S(\underset{\sim}{\phi})/(n - p). \tag{124}$$

One of the basic assumptions of the least squares method is that the residuals are independent and normally distributed. This assumption can be tested at the completion of the search by computing the Chi-square statistic for the residuals.

UNCERTAINTY IN THE ESTIMATED PARAMETERS

In the p-dimensional parameter space, the contours of constant $S(\underset{\sim}{\phi})$, and hence the likelihood contours, are a series of concentric ellipsoids (or hyperellipsoids) centered about $\hat{\underset{\sim}{\phi}}$. The contours indicate the way in which the likelihood falls off as one moves away from $\hat{\underset{\sim}{\phi}}$. If a dichotomy of likely and unlikely values is desired, then one can choose a particular contour at a suitable level of likelihood and regard all those points within the contour as likely, and those outside as unlikely.

The boundary of a region with confidence coefficient $1 - \alpha$ in the parameter space is formed by the values of $\underset{\sim}{\phi}$ which satisfy the relationship (66, 67)

$$(\underset{\sim}{\phi} - \hat{\underset{\sim}{\phi}})^T \underset{\sim}{J}^T\underset{\sim}{J} (\underset{\sim}{\phi} - \hat{\underset{\sim}{\phi}}) = s^2 p \, F_{\alpha(p,n-p)} \tag{125}$$

where $F_{\alpha(p,n-p)}$ is the α percentage point of the F-distribution with p and $n-p$ degrees of freedom; s^2 is an independent estimate of the error variance based on $n-p$ degrees of freedom, i.e., $s^2 = S(\underset{\sim}{\phi})/(n-p)$. The boundary of such a region is a hyperellipsoid with a volume proportional to the square root of the reciprocal of the determinant $|\underset{\sim}{J}^T\underset{\sim}{J}|$. Thus, for a given value of $F_{\alpha(p,n-p)}$ and s^2, the volume will decrease as the value of the determinant increases. The variance-covariance matrix for the parameters $\underset{\sim}{\phi}$ is of the form $(\underset{\sim}{J}^T\underset{\sim}{J})^{-1} \sigma^2$.

All of the above statements hold exactly true for the linear regression case, but unfortunately are only approximately true for the nonlinear case. When the model is nonlinear, the contours of constant $S(\underset{\sim}{\phi})$ in the parameter space are often elongated.

A measure of the nonlinearity of the regression function can be obtained by comparing the relative magnitudes of the eigenvalues ξ_j of the correlation matrix $\underset{\simeq}{A}^*$. In particular, the relative magnitude of the eigenvalues indicate the state

of the conditioning of the likelihood surface, or the state of correlation between the estimated parameters. Therefore, if the estimates are completely uncorrelated, each ξ_j is unity and (59)

$$\sum_{j=1}^{p} \xi_j = p. \tag{126}$$

It is important to recognize that the effect of the very small eigenvalues is to inflate the variance-covariance matrix. The effect of the small eigenvalues is readily made apparent when the variance-covariance matrix is calculated by a generalized inverse method from $\underset{\sim}{J}^T\underset{\sim}{J}$ where the rank r is sequentially reduced by dropping the smallest eigenvalue. Thus, the generalized inverse of $\underset{\sim}{J}^T\underset{\sim}{J}$ is written

$$(\underset{\sim}{J}^T\underset{\sim}{J})^+ = \sum_{j=1}^{r} (1/\xi_j)\, \underset{\sim}{S}_j\, \underset{\sim}{S}_j^T \tag{127}$$

where $\underset{\sim}{S}_j$ is the eigenvector of $\underset{\sim}{J}^T\underset{\sim}{J}$ corresponding to ξ_j (64).

Therefore, one must consider the degree of the nonlinearity when deciding if linearized results provide acceptable approximations (68).

The exact confidence contour is defined by taking $S(\underset{\sim}{\phi})$ = constant, but since one does not generally know the correct distribution properties of $S(\underset{\sim}{\phi})$ in the nonlinear case, one is unable to obtain a specified probability level. However, one can choose a contour such that if the model is linear, it provides an exact ellipsoidal $100(1-\alpha)\%$ boundary, and label it as an approximate $100(1-\alpha)\%$ linear confidence contour in the nonlinear case.

In general, when a nonlinear regression equation is used, all the formulas and analyses of linear regression theory can be applied. Any results obtained are valid only to the extent that the linearized form provides a good approximation to the nonlinear model.

NOMENCLATURE FOR APPENDIX I

$\underset{\sim}{A}$ = p by p matrix of $\underset{\sim}{J}^T\underset{\sim}{J}$

$\underset{\sim}{A}^*$ = scaled A matrix = matrix of correlation coefficients among the $\partial f_i / \partial \phi_j$

$\underset{\sim}{C}$ = arbitrary p by p matrix

$E[L_1^2]$ = estimated average value of squared distance from ϕ to $\hat{\phi}$

f = regression function

$F_{\alpha(p,n-p)}$ = α-percentage point of the F-distribution with p and $n-p$ degrees of freedom

$\underset{\sim}{g}$ = p by 1 gradient vector

$\underset{\sim}{g}^*$ = scaled $\underset{\sim}{g}$ matrix

i = index denoting the set of the experimental observations

$\underset{\sim}{I}$ = identity matrix

j = index denoting the parameter

$\underset{\sim}{J}$ = n by p Jacobian matrix of partial derivatives

k = index denoting the input variable

ℓ = subscript indicating the sub-iteration number

n = the number of sets of experimental observations

p = the number of unknown parameters

r = rank of the matrix

s = superscript indicating the iteration index

s^2 = estimated error variance

$S(\underset{\sim}{\phi})$ = sum of squares of the residuals

$\underset{\sim}{S}_j$ = eigenvector

T = superscript indicating matrix transposition

$VAR[L_1^2]$ = estimated variance of $E[L_1^2]$

x = input variable

X = convergence value

$\underset{\sim}{Y}$ = response variable

$\underset{\sim}{\Gamma}$ = locus of Marquardt's search vector

$\underset{\sim}{\delta}$ = increment vector

$\underset{\sim}{\delta}_{\underline{g}}$ = steepest descent vector

$\underset{\sim}{\delta}_{\underline{M}}$ = Marquardt's vector

$\underset{\sim}{\delta}^{*}_{\underline{M}}$ = Marquardt's vector scaled

$\underset{\sim}{\delta}_{\underline{n}}$ = Newton-Raphson vector

$\underset{\sim}{\delta}_{\underline{R}}$ = scaled steepest descent vector

$\underset{\sim}{\delta}_{\underline{t}}$ = Gauss-Newton vector

∇ = del operator

ε = residual

λ = scaling factor

μ = condition number

ξ = eigenvalues

σ^2 = error variance

$\sum$ = summation

$\underset{\sim}{\phi}$ = parameters

$\underset{\sim}{\hat{\phi}}$ = value of the parameters at the minimum of $\underline{S}(\underset{\sim}{\phi})$

$\underset{\sim}{\phi}^{\circ}$ = value of the parameters at base location of search vector

APPENDIX II

MODIFIED MARQUARDT'S NONLINEAR LEAST SQUARES PROGRAM AND FLOW DIAGRAM

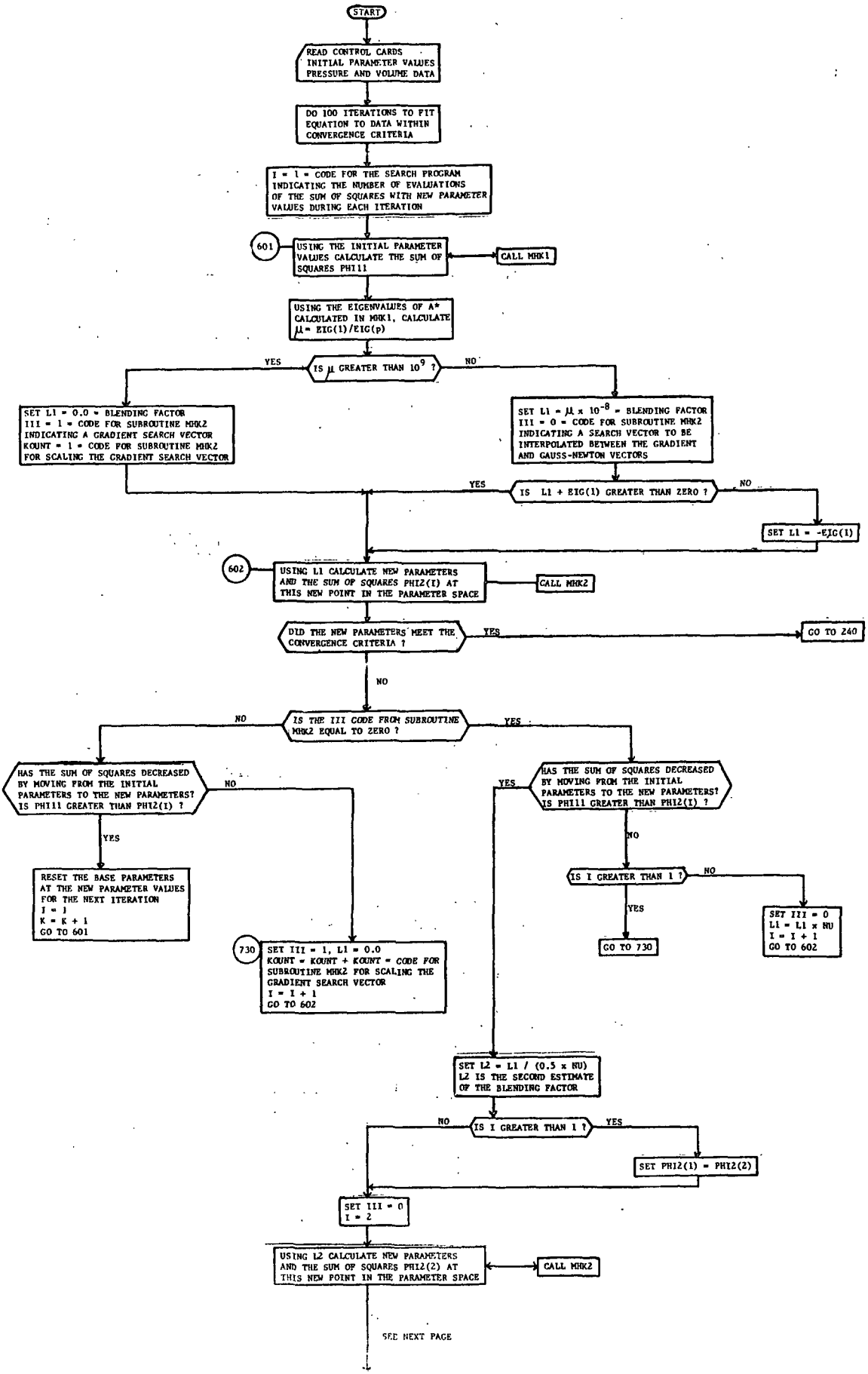

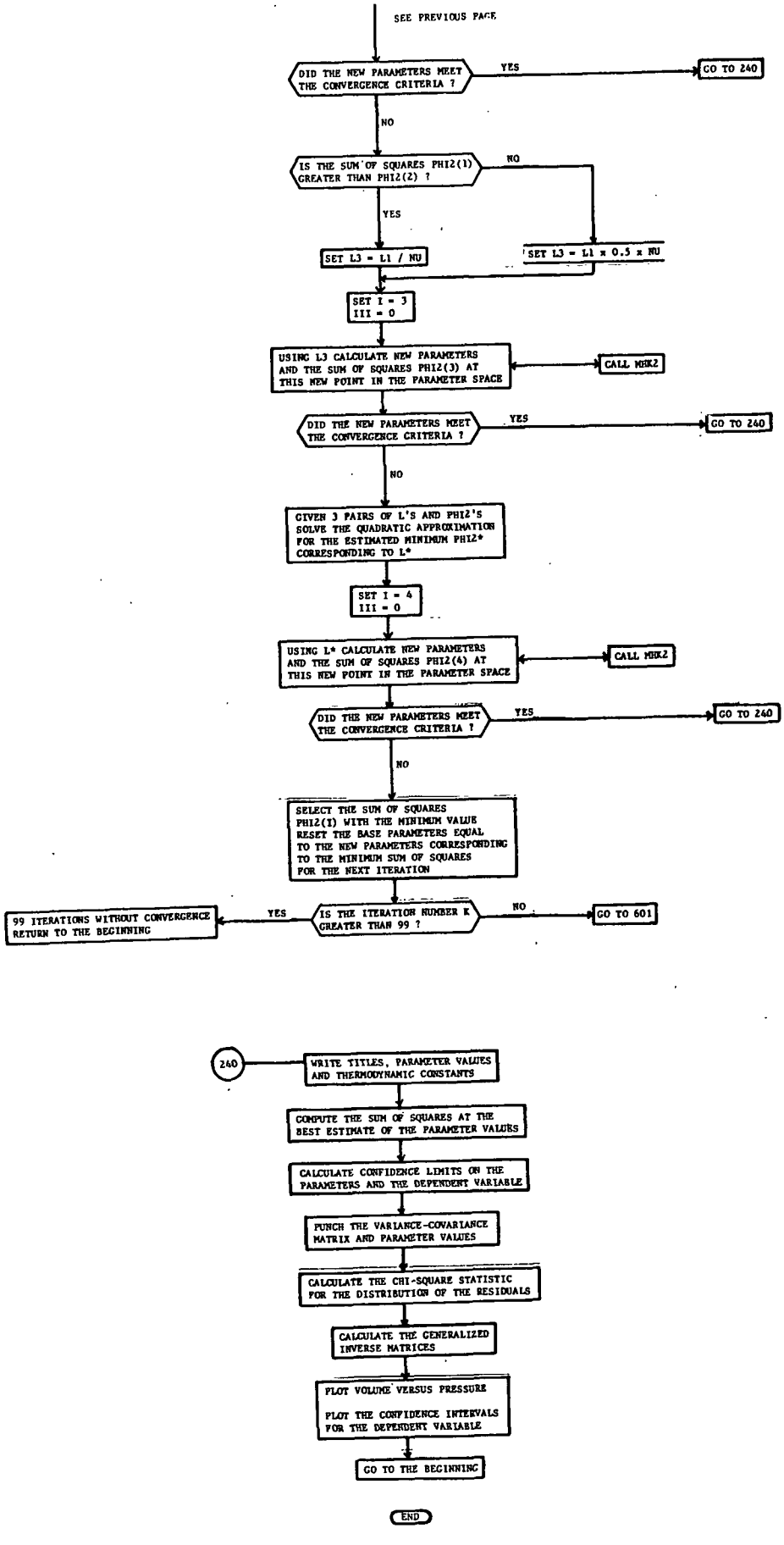
SEE PREVIOUS PAGE
DID THE NEW PARAMETERS MEET THE CONVERGENCE CRITERIA ?
YES
GO TO 240
NO
IS THE SUM OF SQUARES PHI2(1) GREATER THAN PHI2(2) ?
NO
YES
SET L3 = L1 / NU
SET L3 = L1 x 0.5 x NU
SET I = 3
III = 0
USING L3 CALCULATE NEW PARAMETERS AND THE SUM OF SQUARES PHI2(3) AT THIS NEW POINT IN THE PARAMETER SPACE
CALL MRK2
DID THE NEW PARAMETERS MEET THE CONVERGENCE CRITERIA ?
YES
GO TO 240
NO
GIVEN 3 PAIRS OF L'S AND PHI2'S SOLVE THE QUADRATIC APPROXIMATION FOR THE ESTIMATED MINIMUM PHI2* CORRESPONDING TO L*
SET I = 4
III = 0
USING L* CALCULATE NEW PARAMETERS AND THE SUM OF SQUARES PHI2(4) AT THIS NEW POINT IN THE PARAMETER SPACE
CALL MRK2
DID THE NEW PARAMETERS MEET THE CONVERGENCE CRITERIA ?
YES
GO TO 240
NO
SELECT THE SUM OF SQUARES PHI2(I) WITH THE MINIMUM VALUE RESET THE BASE PARAMETERS EQUAL TO THE NEW PARAMETERS CORRESPONDING TO THE MINIMUM SUM OF SQUARES FOR THE NEXT ITERATION
IS THE ITERATION NUMBER K GREATER THAN 99 ?
YES
99 ITERATIONS WITHOUT CONVERGENCE RETURN TO THE BEGINNING
NO
GO TO 601
240
WRITE TITLES, PARAMETER VALUES AND THERMODYNAMIC CONSTANTS
COMPUTE THE SUM OF SQUARES AT THE BEST ESTIMATE OF THE PARAMETER VALUES
CALCULATE CONFIDENCE LIMITS ON THE PARAMETERS AND THE DEPENDENT VARIABLE
PUNCH THE VARIANCE-COVARIANCE MATRIX AND PARAMETER VALUES
CALCULATE THE CHI-SQUARE STATISTIC FOR THE DISTRIBUTION OF THE RESIDUALS
CALCULATE THE GENERALIZED INVERSE MATRICES
PLOT VOLUME VERSUS PRESSURE
PLOT THE CONFIDENCE INTERVALS FOR THE DEPENDENT VARIABLE
GO TO THE BEGINNING
END

```
C
C
C     ************************************************************************
C
C     MODIFIED MARQUARDT'S NON-LINEAR LEAST SQUARES PROGRAM
C
C     ************************************************************************
C
C     MAINLINE PROGRAM, MRQDT, IS A NON-LINEAR LEAST SQUARES PROGRAM
C     WHICH USES A MODIFIED MARQUARDT'S COMPROMISE SEARCHING TECHNIQUE.
C     MRQDT, IN ITS PRESENT VERSION, IS WRITTEN SPECIFICALLY TO FIT
C     EITHER OF 2 GAS ADSORPTION MODEL EQUATIONS TO EXPERIMENTAL DATA.
C     THE SINGLE LAYER ROSS & OLIVIER MODEL OR A MULTILAYER ADSORPTION
C     MODEL MAY BE USED.  BOTH MODELS USE A LOG-NORMAL DISTRIBUTION OF
C     ADSORPTIVE POTENTIALS.
C
C     THE NUMBER OF DATA POINTS, NDATA, MUST BE NO GREATER THAN 50.
C     THE APPROPRIATE SUBROUTINES ARE INCLUDED FOR ARGON(ARGN),
C     NITROGEN(NITR) AND TRICHLOROMONOFLUOROMETHANE(CFCL) ADSORBATE
C     MOLECULES
C     THE PLOTTING OPTION, NPLOT, INDICATES NO PLOT, PLOT VOLUME VERSUS
C     PRESSURE, OR PLOT VOLUME VERSUS PRESSURE AND PLOT THE CONFIDENCE
C     LIMITS ON THE DEPENDENT VARIABLE.  PLOTTER SUBROUTINES REQUIRED -
C     ITLZ,AXIS,LINE,DPT,PLOT,SCALE,FINAL
C     THE NUMBER OF SEARCHING PARAMETERS, NP, CAN BE AS LARGE AS 6,
C     BUT USUALLY SHOULD NOT BE GREATER THAN 4.  INCLUSION OF ALPHA AND
C     BETA AS VARIABLE PARAMETERS OFTEN CAUSES ILL CONDITIONING DUE TO
C     VERY SMALL EIGENVALUES ASSOCIATED WITH THE CORRELATION MATRIX.
C
C     SCIENTIFIC SUBROUTINE PROGRAMS REQUIRED ARE -
C     ARRAY,EIGEN,MINV,GMPRD AND GMTRA IN DOUBLE PRECISION
C     SIMQ AND QSF IN SINGLE PRECISION
C     OTHER SUBROUTINES CALLED ARE MLTAD1,MHK1,MHK2,COVE3
C
C     MRQDT AND ITS SUBROUTINES REQUIRE 101K BYTES OF WORKING SPACE IN
C     CORE RUNNING UNDER IBM 360/44 PS VERSION 3, LEVEL 2.
C
C     ************************************************************************
C
0001        REAL*4 NU,L1,L2,L3,LSTAR
0002        REAL LO
C
0003        COMMON AN,UPLIM,BOTLIM,VCAL(50),TCOV(50),THETA(100,5),A,RES(50)
0004        COMMON UADS(100,5),SDELTA,STR,SROT,SVIB,EKIN,FREQ(100)
0005        COMMON NCALL,NPLOT,NANAL,NP
0006        COMMON PAO,C1,TEMP,II,JJ,ORNT
0007        COMMON P(50),V(50)
C
C
```

```
0008              DIMENSION BASE(6),PARAM1(6),PARAM2(6),PARAM3(6),PSTAR(6)
0009              DIMENSION AARAY(6,6),ASTAR(6,6),GSTAR(6),B(3),AA(9),VPLT(50)
0010              DIMENSION WORK1(6),WORK2(6),S(6),COR(6,6),CINVL(6),CINV(36)
0011              DIMENSION PHI2(20),PARAY(50,6),SF(50),CONF(50),TH(6),TL(6)
0012              DIMENSION ADUMY(21),EIG(6),R(36),RT(36)
0013              DIMENSION DCINV(36),RESULT(36),AINV(6,6)
0014              DIMENSION PX(15),EX(15),FREK(12),CHI(12),PROB(11)
                C
0015              DOUBLE PRECISION AN,UPLIM,BOTLIM,H,UAVE,G,VMOL,VIB,ALPHA,BETA,A
0016              DOUBLE PRECISION BASE,PARAM1,PARAM2,PARAM3,PSTAR
0017              DOUBLE PRECISION PHI11,PHI2,PHIMIN,VCAL,TCOV,THETA,UADS
0018              DOUBLE PRECISION DET,PARAY,AARAY,ASTAR,ADUMY,VARY,R,EIG,CINV,WORK1
0019              DOUBLE PRECISION WORK2,GSTAR,RES,FUDGE,RT
0020              DOUBLE PRECISION SSY,DCINV,RESULT
0021              DOUBLE PRECISION DIST,SIGDIS,AINV
0022              DOUBLE PRECISION SUM
                C
0023              EQUIVALENCE (BASE(1),G), (BASE(2),UAVE), (BASE(4),VIB)
0024              EQUIVALENCE (BASE(3),VMOL),(BASE(5),ALPHA),(BASE(6),BETA)
                C
                C
                C     READ CONTROL CARDS
0025                1 READ(5,100) NDATA,NCALL,NPLOT,NANAL,NP
0026              100 FORMAT(I2,4I1)
                C     NDATA = NUMBER OF DATA POINTS, BLANK DATA CARD INDICATES
                C     TERMINATION OF THE PROGRAM
                C     NCALL=CODE FOR TYPE OF MOLECULE  0=ARGON, 1=NITROGEN, 2=CFCL3
                C     NPLOT=CODE FOR  0=RETURN TO BEGN  1=PLOT  2=PLOT CONF LIMITS
                C     NANAL=CODE FOR TYPE OF ANALYSIS  0=ROSS & OLIVIER
                C     1=MULTILAYER MODEL
                C     NP = NUMBER OF PARAMETERS, GAMMA,UAVE,VMOL,VIB,ALPHA,BETA
                C
0027              IF(NDATA) 500,500,2
0028              500 END FILE 6
                C     END FILE STATEMENT FOR USE WITH MAGNETIC TAPE OUTPUT
0029              CALL EXIT
                C
0030                2 READ(5,101) (P(I),V(I),I=1,NDATA)
0031              101 FORMAT(2F10.0)
                C     PRESSURE DATA IN TORR, VOLUME IN ML(STP) PER GRAM
                C
0032              READ(5,3) CONVER
0033                3 FORMAT(1F10.0)
                C     CONVER IS CONVERGENCE CRITERIA EG. 0.001 - 0.00001
                C
0034              WRITE(6,243)
0035              243 FORMAT(1H1,'  K     I      LAMBDA',8X,'SUM OF',8X,'GAMMA        MEAN
                  1ADSP.      MONOLAYER     VIBRATIONAL     ALPHA',10X,'BETA'/1H ,27X,
                  1'SQUARES',19X,'POTENTIAL       VOLUME          FREQUENCY'//)
```

```
      C
0036        READ(5,102) C1,TEMP,NU,BASE
0037      102 FORMAT(7F10.0)
      C     C1 = IDEAL 2*ALPHA/BETA IN KCAL PER MOLE
      C     TEMP IN DEGREES KELVIN
      C     NU = SCALING FACTOR EG. 5 - 10
      C     BASE = INITIAL GUESS OF PARAMETER VALUES IN THE FOLLOWING ORDER
      C     BASE(1) = GAMMA = HETEROGENEITY PARAMETER
      C     BASE(2) = UAVE = MEDIAN ADSORPTIVE POTENTIAL
      C     BASE(3) = VMOL = MONOLAYER VOLUME
      C     BASE(4) = VIB = VIBRATIONAL FREQUENCY OF THE MOLECULE X 10**-12
      C     BASE(5) = ALPHA = 2-DIMENSIONAL VAN DER WAAL'S GAS CONSTANT
      C     BASE(6) = BETA = 2-DIMENSIONAL VAN DER WAAL'S GAS CONSTANT
      C
0038        READ(5,105) TVAL
0039      105 FORMAT(F10.0)
      C     TVAL = F DISTRIBUTION VALUE FOR (NP),(NDATA-NP) DEGREES OF FREEDOM
      C
0040        IF(NP-5) 610,611,612
0041      611 READ(5,106) TL(5),TH(5)
0042      106 FORMAT(4F10.0)
      C     TL, TH ARE LOWER AND UPPER BOUNDS ON ALPHA OR BETA TO PREVENT
      C     UNREASONABLE VALUES DURING THE SEARCH
0043        GO TO 610
0044      612 READ(5,106) TL(5),TH(5),TL(6),TH(6)
0045      610 CONTINUE
      C
      C     ***************************************************************
      C
      C     BEGIN ITERATIVE DO LOOP
0046        DO 600 K = 1,100
0047        KEND = K
0048        I = 1
0049      601 CALL MHK1(BASE,PHI11,NDATA,AARAY,ASTAR,GSTAR,PARAY)
0050        WRITE(6,550)
0051      550 FORMAT(1HO,'BASE POINT FOR SEARCH VECTOR')
0052        WRITE(6,103) K,PHI11,BASE
0053      103 FORMAT(1H ,I3,19X,7E14.5)
0054        KOUNT=0
      C
      C     STORE ASTAR IN TRIANGULAR FORM
0055        NN=0
0056        DO 700 J=1,NP
0057        DO 700 IC=1,J
0058        NN=NN+1
0059      700 ADUMY(NN)=ASTAR(IC,J)
      C
0060        CALL EIGEN(ADUMY,R,NP,1)
0061        JC=0
```

```
0062              DIST = 0.0
                C     DIST = ESTIMATED DISTANCE TO THE TRUE PARAMETER VALUES
0063              SIGDIS = 0.0
                C     SIGDIS = VARIANCE OF 'DIST'
0064              DO 701 J=1,NP
0065              JC=J+JC
0066              EIG(J) = ADUMY(JC)
                C     EIG(J) ARRAY CONTAINS EIGENVALUES
0067              DIST = DIST + 1.0/EIG(J)
0068            701 SIGDIS=SIGDIS + (1.0/EIG(J))**2
0069              FUDGE = PHI11/(NDATA-NP)
0070              DIST = DIST * FUDGE
0071              SIGDIS = 2*(FUDGE**2)*SIGDIS
0072              WRITE(6,901) DIST,SIGDIS,EIG
0073            901 FORMAT(1H ,'EST. DISTANCE TO TRUE PARAMETER =',E14.7/1H ,'EST. VAR
                   1IANCE OF DISTANCE =',E15.7/1H ,'EIGENVALUES =',6E16.7)
                C
0074              EMU=EIG(1)/EIG(NP)
0075              IF(EMU-1.0E+09) 703,800,800
0076            703 L1=(1.0E-08)*EMU
0077              III=0
0078              IF(L1+EIG(1)) 704,704,602
0079            704 L1=-EIG(1)
0080              GO TO 602
0081            800 III=1
0082              L1=0.
0083              KOUNT=1
                C
0084            602 CALL MHK2(BASE,L1,PHI2(I),PARAM1,NCONV,ASTAR,GSTAR,AARAY,NDATA,TH,
                   1TL,III,KOUNT,CONVER)
0085              WRITE(6,508) K,I,L1,PHI2(I),PARAM1
0086            508 FORMAT(1H ,I3,2X,I3,8E14.5)
0087              IF(NCONV-1) 229,231,240
0088            229 IF(III) 707,707,708
0089            708 IF(PHI11 - PHI2(I)) 730,730,709
0090            709 DO 710 L=1,NP
0091            710 BASE(L)=PARAM1(L)
0092              I=1
0093              K=K+1
0094              GO TO 601
0095            707 IF(PHI11 - PHI2(I)) 501,501,504
0096            501 IF(I-1) 720,720,730
0097            720 III=0
0098              L1=L1*NU
0099              I=I+1
0100              GO TO 602
0101            730 III=1
0102              L1=0.
0103              KOUNT = KOUNT + KOUNT
```

```
0104              I=I+1
0105              GO TO 602
0106            504 L2 = L1/(0.5*NU)
0107              IF(I-1) 740,740,750
0108            750 PHI2(1) = PHI2(2)
                C
0109            740 I=2
0110              III=0
0111              CALL MHK2(BASE,L2,PHI2(I),PARAM2,NCONV,ASTAR,GSTAR,AARAY,NDATA,TH,
                 1TL,III,KOUNT,CONVER)
0112              WRITE(6,508) K,I,L2,PHI2(I),PARAM2
0113              IF(NCONV-1) 230,231,240
0114            230 IF(PHI2(1) - PHI2(2)) 227,227,228
0115            227 L3=L1*(.5*NU)
0116              GO TO 226
0117            228 L3=L1/NU
0118            226 I=3
0119              III=0
                C
0120              CALL MHK2(BASE,L3,PHI2(I),PARAM3,NCONV,ASTAR,GSTAR,AARAY,NDATA,TH,
                 1TL,III,KOUNT,CONVER)
0121              WRITE(6,508) K,I,L3,PHI2(I),PARAM3
0122              IF(NCONV-1) 232,231,240
                C
                C     SOLVE QUADRATIC FOR BEST ESTIMATE OF MINIMUM SUM OF SQUARES AND
                C     CORRESPONDING L = LSTAR
0123            232 AA(4) = L1
0124              AA(5) = L2
0125              AA(6) = L3
0126              AA(1) = L1**2
0127              AA(2) = L2**2
0128              AA(3) = L3**2
0129              DO 233 I = 1,3
0130              AA(6+I) = 1.0
0131            233 B(I) = PHI2(I)
0132              CALL SIMQ(AA,B,3,KS)
0133              IF(KS) 250,234,250
0134            250 WRITE(6,255)
0135            255 FORMAT(1H ,'SINGULAR SET OF EQUATIONS')
0136              GO TO 1
0137            234 LSTAR = -B(2)/(2.0*B(1))
                C
0138              I = 4
0139              III=0
0140              CALL MHK2(BASE,LSTAR,PHI2(I),PSTAR,NCONV,ASTAR,GSTAR,AARAY,NDATA,
                 1TH,TL,III,KOUNT,CONVER)
0141              WRITE(6,508) K,I,LSTAR,PHI2(I),PSTAR
0142              IF(NCONV-1) 244,231,240
0143            244 PHIMIN = PHI2(1)
```

```
0144              II = 1
0145              DO 306 I = 2,4
0146              IF(PHIMIN - PHI2(I)) 306,306,307
0147            307 PHIMIN = PHI2(I)
0148              II = I
0149            306 CONTINUE
0150              IF(II-2) 236,237,238
0151            236 DO 251 KK = 1,NP
0152            251 BASE(KK) = PARAM1(KK)
0153              GO TO 600
0154            237 DO 252 KK = 1,NP
0155            252 BASE(KK) = PARAM2(KK)
0156              GO TO 600
0157            238 IF(II-3) 239,239,241
0158            239 DO 253 KK = 1,NP
0159            253 BASE(KK) = PARAM3(KK)
0160              GO TO 600
0161            241 DO 254 KK = 1,NP
0162            254 BASE(KK) = PSTAR(KK)
0163            600 CONTINUE
                C
                C     ***************************************************************************
                C
0164              WRITE(6,224)
0165            224 FORMAT(1HO,' 99 ITERATIONS WITHOUT CONVERGENCE TO WITHIN LIMITS')
0166              GO TO 1
                C
                C     ***************************************************************************
                C
                C     WRITE OUT THE PARAMETER VALUES AND THERMODYNAMIC ADSORPTION DATA
0167            240 CONTINUE
0168            231 WRITE(6,235)   KEND
0169            235 FORMAT(1H ,' CONVERGENCE AT ITERATION = ',I3)
0170              4 IF(NANAL) 195,195,196
0171            196 WRITE(6,201)
0172            201 FORMAT(1H1,'  MULTILAYER MODIFICATION TO R + O MODEL',/)
0173              GO TO 249
0174            195 WRITE(6,198)
0175            198 FORMAT(1H1,'  ROSS AND OLIVIER MODEL - SINGLE LAYER ADSP')
                C
0176            249 WRITE(6,202) UAVE
0177            202 FORMAT(1HO,' MEDIAN ADSORPTIVE POTENTIAL =',F8.3)
0178              UMEAN=DEXP(DLOG(UAVE)+1./(4.*G))
0179              WRITE(6,190) UMEAN
0180            190 FORMAT(1H ,' MEAN ADSORPTIVE POTENTIAL =',F8.3)
0181              UMODE=DEXP(DLOG(UAVE)-1./(2.*G))
0182              WRITE(6,191) UMODE
0183            191 FORMAT(1H ,' MODE ADSORPTIVE POTENTIAL =',F8.3)
0184              WRITE(6,203) G
```

```
0185          203 FORMAT(1H ,' GAMMA =',F8.3)
0186              WRITE(6,204) C1
0187          204 FORMAT(1H ,' 2*ALPHA/BETA(IDEAL) =',F8.3)
0188              WRITE(6,260) ALPHA
0189          260 FORMAT(1H ,' ALPHA =',F8.3)
0190              WRITE(6,261) BETA
0191          261 FORMAT(1H ,' BETA =',F8.3)
0192              IF(NCALL-1) 262,263,262
0193          263 WRITE(6,264) ORNT
0194          264 FORMAT(1H ,' FRACTION OF NITROGEN IN FLAT POSITION =',F7.4)
0195          262 WRITE(6,205) TEMP
0196          205 FORMAT(1H ,' TEMPERATURE =',F7.2)
0197              WRITE(6,220) VMOL
0198          220 FORMAT(1H ,' MONOLAYER VOLUME =',F7.4)
0199              WRITE(6,206) BOTLIM,FREQ(1)
0200          206 FORMAT(1H ,' LOWER LIMIT OF DIST = ',F8.3,' FREQUENCY =',F8.3)
0201              WRITE(6,207) UPLIM,FREQ(100)
0202          207 FORMAT(1H ,' UPPER LIMIT OF DIST =',F8.3,' FREQUENCY =',F8.3)
0203              WRITE(6,208) AN
0204          208 FORMAT(1H ,' NORMALIZATION FACTOR =',F8.3)
0205              WRITE(6,209) SDELTA
0206          209 FORMAT(1H ,' AREA UNDER DIST.CURVE =',F8.4,////)
0207              WRITE(6,210)
0208          210 FORMAT(1H ,'  THERMODYNAMIC ADSORPTION DATA',/)
0209              WRITE(6,211) STR
0210          211 FORMAT(1H ,' CHANGE IN TRANS. ENTROPY =',E11.5)
0211              WRITE(6,212) SROT
0212          212 FORMAT(1H ,' CHANGE IN ROT. ENTROPY =',E11.5)
0213              WRITE(6,213) SVIB
0214          213 FORMAT(1H ,' CHANGE IN VIB. ENTROPY =',E11.5)
0215              VIBB = VIB*1.0E+12
0216              WRITE(6,214) VIBB
0217          214 FORMAT(1H ,' VIBRATIONAL FREQ. =',E11.5)
0218              WRITE(6,215) EKIN
0219          215 FORMAT(1H ,' CHANGE IN KINETIC ENERGY =',E11.5)
0220              WRITE(6,219) A
0221          219 FORMAT(1H ,' A =',E11.5)
              C
0222              CALL MLTAD1(BASE,NDATA)
0223              SUM = 0.0
0224              SUMSQ = 0.0
0225              DO 90 I = 1,NDATA
0226              RES(I)=V(I)-VCAL(I)
0227              SUM=SUM+RES(I)
0228           90 SUMSQ = SUMSQ + RES(I)**2
              C
              C     CALCULATE CONFIDENCE LIMITS
0229              CALL ARRAY(2,NP,NP,6,6,CINV,AARAY)
0230              CALL MINV(CINV,NP,DET,WORK1,WORK2)
```

```
0231              FUDGE = SUMSQ/(NDATA-NP)
0232              WRITE(6,490)
0233           490 FORMAT(1H1,'PARAY(TRANSPOSE) * PARAY MATRIX'/)
0234              WRITE(6,452) AARAY
0235              WRITE(6,460) DET
0236              WRITE(6,455)
0237           455 FORMAT(1HO,'INVERSE MATRIX BY GAUSS-JORDAN METHOD'/)
0238              CALL ARRAY(1,NP,NP,6,6,CINV,AINV)
0239              WRITE(6,452) AINV
0240              CALL ARRAY(2,NP,NP,6,6,DCINV,AARAY)
0241              CALL GMPRD(CINV,DCINV,RESULT,NP,NP,NP)
0242              WRITE(6,451)
0243           451 FORMAT(1HO,'COMPUTED IDENTITY MATRIX'/)
              C
0244              DO 1870 K = 1,NP
0245              NT = (K-1)*NP + 1
0246              NS = NT + NP - 1
0247          1870 WRITE(6,452) (RESULT(J),J=NT,NS)
0248              DO 1265 J = 1,NP
0249              NN = NP*(J-1) + J
0250          1265 S(J) = DSQRT(FUDGE*DABS(CINV(NN)))
0251              DO 1271 I = 1,NDATA
0252              DO 1270 J = 1,NP
0253          1270 WORK1(J) = PARAY(I,J)
0254              CALL GMPRD(WORK1,CINV,WORK2,1,NP,NP)
0255              VARY = 0.0
0256              DO 1272 L = 1,NP
0257          1272 VARY = VARY + WORK1(L)*WORK2(L)
0258          1271 SF(I) = DSQRT(DABS(FUDGE*VARY))
              C
0259              DO 489 I = 1,6
0260              DO 489 J = 1,6
0261           489 COR(I,J) = 0.0
0262              DO 491 J = 1,NP
0263              DO 491 I = 1,NP
0264           491 COR(I,J) = AINV(I,J)/DSQRT(AINV(I,I)*AINV(J,J))
0265              WRITE(6,450)
0266              WRITE(6,452) COR
0267              DO 492 I = 1,NP
0268              DO 492 J = 1,NP
0269           492 AINV(I,J) = AINV(I,J)*FUDGE
0270              WRITE(6,493)
0271           493 FORMAT(1HO,'COVARIANCE MATRIX'/)
0272              WRITE(6,452) AINV
0273              DO 1401 I = 1,NP
0274          1401 CINVL(I) = TVAL*S(I)
0275              WRITE(6,300)
0276           300 FORMAT(1HO,2X,'PARAMETER NO.',6X,'MEAN VALUE',4X,'CONFIDENCE INTER
                 1VAL',/)
```

```
0277              DO 1301 J = 1,NP
0278            1301 WRITE(6,302) J,BASE(J),CINVL(J)
0279             302 FORMAT(1H ,6X,I1,14X,E11.6,7X,E11.6)
                C
                C     PUNCH VARIANCE-COVARIANCE MATRIX AND ESTIMATED PARAMETER VALUES
0280              NN=0
0281              DO 2000 J=1,NP
0282              DO 2000 IC=1,J
0283              NN=NN+1
0284            2000 ADUMY(NN)=AINV(IC,J)
0285              WRITE(7,290) ADUMY
0286             290 FORMAT(6E10.4)
0287              WRITE(7,290) BASE
                C
                C     DETERMINATION OF CHI SQUARE VALUE FOR THE RESIDUAL DISTRIBUTION
0288               80 PX(1)=.1151
0289                  PX(2) = 0.0968
0290                  PX(3) = 0.1327
0291                  PX(4) = 0.1554
0292                  PX(5) = 0.1554
0293                  PX(6) = 0.1327
0294                  PX(7) = 0.0968
0295                  PX(8) = 0.1151
0296                  SUMEX = 0.0
0297                  DO 723 I = 1,8
0298                  EX(I) = NDATA * PX(I)
0299                  SUMEX = EX(I) + SUMEX
0300             723  FREK(I) = 0.0
0301                  SIGMA=DSQRT((SUMSQ-(SUM**2)/NDATA)/(NDATA-1))
0302                  DO 733 I = 1,NDATA
0303                  UND = RES(I)/SIGMA
0304                  IF(UND - 1.2) 721,731,731
0305             721  IUND = IFIX((1.2-UND)/0.4)
0306                  IX =  7 - IUND
0307                  GO TO 733
0308             731  IX = 8
0309             733  FREK(IX) = FREK(IX) + 1
0310                  CKISQ = 0.0
0311                  DO 735 I = 1,8
0312                  CHI(I) = FREK(I)**2/EX(I)
0313             735  CKISQ = CKISQ + CHI(I)
0314                  WRITE(6,746)
0315             746  FORMAT(1H1,'   CLASS',9X,'NUMBER',7X,'PROBABILITY     EXPECTED N
                    1 CHI(I)')
0316                  LO = -1.2
0317                  WRITE(6,741) LO,FREK(1),PX(1),EX(1),CHI(1)
0318             741  FORMAT(1H ,6X,F4.1,9X,F4.0,10X,F6.4, 9X,F4.2,7X,F8.4)
0319                  DO 742 I = 2,7
0320                  LO = -1.2 + 0.4*(I-1)
```

```
0321            HI = -1.2 + 0.4*I
0322          742 WRITE(6,743) LO,HI,FREK(I),PX(I),EX(I),CHI(I)
0323          743 FORMAT(1H ,F4.1,2X,F4.1,9X,F4.0,10X,F6.4, 9X,F4.2,7X,F8.4)
0324            LO = +1.2
0325            WRITE(6,744) LO,FREK(6),PX(8),EX(8),CHI(8)
0326          744 FORMAT(1H ,F4.1,6X,9X,F4.0,10X,F6.4, 9X,F4.2,7X,F8.4)
0327            ONE = 1.0
0328            WRITE(6,745) NDATA,ONE,SUMEX,CKISQ
0329          745 FORMAT(1H0,'TOTAL',11X,3X,I3,11X,F6.4,8X,F5.2,9X,F8.4//)
0330            CKISQ = CKISQ - NDATA
0331            WRITE(6,20) CKISQ
0332           20 FORMAT(1H0,'CHI-SQUARED STATISTIC =',F6.3,' FOR 7 DEGREES OF FREED
                  1OM')
              C     END OF CHI-SQUARED SECTION
              C
0333            WRITE(6,216)
0334          216 FORMAT(1H0,'  PRESSURE        VOLUME        MODEL VOLUME   CONF. BAN
                 1D    RESIDUAL       COVERAGE'/)
0335            WRITE(6,217) (P(J),V(J),VCAL(J),SF(J),RES(J),TCOV(J),J=1,NDATA)
0336          217 FORMAT(1H ,1X,F8.3,7X,F7.4,9X,F7.4,7X,F7.4,7X,F7.4,7X,F7.3)
0337            WRITE(6,218) SUMSQ
0338          218 FORMAT(////,1H ,' SUM OF RESIDUAL SQUARES =',F9.4)
              C
              C     CALCULATE VARIANCE-COVARIANCE MATRIX BY GENERALIZED INVERSE
              C     STORE AARAY IN TRIANGULAR FORM
0339            NN = 0
0340            DO 1700 J = 1,NP
0341            DO 1700 IC = 1,J
0342            NN = NN + 1
0343         1700 ADUMY(NN) = AARAY(IC,J)
0344            CALL EIGEN(ADUMY,R,NP,0)
0345            JC = 0
0346            DO 1701 J = 1,NP
0347            JC = JC + J
0348         1701 EIG(J) = ADUMY(JC)
0349            DO 933 KC=1,NP
0350          933 WORK1(KC)=EIG(KC)
0351            DO 934 KB=1,NP
0352            KA=NP-(KB-1)
0353          934 EIG(KB)=WORK1(KA)
0354            DO 935 KD=1,36
0355          935 RESULT(KD)=R(KD)
0356            DO 936 KE=1,NP
0357            DO 936 KF=1,NP
0358            KG=NP*(KE-1)+KF
0359            KH=NP*(NP-KE)+KF
0360          936 R(KG)=RESULT(KH)
0361            NQ = 1
              C
```

```
0362          1991 DO 932 I=1,NP
0363               DO 932 J=1,NP
0364               AINV(I,J)=0.0
0365               DO 932 K = NQ,NP
0366               NI=NP*(K-1)+I
0367               NJ=NP*(K-1)+J
0368           932 AINV(I,J)=AINV(I,J)+R(NI)*R(NJ)/EIG(K)
0369               DET=1.0
0370               DO 937 K = NQ,NP
0371           937 DET=DET*EIG(K)
0372               WRITE(6,1999)
0373          1999 FORMAT(1H1)
0374               WRITE(6,1750) EIG
0375          1750 FORMAT(1HO,'EIGENVALUE =',6E16.7)
0376               WRITE(6,1751)
0377          1751 FORMAT(1HO,'EIGENVECTOR MATRIX'/)
0378               DO 1775 K = 1,NP
0379               NT = (K-1)*NP + 1
0380               NS = NT + NP - 1
0381          1775 WRITE(6,452) (R(J),J=NT,NS)
              C
0382               DO 495 I = 1,NP
0383               DO 495 J = 1,NP
0384           495 COR(I,J) = AINV(I,J)/DSQRT(AINV(I,I)*AINV(J,J))
0385               WRITE(6,456)
0386           456 FORMAT(1HO,'CORRELATION MATRIX'/)
0387               WRITE(6,452) COR
0388               WRITE(6,460) DET
0389               NC=NP-NQ+1
0390               WRITE(6,1998) NC
0391          1998 FORMAT(1HO,'GENERALIZED INVERSE OF RANK =',I1/)
0392               WRITE(6,452) AINV
0393               CALL ARRAY(2,NP,NP,6,6,DCINV,AARAY)
0394               CALL GMTRA(R,RT,NP,NP)
0395               CALL GMPRD(RT,DCINV,RESULT,NP,NP,NP)
0396               CALL GMPRD(RESULT,R,CINV,NP,NP,NP)
0397               WRITE(6,1997)
0398          1997 FORMAT(1HO,'EIGENVALUE DIAGONAL MATRIX'/)
0399               DO 1996 K = 1,NP
0400               NT = (K-1)*NP + 1
0401               NS = NT + NP -1
0402          1996 WRITE(6,452) (CINV(J),J=NT,NS)
0403               CALL ARRAY(2,NP,NP,6,6,CINV,AINV)
0404               DO 1995 J = 1,NP
0405               NN = NP*(J-1) + J
0406          1995 S(J) = DSQRT(FUDGE*DABS(CINV(NN)))
0407               DO 496 I = 1,NP
0408               DO 496 J = 1,NP
0409           496 AINV(I,J) = AINV(I,J)*FUDGE
```

```
0410            WRITE(6,493)
0411            WRITE(6,452) AINV
0412            DO 1994 I = 1,NP
0413         1994 CINVL(I) = TVAL*S(I)
0414            WRITE(6,300)
0415            DO 1993 J = 1,NP
0416         1993 WRITE(6,302) J,BASE(J),CINVL(J)
0417            NQ = NQ + 1
0418            IF(NQ-NP) 1991,1991,1992
0419         1992 CONTINUE
             C
             C
0420            IF(NPLOT-1) 50,40,40
0421          40 CALL ITLZ
0422            CALL DPT(1,4)
0423            CALL PLOT(0.,-11.,3)
0424            CALL PLOT(0.,-9.5,-3)
0425            CALL SCALE(P,5.,NDATA,1)
0426            CALL SCALE(V,6.,NDATA,1)
0427            CALL AXIS(0.,0.,'PRESSURE - TORR',-15,5.,0.,P(NDATA+1),P(NDATA+2))
0428            CALL AXIS(0.,0.,'VOLUME - (ML(S.T.P.)/GRAM)',26,6.,90.,V(NDATA+1),
                1V(NDATA+2))
0429            DO 35 K=1,NDATA
0430          35 VPLT(K)=VCAL(K)
0431            VPLT(NDATA+1)=V(NDATA+1)
0432            VPLT(NDATA+2)=V(NDATA+2)
0433            CALL LINE(P,V,NDATA,1,-1,1)
0434            CALL LINE(P,VPLT,NDATA,1,0,1)
0435            IF (NPLOT-2) 76,75,75
0436          75 DO 503 K = 1,NDATA
0437         503 CONF(K) = VCAL(K) + SF(K)
0438            CONF(NDATA+1) = V(NDATA+1)
0439            CONF(NDATA+2) = V(NDATA+2)
0440            CALL LINE(P,CONF,NDATA,1,-1,10)
0441            DO 502 KT = 1,NDATA
0442         502 CONF(KT) = VCAL(KT) - SF(KT)
0443            CALL LINE(P,CONF,NDATA,1,-1,8)
0444          76 CALL FINAL
             C
0445          50 GO TO 1
             C
0446         452 FORMAT(1H ,6E20.7)
0447         450 FORMAT(1HO,'CORRELATION MATRIX'/)
0448         460 FORMAT(1HO,'DETERMINANT =',E15.6)
0449            END
```

```
0001              SUBROUTINE MHK1(BASE,PHI11,NDATA,AARAY,ASTAR,GSTAR,PARAY)
                  C
                  C     SUBROUTINE CALLED BY MRQDT TO EVALUATE THE SUM OF SQUARES AT THE
                  C     BASE PARAMETERS, AND TO SET UP THE JACOBIAN MATRIX, AND TO
                  C     CALCULATE ASTAR AND GSTAR ARRAYS
                  C
0002              COMMON AN,UPLIM,BOTLIM,VCAL(50),TCOV(50),THETA(100,5),A,RES(50)
0003              COMMON UADS(100,5),SDELTA,STR,SROT,SVIB,EKIN,FREQ(100)
0004              COMMON NCALL,NPLOT,NANAL,NP
0005              COMMON PAO,C1,TEMP,II,JJ,ORNT
0006              COMMON P(50),V(50)
                  C
0007              DIMENSION BASE(6),PARAM(6),DUMY(6)
0008              DIMENSION AARAY(6,6),ASTAR(6,6),GSTAR(6),GARAY(6)
0009              DIMENSION PARAY(50,6),VHI(50),VLO(50)
                  C
0010              DOUBLE PRECISION AN,UPLIM,BOTLIM,H,UAVE,G,VMOL,VIB,ALPHA,BETA,A
0011              DOUBLE PRECISION BASE,PHI11,DUMY,PARAY
0012              DOUBLE PRECISION VCAL,VHI,VLO,TCOV,THETA,UADS
0013              DOUBLE PRECISION AARAY,ASTAR,GSTAR,GARAY,RES,DRV,DRVDL
                  C     SET UP JACOBIAN MATRIX = PARAY(I,J)
                  C     I = DATA POINT INDEX    J = PARAMETER INDEX
                  C
0014                  PHI11 = 0.0
0015                  CALL MLTAD1(BASE,NDATA)
0016                  DO 13 I = 1,NDATA
0017                  VHI(I)=VCAL(I)
0018                  RES(I)=V(I)-VCAL(I)
0019             13   PHI11 = PHI11 + RES(I)**2
                  C
0020                  DO 10 J=1,NP
0021             30   DRVDL=BASE(J)*1.0D-05
0022             32   XLO = BASE(J)  - DRVDL
0023                  DO 9 JA = 1,6
0024              9   DUMY(JA) = BASE(JA)
0025                  DUMY(J) = XLO
0026                  CALL MLTAD1(DUMY,NDATA)
0027                  DO 16 I = 1,NDATA
0028             16   VLO(I) = VCAL(I)
0029                  DO 10 I = 1,NDATA
0030             10   PARAY(I,J)=(VHI(I)-VLO(I))/DRVDL
                  C
0031                  DO 50 LA=1,NP
0032                  DRV=BASE(J)*5.0D-06
0033             50   BASE(LA)=BASE(LA)-DRV
                  C     SET UP AARAY
0034                  DO 19 JI = 1,NP
0035                  DO 19 IJ = 1,NP
0036             19   AARAY(IJ,JI) = 0.0
```

```
0037              DO 20 IJ = 1,NP
0038              DO 20 JI = 1,NP
0039              DO 20 I = 1,NDATA
0040           20 AARAY(IJ,JI) = AARAY(IJ,JI) + PARAY(I,IJ)*PARAY(I,JI)
0041              DO 11 J = 1,NP
0042              DO 11 JK= 1,NP
0043           11 ASTAR(J,JK) = AARAY(J,JK)/(DSQRT(DABS(AARAY(J,J)))*
                 1DSQRT(DABS(AARAY(JK,JK))))
               C
0044              DO 12 JX = 1,NP
0045           12 GARAY(JX) = 0.0
0046              DO 15 J = 1,NP
0047              DO 14 I = 1,NDATA
0048           14 GARAY(J)=GARAY(J)+RES(I)*PARAY(I,J)
0049           15 GSTAR(J) = GARAY(J)/DSQRT(DABS(AARAY(J,J)))
0050              RETURN
0051              END
```

```
0001            SUBROUTINE MHK2(BASE,Z,SUMSQ,PARAM,NCONV,ASTAR,GSTAR,AARAY,NDATA,
               1TH,TL,III,KOUNT,CONVER)
                C
                C     SUBROUTINE CALLED BY MRQDT TO COMPUTE THE ITERATIVE  PARAMETER
                C     STEP SIZE, THE NEW PARAMETERS, THE SUM OF SQUARES AT THE NEW
                C     PARAMETERS, AND TO TEST FOR CONVERGENCE USING THE NEW PARAMETERS.
                C
0002            COMMON AN,UPLIM,BOTLIM,VCAL(50),TCOV(50),THETA(100,5),A,RES(50)
0003            COMMON UADS(100,5),SDELTA,STR,SROT,SVIB,EKIN,FREQ(100)
0004            COMMON NCALL,NPLOT,NANAL,NP
0005            COMMON PAO,C1,TEMP,II,JJ,ORNT
0006            COMMON P(50),V(50)
                C
0007            DIMENSION BASE(6),PARAM(6),DELTA(6),WORK1(6),WORK2(6)
0008            DIMENSION AARAY(6,6),ASTAR(6,6),GSTAR(6),DDENOM(36),TL(6),TH(6)
0009            DIMENSION DCINV(36),PROD(36)
                C
0010            DOUBLE PRECISION AN,UPLIM,BOTLIM,H,UAVE,G,VMOL,VIB,ALPHA,BETA,A
0011            DOUBLE PRECISION BASE,SUMSQ,PARAM,VCAL,TCOV,THETA,UADS
0012            DOUBLE PRECISION DDENOM,DET,AARAY,ASTAR,WORK1,WORK2,GSTAR,DELTA
0013            DOUBLE PRECISION DLEN,GLEN,ALNGTH,ANGL,ANGLE,GRNUM,FACTR,RES
0014            DOUBLE PRECISION DCINV,PROD
                C
                C     III = CODE TO INDICATE WHETHER A GRADIENT VECTOR  OR INTERPOLATED
                C     VECTOR IS TO BE CALCULATED
0015            IF(III) 100,100,200
                C
                C     ENTRY POINT TO SEARCH WITH AN INTERPOLATED VECTOR
0016          100 DO 45 K = 1,6
0017           45 DELTA(K) = 0.0
                C
                C     SET UP DENOMINATOR ASTAR + (LMBDA*I)
0018            KOUNT=1
0019            NCONV = 0
0020            DO 14 J = 1,NP
0021            DO 14 I = 1,NP
0022            NN = NP*(J-1) + I
0023           14 DDENOM(NN) = ASTAR(I,J)
0024            DO 15 J = 1,NP
0025            NN = NP*(J-1) + J
0026           15 DDENOM(NN) = ASTAR(J,J) + Z*1.0
0027            DO 300 L=1,36
0028          300 DCINV(L)=DDENOM(L)
                C
0029            CALL MINV(DDENOM,NP,DET,WORK1,WORK2)
0030            CALL GMPRD(DDENOM,DCINV,PROD,NP,NP,NP)
                C     TEST OFF DIAGONAL ELEMENTS OF THE PRODUCT MATRIX
0031            DO 301 K = 2,NP
0032            K1 = K - 1
```

```
0033              DO 301 KK = 1,K1
0034              NC = NP*K1 + KK
0035              ITEST = DABS(PROD(NC)) - 1.0D-10
0036              IF(ITEST) 301,301,302
0037            301 CONTINUE
0038              GO TO 303
0039            302 WRITE(6,305)
0040            305 FORMAT(1H ,'WARNING MATRIX INVERSION ILL-BEHAVED')
0041              WRITE(6,306) DET
0042            306 FORMAT(1H ,'DETERMINANT =',E14.7)
0043              WRITE(6,307)
0044            307 FORMAT(1H ,'COMPUTED IDENTITY MATRIX')
0045              DO 308 L=1,NP
0046              NT=(L-1)*NP+1
0047              NS=NT+NP-1
0048            308 WRITE(6,309) (PROD(J),J=NT,NS)
0049            309 FORMAT(1H ,6E20.7)
0050            303 CALL GMPRD(DDENOM,GSTAR,DELTA,NP,NP,1)
0051              DO 16 J = 1,NP
0052             16 DELTA(J) = DELTA(J) /DSQRT(DABS(AARAY(J,J)))
                C
0053              DLEN = 0.0
0054              GLEN = 0.0
0055              DO 33 J = 1,NP
0056              DLEN = DLEN + DELTA(J)**2
0057             33 GLEN = GLEN + GSTAR(J)**2
0058              ALNGTH = (DSQRT(DLEN))*(DSQRT(GLEN))
0059              ANGL = 0.0
0060              DO 32 J = 1,NP
0061             32 ANGL = ANGL + GSTAR(J)*DELTA(J)
0062              ANGLE = ANGL/ALNGTH
0063              ANGLE =DARCOS(ANGLE)
0064              DANGLE=ANGLE*180./3.1416
0065              WRITE(6,501)
0066            501 FORMAT(1H ,'SEARCH VECTOR INTERPOLATED BETWEEN GAUSS-NEWTON AND GR
                   1ADIENT VECTOR')
0067              WRITE(6,35) DANGLE
0068             35 FORMAT(1H ,'ANGLE =',E12.5)
0069              IF(DABS(ANGLE)-(3.1416/6.0)) 250,250,101
0070            250 WRITE(6,502)
0071            502 FORMAT(1H ,'ANGLE TOO SMALL USE GRADIENT VECTOR')
0072              III=1
0073              KOUNT=1
                C
                C     ENTRY POINT TO SEARCH WITH GRADIENT VECTOR   CODE III = 1
0074            200 GRNUM = 0.0
0075              NCONV=0
0076              DO 206 K=1,6
0077            206 WORK1(K)=0.0
```

```
0078              DO 201 J = 1,NP
0079              GRNUM = GRNUM + GSTAR(J)**2
0080              DO 201 I = 1,NP
0081            201 WORK1(J)=WORK1(J)+GSTAR(I)*ASTAR(I,J)
0082              FACTR = 0.0
0083              DO 202 J = 1,NP
0084            202 FACTR = FACTR + WORK1(J)*GSTAR(J)
0085              FACTR = GRNUM/FACTR
0086              FACTR=FACTR/KOUNT
0087              WRITE(6,503)
0088            503 FORMAT(1H ,'SEARCH VECTOR IS GRADIENT VECTOR')
0089              WRITE(6,204) FACTR
0090            204 FORMAT(1H ,'FACTOR =',E12.5)
0091              DO 203 J = 1,NP
0092            203 DELTA(J) = FACTR*GSTAR(J)
0093              WRITE(6,205) DELTA
0094            205 FORMAT(1H ,'DELTAS =',6E16.7)
                C
                C     TEST NEW PARAMETERS FOR CONVERGENCE
0095            101 DO 17 J = 1,NP
0096              TEST=DABS(DELTA(J))/(.001+DABS(BASE(J)))-CONVER
0097              IF (TEST) 17,18,18
0098             17 CONTINUE
0099              NCONV = 1
0100             18 DO 19 J = 1,6
0101             19 PARAM(J) =  BASE(J) + DELTA(J)
0102              TL(1)=3.5
0103              TH(1)=1000.
0104              TL(2)=0.5
0105              TH(2)=7.0
0106              TL(3)=.05
0107              TH(3)=10.0
0108              TL(4)=1.0E-04
0109              TH(4)=1.0E+02
0110              DO 82 J = 1,NP
0111              IF(PARAM(J)-TL(J)) 80,80,81
0112             80 PARAM(J) = TL(J)
0113              GO TO 82
0114             81 IF(PARAM(J) - TH(J)) 82,82,83
0115             83 PARAM(J) = TH(J)
0116             82 CONTINUE
                C
0117             25 CALL MLTAD1(PARAM,NDATA)
0118              SUMSQ = 0.0
0119              DO 30 I = 1,NDATA
0120              RES(I)=V(I)-VCAL(I)
0121             30 SUMSQ = SUMSQ + RES(I)**2
0122              RETURN
0123              END
```

```
0001            SUBROUTINE MLTAD1(BASE,NDATA)
                C
                C     SUBROUTINE CALLED BY THE MAINLINE PROGRAM AND SUBROUTINES MHK1 AND
                C     MHK2 TO CALCULATE THE VOLUME OF GAS ADSORBED.  EITHER THE ROSS &
                C     OLIVIER MODEL OR THE MULTILAYER MODEL MAY BE USED.
                C
0002            COMMON AN,UPLIM,BOTLIM,VCAL(50),TCOV(50),THETA(100,5),A,RES(50)
0003            COMMON UADS(100,5),SDELTA,STR,SROT,SVIB,EKIN,FREQ(100)
0004            COMMON NCALL,NPLOT,NANAL,NP
0005            COMMON PAO,C1,TEMP,II,JJ,ORNT
0006            COMMON P(50),V(50)
                C
0007            DIMENSION BASE(6),USURF(102),COV(100),DELTA(100)
0008            DIMENSION Z(500)
                C
0009            DOUBLE PRECISION AN,UPLIM,BOTLIM,H,UAVE,G,VMOL,VIB,ALPHA,BETA,A
0010            DOUBLE PRECISION BASE,U,VCAL,COV,TCOV,THETA,DELTA
0011            DOUBLE PRECISION USPACE,U1,U2,USURF,U3,UADS,RES
0012            DOUBLE PRECISION HLO,HUP
                C
0013            G=BASE(1)
0014            UAVE=BASE(2)
0015            VMOL=BASE(3)
0016            VIB=BASE(4)
0017            ALPHA=BASE(5)
0018            BETA=BASE(6)
                C
0019            DO 70 K1=1,100
0020            DO 70 K2=1,5
0021          70 THETA(K1,K2) = 0.0
                C
                C     CALCULATE THE STATISTICAL THERMODYNAMIC FUNCTIONS FOR THE SPECIFIED
                C     ADSORBATE MOLECULE
0022            IF(NCALL -1) 30,31,32
0023          30 CALL ARGN(VIB)
0024            GO TO 33
0025          31 ORNT=(BASE(5)-52.5)/(45.0-52.5)
0026            CALL NITR(VIB,AREA)
0027            BASE(6)=AREA
0028            BETA=AREA
0029            GO TO 33
0030          32 CALL CFCL(VIB)
0031          33 CONTINUE
                C
                C     CALCULATE THE LOG-NORMAL DISTRIBUTION OF THE ADSORPTIVE POTENTIALS
                C     CALCULATE THE NORMALIZATION FACTOR TO 10 KCAL/MOLE RANGE
0032            HUP=((2.*DLOG(UAVE)-1./G)+DSQRT((2.*DLOG(UAVE)-1./G)**2
                1-4.*((DLOG(UAVE))**2+DLOG(1.D-05)/G)))/2.0
0033            HUP=DEXP(HUP)
```

```
0034              HLO=((2.*DLOG(UAVE)-1./G)-DSQRT((2.*DLOG(UAVE)-1./G)**2
                 1-4.*((DLOG(UAVE))**2+DLOG(1.D-05)/G)))/2.0
0035              HLO=DEXP(HLO)
0036              H=(HUP-HLO)/500.
0037              U=HLO
0038              DO 1 J=1,500
0039              Z(J)=DEXP(-G*(DLOG(U)-DLOG(UAVE))**2)/U
0040            1 U=U+H
0041              USTEP=H
0042              CALL QSF(USTEP,Z,Z,500)
                C
0043              AN=Z(500)
0044              UPLIM=((2.*DLOG(UAVE)-1./G)+DSQRT((2.*DLOG(UAVE)-1./G)**2-4.*((DL
                 1G(UAVE))**2 + DLOG(0.001*AN)/G)))/2.0
0045              UPLIM=DEXP(UPLIM)
0046              BOTLIM=((2.*DLOG(UAVE)-1./G)-DSQRT((2.*DLOG(UAVE)-1./G)**2-4.*((DL
                 1OG(UAVE))**2 + DLOG(0.001*AN)/G)))/2.0
0047              BOTLIM=DEXP(BOTLIM)
0048              IF(UPLIM-10.) 58,59,59
0049           59 UPLIM=10.
0050           58 IF(BOTLIM) 60,61,61
0051           60 BOTLIM=0.0
0052           61 USPACE=(UPLIM-BOTLIM)/200.
0053              U=BOTLIM
0054              SDELTA=0.0
0055              DO 4 I=1,100
0056              U1=DEXP(-G*(DLOG(U)-DLOG(UAVE))**2)/(U*AN)
0057              U=U+USPACE
0058              U2=DEXP(-G*(DLOG(U)-DLOG(UAVE))**2)/(U*AN)
0059              USURF(I)=U
0060              FREQ(I)=U2
0061              U=U+USPACE
0062              U3=DEXP(-G*(DLOG(U)-DLOG(UAVE))**2)/(U*AN)
0063              DELTA(I)=(USPACE/3.0)*(U1+4.*U2+U3)
0064            4 SDELTA=SDELTA+DELTA(I)
                C
                C     CALC UADS(I,J) ARRAY
                C     I INDEX, 1-100, REFERS TO THE ADSORPTIVE POTENTIAL DISTRIBUTION
                C     J INDEX INDICATES THE NUMBER OF THE LAYER 1-5
                C
0065              CSAVE = C1
0066              DO 50 M = 1,NDATA
0067              PAO = P(M)
0068              TCOV(M) = 0.0
0069              DO 17 I = 1,100
0070              IF(NANAL) 100,100,101
0071          100 UADS(I,1) = USURF(I)
0072              C1 = (2.*ALPHA/BETA)*0.143883
0073              J=1
```

```
0074              GO TO 11
0075            101 DO 17 J=1,5
0076              UADS(I,J) = USURF(I)/(J**3)
0077              C1 = (2.*ALPHA/BETA)*0.143883
0078              IF(J-2) 11,12,12
0079             12 UADS(I,J) = UADS(I,J) + C1*THETA(I,1)/(J-1)**3
0080              IF(J-2) 20,20,19
0081             19 DO 13 K = 3,J
0082             13 UADS(I,J) = UADS(I,J) + CSAVE*THETA(I,K-1)/(J-K+1)**3
0083             20 C1 = CSAVE
0084              IF(UADS(I,J)-.0019872*TEMP) 15,15,11
0085             15 UADS(I,J) = 0.0
0086              GO TO 17
0087             11 II = I
0088              JJ = J
0089              CALL COVE3
0090             17 CONTINUE
                C
0091              DO 14 JC = 1,100
0092              COV(JC) = 0.0
0093              DO 14 J8=1,5
0094             14 COV(JC) = COV(JC) + THETA(JC,J8)
0095              DO 18 JA = 1,100
0096             18 TCOV(M) = TCOV(M) + DELTA(JA)*COV(JA)
0097             50 VCAL(M)=TCOV(M)*VMOL
                C
0098              C1 = CSAVE
0099              RETURN
0100              END
```

```
0001            SUBROUTINE ARGN(VIB)
                C
                C     SUBROUTINE CALLED BY MLTADI TO COMPUTE THE TRANSLATIONAL, ROTATIONAL, AND
                C     VIBRATIONAL PARTITION FUNCTIONS FOR THE ARGON ADSORBATE MOLECULE.
                C     A IS THE CONSTANT IN THE LOCAL ISOTHERM EQUATION.
                C
0002            COMMON AN,UPLIM,BOTLIM,VCAL(50),TCOV(50),THETA(100,5),A,RES(50)
0003            COMMON UADS(100,5),SDELTA,STR,SROT,SVIB,EKIN,FREQ(100)
0004            COMMON NCALL,NPLOT,NANAL,NP
0005            COMMON PAO,C1,TEMP,II,JJ,ORNT
0006            COMMON P(50),V(50)
0007            DOUBLE PRECISION AN,UPLIM,BOTLIM,H,UAVE,G,VMOL,VIB,ALPHA,BETA ,A
0008            DOUBLE PRECISION VCAL,TCOV,THETA,X,FVIB,UADS,RES
0009            STR = (1.9872*ALOG(39.944))/2.0+(1.9872*ALOG(TEMP))/2.0 + 2.30
0010            DSTR = STR/1.9872
0011            STR = -STR/1000.
0012            SROT = 0.0
0013            X = 48.0*VIB/TEMP
0014            SVIB = 0.0019872*X/(DEXP(X)-1.)-0.0019872*DLOG(1.-1./DEXP(X))
0015            FVIB = DLOG(1.-1.0/DEXP(X))
0016            TS = 13.6/(4.08*TEMP)
0017            EKIN = -0.5*0.0019872*TEMP
0018            A = DSTR + FVIB - 0.5 - ALOG(TS/(1.-TS)) + ALOG(760.)
0019            A =DEXP(A)
0020            RETURN
0021            END
```

```
0001            SUBROUTINE NITR(VIB,AREA)
                C
                C     SUBROUTINE CALLED BY MLTAD1 TO COMPUTE THE TRANSLATIONAL, ROTATIONAL AND
                C     VIBRATIONAL PARTITION FUNCTIONS FOR THE NITROGEN ADSORBATE MOLECULE.
                C     A IS THE CONSTANT IN THE LOCAL ISOTHERM EQUATION
                C     ORNT IS THE FRACTION OF NITROGEN MOLECULES ADSORBED IN A FLAT POSITION.
                C
0002            COMMON AN,UPLIM,BOTLIM,VCAL(50),TCOV(50),THETA(100,5),A,RES(50)
0003            COMMON UADS(100,5),SDELTA,STR,SROT,SVIB,EKIN,FREQ(100)
0004            COMMON NCALL,NPLOT,NANAL,NP
0005            COMMON PAO,C1,TEMP,II,JJ,ORNT
0006            COMMON P(50),V(50)
0007            DOUBLE PRECISION AN,UPLIM,BOTLIM,H,UAVE,G,VMOL,VIB,ALPHA,BETA,A
0008            DOUBLE PRECISION VCAL,TCOV,THETA,X,FVIB,UADS,RES
0009            AREA=ORNT*17.1+(1.-ORNT)*12.3
0010            STR = (1.9872*ALOG(28.014))/2.0 + (1.9872*ALOG(TEMP))/2.+2.30
0011            DSTR = STR/1.9872
0012            STR = -STR/1000.
0013            DSROT =ALOG((8*(3.1416**3)*1.3942*0.138*TEMP/(6.625**2))**0.5)+0.5
0014            DSROT=ORNT*DSROT
0015            SROT = -0.0019872*DSROT
0016            X = 48.0*VIB/TEMP
0017            SVIB= 0.0019872*2.*X/(DEXP(X)-1.)-2.*0.0019872*DLOG(1.-DEXP(-X))
0018            SVIB=ORNT*SVIB+(1.-ORNT)*(.0019872*X/(DEXP(X)-1.)-.0019872*DLOG(1.
               1-1./DEXP(X)))
0019            FVIB = 2.*DLOG(1.-1./DEXP(X))
0020            FVIB=ORNT*FVIB+(1.-ORNT)*(DLOG(1.-1./DEXP(X)))
0021            EKIN = 0.0019872*TEMP
0022            EKIN=ORNT*EKIN+(1.-ORNT)*(.0019872*.5*TEMP)
0023            TS=AREA/(4.08*TEMP)
0024            A=DSTR+DSROT+FVIB-ORNT-(1.-ORNT)*.5-ALOG(TS/(1.-TS))+ALOG(760.)
0025            A =DEXP(A)
0026            RETURN
0027            END
```

```
0001            SUBROUTINE CFCL(VIB)
                C
                C     SUBROUTINE CALLED BY MLTAD1 TO COMPUTE THE TRANSLATIONAL, ROTATIONAL AND
                C     VIBRATIONAL PARTITION FUNCTIONS FOR THE CFCL3 ADSORBATE MOLECULE.
                C     THESE CALCULATIONS ASSUME THAT THE POLAR GAS BEHAVES AS AN IDEAL
                C     ADSORBATE WITH NO PREFERENTIAL ORIENTATION.
                C     A IS THE CONSTANT IN THE LOCAL ISOTHERM EQUATION
                C
0002            COMMON AN,UPLIM,BOTLIM,VCAL(50),TCOV(50),THETA(100,5),A,RES(50)
0003            COMMON UADS(100,5),SDELTA,STR,SROT,SVIB,EKIN,FREQ(100)
0004            COMMON NCALL,NPLOT,NANAL,NP
0005            COMMON PAO,C1,TEMP,II,JJ,ORNT
0006            COMMON P(50),V(50)
0007            DOUBLE PRECISION AN,UPLIM,BOTLIM,H,UAVE,G,VMOL,VIB,ALPHA,BETA
0008            DOUBLE PRECISION VCAL,TCOV,THETA,X,FVIB,A,UADS,RES
0009          1 STR = (1.9872*ALOG(137.382))/2.0+(1.9872*ALOG(TEMP))/2.0 + 2.30
0010            DSTR = STR/1.9872
0011            STR = -STR/1000.
0012            DSROT=0.0
0013            SROT = -0.0019872*DSROT
0014          3 X=(48.*VIB)/TEMP
0015            SVIB=.0019872*X/(DEXP(X)-1.)-.0019872*DLOG(1.-1./DEXP(X))
0016            FVIB=DLOG(1.-1./DEXP(X))
0017            EKIN=-.0019872*TEMP/2.
0018            TS = 31.2/(4.08*TEMP)
0019            A=DSTR+DSROT+FVIB-1./2.-ALOG(TS/(1.-TS))+ALOG(760.)
0020            A =DEXP(A)
0021            RETURN
0022            END
```

```
0001              SUBROUTINE COVE3
                  C
                  C     SUBROUTINE CALLED BY MLTADI TO CALCULATE THETA(I,J) THE FRACTIONAL
                  C     COVERAGE
                  C     COVE3 IS A MODIFIED FORM OF SUBROUTINE DRTMI FROM THE IBM SCIENTIFIC
                  C     SUBROUTINE PACKAGE.  THE PURPOSE OF THE PROGRAM IS TO SOLVE A GENERAL
                  C     NON LINEAR EQUATION OF THE FORM FCT(X) = 0 BY MEANS OF MJELLER'S
                  C     ITERATION METHOD
                  C
                  C     I INDEX 1-100 REFERS TO THE ADSORPTIVE POTENTIAL DISTRIBJTION
                  C     J INDEX 1-5 INDICATES THE LAYER
                  C
0002              COMMON AN,UPLIM,BOTLIM,VCAL(50),TCOV(50),THETA(100,5),A,RES(50)
0003              COMMON UADS(100,5),SDELTA,STR,SROT,SVIB,EKIN,FREQ(100)
0004              COMMON NCALL,NPLOT,NANAL,NP
0005              COMMON PAO,C1,TEMP,II,JJ,ORNT
0006              COMMON P(50),V(50)
0007              DOUBLE PRECISION AN,UPLIM,BOTLIM,H,UAVE,G,VMOL,VIB,ALPHA,BETA,A
0008              DOUBLE PRECISION B,AD,UD,C1D,PD,TD,X,XL,XR,FL,FR,TOL,TOLF
0009              DOUBLE PRECISION A1,DX,XM,FM
0010              DOUBLE PRECISION VCAL,TCOV,THETA,UADS,RES
0011              PD = DBLE(PAO)
0012              C1D = DBLE(C1)
0013              UD=UADS(II,JJ)
0014              AD = A
0015              TD = DBLE(TEMP)
                  C
                  C     PREPARE ITERATION
0016              IER = 0
0017           30 XL=0.0
0018           32 XR=.98
0019              X = XL
0020              B = (X/(1.-X))*DEXP((X/(1.-X))-C1D*X/(0.0019872*TD))
                 1-PD/(AD*DEXP(-UD/(0.0019872*TD)))
0021              IF(B) 1,16,1
0022            1 FL = B
0023              X = XR
0024              B = (X/(1.-X))*DEXP((X/(1.-X))-C1D*X/(0.0019872*TD))
                 1-PD/(AD*DEXP(-UD/(0.0019872*TD)))
0025              IF(B) 2,16,2
0026            2 FR = B
0027              IF(DSIGN(1.D0,FL)+DSIGN(1.D0,FR)) 25,3,25
0028            3 I = 0
0029              IF(THETA(II-1,JJ)-.95) 40,41,41
0030           40 EPS=.00001
0031              GO TO 42
0032           41 EPS=.001
0033           42 TOLF=100.*EPS
                  C
```

```
C
C     START IERATION LOOP
0034      4 I = I + 1
0035        DO 13 K=1,10000
0036        X = 0.5D0*(XL+XR)
0037        B = (X/(1.-X))*DEXP((X/(1.-X))-C1D*X/(0.0019872*TD))
           1-PD/(AD*DEXP(-UD/(0.0019872*TD)))
0038        IF(B) 5,16,5
0039      5 IF(DSIGN(1.D0,B)+DSIGN(1.D0,FR)) 7,6,7
C
C     INTERCHANGE XL AND XR IN ORDER TO GET THE SAME SIGN IN B AND FR
0040      6 TOL = XL
0041        XL = XR
0042        XR = TOL
0043        TOL = FL
0044        FL = FR
0045        FR = TOL
0046      7 TOL = B-FL
0047        A1= B*TOL
0048        A1 = A1 + A1
0049        IF(A1- FR*(FR-FL)) 8,8,9
0050      8 IF(I-10000) 17,17,9
0051      9 XR = X
0052        FR = B
C
C     TEST ON SATISFACTORY ACCUARCY IN BISECTION LOOP
0053        TOL=EPS
0054        A1= DABS(XR)
0055        IF(A1- 1.D0) 11,11,10
0056     10 TOL = TOL * A1
0057     11 IF(DABS(XR-XL)-TOL) 12,12,13
0058     12 IF(DABS(FR-FL)-TOLF) 14,14,13
0059     13 CONTINUE
C
C     END OF BISECTION LOOP
0060        IER = 1
0061        WRITE(6,300) II,JJ,UADS(II,JJ),B,X
0062    300 FORMAT(1H ,I3,5X,I3,5X,3E20.7)
0063        RETURN
C
0064     14 IF(DABS(FR)-DABS(FL))16,16,15
0065     15 THETA(II,JJ)=XL
0066        RETURN
0067     16 THETA(II,JJ)=X
0068        RETURN
C     GENERATION OF ITERATED X VALUE BY INVERSE PARABOLIC INTERPOLATION
0069     17 A1= FR - B
0070        DX = (X-XL)*FL*(1.D0+B*(A1-TOL)/(A1*(FR-FL)))/TOL
0071        XM = X
```

```
0072                FM = B
0073                X = XL - DX
0074                TOL = X
0075                B = (X/(1.-X))*DEXP((X/(1.-X))-C1D*X/(0.0019872*TD))
                   1-PD/(AD*DEXP(-UD/(0.0019872*TD)))
0076                IF(B) 18,16,18
                C
                C     TEST ON SATISFACTORY ACCURACY IN ITERATION LOOP
0077             18 TOL = 0.00001
0078                A1= DABS(X)
0079                IF(A1- 1.D0) 20,20,19
0080             19 TOL = TOL * A1
0081             20 IF(DABS(DX)-TOL) 21,21,22
0082             21 IF(DABS(B) - TOLF) 16,16,22
                C
                C
                C     PREPARATION OF NEXT BISECTION LOOP
0083             22 IF(DSIGN(1.D0,B)+DSIGN(1.D0,FL)) 24,23,24
0084             23 XR = X
0085                FR = B
0086                GO TO 4
0087             24 XL = X
0088                FL = B
0089                XR = XM
0090                FR = FM
0091                GO TO 4
0092             25 IER = 2
0093                WRITE(6,300) IER
0094                RETURN
0095                END
```

```
0001                SUBROUTINE ARRAY(MODE,I,J,N,M,S,D)
                C
                C     IBM SCIENTIFIC SUBROUTINE PACKAGE PROGRAM MODIFIED TO DOUBLE
                C     PRECISION.
                C
                C     CONVERT DATA ARRAY FROM SINGLE TO DOUBLE DIMENSION OR VICE
                C     VERSA.  THIS SUBROUTINE IS USED TO LINK THE MAINLINE PROGRAM
                C     WHICH HAS DOUBLE DIMENSION ARRAYS AND THE SSP SUBROUTINES
                C     WHICH OPERATE ON ARRAYS OF DATA IN A VECTOR FASHION.
                C
0002                DIMENSION S(1),D(1)
0003                DOUBLE PRECISION S,D
0004                NI = N-I
                C     TEST TYPE OF CONVERSION
0005                IF(MODE -1) 100,100,120
                C     CONVERT FROM SINGLE TO DOUBLE PRECISION
0006              100 IJ = I*J+1
0007                  NM = N*J+1
0008                  DO 110 K = 1,J
0009                  NM = NM - NI
0010                  DO 110 L = 1,I
0011                  IJ = IJ - 1
0012                  NM = NM - 1
0013              110 D(NM) = S(IJ)
0014                  GO TO 140
                C     CONVERT FROM DOUBLE TO SINGLE DIMENSION
                C
0015              120 IJ = 0
0016                  NM = 0
0017                  DO 130 K = 1,J
0018                  DO 125 L = 1,I
0019                  IJ = IJ + 1
0020                  NM = NM + 1
0021              125 S(IJ) = D(NM)
0022              130 NM = NM + NI
                C
0023              140 RETURN
0024                  END
```

```
0001                  SUBROUTINE GMTRA(A,R,N,M)
                C
                C     IBM SCIENTIFIC SUBROUTINE PACKAGE PROGRAM MODIFIED TO DOUBLE
                C     PRECISION.
                C
                C     TRANSPOSE A GENERAL MATRIX
                C
0002                  DIMENSION A(1),R(1)
0003                  DOUBLE PRECISION A,R
0004                  IR=0
0005                  DO 10 I=1,N
0006                  IJ=I-N
0007                  DO 10 J=1,M
0008                  IJ=IJ+N
0009                  IR=IR+1
0010                10 R(IR)=A(IJ)
0011                  RETURN
0012                  END
```

```
0001            SUBROUTINE GMPRD(A,B,R,N,M,L)
                C
                C     IBM SCIENTIFIC SUBROUTINE PACKAGE PROGRAM MODIFIED TO DOUBLE
                C     PRECISION.
                C
                C     MULTIPLY TWO GENERAL MATRICES TO FORM A RESULTANT GENERAL MATRIX
                C
0002            DIMENSION A(1),B(1),R(1)
0003            DOUBLE PRECISION A,B,R
0004            IR = 0
0005            IK = -M
0006            DO 10 K = 1,L
0007            IK = IK + M
0008            DO 10 J = 1,N
0009            IR = IR + 1
0010            JI = J - N
0011            IB = IK
0012            R(IR) = 0
0013            DO 10 I = 1,M
0014            JI = JI + N
0015            IB = IB + 1
0016         10 R(IR) = R(IR) + A(JI)*B(IB)
0017            RETURN
0018            END
```

```
0001                SUBROUTINE EIGEN(A,R,N,MV)
                C
                C     IBM SCIENTIFIC SUBROUTINE PACKAGE PROGRAM MODIFIED TO DOJBLE
                C     PRECISION.
                C
                C     COMPUTE EIGENVALUES AND EIGENVECTORS OF A REAL SYMMETRIC MATRIX
                C
0002                DIMENSION A(1),R(1)
0003                DOUBLE PRECISION A,R,ANORM,ANRMX,THR,X,Y,SINX,SINX2,COSX,COSX2,
                   1SINCS,RANGE
                C     GENERATE IDENTITY MATRIX
0004                 5 RANGE=1.0D-12
0005                  IF(MV-1) 10,25,10
0006                10 IQ=-N
0007                   DO 20 J=1,N
0008                   IQ=IQ+N
0009                   DO 20 I=1,N
0010                   IJ=IQ+I
0011                   R(IJ)=0.0
0012                   IF(I-J) 20,15,20
0013                15 R(IJ) = 1.0
0014                20 CONTINUE
                C     COMPUTE INITIAL AND FINAL NORMS (ANORM AND ANORMX)
0015                25 ANORM=0.0
0016                   DO 35 I=1,N
0017                   DO 35 J=I,N
0018                   IF(I-J) 30,35,30
0019                30 IA=I+(J*J-J)/2
0020                   ANORM=ANORM+A(IA)*A(IA)
0021                35 CONTINUE
0022                   IF(ANORM) 165,165,40
0023                40 ANORM=1.414*DSQRT(ANORM)
0024                   ANRMX=ANORM*RANGE/FLOAT(N)
                C     INITIALIZE INDICATORS AND COMPUTE THRESHOLD, THR
0025                   IND=0
0026                   THR=ANORM
0027                45 THR=THR/FLOAT(N)
0028                50 L=1
0029                55 M=L+1
                C     COMPUTE SIN AND COS
0030                60 MQ=(M*M-M)/2
0031                   LQ=(L*L-L)/2
0032                   LM=L+MQ
0033                62 IF(DABS(A(LM))-THR) 130,65,65
0034                65 IND=1
0035                   LL=L+LQ
0036                   MM=M+MQ
0037                   X=0.5*(A(LL)-A(MM))
0038                68 Y=-A(LM)/DSQRT(A(LM)*A(LM)+X*X)
```

```
0039              IF(X) 70,75,75
0040           70 Y=-Y
0041           75 SINX=Y/DSQRT(2.0*(1.0+(DSQRT(1.0-Y*Y))))
0042              SINX2=SINX*SINX
0043           78 COSX=DSQRT(1.0-SINX2)
0044              COSX2=COSX*COSX
0045              SINCS=SINX*COSX
                C     ROTATE L AND M COLUMNS
0046              ILQ=N*(L-1)
0047              IMQ=N*(M-1)
0048              DO 125 I=1,N
0049              IQ=(I*I-I)/2
0050              IF(I-L) 80,115,80
0051           80 IF(I-M) 85,115,90
0052           85 IM=I+MQ
0053              GO TO 95
0054           90 IM=M+IQ
0055           95 IF(I-L) 100,105,105
0056          100 IL=I+LQ
0057              GO TO 110
0058          105 IL=L+IQ
0059          110 X=A(IL)*COSX-A(IM)*SINX
0060              A(IM)=A(IL)*SINX+A(IM)*COSX
0061              A(IL)=X
0062          115 IF(MV-1) 120,125,120
0063          120 ILR=ILQ+I
0064              IMR=IMQ+I
0065              X=R(ILR)*COSX-R(IMR)*SINX
0066              R(IMR)=R(ILR)*SINX+R(IMR)*COSX
0067              R(ILR)=X
0068          125 CONTINUE
0069              X=2.0*A(LM)*SINCS
0070              Y=A(LL)*COSX2+A(MM)*SINX2-X
0071              X=A(LL)*SINX2+A(MM)*COSX2+X
0072              A(LM)=(A(LL)-A(MM))*SINCS+A(LM)*(COSX2-SINX2)
0073              A(LL)=Y
0074              A(MM)=X
                C      TESTS FOR COMPLETION
                C     TEST FOR M=LAST COLUMN
0075          130 IF(M-N) 135,140,135
0076          135 M=M+1
0077              GO TO 60
                C     TEST FOR L=SECOND FROM LAST COLUMN
0078          140 IF(L-(N-1)) 145,150,145
0079          145 L=L+1
0080              GO TO 55
0081          150 IF(IND-1) 160,155,160
0082          155 IND=0
0083              GO TO 50
```

```
C     COMPARE THRESHOLD WITH FINAL NORM
  160 IF(THR-ANRMX) 165,165,45
C     SORT EIGENVALUES AND EIGENVECTORS
  165 IQ=-N
      DO 185 I=1,N
      IQ=IQ+N
      LL=I+(I*I-I)/2
      JQ=N*(I-2)
      DO 185 J=I,N
      JQ=JQ+N
      MM=J+(J*J-J)/2
      IF(A(LL)-A(MM)) 170,185,185
  170 X=A(LL)
      A(LL)=A(MM)
      A(MM)=X
      IF(MV-1) 175,185,175
  175 DO 180 K=1,N
      ILR=IQ+K
      IMR=JQ+K
      X=R(ILR)
      R(ILR)=R(IMR)
  180 R(IMR)=X
  185 CONTINUE
      RETURN
      END
```

```
0001            SUBROUTINE MINV(A,N,D,L,M)
                C
                C       IBM SCIENTIFIC SUBROUTINE PACKAGE PROGRAM MODIFIED TO DOUBLE
                C       PRECISION.
                C
                C       INVERT A MATRIX
                C
0002            DIMENSION A(1),L(1),M(1)
0003            DOUBLE PRECISION A,D,BIGA,HOLD
                C       INVERT THE SUBMATRIX OF CORRELATION COEFFICIENTS
                C       SEARCH FOR LARGEST ELEMENT
0004            D=1.0
0005            NK=-N
0006            DO 228 K=1,N
0007            NK=NK+N
0008            L(K)=K
0009            M(K)=K
0010            KK=NK+K
0011            BIGA=A(KK)
0012            DO 209 J=K,N
0013            IZ=N*(J-1)
0014            DO 209 I=K,N
0015            IJ=IZ+I
0016          210 IF(DABS(BIGA) - DABS(A(IJ))) 211,209,209
0017          211 BIGA=A(IJ)
0018            L(K)=I
0019            M(K)=J
0020          209 CONTINUE
                C       INTERCHANGE ROWS
0021            J=L(K)
0022            IF(J-K) 212,212,213
0023          213 KI=K-N
0024            DO 214 I=1,N
0025            KI=KI+N
0026            HOLD=-A(KI)
0027            JI=KI-K+J
0028            A(KI)=A(JI)
0029          214 A(JI)=HOLD
                C       INTERCHANGE ROWS
0030          212 I=M(K)
0031            IF(I-K) 215,215,216
0032          216 JP=N*(I-1)
0033            DO 217 J=1,N
0034            JK=NK+J
0035            JI=JP+J
0036            HOLD=-A(JK)
0037            A(JK)=A(JI)
0038          217 A(JI)=HOLD
                C       DIVIDE COLUMN BY MINUS PIVOT
```

```
0039          215 IF(BIGA) 218,219,218
0040          219 D=0.0
0041              RETURN
0042          218 DO 221 I=1,N
0043              IF(I-K) 222,221,222
0044          222 IK=NK+I
0045              A(IK)=A(IK)/(-BIGA)
0046          221 CONTINUE
              C   REDUCE MATRIX
0047              DO 223 I=1,N
0048              IK=NK+I
0049              HOLD=A(IK)
0050              IJ=I-N
0051              DO 223 J=1,N
0052              IJ=IJ+N
0053              IF(I-K) 224,223,224
0054          224 IF(J-K) 225,223,225
0055          225 KJ=IJ-I+K
0056              A(IJ)=HOLD*A(KJ)+A(IJ)
0057          223 CONTINUE
              C   DIVIDE ROW BY PIVOT
0058              KJ=K-N
0059              DO 226 J=1,N
0060              KJ=KJ+N
0061              IF(J-K) 227,226,227
0062          227 A(KJ)=A(KJ)/BIGA
0063          226 CONTINUE
              C   PRODUCT OF PIVOTS
0064              D=D*BIGA
              C   REPLACE PIVOT BY RECIPROCAL
0065              A(KK)=1.0/BIGA
0066          228 CONTINUE
              C   FINAL ROW AND COLUMN INTERCHANGE
0067              K=N
0068          229 K=(K-1)
0069              IF(K) 230,230,231
0070          231 I=L(K)
0071              IF(I-K) 232,232,233
0072          233 JQ=N*(K-1)
0073              JR=N*(I-1)
0074              DO 234 J=1,N
0075              JK=JQ+J
0076              HOLD=A(JK)
0077              JI=JR+J
0078              A(JK)=-A(JI)
0079          234 A(JI)=HOLD
0080          232 J=M(K)
0081              IF(J-K) 229,229,235
0082          235 KI=K-N
```

```
0083              DO 236 I=1,N
0084              KI=KI+N
0085              HOLD=A(KI)
0086              JI=KI-K*J
0087              A(KI)=-A(JI)
0088          236 A(JI)=HOLD
0089              GO TO 229
0090          230 RETURN
0091              END
```

```
0001            SUBROUTINE SIMQ(A,B,N,KS)
                C
                C       IBM SCIENTIFIC SUBROUTINE PACKAGE PROGRAM
                C       SOLUTION OF SIMULTANEOUS LINEAR ALGEBRAIC EQUATIONS
                C
0002            DIMENSION A(1),B(1)
                C       FORWARD SOLUTION
0003            TOL=0.0
0004            KS=0
0005            JJ=-N
0006            DO 65 J=1,N
0007            JY=J+1
0008            JJ=JJ+N+1
0009            BIGA=0
0010            IT=JJ-J
0011            DO 30 I=J,N
                C       SEARCH FOR MAXIMUM COEFFICIENT IN COLUMN
0012            IJ=IT+I
0013            IF(ABS(BIGA)-ABS(A(IJ))) 20,30,30
0014         20 BIGA=A(IJ)
0015            IMAX=I
0016         30 CONTINUE
                C       TEST FOR PIVOT LESS THAN TOLERANCE (SINGULAR MATRIX)
0017            IF(ABS(BIGA)-TOL) 35,35,40
0018         35 KS=1
0019            RETURN
                C       INTERCHANGE ROWS IF NECESSARY
0020         40 I1=J+N*(J-2)
0021            IT=IMAX-J
0022            DO 50 K=J,N
0023            I1=I1+N
0024            I2=I1+IT
0025            SAVE=A(I1)
0026            A(I1)=A(I2)
0027            A(I2)=SAVE
                C       DIVIDE EQUATION BY LEADING COEFFICIENT
0028         50 A(I1)=A(I1)/BIGA
0029            SAVE=B(IMAX)
0030            B(IMAX)=B(J)
0031            B(J)=SAVE/BIGA
                C       ELIMINATE NEXT VARIABLE
0032            IF(J-N) 55,70,55
0033         55 IQS=N*(J-1)
0034            DO 65 IX=JY,N
0035            IXJ=IQS+IX
0036            IT=J-IX
0037            DO 60 JX=JY,N
0038            IXJX=N*(JX-1)+IX
0039            JJX=IXJX+IT
```

```
0040            60 A(IXJX)=A(IXJX)-(A(IXJ)*A(JJX))
0041            65 B(IX)=B(IX)-(B(J)*A(IXJ))
                C     BACK SOLUTION
0042            70 NY=N-1
0043               IT=N*N
0044               DO 80 J=1,NY
0045               IA=IT-J
0046               IB=N-J
0047               IC=N
0048               DO 80 K=1,J
0049               B(IB)=B(IB)-A(IA)*B(IC)
0050               IA=IA-N
0051            80 IC=IC-1
0052               RETURN
0053               END
```

```
0001            SUBROUTINE QSF(H,Y,Z,NDIM)
                C
                C     IBM SCIENTIFIC SUBROUTINE PACKAGE PROGRAM
                C INTEGRATION BY SIMPSON,S RULE
                C
0002            DIMENSION Y(1),Z(1)
0003            HT=.3333333*H
0004            IF(NDIM-5) 7,8,1
                C NDIM GREATER THAN 5
0005          1 SUM1=Y(2)+Y(2)
0006            SUM1=SUM1+SUM1
0007            SUM1=HT*(Y(1)+SUM1+Y(3))
0008            AUX1=Y(4)+Y(4)
0009            AUX1=AUX1+AUX1
0010            AUX1=SUM1+HT*(Y(3)+AUX1+Y(5))
0011            AUX2=HT*(Y(1)+3.875*(Y(2)+Y(5))+2.625*(Y(3)+Y(4))+Y(6))
0012            SUM2=Y(5)+Y(5)
0013            SUM2=SUM2+SUM2
0014            SUM2=AUX2-HT*(Y(4)+SUM2+Y(6))
0015            Z(1)=0.
0016            AUX=Y(3)+Y(3)
0017            AUX=AUX+AUX
0018            Z(2)=SUM2-HT*(Y(2)+AUX+Y(4))
0019            Z(3)=SUM1
0020            Z(4)=SUM2
0021            IF(NDIM-6) 5,5,2
0022          2 DO 4 I=7,NDIM,2
0023            SUM1=AUX1
0024            SUM2=AUX2
0025            AUX1=Y(I-1)+Y(I-1)
0026            AUX1=AUX1+AUX1
0027            AUX1=SUM1+HT*(Y(I-2)+AUX1+Y(I))
0028            Z(I-2)=SUM1
0029            IF(I-NDIM) 3,6,6
0030          3 AUX2=Y(I)+Y(I)
0031            AUX2=AUX2+AUX2
0032            AUX2=SUM2+HT*(Y(I-1)+AUX2+Y(I+1))
0033          4 Z(I-1)=SUM2
0034          5 Z(NDIM-1)=AUX1
0035            Z(NDIM)=AUX2
0036            RETURN
0037          6 Z(NDIM-1)=SUM2
0038            Z(NDIM)=AUX1
0039            RETURN
0040          7 IF(NDIM-3) 12,11,8
0041          8 SUM2=1.125*HT*(Y(1)+Y(2)+Y(2)+Y(2)+Y(3)+Y(3)+Y(3)+Y(4))
0042            SUM1=Y(2)+Y(2)
0043            SUM1=SUM1+SUM1
0044            SUM1=HT*(Y(1)+SUM1+Y(3))
```

```
0045              Z(1)=0.
0046              AUX1=Y(3)+Y(3)
0047              AUX1=AUX1+AUX1
0048              Z(2)=SUM2-HT*(Y(2)+AUX1+Y(4))
0049              IF(NDIM-5) 10,9,9
0050            9 AUX1=Y(4)+Y(4)
0051              AUX1=AUX1+AUX1
0052              Z(5)=SUM1+HT*(Y(3)+AUX1+Y(5))
0053           10 Z(3)=SUM1
0054              Z(4)=SUM2
0055              RETURN
0056           11 SUM1=HT*(1.25*Y(1)+Y(2)+Y(2)-.25*Y(3))
0057              SUM2=Y(2)+Y(2)
0058              SUM2=SUM2+SUM2
0059              Z(3)=HT*(Y(1)+SUM2+Y(3));
0060              Z(1)=0.
0061              Z(2)=SUM1
0062           12 RETURN
0063              END
```

```
C     SAMPLE DATA FOR ARGON, 77.5 DEGREES, 37 DATA POINTS                    DAT00010
C                                                                            DAT00020
C                                                                            DAT00030
370114                                                                       DAT00040
.042        .03903                                                           DAT00050
.052        .03676                                                           DAT00060
.078        .04989                                                           DAT00070
.129        .05589                                                           DAT00080
.151        .06334                                                           DAT00090
.281        .08149                                                           DAT00100
.318        .08567                                                           DAT00110
.529        .11036                                                           DAT00120
.716        .12827                                                           DAT00130
1.092       .14859                                                           DAT00140
1.514       .17549                                                           DAT00150
2.035       .19983                                                           DAT00160
3.016       .23974                                                           DAT00170
5.120       .31327                                                           DAT00180
7.664       .37721                                                           DAT00190
10.637      .43619                                                           DAT00200
12.949      .47291                                                           DAT00210
15.060      .50092                                                           DAT00220
17.355      .52919                                                           DAT00230
20.186      .56719                                                           DAT00240
22.503      .58564                                                           DAT00250
25.169      .61481                                                           DAT00260
27.673      .62818                                                           DAT00270
30.355      .65811                                                           DAT00280
35.270      .68133                                                           DAT00290
40.022      .72643                                                           DAT00300
45.177      .73859                                                           DAT00310
49.712      .77502                                                           DAT00320
55.119      .79345                                                           DAT00330
60.097      .82079                                                           DAT00340
65.199      .84008                                                           DAT00350
69.988      .87064                                                           DAT00360
74.749      .88162                                                           DAT00370
79.597      .91093                                                           DAT00380
84.442      .92181                                                           DAT00390
89.801      .96044                                                           DAT00400
94.937      .96683                                                           DAT00410
0.001                                                                        DAT00420
1.002       77.5        10.0        7.4456      1.3570      1.390       2.2637  DAT00430
47.4        13.6                                                             DAT00440
2.67                                                                         DAT00450
                                                                             DAT00460
```

K	I	LAMBDA	SUM OF SQUARES	GAMMA	MEAN ADSP. POTENTIAL	MONOLAYER VOLUME	VIBRATIONAL FREQUENCY	ALPHA	BETA

BASE POINT FOR SEARCH VECTOR

1 0.25264D-02 0.74456D 01 0.13570D 01 0.13900D 01 0.22637D 01 0.47400D 02 0.13600D 02

EST. DISTANCE TO TRUE PARAMETER = 0.1613432D-01

EST. VARIANCE OF DISTANCE = 0.2792011D-03

EIGENVALUES = 0.3564740D 01 0.4138917D 00 0.1406687D-01 0.7301114D-02 0.0 0.0

SEARCH VECTOR INTERPOLATED BETWEEN GAUSS-NEWTON AND GRADIENT VECTOR

ANGLE = 0.19720E 02

ANGLE TOO SMALL USE GRADIENT VECTOR

SEARCH VECTOR IS GRADIENT VECTOR

FACTOR = 0.53665D 00

DELTAS = 0.3465129D-02 -0.8761092D-03 0.3230192D-05 0.1010274D-02 0.0 0.0

1 1 0.48825E-05 0.25417D-02 0.74491D 01 0.13561D 01 0.13900D 01 0.22647D 01 0.47400D 02 0.13600D 02

CONVERGENCE AT ITERATION = 1

MEDIAN ADSORPTIVE POTENTIAL = 1.357
MEAN ADSORPTIVE POTENTIAL = 1.403
MODE ADSORPTIVE POTENTIAL = 1.269
GAMMA = 7.446
2*ALPHA/BETA(IDEAL) = 1.002
ALPHA = 47.400
BETA = 13.600
TEMPERATURE = 77.50
MONOLAYER VOLUME = 1.3900
LOWER LIMIT OF DIST = 0.479 FREQUENCY = 0.002
UPPER LIMIT OF DIST = 3.359 FREQUENCY = 0.001
NORMALIZATION FACTOR = 0.649
AREA UNDER DIST.CURVE = 0.9998

THERMODYNAMIC ADSORPTION DATA

CHANGE IN TRANS. ENTROPY =-.10286E-01
CHANGE IN ROT. ENTROPY =0.0
CHANGE IN VIB. ENTROPY =0.14701E-02
VIBRATIONAL FREQ. =0.22637E 13
CHANGE IN KINETIC ENERGY =-.77004E-01
A =0.13691D 07

CLASS		NUMBER	PROBABILITY	EXPECTED N	CHI(I)
	-1.2	4.	0.1151	4.26	3.7570
-0.8	-0.4	3.	0.0968	3.58	2.5128
-0.4	0.0	1.	0.1327	4.91	0.2037
0.0	0.4	7.	0.1554	5.75	8.5220
0.4	0.8	5.	0.1554	5.75	4.3480
0.8	1.2	6.	0.1327	4.91	7.3321
1.2	1.6	5.	0.0968	3.58	6.9801
1.2		5.	0.1151	4.26	5.8703
TOTAL		37	1.0000	37.00	39.5261

CHI-SQUARED STATISTIC = 2.526 FOR 7 DEGREES OF FREEDOM

PRESSURE	VOLUME	MODEL VOLUME	CONF. BAND	RESIDUAL	COVERAGE
0.042	0.0390	0.0245	0.0012	0.0146	0.018
0.052	0.0368	0.0278	0.0012	0.0090	0.020
0.078	0.0499	0.0354	0.0014	0.0145	0.025
0.129	0.0559	0.0480	0.0016	0.0079	0.035
0.151	0.0633	0.0527	0.0021	0.0107	0.038
0.281	0.0815	0.0748	0.0017	0.0067	0.054
0.318	0.0857	0.0805	0.0025	0.0052	0.058
0.529	0.1104	0.1056	0.0025	0.0048	0.076
0.716	0.1283	0.1248	0.0018	0.0034	0.090
1.092	0.1486	0.1549	0.0019	-0.0063	0.111
1.514	0.1755	0.1836	0.0017	-0.0081	0.132
2.035	0.1998	0.2127	0.0040	-0.0129	0.153
3.016	0.2397	0.2569	0.0022	-0.0171	0.185
5.120	0.3133	0.3247	0.0044	-0.0114	0.234
7.664	0.3772	0.3873	0.0022	-0.0101	0.279
10.637	0.4362	0.4394	0.0023	-0.0032	0.316
12.949	0.4729	0.4748	0.0029	-0.0019	0.342
15.060	0.5009	0.5025	0.0025	-0.0016	0.362
17.355	0.5292	0.5311	0.0028	-0.0019	0.382
20.186	0.5672	0.5621	0.0027	0.0051	0.404
22.503	0.5856	0.5815	0.0025	0.0041	0.418
25.169	0.6148	0.6065	0.0030	0.0083	0.436
27.673	0.6282	0.6265	0.0042	0.0017	0.451
30.355	0.6581	0.6470	0.0030	0.0111	0.465
35.270	0.6813	0.6821	0.0028	-0.0007	0.491
40.022	0.7264	0.7098	0.0036	0.0167	0.511
45.177	0.7386	0.7397	0.0030	-0.0012	0.532
49.712	0.7750	0.7667	0.0021	0.0083	0.552
55.119	0.7934	0.7922	0.0028	0.0012	0.570
60.097	0.8208	0.8197	0.0021	0.0011	0.590
65.199	0.8401	0.8425	0.0030	-0.0024	0.606
69.988	0.8706	0.8647	0.0037	0.0060	0.622
74.749	0.8816	0.8890	0.0030	-0.0074	0.640
79.597	0.9109	0.9093	0.0034	0.0016	0.654
84.442	0.9218	0.9312	0.0049	-0.0094	0.670
89.801	0.9604	0.9575	0.0039	0.0030	0.689
94.937	0.9668	0.9786	0.0042	-0.0118	0.704

SUM OF RESIDUAL SQUARES = 0.0025

PARAY(TRANSPOSE) * PARAY MATRIX

0.98970690-02	-0.61750460 00	-0.16154530 00	0.21203430-01	0.0	0.0
-0.61750460 00	0.54906610 02	0.17847060 02	-0.20914150 01	0.0	0.0
-0.16154530 00	0.17847060 02	0.65155880 01	-0.72829420 00	0.0	0.0
0.21203430-01	-0.20914150 01	-0.72829420 00	0.84534600-01	0.0	0.0
0.0	0.0	0.0	0.0	0.0	0.0
0.0	0.0	0.0	0.0	0.0	0.0

DETERMINANT = 0.453545D-04

INVERSE MATRIX BY GAUSS-JORDAN METHOD

0.13672630 04	0.35014210 02	-0.94968060 02	-0.29486280 03	0.0	0.0
0.35014210 02	0.12253290 01	-0.21986740 01	0.25902850 01	0.0	0.0
-0.94968060 02	-0.21986740 01	0.10909930 02	0.63417220 02	0.0	0.0
-0.29486280 03	0.25902850 01	0.63417220 02	0.69623390 03	0.0	0.0
0.0	0.0	0.0	0.0	0.0	0.0
0.0	0.0	0.0	0.0	0.0	0.0

COMPUTED IDENTITY MATRIX

0.10000000 01	-0.52041700-16	-0.22204460-15	-0.22204460-15
-0.28421710-12	0.10000000 01	0.24869000-13	0.56843420-13
-0.12434500-12	-0.33306690-14	0.10000000 01	0.0
0.71054270-14	-0.11102230-15	-0.88817840-15	0.10000000 01

CORRELATION MATRIX

0.1000000E 01	0.8554447E 00	-0.7775719E 00	-0.3022152E 00	0.0	0.0
0.8554447E 00	0.1000000E 01	-0.6013446E 00	0.8868361E-01	0.0	0.0
-0.7775719E 00	-0.6013446E 00	0.1000000E 01	0.7276433E 00	0.0	0.0
-0.3022152E 00	0.8868361E-01	0.7276433E 00	0.1000000E 01	0.0	0.0
0.0	0.0	0.0	0.0	0.0	0.0
0.0	0.0	0.0	0.0	0.0	0.0

COVARIANCE MATRIX

0.10466300 00	0.26803130-02	-0.72697360-02	-0.22571530-01	0.0	0.0
0.26803130-02	0.93798070-04	-0.16830690-03	0.19828450-03	0.0	0.0
-0.72697360-02	-0.16830690-03	0.83514740-03	0.48545420-02	0.0	0.0
-0.22571530-01	0.19828450-03	0.48545420-02	0.53296200-01	0.0	0.0
0.0	0.0	0.0	0.0	0.0	0.0
0.0	0.0	0.0	0.0	0.0	0.0

PARAMETER NO.	MEAN VALUE	CONFIDENCE INTERVAL
1	.744559D 01	.863789E 00
2	.135699D 01	.258588E-01
3	.138999D 01	.771601E-01
4	.226369D 01	.616395E 00

EIGENVALUE = 0.6722733D-03 0.1704776D-02 0.6501991D 00 0.6086405D 02 0.0 0.0

EIGENVECTOR MATRIX

0.9322207D 00	0.2145712D-01	-0.7516468D-01	-0.3533474D 00
0.3565586D 00	0.2529150D-01	0.4385209D-01	0.9329005D 00
0.6099776D-01	-0.3127717D 00	0.9460107D 00	-0.5930254D-01
-0.1047386D-01	0.9492491D 00	0.3122354D 00	-0.3640856D-01

CORRELATION MATRIX

0.1000000E 01	0.8554447E 00	-0.7775719E 00	-0.3022152E 00	0.0	0.0
0.8554447E 00	0.1000000E 01	-0.6013446E 00	0.8868361E-01	0.0	0.0
-0.7775719E 00	-0.6013446E 00	0.1000000E 01	0.7276433E 00	0.0	0.0
-0.3022152E 00	0.8868361E-01	0.7276433E 00	0.1000000E 01	0.0	0.0
0.0	0.0	0.0	0.0	0.0	0.0
0.0	0.0	0.0	0.0	0.0	0.0

DETERMINANT = 0.453545D-04

GENERALIZED INVERSE OF RANK =4

0.1367263D 04	0.3501421D 02	-0.9496806D 02	-0.2948628D 03	0.0	0.0
0.3501421D 02	0.1225329D 01	-0.2198674D 01	0.2590285D 01	0.0	0.0
-0.9496806D 02	-0.2198674D 01	0.1090993D 02	0.6341722D 02	0.0	0.0
-0.2948628D 03	0.2590285D 01	0.6341722D 02	0.6962339D 03	0.0	0.0
0.0	0.0	0.0	0.0	0.0	0.0
0.0	0.0	0.0	0.0	0.0	0.0

EIGENVALUE DIAGONAL MATRIX

0.6722733D-03	-0.3523657D-17	0.1575996D-14	0.1415534D-14
0.1345088D-17	0.1704776D-02	0.7112366D-16	-0.4440892D-15
0.1497274D-14	0.8503194D-16	0.6501991D 00	-0.2914335D-15
0.1219789D-14	-0.3778275D-15	0.3943677D-14	0.6086405D 02

COVARIANCE MATRIX

0.1046630D 00	0.2680313D-02	-0.7269736D-02	-0.2257153D-01	0.0	0.0
0.2680313D-02	0.9379807D-04	-0.1683069D-03	0.1982845D-03	0.0	0.0
-0.7269736D-02	-0.1683069D-03	0.8351474D-03	0.4854542D-02	0.0	0.0
-0.2257153D-01	0.1982845D-03	0.4854542D-02	0.5329620D-01	0.0	0.0
0.0	0.0	0.0	0.0	0.0	0.0
0.0	0.0	0.0	0.0	0.0	0.0

PARAMETER NO.	MEAN VALUE	CONFIDENCE INTERVAL
1	.744559D 01	.863789E 00
2	.135699D 01	.258588E-01
3	.138999D 01	.771601E-01
4	.226369D 01	.616395E 00

EIGENVALUE = 0.67227330-03 0.17047760-02 0.6501991D 00 0.60864050 02 0.0 0.0

EIGENVECTOR MATRIX

0.9322207D 00	0.2145712D-01	-0.7516468D-01	-0.3533474D 00
0.3565586D 00	0.2529150D-01	0.4385209D-01	0.9329005D 00
0.6099776D-01	-0.3127717D 00	0.9460107D 00	-0.5930254D-01
-0.1047386D-01	0.9492491D 00	0.3122354D 00	-0.3640856D-01

CORRELATION MATRIX

0.1000000E 01	0.8285267E 00	0.6773727E 00	0.9999278E 00	0.0	0.0
0.8285267E 00	0.1000000E 01	0.1721730E 00	0.8348847E 00	0.0	0.0
0.6773727E 00	0.1721730E 00	0.1000000E 01	0.6684896E 00	0.0	0.0
0.9999278E 00	0.8348847E 00	0.6684896E 00	0.1000000E 01	0.0	0.0
0.0	0.0	0.0	0.0	0.0	0.0
0.0	0.0	0.0	0.0	0.0	0.0

DETERMINANT = 0.6746440-01

GENERALIZED INVERSE OF RANK =3

0.7458095D 02	0.5260282D 01	0.9260482D 01	0.1951132D 03	0.0	0.0
0.5260282D 01	0.5404768D 00	0.2003760D 00	0.1386816D 02	0.0	0.0
0.9260482D 01	0.2003760D 00	0.2506016D 01	0.2391060D 02	0.0	0.0
0.1951132D 03	0.1386816D 02	0.2391060D 02	0.5105143D 03	0.0	0.0
0.0	0.0	0.0	0.0	0.0	0.0
0.0	0.0	0.0	0.0	0.0	0.0

EIGENVALUE DIAGONAL MATRIX

0.6722733D-03	-0.3523657D-17	0.1575996D-14	0.1415534D-14
0.1345088D-17	0.1704776D-02	0.7112366D-16	-0.4440892D-15
0.1497274D-14	0.8503194D-16	0.6501991D 00	-0.2914335D-15
0.1219789D-14	-0.3778275D-15	0.3943677D-14	0.6086405D 02

COVARIANCE MATRIX

0.5709118D-02	0.4026707D-03	0.7088832D-03	0.1493577D-01	0.0	0.0
0.4026707D-03	0.4137311D-04	0.1533864D-04	0.1061598D-02	0.0	0.0
0.7088832D-03	0.1533864D-04	0.1918337D-03	0.1830339D-02	0.0	0.0
0.1493577D-01	0.1061598D-02	0.1830339D-02	0.3907950D-01	0.0	0.0
0.0	0.0	0.0	0.0	0.0	0.0
0.0	0.0	0.0	0.0	0.0	0.0

PARAMETER NO.	MEAN VALUE	CONFIDENCE INTERVAL
1	.744559D 01	.201742E 00
2	.135699D 01	.171739E-01
3	.138999D 01	.369806E-01
4	.226369D 01	.527820E 00

EIGENVALUE = 0.6722733D-03 0.1704776D-02 0.6501991D 00 0.6086405D 02 0.0 0.0

EIGENVECTOR MATRIX

0.9322207D 00	0.2145712D-01	-0.7516468D-01	-0.3533474D 00
0.3565586D 00	0.2529150D-01	0.4385209D-01	0.9329005D 00
0.6099776D-01	-0.3127717D 00	0.9460107D 00	-0.5930254D-01
-0.1047386D-01	0.9492491D 00	0.3122354D 00	-0.3640856D-01

CORRELATION MATRIX

0.1000000E 01	-0.9593180E 00	0.9986563E 00	-0.9967118E 00	0.0	0.0
-0.9593180E 00	0.1000000E 01	-0.9433979E 00	0.9332873E 00	0.0	0.0
0.9986563E 00	-0.9433979E 00	0.1000000E 01	-0.9995716E 00	0.0	0.0
-0.9967118E 00	0.9332873E 00	-0.9995716E 00	0.1000000E 01	0.0	0.0
0.0	0.0	0.0	0.0	0.0	0.0
0.0	0.0	0.0	0.0	0.0	0.0

DETERMINANT = 0.395738D 02

GENERALIZED INVERSE OF RANK =2

0.5724245D-02	-0.2950571D-01	0.8869530D-01	-0.5557141D-02	0.0	0.0
-0.2950571D-01	0.1652604D 00	-0.4501993D 00	0.2795905D-01	0.0	0.0
0.8869530D-01	-0.4501993D 00	0.1378005D 01	-0.8646933D-01	0.0	0.0
-0.5557141D-02	0.2795905D-01	-0.8646933D-01	0.5430570D-02	0.0	0.0
0.0	0.0	0.0	0.0	0.0	0.0
0.0	0.0	0.0	0.0	0.0	0.0

EIGENVALUE DIAGONAL MATRIX

0.6722733D-03	-0.3523657D-17	0.1575996D-14	0.1415534D-14
0.1345088D-17	0.1704776D-02	0.7112366D-16	-0.4440892D-15
0.1497274D-14	0.8503194D-16	0.6501991D 00	-0.2914335D-15
0.1219789D-14	-0.3778275D-15	0.3943677D-14	0.6086405D 02

COVARIANCE MATRIX

0.4381868D-06	-0.2258641D-05	0.5789560D-05	-0.4253951D-06	0.0	0.0
-0.2258641D-05	0.1265056D-04	-0.3446243D-04	0.2140245D-05	0.0	0.0
0.5789560D-05	-0.3446243D-04	0.1054853D-03	-0.6619164D-05	0.0	0.0
-0.4253951D-06	0.2140245D-05	-0.6619164D-05	0.4157062D-06	0.0	0.0
0.0	0.0	0.0	0.0	0.0	0.0
0.0	0.0	0.0	0.0	0.0	0.0

PARAMETER NO.	MEAN VALUE	CONFIDENCE INTERVAL
1	.744559D 01	.176742E-02
2	.135699D 01	.949655E-02
3	.138999D 01	.274225E-01
4	.226369D 01	.172149E-02

EIGENVALUE = 0.6722733D-03 0.1704776D-02 0.5501991D 00 0.6086405D 02 0.0 0.0

EIGENVECTOR MATRIX

0.9322207D 00	0.2145712D-01	-0.7516468D-01	-0.3533474D 00
0.3565586D 00	0.2529150D-01	0.4385209D-01	0.9329005D 00
0.6099776D-01	-0.3127717D 00	0.9460107D 00	-0.5930254D-01
-0.1047386D-01	0.9492491D 00	0.3122354D 00	-0.3640856D-01

CORRELATION MATRIX

0.1000000E 01	-0.9999999E 00	-0.1000000E 01	0.9999999E 00	0.0	0.0
-0.9999999E 00	0.1000000E 01	0.1000000E 01	-0.1000000E 01	0.0	0.0
-0.1000000E 01	0.1000000E 01	0.1000000E 01	-0.1000000E 01	0.0	0.0
0.9999999E 00	-0.1000000E 01	-0.1000000E 01	0.1000000E 01	0.0	0.0
0.0	0.0	0.0	0.0	0.0	0.0
0.0	0.0	0.0	0.0	0.0	0.0

DETERMINANT = 0.6086410 02

GENERALIZED INVERSE OF RANK =1

0.1802406D-05	-0.1633526D-03	-0.5373138D-04	0.6265408D-05	0.0	0.0
-0.1633526D-03	0.1480470D-01	0.4869692D-02	-0.5678359D-03	0.0	0.0
-0.5373138D-04	0.4869692D-02	0.1601782D-02	-0.1867776D-03	0.0	0.0
0.6265408D-05	-0.5678359D-03	-0.1867776D-03	0.2177941D-04	0.0	0.0
0.0	0.0	0.0	0.0	0.0	0.0
0.0	0.0	0.0	0.0	0.0	0.0

EIGENVALUE DIAGONAL MATRIX

0.6722733D-03	-0.3523657D-17	0.1575996D-14	0.1415534D-14
0.1345088D-17	0.1704776D-02	0.7112366D-16	-0.4440892D-15
0.1497274D-14	0.8503194D-16	0.6501991D 00	-0.2914335D-15
0.1219789D-14	-0.3778275D-15	0.3943677D-14	0.6086405D 02

COVARIANCE MATRIX

0.1379728D-09	-0.1250452D-07	-0.4113098D-08	0.4796124D-09	0.0	0.0
-0.1250452D-07	0.1133289D-05	0.3727713D-06	-0.4346742D-07	0.0	0.0
-0.4113098D-08	0.3727713D-06	0.1226153D-06	-0.1429769D-07	0.0	0.0
0.4796124D-09	-0.4346742D-07	-0.1429769D-07	0.1667198D-08	0.0	0.0
0.0	0.0	0.0	0.0	0.0	0.0
0.0	0.0	0.0	0.0	0.0	0.0

PARAMETER NO.	MEAN VALUE	CONFIDENCE INTERVAL
1	.7445590 01	.313623E-04
2	.1356990 01	.284237E-02
3	.1389990 01	.934939E-03
4	.2263690 01	.109020E-03

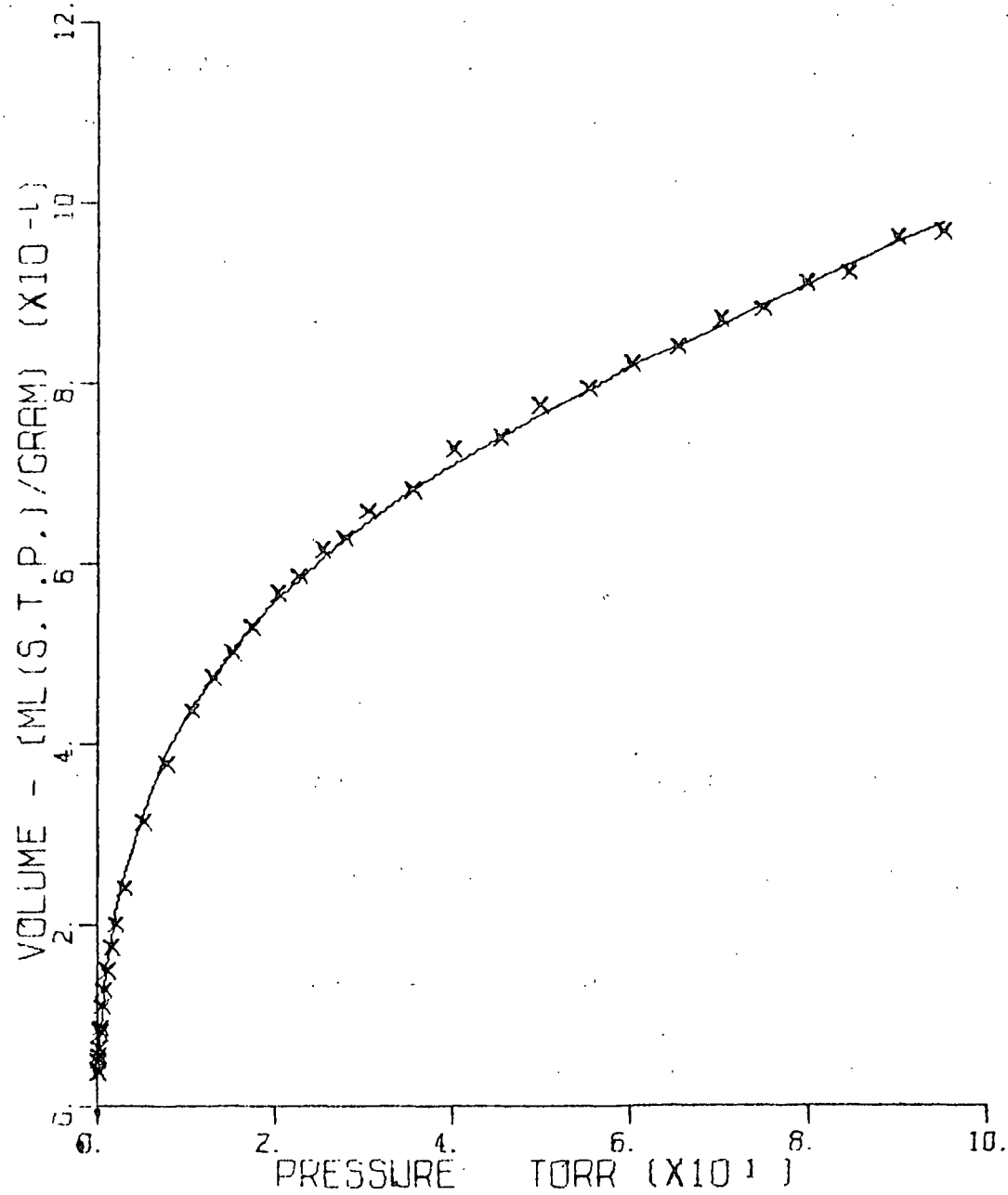
VOLUME - (ML (S.T.P.)/GRAM) (X10 -1)
12.
10.
8.
6.
4.
2.
0.
2.
4.
6.
8.
10.
PRESSURE TORR (X10 1)

APPENDIX III

A SIMPLIFIED DERIVATION OF CLUSTERING THEORY FOR APPLICATION OF BINARY SYSTEMS

Consider for simplicity a two-component system with volume, $\underline{V}$, temperature, $\underline{T}$, and chemical potentials, μ_1 and μ_2. For an open isothermal system whose thermodynamic state is specified by the variables $\underline{V}$, $\underline{T}$, μ_1 and μ_2, the probability that such a system contains $\underline{N}$ molecules and is in energy state $\underline{E}_j(\underline{N}_1, \underline{N}_2, \underline{V})$ is

$$P_j(N_1,N_2,V,T,\mu_1,\mu_2) = \frac{\exp[-E_j(N_1,N_2V)/kT]\ \lambda_1^{N_1}\ \lambda_2^{N_2}}{\Xi(N_1,N_2,V,T,\mu_1,\mu_2)} \tag{128}$$

where

$$N = N_1 + N_2 \tag{129}$$

$$\Xi = \sum_{N_1,N_2} Q(N_1,N_2,V,T)\lambda_1^{N_1}\ \lambda_2^{N_2} \tag{130}$$

and

$$\lambda_1 = \exp[\mu_1/kT] \qquad \lambda_2 = \exp[\mu_2/kT]. \tag{131}$$

Ξ is called the "grand partition function" and is defined in the relationship

$$\begin{aligned}\Xi &= \sum_{j,N} \exp[-E_j(N_1,N_2,V)/kT]\ \exp[N_1\mu_1/kT]\ \exp[N_2\mu_2/kT] \\ &= \sum_{N} \{\exp[N_1\mu_1/kT]\ \exp[N_2\mu_2/kT] \sum_{j} \exp[-E_j(N_1,N_2,V)/kT]\} \\ &= \sum_{N_1,N_2} Q(N_1,N_2,V,T)\ \exp[N_1\mu_1/kT]\ \exp[N_2\mu_2/kT].\end{aligned} \tag{132}$$

If one substitutes Equation (128) into the relationship defining the entropy of mixing

$$S = -k \sum_{j,N} P_j(N)\ \ln P_j(N) \tag{133}$$

one finds

$$S = E/T - N_1\mu_1/T - N_2\mu_2/T + k \ln \Xi \tag{134}$$

where

$$E = \sum_{j,N} P_j(N)\, E_j(N_1,N_2,V). \tag{135}$$

From classical thermodynamics one can obtain the relationship

$$S = E/T - N_1\mu_1/T - N_2\mu_2/T + pV/T. \tag{136}$$

Hence,

$$pV = kT \ln \Xi\,(N_1,N_2,V,T,\mu_1,\mu_2). \tag{137}$$

Equation (137) is recognized as an equation of state for the system in terms of the grand partition function.

The next portion of this derivation will concern the application of the grand partition function to reduce a many-body problem in statistical mechanics to a one-body, two-body, etc., problem.

The grand partition function is most conveniently used as a power series in the absolute activity λ_1 and λ_2, i.e.,

$$\Xi\,(N_1,N_2,V,T,\lambda_1,\lambda_2) = \exp[pV/kT] = \sum_{N_1,N_2\geq 0} Q_{N_1,N_2}(V,T)\lambda_1^{N_1}\,\lambda_2^{N_2}$$

$$= 1 + \sum_{N_1,N_2\geq 1} Q_{N_1,N_2}\,\lambda_1^{N_1}\,\lambda_2^{N_2}. \tag{138}$$

In Equation (138), we have put $\underline{Q}_{o,o} = 1$ since when $\underline{N}_1$, $\underline{N}_2 = 0$ the system has only one state with energy $\underline{E} = 0$.

The partition function $\underline{Q}$ is defined by the relationship

$$Q = \frac{1}{h^{3N}\,N!} \int \ldots \int \exp[-H/kT]\, dp_1 \ldots dp_N,\, dr_1 \ldots dr_N. \tag{139}$$

The Hamiltonian expression for the external energy is

$$H = \sum_{i=1}^{N} \frac{1}{2m} (p_{xi}^2 + p_{yi}^2 + p_{zi}^2) + U(r_i, \ldots, r_N) \qquad (140)$$

where $\underline{U}$ is the potential energy of interaction of all the pairs of molecules present and the $\underline{p}$'s represent the momenta terms.

Substituting Equation (140) into Equation (139) and carrying out the momenta integrations, one obtains the result

$$Q_{N_1,N_2} = Z_{N_1,N_2}/(N_1!\, N_2!\, \Lambda_1^{3N_1}\, \Lambda_2^{3N_2}) \qquad (141)$$

where

$$\Lambda_1 = h/(2\pi m_1 kT)^{1/2} \qquad \Lambda_2 = h/(2\pi m_2 kT)^{1/2} \qquad (142)$$

and

$$Z_{N_1,N_2} = \int \ldots \int \exp[-U_{N_1,N_2}/kT]\, d[N_1]\, d[N_2] \qquad (143)$$

where $d[\underline{N}_1]$ means $d\underline{r}_1 \ldots d\underline{r}_{\underline{N}}$ for Species 1, etc., and $\underline{Z}_{\underline{N}_1,\underline{N}_2}$ is the so-called "configuration integral." Equation (143) involves a very complicated $3\underline{N}$-fold integration which in general cannot be solved.

As already mentioned, the potential energy $\underline{U}$ is the sum of the potentials due to the interaction of molecular pairs. That is,

$$U(r_1, \ldots, r_N) = \sum_{\substack{1 \leq i \leq N \\ 1 \leq j \leq N}} u(r_{ij}) \qquad (144)$$

where $\underline{u}(\underline{r}_{\underline{i}\underline{j}})$ is the potential energy of interaction between molecules $\underline{i}$ and $\underline{j}$ as a function of the distance $\underline{r}_{\underline{i}\underline{j}}$ between the molecules.

If one introduces the function $\underline{f}_{\underline{i}\underline{j}}$ which is defined by

$$f_{ij} = \exp[-u(r_{ij})/kT] - 1 \qquad (145)$$

then,

$$\exp[-U/kT] = \exp[-\Sigma\, u(r_{ij})/kT] = \Pi \exp[-u(r_{ij})/kT]. \qquad (146)$$

If this product is multiplied out, one has

$$\exp[-U/kT] = \Pi\, (1 + f_{ij}) = 1 + \Sigma\, f_{ij} + \Sigma\, f_{ij}\, f_{k\ell} + \ldots \qquad (147)$$

By introducing the f functions, the effects of the intermolecular forces are more clearly exposed. In the absence of intermolecular forces (i.e., a perfect gas) all the f's are zero, and only the leading term on the right-hand side of Equation (147) remains. In this case, $Z = V^N$. In each configuration $r_1 \ldots r_N$ of the N molecules, the f's represent the contribution to $\exp[-U/kT]$ of the nonzero intermolecular forces. In general, $f(r_{ij})$ is zero except when r_{ij} is small, i.e., of the order of several molecular diameters or less.

In Equation (147), there is a term corresponding to each possible combination from zero to all $N(N-1)/2$ f's. Any such term may be represented by a diagram consisting of circles for the molecules and a line segment between the ith and jth molecule for each factor f_{ij} which occurs as a term. See Fig. 43.

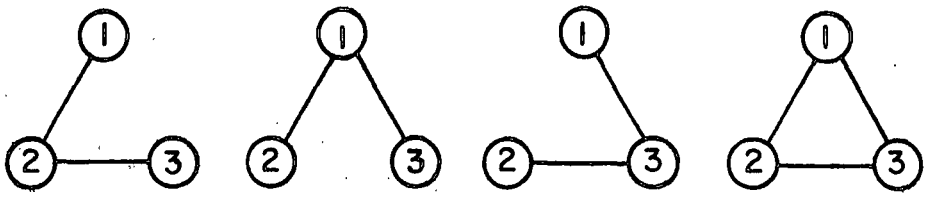

Figure 43. Clusters of Three Molecules

There are, in general, many ways in which any given set of molecules may be connected together into a cluster. For example, a set of three molecules may be connected into a cluster in four ways.

The cluster sum $S_{i,j,k\ldots}$ is defined as the sum of all terms which connect in a cluster each of the molecules i, j, $k\ldots$, no other molecules being connected to this cluster. For example,

$$S_{1,2,3} = f_{1,2}\, f_{2,3} + f_{1,2}\, f_{1,3} + f_{1,3}\, f_{2,3} + f_{1,2}\, f_{1,3}\, f_{2,3}. \quad (148)$$

Also, $S_{1,2} = f_{1,2}$ and the unit cluster is defined as $S_1 = 1$.

Consider now, a product of $S_{i,j,k,}$'s such that in the product each molecule occurs once and only once as a subscript. Thus, to include every term in Equation (147), one must take the sum of all possible different products of the $S_{i,j,k,}$'s, each product containing every molecule once and only once as a subscript. Each such product corresponds to a different possible division of the N molecules into groups or clusters.

The cluster integrals, b_ℓ, are defined as

$$b_\ell(V,T) = (1/\ell!V) \int\ldots\int S_{1,2,\ldots,\ell}\, dr_1, dr_2, \ldots, dr_\ell \quad (149)$$

or

$$b_\ell(V,T) = (1/\ell!V) \int\ldots\int \sum_{\substack{\ell\geq 1 \\ j\geq 2 \\ i\neq j}} \prod f_{ij}\, dr_i \ldots dr_\ell. \quad (150)$$

The summation is taken over all the products of the f_{ij} terms for connected pairs of molecules that can take part in a cluster of the same ℓ molecules. The $1/\ell!V$ in Equations (149) and (150) is introduced for normalization purposes; this makes the cluster integral have the dimension of $V^{\ell-1}$, where V is the volume of the whole system.

For $\ell = 1$, the cluster integral is

$$b_1 = (1/V) \int dr_1 = 1 \quad (151)$$

which is equal to unity, since integration over the coordinates of the molecules gives simply the volume of the containing vessel.

The cluster integral for $\underline{\ell} = 2$ is

$$b_2 = (1/2V) \iint f_{1,2}\, dr_1\, dr_2$$

$$= (1/2V) \iint (\exp[-u(r_{12})/kT] - 1)\, dr_1\, dr_2. \qquad (152)$$

The definition of $S_{\underline{i},\underline{j},\underline{k}}\ldots$ depends only on the coordinates of the molecules appearing as subscripts. Therefore, the multiple integral over all coordinates of a product of these $\underline{S}$'s is merely the product of the integrals of the several $\underline{S}$'s. In general, a product of the $\underline{S}$'s which represents $\underline{m}_1$ unit clusters, $\underline{m}_2$ clusters of two molecules, ..., $\underline{m}_{\underline{\ell}}$ clusters of $\underline{\ell}$ molecules, yields an integral over $d\underline{r}_1 \ldots d\underline{r}_{\underline{N}}$ of

$$I = (1!Vb_1)^{m_1}\, (2!Vb_2)^{m_2} \ldots (\ell!Vb_\ell)^{m_\ell}. \qquad (153)$$

The question now arises, how many $S_{\underline{i},\underline{j},\underline{k}}$ products out of all possible $S_{\underline{i},\underline{j},\underline{k}}$ products yield the result in Equation (153)? That is, in how many different ways can $\underline{N}$ molecules be divided into groups or clusters so that there are $\underline{m}_1$ unit clusters, $\underline{m}_2$ clusters of two molecules, ... $\underline{m}_{\underline{\ell}}$ clusters of $\underline{\ell}$ molecules. It can be shown that

$$N!/\prod_{\ell=1}^{N} (\ell!)^{m_\ell}\, m_\ell! \qquad (154)$$

is the possible number of cluster arrangements.

The product of Equation (153) and (154) is the contribution to the integral in Equation (143) owing to all the terms in Equation (147) associated with those products of $S_{\underline{i},\underline{j},\underline{k}}$'s which represent the cluster partition $\underline{m}_1$, $\underline{m}_2$, ..., $\underline{m}_{\underline{\ell}}$. This contribution to $\underline{Z}$ is

$$N! \prod_{\ell=1}^{N} [(Vb_\ell)^{m_\ell}/(M_\ell!)]. \qquad (155)$$

There will be a contribution of this form to Z for each different set of positive integers m_1, m_2, ... m_ℓ consistent with the condition $\sum_{\ell=1} \ell m_\ell = N$. Hence, one can write

$$Z_N = N! \sum_m \left[\prod_{\ell=1}^{N} \{(Vb_\ell)^{m_\ell}/(M_\ell!)\} \right] \tag{156}$$

and

$$Q = (1/\Lambda^{3N}) \sum_m \left[\prod_{\ell=1}^{N} \{(Vb_\ell)^{m_\ell}/(m_\ell!)\} \right]. \tag{157}$$

Equation (157) is now in a form which is much more convenient to work with than Q as defined in Equation (139).

This part of the derivation is concluded with a few remarks concerning clusters and cluster integrals. Let us imagine that in Equation (150) for ℓ small compared to V/r_o^3, where r_o is of the order of a molecular diameter, we keep the ℓth molecule fixed at some point r_ℓ and carry out the integrations over r_1, r_2, ..., $r_{\ell-1}$. Since each f_{ij} is nonzero only when r_{ij} is less than a few molecular diameters, each product of f's in $S_{1,2,\ldots,\ell}$ is nonzero only when all r_{ij}'s corresponding to the f's in the product are small. Since the ℓ molecules are connected to each other directly or indirectly in every product of f's in $S_{1,2,\ldots,\ell}$, $S_{1,2,\ldots,\ell}$ is nonzero only in those regions of the configurational space where molecules $1,2,\ldots,\ell$ are rather close together. This is the origin of the term "cluster." The reader will note that the clustering theory derivation since Equation (143) has considered a one-component system for simplicity.

Consider now the use of the grand partition function to obtain the expansion of p/kT in powers of the activity.

$$\Xi(N_1,N_2,V,T,\lambda_1,\lambda_2) = \exp[pV/kT] = \sum_{N_1,N_2 \geq 0} Q_{N_1,N_2}(V,T)\, \lambda_1^{N_1}\, \lambda_2^{N_2}$$

$$= \sum_{N_1,N_2 \geq 0} \{[Z_{N_1,N_2}/(N_1!\, N_2!)]\, z_1^{N_1}\, z_2^{N_2}\} \tag{158}$$

with

$$\lambda_1 = \exp[\mu_1/kT] \qquad \lambda_2 = \exp[\mu_2/kT] \tag{159}$$

and

$$z_1 = \lambda_1/\Lambda_1^3 \qquad z_2 = \lambda_2/\Lambda_2^3 \tag{160}$$

where λ is the absolute activity and $\underline{z}$ the activity.

Let us digress briefly to discuss the activity, $\underline{z}$. For an infinitely dilute (perfect) gas,

$$\mu/RT = \ln \Lambda^3 + \ln(N/V) \qquad \text{as } N/V \to 0. \tag{161}$$

If we define an active number density or activity, $\underline{z}$, which bears the same relation to μ at any density that $\underline{N}/\underline{V}$ does as $\underline{N}/\underline{V} \to 0$, then

$$\mu/RT = \ln \Lambda^3 + \ln z \tag{162}$$

where

$$\lim_{N/V \to 0} z = N/V. \tag{163}$$

This is seen to be the same $\underline{z}$ as in Equation (160). It should be noted that the fugacity, $\underline{f}$, of chemical thermodynamics is defined by

$$\mu/RT = \ln(\Lambda^3/RT) + \ln p \qquad \text{as } p \to 0 \tag{164}$$

$$\mu/RT = \ln(\Lambda^3/RT) + \ln f \tag{165}$$

where

$$\lim_{p \to 0} f = p. \tag{166}$$

Therefore, $\underline{f}/\underline{kt} = \underline{z}$.

Returning now to Equation (158)

$$\Xi(N_1,N_2,V,T,\lambda_1,\lambda_2) = \exp[pV/kT] = 1 + \sum_{N_1,N_2 \geq 1} \left\{ [Z_{N_1,N_2}/(N_1!\, N_2!)]\, z_1^{N_1}\, z_2^{N_2} \right\} \quad (167)$$

since when $\underline{N} = 0$, the system has only one state.

After taking the logarithm of both sides of Equation (167), expanding the logarithm on the right, and dividing by $\underline{V}$, one obtains an expression for $\underline{p}$ in powers of $\underline{z}$:*

$$p/kT = z_1 + z_2 + \frac{1}{2}\left(\frac{Z_{2,0}}{V} - V\right) z_1^2 + \left(\frac{Z_{1,1}}{V} - V\right) z_1 z_2 + \frac{1}{2}\left(\frac{Z_{0,2}}{V} - V\right) z_2^2 + \ldots \quad (168)$$

Comparing the coefficients of the power series in Equation (168) with the relationship developed in Equation (156), it becomes apparent that

$$b_{1,0} = b_{0,1} = 1 \qquad b_{2,0} = \frac{1}{2}\left(\frac{Z_{2,0}}{V} - V\right) \quad (169)$$

$$b_{1,1} = \frac{Z_{1,1}}{V} - V \qquad b_{0,2} = \frac{1}{2}\left(\frac{Z_{0,2}}{V} - V\right) \quad (170)$$

therefore the power series can be rewritten as follows

$$p/kT = b_{1,0}\, z_1 + b_{0,1}\, z_2 + b_{2,0}\, z_1^2 + b_{1,1}\, z_1 z_2 + b_{0,2}\, z_2^2 + \ldots \quad (171)$$

in terms of the cluster integrals and activities.

All of the theory up to Equation (171) is essentially a simplified version of the classical paper presented by Mayer and McMillan (28). A later version of the theory was developed by Kirkwood and Buff (29) employing the more recent development of molecular distribution functions. Additional background material is available in the following texts (69-72).

*Note: $\ln(1-x) = x - \frac{1}{2}x^2 + \frac{1}{3}x^3 - \ldots \cong x - \frac{1}{2}x^2$.

Turning now to the work of Zimm (30), a relationship is derived for the chemical potential, compressibility, and one of the clustering integrals of a binary mixture. From the power series in Equation (171) for pressure, p, in terms of the activity, z, one may identify the coefficients by developing a corresponding Taylor series. The Taylor series for $p(z_1, z_2)$ is*

$$p(z_1 + x, z_2 + y) = p(z_1, z_2) + x \frac{\partial p(z_1, z_2)}{\partial z_1} + y \frac{\partial p(z_1, z_2)}{\partial z_2}$$

$$+ \frac{x^2}{2!} \frac{\partial^2 p(z_1, z_2)}{\partial^2 z_1} + \frac{2xy}{2!} \frac{\partial^2 p(z_1, z_2)}{\partial z_1 \partial z_2} + \frac{y^2}{2!} \frac{\partial^2 p(z_1, z_2)}{\partial z_2^2} + \ldots \quad (172)$$

Comparing the Taylor series of Equation (172) with Equation (171), it is obvious that

$$kT\, b_{2,0} = \frac{x^2}{2!} \left(\frac{\partial^2 p}{\partial x_1^2} \right)_{z_2, T} . \quad (173)$$

Equation (173) can be rearranged to the following form

$$2b_{2,0} = \frac{1}{kT} \frac{z_1^2}{c_1^2} \left(\frac{\partial^2 p}{\partial z_1^2} \right)_{z_2, T} \quad (174)$$

where the increment x is defined as z_1/c_1, and c_i is the bulk molecular concentration of Species i.

$$c_i = \langle N_i \rangle_{Av} / V. \quad (175)$$

---

*Note: Taylor series for a function of two variables:

$$f(a+h, b+k) = f(a,b) + \left(h \frac{\partial}{\partial x} + k \frac{\partial}{\partial y} \right) f(x,y) \Big|_{\substack{x=a \\ y=b}}$$

$$+ \frac{1}{n!} \left(h \frac{\partial}{\partial x} + k \frac{\partial}{\partial y} \right)^n f(x,y) \Big|_{\substack{x=a \\ y=b}}$$

In order to better understand the meaning of the cluster integrals, the paper of Kirkwood and Buff (29) will be cited in detail. They defined the molecular pair distribution function, $\underline{F}_2(\underline{i},\underline{j})$ by the statement that,

$$(1/V^2)\, F_2(i,j)\, d(i)\, d(j) \tag{176}$$

is the probability that the molecular Species $\underline{i}$ and $\underline{j}$ are each at the positions specified by the coordinates $\underline{i},\underline{j}$ in the range of the coordinates $d(\underline{i})$ and $d(\underline{j})$. The cluster integral, $\underline{G}_{11}$, is defined by

$$G_{11} = (1/V) \iint [F_2(i,j) - 1]\, d(i)\, d(j) \tag{177}$$

where $\underline{i}$ and $\underline{j}$ are now the same component of the binary mixture. A relationship was derived between the radial distribution function $\underline{F}_2(\underline{i},\underline{j})$ and the density fluctuations,

$$G_{ij} = V \frac{\langle N_i N_j \rangle_{Av} - \langle N_i \rangle_{Av} \langle N_j \rangle_{Av}}{\langle N_i \rangle_{Av} \langle N_j \rangle_{Av}} - \frac{\delta_{ij}}{c_i} \tag{178}$$

where $\delta_{\underline{ij}}$ is the Kronecker delta function which equals unity for $\underline{i} = \underline{j}$, and equals zero for $\underline{i} \neq \underline{j}$.

It can be shown that $\underline{G}_{11}/\underline{v}_1$ is equal to minus one molecular volume, $\underline{v}_1$, when pecies 1 is randomly distributed in the system. Obviously, values of $\underline{G}_{11}/\underline{v}_1$ greater than minus one molecular volume indicate clustering; values less than minus one molecular volume indicate an exclusion of volume for the Species 1 molecules. Letting ϕ_1 represent the volume fraction of molecular pecies 1, it can be shown that $\phi_1\underline{G}_{11}/\underline{v}_1$ is equal to the mean number of Type 1 molecules in excess of the mean concentration of Type 1 molecules in the neighborhood of a given Type 1 molecule.

Thus, $\phi_1\underline{G}_{11}/\underline{v}_1$ measures the clustering tendency of the Type 1 molecules. Also it should be obvious from Equation (177) and Equation (152) that $2\underline{b}_{2,0} = \underline{G}_{11}$.

Returning to Equation (174)

$$2b_{2,0} = G_{11} = \frac{1}{kT}\frac{z_1^2}{c_1^2}\left(\frac{\partial^2 p}{\partial z_1^2}\right)_{z_2,T} \tag{179}$$

in this equation, c_1 is the molecular concentration N_1/V, of Component 1. The activity z_x is related to the chemical potential μ_x by the relation

$$\mu_x = kT \ln(z_x/z_{xo}) \tag{180}$$

with z_{xo} a constant.

One may use the equation of differential calculus

$$dc_1 = \left(\frac{\partial c_1}{\partial p}\right)_{\mu_2} dp + \left(\frac{\partial c_1}{\partial \mu_2}\right)_p d\mu_2 \tag{181}$$

giving

$$\left(\frac{\partial c_1}{\partial p}\right)_{\mu_2} = \left(\frac{\partial c_1}{\partial p}\right)_{N_1/N_2} - \left(\frac{\partial c_1}{\partial \mu_2}\right)_p \left(\frac{\partial \mu_2}{\partial p}\right)_{N_1/N_2} \tag{182}$$

and the classical thermodynamic equation for the Gibbs free energy, G,

$$dG = d(\mu_1 N_1 + \mu_2 N_2) = Vdp + \mu_1 dN_1 + \mu_2 dN_2 - SdT \tag{183}$$

with the corollaries

$$\left(\frac{\partial \mu_2}{\partial p}\right)_{N_1,N_2,T} = \left(\frac{\partial \mu_2}{\partial p}\right)_{N_1/N_2,T} = \left(\frac{\partial V}{\partial N_2}\right)_{p,T,N_1} = v_2 \tag{184}$$

and

$$\left(\frac{\partial \mu_1}{\partial \mu_2}\right)_{p,T} = -\frac{N_2}{N_1} = \frac{c_2}{c_1} \tag{185}$$

the latter being the Gibbs-Duhem equation. With these relations, Equation (179) may be transformed into the form

$$G_{11} = kT\left(\frac{\partial c_1}{\partial p}\right)_{T,\mu_2} - 1. \tag{186}$$

Substituting Equation (182) into Equation (186)

$$G_{11}c_1 = kT\left[\left(\frac{\partial c_1}{\partial p}\right)_{N_1/N_2,T} - \left(\frac{\partial c_1}{\partial \mu_2}\right)_{p,T}\left(\frac{\partial \mu_2}{\partial p}\right)_{N_1/N_2,T}\right] - 1 \qquad (187)$$

noting that since $\underline{c}_1 = \underline{N}_1/\underline{V}$

$$\left(\frac{\partial c_1}{\partial p}\right)_{N_1/N_2,T} = -\frac{N_1}{V^2}\left(\frac{\partial V}{\partial p}\right)_T \qquad (188)$$

and

$$G_{11} = kT\left[-\frac{N_1}{V^2}\left(\frac{\partial V}{\partial p}\right)_T - \left(\frac{\partial c_1}{\partial \mu_2}\right)_{p,T} v_2\right] - 1 \qquad (189)$$

rearranging

$$G_{11}c_1 = kT\left[-\frac{N_1}{V^2}\left(\frac{\partial \ln V}{\partial p}\right)_T - v_2\left(\frac{\partial c_1}{\partial \mu_2}\right)_{p,T}\right] - 1. \qquad (190)$$

Using the definition of isothermal compressibility, i.e., $\kappa = -(\partial \ln \underline{V}/\partial \underline{p})_{\underline{T}}$ and the Gibbs-Duhem relationship, one obtains

$$\frac{G_{11}}{v_1} = kT\left[\frac{\kappa}{v_2} + \frac{v_2 c_2}{v_1 c_1^2}\left(\frac{\partial c_2}{\partial \mu_1}\right)_{p,T}\right] - \frac{1}{c_1 v_1}. \qquad (191)$$

For many systems the compressibility is small so that this term may be neglected in Equation (191). With the neglect of this term, and after the introduction of the volume fractions

$$\phi_x = c_x v_x. \qquad (192)$$

Equation (191) may be written simply in the form below.

$$G_{11}/v_1 = kT\,(\phi_2/\phi_1)\,(\partial \ln \phi_1/\partial \mu_1)_{p,T} - 1/\phi_1. \qquad (193)$$

Using Equation (180) and assuming the additivity of volumes, i.e., $\phi_1 + \phi_2 = 1$, Equation (193) can be changed to the form

$$G_{11}/v_1 = -\phi_2\,(\partial(z_1/\phi_1)/\partial z_1)_{p,T} - 1. \qquad (194)$$

It can be seen that the cluster integral is exactly minus one molecular volume for any incompressible system in which the activity is proportional to the volume fraction. On the other hand, the integral is large and positive, indicating the presence of large clusters of molecules in the system, where the activity varies little with the volume fraction.

NOMENCLATURE FOR APPENDIX III

b_ℓ = cluster integral

c_i = bulk molecular concentration of Species i

E = total energy

E_j = energy state

f_{ij} = defined in text

F_{2ij} = molecular pair distribution function

G = Gibbs free energy

G_{11} = cluster integral

h = Planck's constant

H = Hamiltonian expression for external energy

I = product of the cluster sums

k = Boltzmann's constant

m_ℓ = mass of the molecule; number of clusters of ℓ molecules

N = total number of molecules

p = pressure

p_i = momentum

P_j = probability

Q = partition function

r_{ij} = distance between molecules

S = entropy

$S_{ijk\ldots}$ = cluster sum

T = temperature

$u(r_{ij})$ = potential energy of interaction between molecules

U = potential energy

v_i = partial molecular volume of Species i

V = total volume

$\underline{x}$ = increment

$\underline{y}$ = increment

$\underline{z}$ = activity

$\underline{Z}$ = configuration integral

$\delta_{\underline{ij}}$ = Kronecker delta

κ = isothermal compressibility

Λ = defined in text

$\mu_{\underline{i}}$ = chemical potential of molecular Species $\underline{i}$

Ξ = grand partition function

$\phi_{\underline{i}}$ = volume fraction of molecular Species $\underline{i}$

$\int$ = integral operator

ln = natural logarithm

Π = product operator

e = 2.718281

! = factorial

$\sum$ = summation

∞ = infinity

APPENDIX IV

ADSORPTION CORRECTION DATA

TABLE XXVI

ACID HYDROLYZED HOLOCELLULOSE BUOYANCY DETERMINATION DATA

Gas: Argon
Sample mass: 0.50276 g.
Temperature: 288.15°K

Pressure, torr.	Apparent Mass Change, μg.
5.002	-61.0
10.095	-64.0
20.826	-70.0
40.156	-78.0
59.778	-86.5
79.701	-94.0
99.477	-102.0
118.988	-108.0
139.159	-116.0
159.543	-122.5
179.520	-129.0
199.232	-137.0
220.451	-143.5

Linear Regression Results Slope = -0.3784 μg./torr.

ALKALI EXTRACTED HOLOCELLULOSE BUOYANCY DETERMINATION DATA

Gas: Argon
Sample mass: 0.50237 g.
Temperature: 288.15°K

Pressure, torr.	Apparent Mass Change, μg.
10.208	-79.0
20.177	-83.0
39.780	-93.0
60.529	-104.0
79.335	-114.0
99.985	-121.0
119.249	-129.0
139.701	-139.0
159.378	-148.0
179.406	-156.0
200.269	-166.0
213.730	-171.0

Linear Regression Results Slope = -0.4520 μg./torr.

TABLE XXVI (Continued)

HOLOCELLULOSE BUOYANCY DETERMINATION DATA

Gas: Argon
Sample mass: 0.50415 g.
Temperature: 293.15°K

Pressure, torr.	Apparent Mass Change, μg.
10.294	-61.0
20.167	-65.0
40.128	-76.0
59.842	-83.0
79.672	-94.0
98.957	-103.0
119.329	-109.0
139.177	-116.0
159.848	-124.5
179.367	-132.0
200.696	-142.0
219.839	-150.0

Linear Regression Results Slope = -0.4179 μg./torr.

CAHN BALANCE BEAM BUOYANCY DETERMINATION DATA

Gas: Argon
Temperature: 298.15°K

Pressure, torr.	Apparent Mass Change, μg.
10.782	-60.5
30.998	-57.0
50.573	-53.0
70.241	-50.0
89.652	-46.5
109.708	-44.0
129.311	-40.5
149.432	-35.5
169.685	-32.5
189.403	-29.5
210.827	-25.5
230.185	-24.0

Linear Regression Results Slope = 0.1708 μg./torr.

TABLE XXVII

ARGON THERMOMOLECULAR FLOW CORRECTION DATA

Isotherm Temperature: 77.5°K

Pressure Gage[a] Reading	Apparent Mass Change, μg.
0.035	-34.0
0.071	-44.0
0.131	-49.0
0.263	-56.0
0.535	-62.0
1.068	-67.0
2.119	-69.5
5.282	-74.0
10.882	-71.5
20.554	-66.0
36.752	-59.0
46.619	-54.0
56.481	-48.0
67.548	-46.0
77.124	-42.5
88.177	-39.0
100.378	-32.0

Isotherm Temperature: 90.1°K

Pressure Gage[a] Reading	Apparent Mass Change, μg.
0.032	-33.5
0.076	-45.0
0.138	-51.0
0.264	-55.0
0.524	-60.5
1.073	-63.5
2.187	-68.0
5.991	-68.5
10.374	-69.0
20.190	-66.0
44.280	-54.0
61.969	-48.0
81.537	-39.0
100.855	-31.0
120.706	-22.5
141.079	-13.0
160.482	-4.5
180.585	2.0
201.142	11.0
220.656	16.0
240.548	20.5
260.862	22.0
299.688	34.0

NITROGEN THERMOMOLECULAR FLOW CORRECTION DATA

Isotherm Temperature: 77.5°K

Pressure Gage[a] Reading	Apparent Mass Change, μg.
0.063	-49.0
0.125	-61.0
0.265	-67.0
0.577	-76.5
1.318	-81.0
2.085	-84.0
5.190	-83.5
10.376	-90.0
20.270	-84.0
30.680	-80.5
50.565	-75.5
70.558	-65.0

Isotherm Temperature: 77.5°K (Cont'd)

Pressure Gage[a] Reading	Apparent Mass Change, μg.
90.512	-60.0
110.492	-51.0
130.645	-44.0
150.778	-36.5
171.165	-34.0
190.644	-31.0

[a]Refer to pressure gage calibration table to convert pressure gage units to torr.

TABLE XXVII (Continued)

$CFCl_3$ THERMOMOLECULAR FLOW CORRECTION DATA

Isotherm Temperature: 258.15°K		Isotherm Temperature: 268.15°K	
Pressure Gage[a] Reading	Apparent Mass Change, μg.	Pressure Gage[a] Reading	Apparent Mass Change, μg.
0.035	-27.0	0.033	-19.0
0.070	-31.5	0.067	-26.0
0.130	-36.0	0.131	-33.0
0.260	-40.0	0.259	-35.5
0.517	-43.0	0.530	-37.0
1.030	-46.0	1.063	-40.0
2.074	-47.0	2.280	-42.0
5.266	-48.0	5.037	-41.5
10.296	-44.0	10.309	-42.0
19.930	-40.0	20.434	-34.0
30.595	-33.0	31.231	-26.0
40.261	-26.5	40.834	-20.5
50.457	-20.0	51.091	-14.5
60.457	-20.5	70.434	-7.0
70.010	-19.5	90.273	-3.0
80.620	-27.0	110.658	-5.0
89.998	-34.5	130.270	-10.0
101.480	-49.0	150.859	-22.5
Isotherm Temperature: 278.15°K		Isotherm Temperature: 288.15°K	
Pressure Gage[a] Reading	Apparent Mass Change, μg.	Pressure Gage[a] Reading	Apparent Mass Change, μg.
0.039	-24.0	0.041	-25.0
0.069	-30.0	0.067	-27.0
0.155	-34.0	0.134	-31.0
0.275	-39.0	0.260	-35.0
0.540	-37.0	0.529	-41.0
1.019	-41.5	1.059	-45.0
2.163	-43.0	2.034	-46.0
5.108	-43.0	5.320	-47.5
10.190	-42.0	10.572	-45.0
20.239	-33.0	20.220	-35.5
30.824	-27.5	29.978	-30.0
40.819	-22.0	40.964	-24.0
50.399	-17.0	50.980	-18.0
70.701	-8.0	70.541	-10.0
90.503	-2.5	90.274	-6.0
110.477	0.0	110.283	-3.0
130.421	4.0	131.151	1.0
150.792	-1.5	150.060	6.0
170.563	-5.0	170.245	6.0
190.491	-9.0	190.227	8.0

[a]Refer to pressure gage calibration table to convert pressure gage units to torr.

TABLE XXVII (Continued)

$CFCl_3$ THERMOMOLECULAR FLOW CORRECTION DATA

Isotherm Temperature: 298.15°K

Pressure Gage[a] Reading	Apparent Mass Change, μg.
0.030	-15.5
0.065	-20.0
0.121	-24.5
0.264	-26.0
0.529	-28.0
1.058	-30.5
2.026	-31.0
5.119	-30.5
10.205	-27.0
20.212	-21.0
30.171	-12.0
40.033	-3.0
50.330	2.5
70.594	11.0
90.285	18.5
110.704	21.0
130.045	25.0
150.386	30.0
170.401	34.0
190.567	36.0

[a]Refer to pressure gage calibration table to convert pressure gage units to torr.

TABLE XXVIII

PRESSURE GAGE CALIBRATION TABLE

True Corrected Pressure, torr.	Pressure Gage Reading
0.0000	0.000
14.9764	15.155
30.0109	30.296
45.0226	45.450
59.9965	60.599
75.0183	75.748
90.0149	90.871
105.0065	105.965
120.0334	121.031
135.0275	136.051
150.0241	151.049
165.0232	166.041
180.0198	181.009
195.0088	195.969
210.0079	210.925
225.0298	225.863
240.0238	240.768
255.0204	255.646
269.9893	270.511
284.9859	285.361

Calibration Temperature: 44.1°C.

APPENDIX V

ADSORBENT SAMPLE PREPARATION PROCEDURES

HOLOCELLULOSE PREPARATION PROCEDURE

A holocellulose pulp was prepared from black spruce (Picea mariana) chips using a modified chlorite method. The chips were cut by hand to approximate dimensions of 2 x 2 x 0.1 cm. from 2-cm. thick disks cut from a black spruce log.

All of the chips were extracted for 4 hours in a Soxhlet extractor with a chloroform-ethanol (10:1) mixture. Eleven hundred ml. of extraction solvent were used for each 150 grams of chips. After the solvent extraction, the chips were solvent exchanged to water.

The holopulping was accomplished over a 50-hour period by a chlorite treatment at 50°C. (43). The chips (300 g.) were placed in a solution (2.5 liters) containing sodium chlorite (45 g.) adjusted to pH 4 with acetic acid. A trace of formic acid was added to hasten formation of chlorine dioxide. When the sodium chlorite was consumed, fresh chlorite was added. Four changes of chlorite were required at 12-hour intervals.

After completing the pulping, each 200 grams of pulp was washed by filtering with approximately 6 liters of distilled water. The holocellulose was readily dispersed into fibers by soaking in 0.1N sodium hydroxide for 12 hours, and then beating in an Osterizer for 1 min. (43).

At the conclusion of the beating operation, the foamy mass was filtered and resuspended in water adjusted to pH 4 with acetic acid.

Finally, the holocellulose was washed and screened thoroughly using a vibrating flatbox screen. The shives were rejected in the screening operation. The screened

pulp was dewatered to approximately 20% consistency using a centrifuge, and stored in a refrigerated area.

ALKALI-EXTRACTED HOLOCELLULOSE PREPARATION PROCEDURE

The alkali-extracted holocellulose was prepared from the holocellulose pulp by extraction in 4% NaOH at a consistency of approximately 1.4% for 18 hours at 0°C. under an evacuated atmosphere. At the completion of this 18-hour period, the pulp was washed in distilled water. The pulp was then alternatively extracted and washed two more times using the same conditions. Finally, the pulp was neutralized to pH 6 using acetic acid, and allowed to stand two hours before washing exhaustively with distilled water. The extracted pulp was dewatered to approximately 20% consistency and stored in a refrigerated area.

ACID-HYDROLYZED HOLOCELLULOSE PREPARATION PROCEDURE

The acid-hydrolyzed holocellulose was prepared from the alkali-extracted holocellulose by an acid hydrolysis at 1.3% consistency in 2.5N HCl boiling at 105°C. The acid hydrolysis was carried out in a 2000-ml. three-necked flask heated by means of a mantle. A steady stream of nitrogen gas was admitted through one opening of the three-necked flask for the purpose of keeping the temperature of the acid uniform, eliminating bumping, and excluding oxygen from the hydrolyzing medium. The cellulose was left in the boiling HCl solution for 30 minutes. Upon completion of the hydrolysis, the cellulose was washed repeatedly with distilled water, dilute NH_4OH (1%), and more distilled water until acid free.

In order to separate the hydrolysis residue into microcrystallites, the cellulose was subjected to the vigorous mixing of a Waring Blendor at a consistency of 5% for 1 hour. Finally, the acid-hydrolyzed holocellulose was filtered, frozen in liquid nitrogen, and then freeze dried.

APPENDIX VI

ADSORPTION DATA AND MULTILAYER ADSORPTION MODEL RESULTS

TABLE XXIX

ARGON ADSORPTION DATA

Adsorbent: Holocellulose
Sample Mass: 0.50431 g.
Isotherm Temperature: 77.5°K

Equilibrium[a] Pressure, torr.	Apparent Mass Adsorbed, μg.	Corrected[b] Mass Adsorbed, μg.	Specific[c] Volume Adsorbed, ml. (S.T.P.)/g.
	1st. Experimental Run		
0.306	-30.0	28.6	0.0318
1.001	-25.0	44.0	0.0490
2.022	-23.0	50.9	0.0566
4.108	-11.0	72.0	0.0801
7.984	-5.0	85.9	0.0956
12.060	2.0	99.5	0.1107
17.056	4.0	110.1	0.1225
22.444	4.0	119.2	0.1325
35.745	0.0	139.3	0.1549
44.904	-4.0	151.2	0.1682
55.184	-12.0	159.8	0.1777
64.594	-22.0	169.1	0.1881
74.534	-31.0	178.9	0.1990
	2nd. Experimental Run		
0.527	-36.0	27.2	0.0303
1.029	-37.0	32.3	0.0359
2.039	-29.0	45.0	0.0500
4.000	-21.0	61.7	0.0686
6.025	-17.0	70.5	0.0784
9.991	-9.0	85.3	0.0949
14.972	1.0	103.7	0.1153
20.940	2.0	114.5	0.1273
25.306	2.5	122.7	0.1364
29.957	3.5	132.5	0.1474
39.832	0.0	146.5	0.1629
49.671	-4.0	159.1	0.1770
59.678	-15.0	165.3	0.1838
69.602	-25.0	175.9	0.1956
79.468	-39.0	180.3	0.2005

[a] Pressure corrected for thermal transpiration.
[b] Data corrected for buoyancy and thermomolecular flow effect.
[c] Specific volume adsorbed calculated as volume adsorbed per gram of adsorbent.

TABLE XXIX (Continued)

ARGON ADSORPTION DATA

Equilibrium[a] Pressure, torr.	Apparent Mass Adsorbed, μg.	Corrected[b] Mass Adsorbed, μg.	Specific[c] Volume Adsorbed, ml. (S.T.P.)/g.
	3rd Experimental Run		
0.563	-31.0	32.9	0.0366
1.034	-27.0	42.3	0.0470
2.060	-21.0	53.1	0.0590
4.027	-15.0	67.8	0.0754
6.108	-10.0	77.6	0.0863
9.981	-4.0	90.3	0.1004
14.989	3.0	105.7	0.1176
19.926	3.0	113.8	0.1266
25.198	4.0	124.0	0.1379
29.820	5.0	133.8	0.1488
44.792	-5.0	150.0	0.1668
54.645	-14.0	156.8	0.1744
64.521	-23.5	167.5	0.1863
74.453	-32.0	177.8	0.1977
84.404	-41.0	188.1	0.2092

[a] Pressure corrected for thermal transpiration.
[b] Data corrected for buoyancy and thermomolecular flow effect.
[c] Specific volume adsorbed calculated as volume adsorbed per gram of adsorbent.

TABLE XXX

RESULTS OF FITTING MULTILAYER ADSORPTION MODEL TO EXPERIMENTAL DATA

Adsorbent: Holocellulose
Adsorbate: Argon
Temperature: 77.5°K

Model Parameters

$\underline{U}^{Median} = 1.36 \pm 0.06^{a}$ kcal. mole^{-1}

$\underline{U}^{Mean} = 1.43$ kcal. mole^{-1}

$\underline{U}^{Mode} = 1.25$ kcal. mole^{-1}

$\gamma = 5.5 \pm 1.3$

$\underline{V}_{\beta} = 0.31 \pm 0.04$ ml. (S.T.P.) g.$^{-1}$

$\nu = 2.19 \pm 1.04 \times 10^{12}$ sec.$^{-1}$

$2\alpha/\beta$ (Ideal) $= 1.002$ kcal. mole^{-1}

$\alpha = 47.4 \times 10^{-30}$ erg cm.^{2} molecule^{-2}

$\beta = 13.6$ A.^{2} molecule^{-1}

Thermodynamic Data

$\Delta\underline{S}_{s}^{tr} = -0.0103$ kcal. mole^{-1} deg.$^{-1}$

$\Delta\underline{S}^{rot} = 0.0$ kcal. mole^{-1} deg.$^{-1}$

$\Delta\underline{S}^{vib} = 0.0015$ kcal. mole^{-1} deg.$^{-1}$

$\Delta\underline{E}^{kin} = -0.0770$ kcal. mole^{-1}

$\underline{\mathring{A}}. = 0.13476 \times 10^{7}$

---

[a] Approximate 95% linear confidence limits.

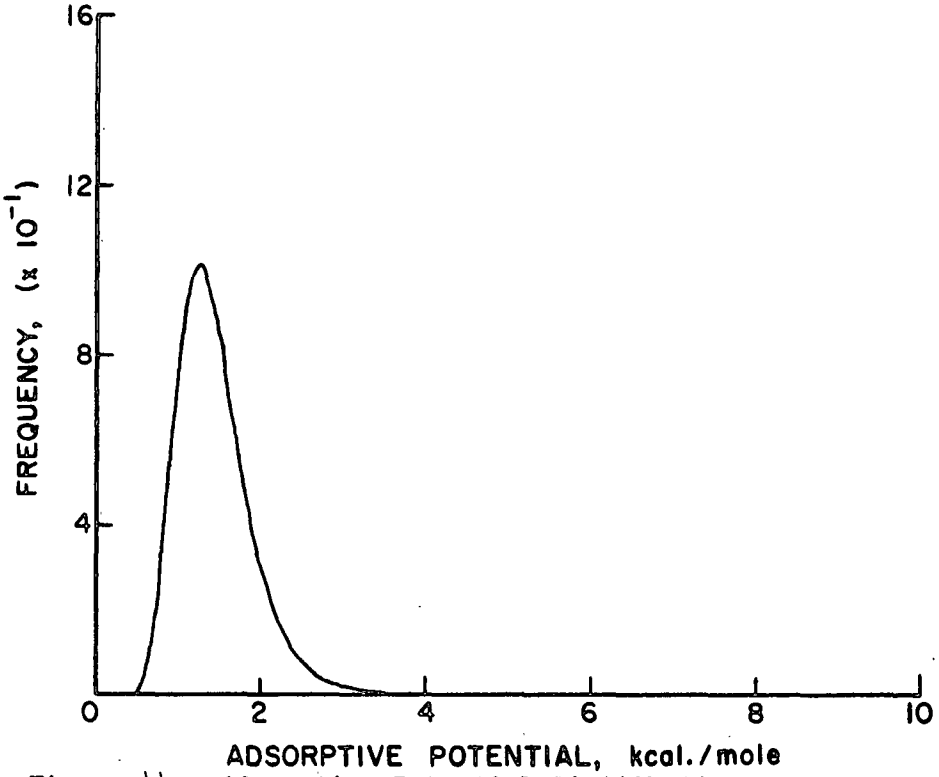

Figure 44. Adsorptive Potential Distribution for Argon Adsorption on Holocellulose at 77.5°K

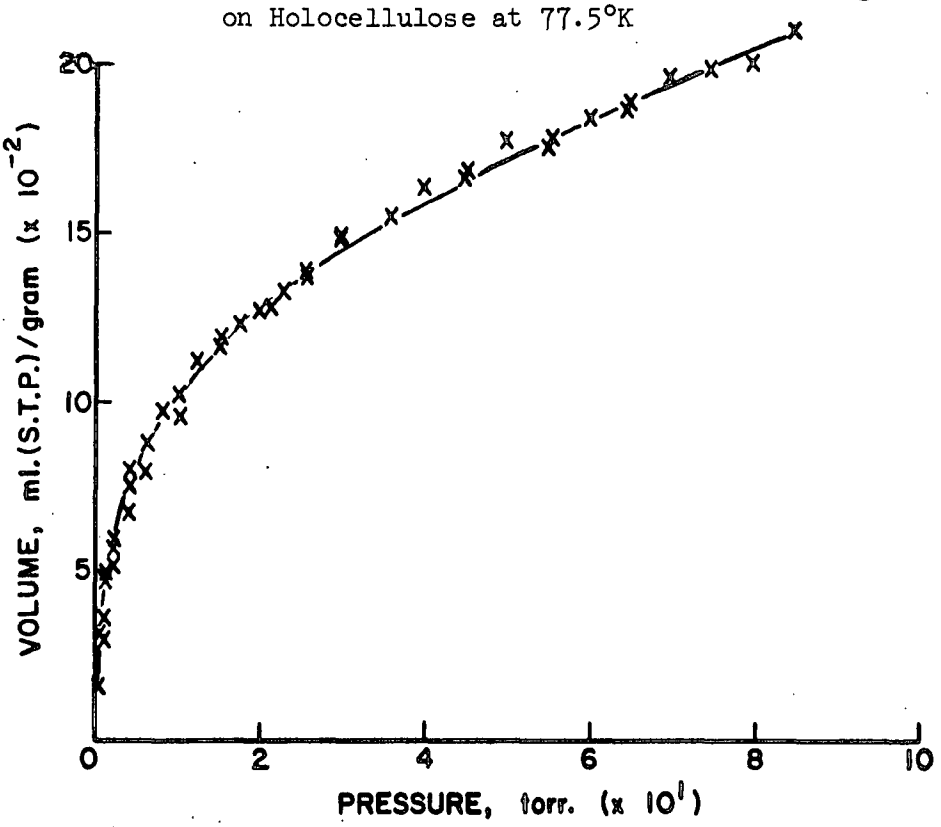

Figure 45. Multilayer Adsorption Model Fitted to the Argon Holocellulose Adsorption Data at 77.5°K

TABLE XXXI

ARGON ADSORPTION DATA

Adsorbent: Holocellulose
Sample Mass: 0.50425 g.
Isotherm Temperature: 90.1°K

Equilibrium[a] Pressure, torr.	Apparent Mass Adsorbed, μg.	Corrected[b] Mass Adsorbed, μg.	Specific[c] Volume Adsorbed, ml. (S.T.P.)/g.
	1st Experimental Run		
1.064	-64.0	1.6	0.0018
2.064	-70.0	1.7	0.0019
5.360	-67.0	13.1	0.0145
10.056	-71.0	17.3	0.0193
20.231	-74.0	30.8	0.0342
40.317	-93.0	40.1	0.0446
79.947	-134.0	59.2	0.0659
99.453	-163.0	59.6	0.0663
119.390	-187.0	65.5	0.0728
139.443	-219.0	62.7	0.0697
159.446	-245.0	66.4	0.0739
179.741	-275.0	68.9	0.0767
199.794	-311.0	62.7	0.0698
222.150	-347.0	64.0	0.0712
	2nd Experimental Run		
1.064	-51.0	14.6	0.0162
2.081	-56.0	15.8	0.0176
5.038	-56.0	24.0	0.0267
10.299	-60.0	28.8	0.0321
20.056	-73.0	31.6	0.0351
29.937	-81.0	38.4	0.0427
49.658	-104.0	43.3	0.0482
69.507	-127.0	51.3	0.0571
89.301	-152.0	55.2	0.0614
109.379	-179.0	58.5	0.0651
129.575	-205.0	62.4	0.0694
149.250	-230.0	66.2	0.0736
169.502	-259.0	68.2	0.0759
188.406	-285.0	72.1	0.0802
210.575	-321.0	70.6	0.0785
230.911	-353.0	72.6	0.0808
250.698	-387.0	73.9	0.0822
270.190	-426.0	71.0	0.0790

[a] Pressure corrected for thermal transpiration.
[b] Data corrected for buoyancy and thermomolecular flow effect.
[c] Specific volume adsorbed calculated as volume adsorbed per gram of adsorbent.

TABLE XXXII

RESULTS OF FITTING MULTILAYER ADSORPTION MODEL TO EXPERIMENTAL DATA

Adsorbent: Holocellulose
Adsorbate: Argon
Temperature: 90.1°K

Model Parameters

$\underline{U}^{Median} = 1.44 \pm 0.42^{a}$ kcal. mole^{-1}

$\underline{U}^{Mean} = 1.50$ kcal. mole^{-1}

$\underline{U}^{Mode} = 1.32$ kcal. mole^{-1}

$\gamma = 5.8 \pm 10.4$

$\underline{V}_{\beta} = 0.14 \pm 0.25$ ml. (S.T.P.) g.$^{-1}$

$\nu = 2.19 \pm 17.3 \times 10^{12}$ sec.$^{-1}$

$2\alpha/\beta$ (Ideal) $= 1.002$ kcal. mole^{-1}

$\alpha = 47.4 \times 10^{-30}$ erg cm.^{2} molecule^{-2}

$\beta = 13.6$ A.^{2} molecule^{-1}

Thermodynamic Data

$\Delta\underline{S}_{s}^{tr} = -0.0104$ kcal. mole^{-1} deg.$^{-1}$

$\Delta\underline{S}^{rot} = 0.0$ kcal. mole^{-1} deg.$^{-1}$

$\Delta\underline{S}^{vib} = 0.0018$ kcal. mole^{-1} deg.$^{-1}$

$\Delta\underline{E}^{kin} = -0.0895$ kcal. mole^{-1}

$\underline{A}^{o} = 0.15766 \times 10^{7}$

[a] Approximate 95% linear confidence limits.

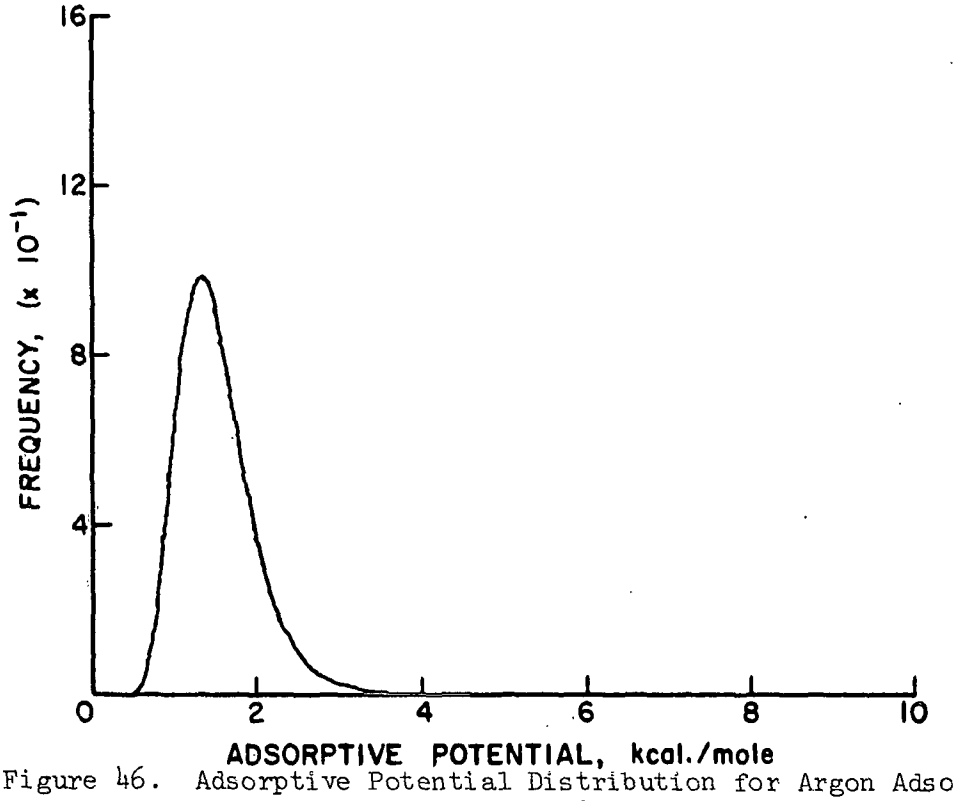

Figure 46. Adsorptive Potential Distribution for Argon Adsorption on Holocellulose at 90.1°K

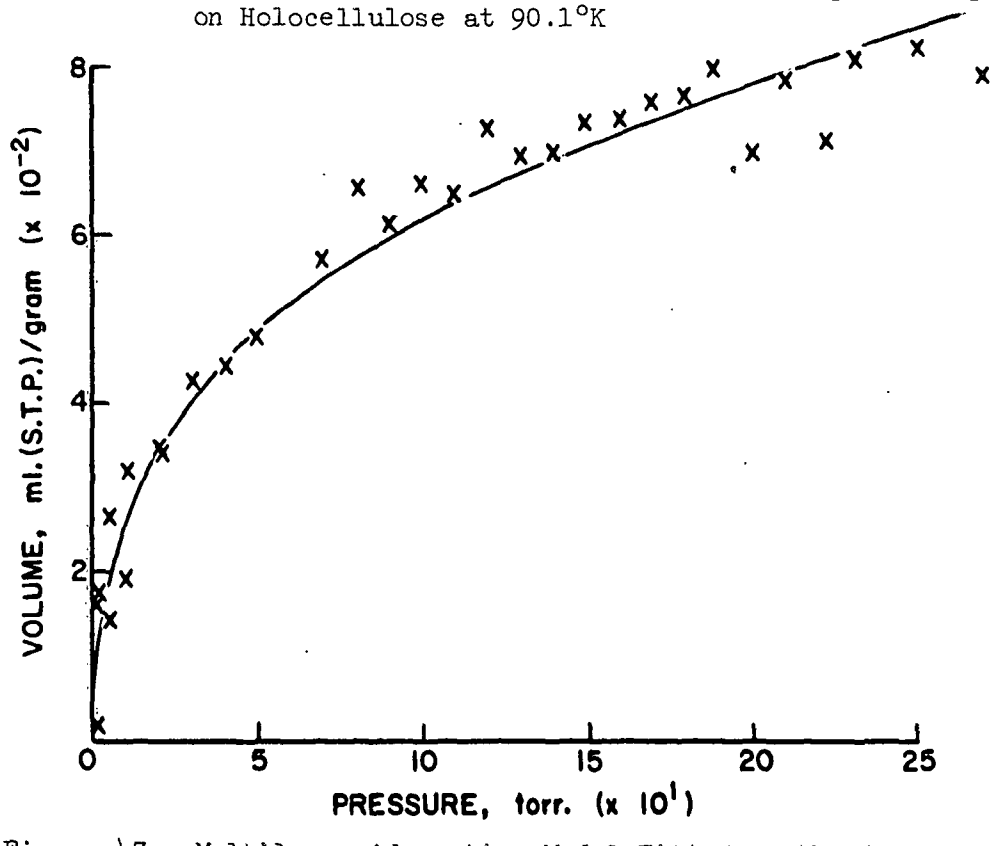

Figure 47. Multilayer Adsorption Model Fitted to the Argon Holocellulose Adsorption Data at 90.1°K

TABLE XXXIII

RESULTS OF FITTING MULTILAYER ADSORPTION MODEL TO EXPERIMENTAL DATA WITH VIBRATIONAL FREQUENCY ELIMINATED AS AN UNKNOWN PARAMETER

Adsorbent: Holocellulose
Adsorbate: Argon
Temperature: 90.1°K

Model Parameters

$\underline{U}^{Median} = 1.44 \pm 0.34^{a}$ kcal. mole^{-1}

$\underline{U}^{Mean} = 1.50$ kcal. mole^{-1}

$\underline{U}^{Mode} = 1.32$ kcal. mole^{-1}

$\gamma = 5.8 \pm 6.7$

$\underline{V}_{\beta} = 0.13 \pm 0.07$ ml. (S.T.P.) g.$^{-1}$

$\nu = 1.86 \times 10^{12}$ sec.$^{-1}$ (Calculated from the median adsorptive potential)

$2\alpha/\beta$ (Ideal) = 1.002 kcal. mole^{-1}

$\alpha = 47.4 \times 10^{-30}$ erg cm.^{2} molecule^{-2}

$\beta = 13.6$ A.^{2} molecule^{-1}

Thermodynamic Data

$\Delta\underline{S}^{tr} = -0.0104$ kcal. mole^{-1} deg.$^{-1}$

$\Delta\underline{S}^{rot} = 0.0$ kcal. mole^{-1} deg.$^{-1}$

$\Delta\underline{S}^{vib} = 0.0021$ kcal. mole^{-1} deg.$^{-1}$

$\Delta\underline{E}^{kin} = -0.0895$ kcal. mole^{-1}

$\underline{A}^{\circ} = 0.14395 \times 10^{7}$

---

[a] Approximate 95% linear confidence limits.

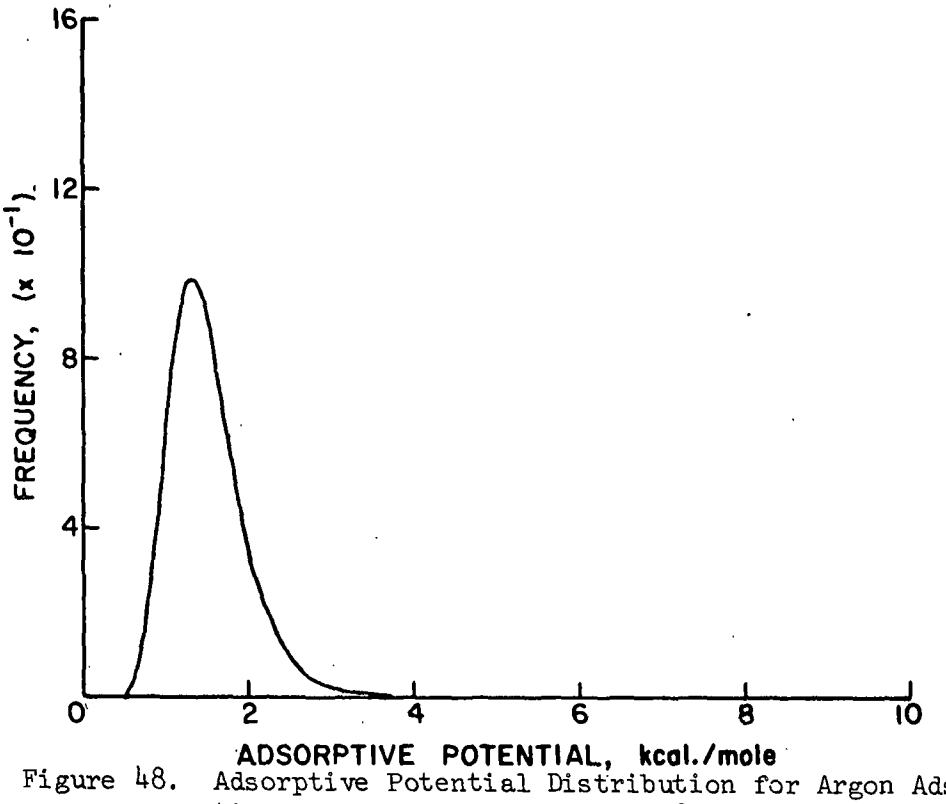

Figure 48. Adsorptive Potential Distribution for Argon Adsorption on Holocellulose at 90.1°K

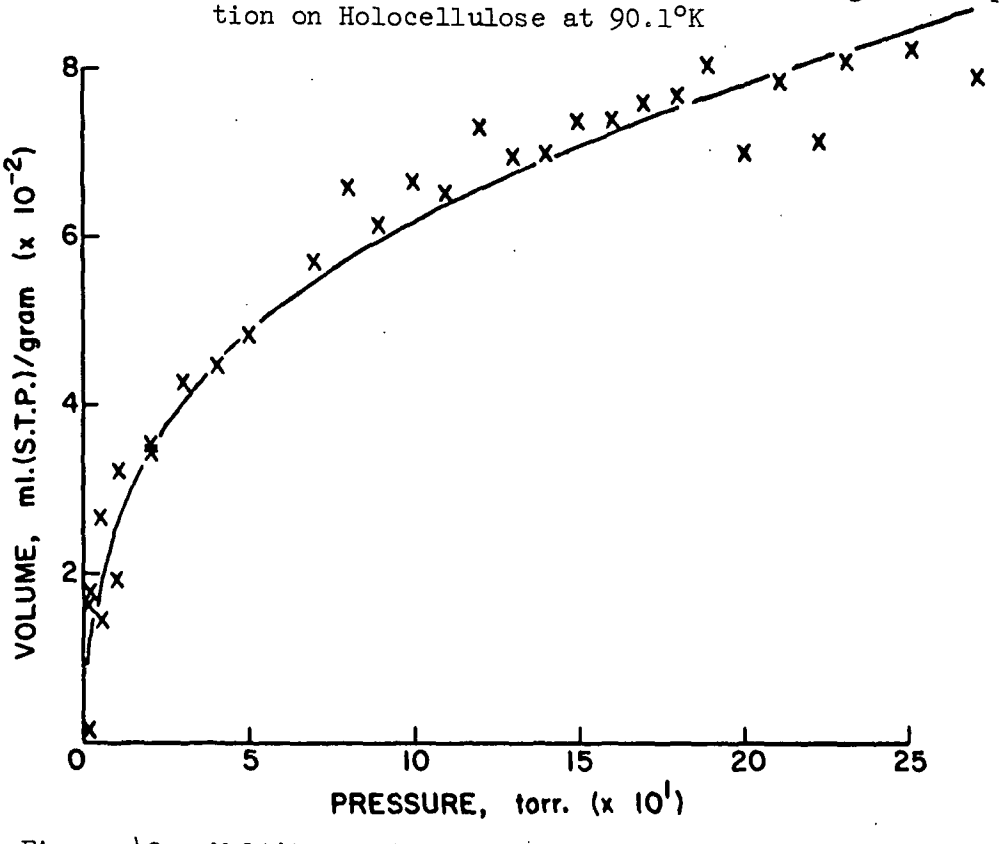

Figure 49. Multilayer Adsorption Model Fitted to the Argon Holocellulose Adsorption Data at 90.1°K with the Vibrational Frequency Eliminated as an Unknown Parameter

TABLE XXXIV

ARGON ADSORPTION DATA

Adsorbent: Alkali Extracted Holocellulose
Sample Mass: 0.52229 g.
Isotherm Temperature: 77.5°K

Equilibrium[a] Pressure, torr.	Apparent Mass Adsorbed, μg.	Corrected[b] Mass Adsorbed, μg.	Specific[c] Volume Adsorbed, ml. (S.T.P.)/g.
		1st Experimental Run	
0.038	-23.0	12.5	0.0139
0.099	-40.0	8.1	0.0090
0.053	-27.0	13.3	0.0149
0.102	-43.0	5.4	0.0060
0.221	-51.0	4.1	0.0045
0.356	-50.0	9.6	0.0108
0.634	-47.5	17.8	0.0198
1.015	-47.0	22.2	0.0248
2.062	-40.0	34.3	0.0383
5.065	-19.0	66.8	0.0746
10.152	-1.0	94.6	0.1056
15.306	14.0	118.8	0.1326
20.174	22.0	135.3	0.1510
30.658	31.0	164.4	0.1835
39.935	35.0	185.7	0.2073
49.901	33.0	201.5	0.2250
59.967	32.0	218.9	0.2444
69.460	30.0	237.6	0.2653
79.487	28.5	255.8	0.2856
89.244	23.0	269.7	0.3012
		2nd Experimental Run	
0.279	-53.0	4.3	0.0048
0.775	-50.0	17.2	0.0193
1.516	-37.0	35.1	0.0392
3.093	-26.0	53.8	0.0600
7.473	-3.0	87.7	0.0980
12.509	14.0	113.4	0.1266
17.645	20.0	128.9	0.1439
24.970	29.0	151.1	0.1687
35.081	33.0	174.6	0.1950
44.941	32.0	191.8	0.2141
54.630	33.0	209.3	0.2336
64.852	30.5	228.6	0.2553
74.600	26.0	243.5	0.2719
84.242	23.0	260.2	0.2905

[a] Pressure corrected for thermal transpiration.
[b] Data corrected for buoyancy and thermomolecular flow effect.
[c] Specific volume adsorbed calculated as volume adsorbed per gram of adsorbent.

TABLE XXXV

RESULTS OF FITTING MULTILAYER ADSORPTION MODEL TO EXPERIMENTAL DATA

Adsorbent: Alkali Extracted Holocellulose
Adsorbate: Argon
Temperature: 77.5°K

Model Parameters

$\underline{U}^{Median} = 1.29 \pm 0.02^{a}$ kcal. mole^{-1}

$\underline{U}^{Mean} = 1.31$ kcal. mole^{-1}

$\underline{U}^{Mode} = 1.23$ kcal. mole^{-1}

$\gamma = 12.1 \pm 2.3$

$\underline{V}_{\beta} = 0.35 \pm 0.04$ ml. (S.T.P.) g.$^{-1}$

$\nu = 0.74 \pm 0.16 \times 10^{12}$ sec.$^{-1}$

$2\alpha/\beta$ (Ideal) $= 1.002$ kcal. mole^{-1}

$\alpha = 47.4 \times 10^{-30}$ erg cm.^{2} molecule^{-2}

$\beta = 13.6$ A.^{2} molecule^{-1}

Thermodynamic Data

$\Delta\underline{S}^{tr} = -0.0103$ kcal. mole^{-1} deg.$^{-1}$

$\Delta\underline{S}^{rot} = 0.0$ kcal. mole^{-1} deg.$^{-1}$

$\Delta\underline{S}^{vib} = 0.0036$ kcal. mole^{-1} deg.$^{-1}$

$\Delta\underline{E}^{kin} = -0.0770$ kcal. mole^{-1}

$\underline{A}^{o} = 0.66748 \times 10^{6}$

---

[a] Approximate 95% linear confidence limits.

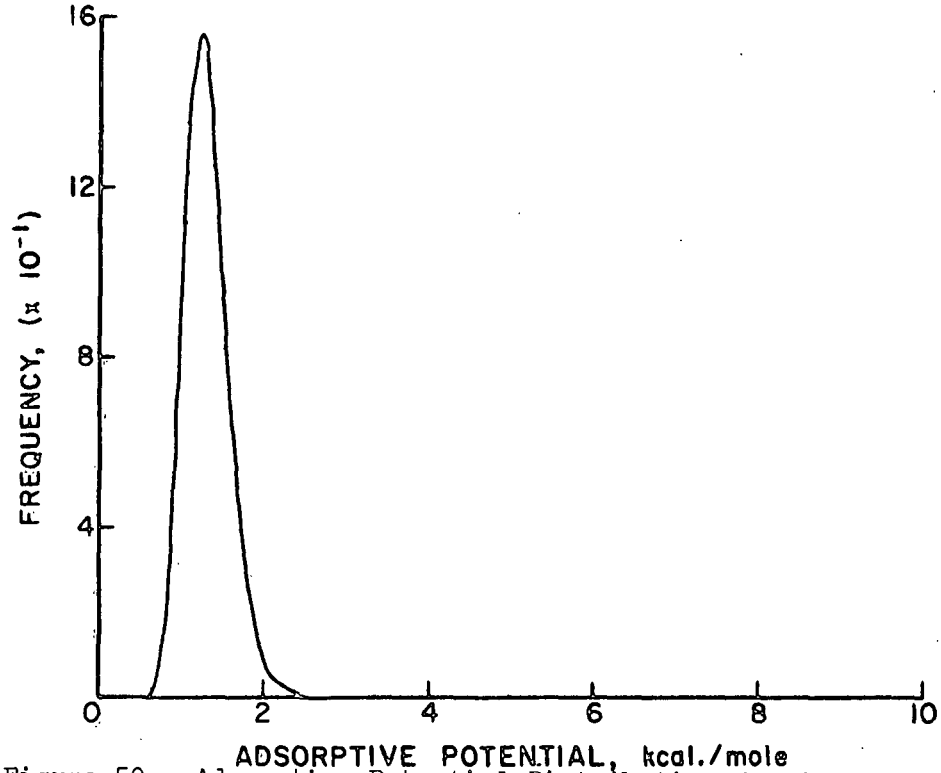

Figure 50. Adsorptive Potential Distribution for Argon Adsorption on Alkali-Extracted Holocellulose at 77.5°K

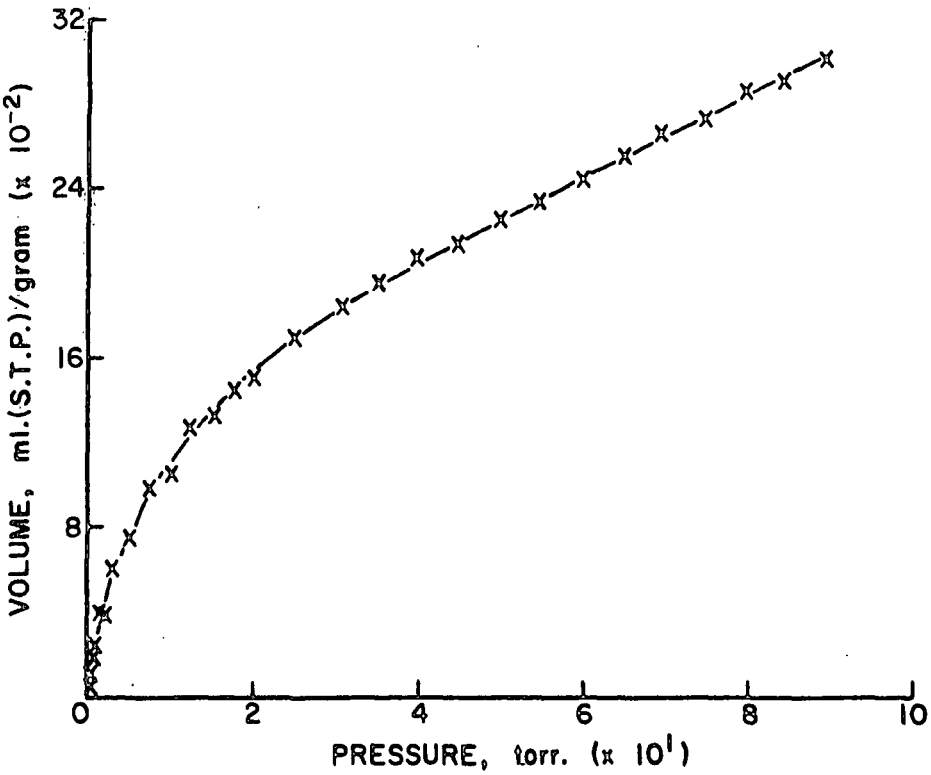

Figure 51. Multilayer Adsorption Model Fitted to the Argon Alkali-Extracted Holocellulose Adsorption Data at 77.5°K

TABLE XXXVI

ARGON ADSORPTION DATA

Adsorbent: Alkali Extracted Holocellulose
Sample Mass: 0.50232 g.
Isotherm Temperature: 90.1°K

Equilibrium[a] Pressure, torr.	Apparent Mass Adsorbed, μg.	Corrected[b] Mass Adsorbed, μg.	Specific[c] Volume Adsorbed, ml. (S.T.P.)/g.
		1st Experimental Run	
5.105	-66.5	14.0	0.0156
10.127	-65.0	24.4	0.0272
20.080	-67.5	38.8	0.0433
40.060	-78.0	58.2	0.0649
59.702	-93.0	75.7	0.0845
79.288	-109.5	89.6	0.1000
99.293	-129.0	101.9	0.1138
119.187	-145.0	117.4	0.1311
139.524	-166.5	127.3	0.1421
160.035	-183.0	143.1	0.1597
179.456	-222.0	136.9	0.1528
201.384	-247.0	146.5	0.1636
220.057	-272.0	154.4	0.1724
239.589	-303.0	158.3	0.1767
260.181	-337.0	164.2	0.1833
279.875	-368.0	176.1	0.1966
		2nd Experimental Run	
5.154	-69.0	11.5	0.0128
10.008	-67.0	22.1	0.0247
20.352	-67.0	39.7	0.0443
30.776	-71.0	52.3	0.0584
49.822	-84.0	67.9	0.0758
69.761	-100.0	84.7	0.0945
89.126	-117.0	97.6	0.1090
109.530	-136.0	111.1	0.1241
129.387	-159.0	119.3	0.1331
149.219	-180.0	129.0	0.1440

[a] Pressure corrected for thermal transpiration.
[b] Data corrected for buoyancy and thermomolecular flow effect.
[c] Specific volume adsorbed calculated as volume adsorbed per gram of adsorbent.

TABLE XXXVII

RESULTS OF FITTING MULTILAYER ADSORPTION MODEL TO EXPERIMENTAL DATA

Adsorbent: Alkali-Extracted Holocellulose
Adsorbate: Argon
Temperature: 90.1°K

Model Parameters

$\underline{U}^{Median} = 1.29 \pm 0.37^{a}$ kcal. mole^{-1}

$\underline{U}^{Mean} = 1.32$ kcal. mole^{-1}

$\underline{U}^{Mode} = 1.23$ kcal. mole^{-1}

$\gamma = 10.4 \pm 4.1$

$\underline{V}_{\beta} = 0.38 \pm 0.38$ ml. (S.T.P.) g.$^{-1}$

$\nu = 2.16 \pm 15.8 \times 10^{12}$ sec.$^{-1}$

$2\alpha/\beta$ (Ideal) $= 1.002$ kcal. mole^{-1}

$\alpha = 47.4 \times 10^{-30}$ erg cm.^{2} molecule^{-2}

$\beta = 13.6$ A.^{2} molecule^{-1}

Thermodynamic Data

$\Delta\underline{S}_{\underline{s}}^{tr} = -0.0104$ kcal. mole^{-1} deg.$^{-1}$

$\Delta\underline{S}^{rot} = 0.0$ kcal. mole^{-1} deg.$^{-1}$

$\Delta\underline{S}^{vib} = 0.0018$ kcal. mole^{-1} deg.$^{-1}$

$\Delta\underline{E}^{kin} = -0.0895$ kcal. mole^{-1}

$\underline{\overset{\circ}{A}} = 0.16197 \times 10^{7}$

[a] Approximate 95% linear confidence limits.

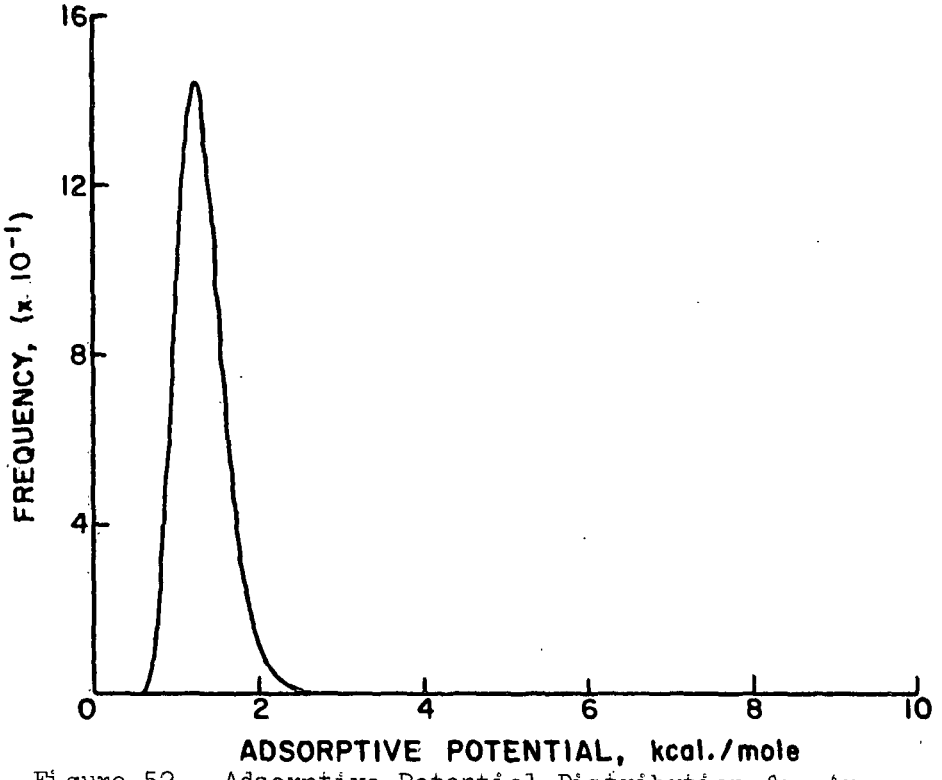

Figure 52. Adsorptive Potential Distribution for Argon Adsorption on Alkali-Extracted Holocellulose at 90.1°K

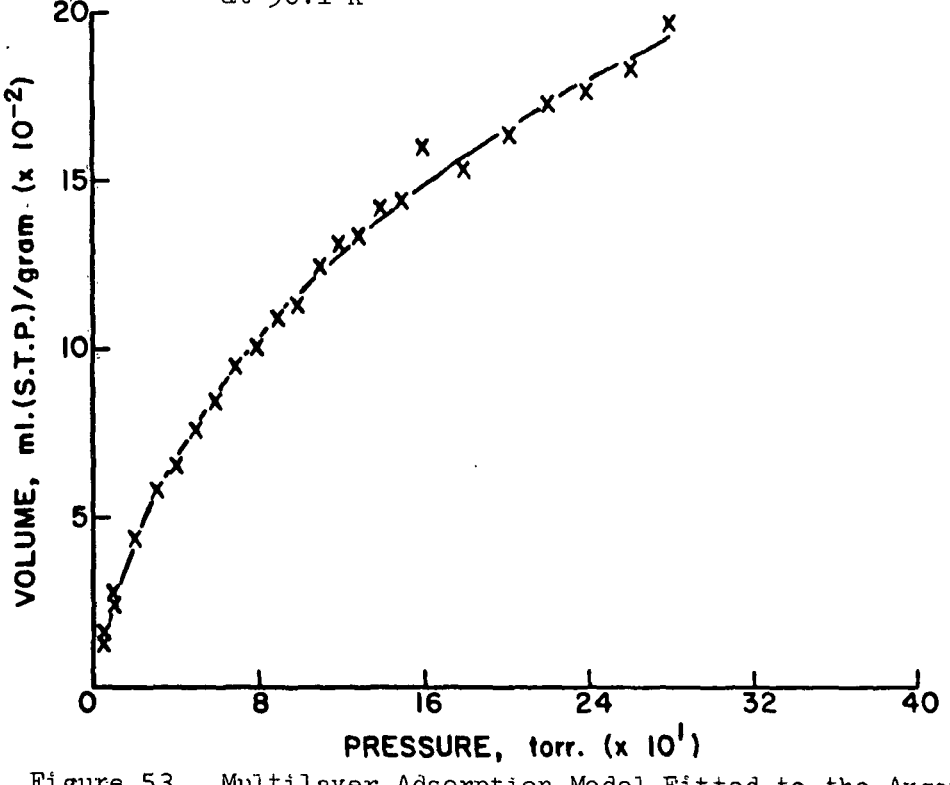

Figure 53. Multilayer Adsorption Model Fitted to the Argon Alkali-Extracted Holocellulose Adsorption Data at 90.1°K

TABLE XXXVIII

RESULTS OF FITTING MULTILAYER ADSORPTION MODEL TO EXPERIMENTAL DATA WITH VIBRATIONAL FREQUENCY ELIMINATED AS AN UNKNOWN PARAMETER

Adsorbent: Alkali-Extracted Holocellulose
Adsorbate: Argon
Temperature: 90.1°K

Model Parameters

$\underline{U}^{Median} = 1.28 \times 0.09^{a}$ kcal. mole^{-1}

$\underline{U}^{Mean} = 1.31$ kcal. mole^{-1}

$\underline{U}^{Mode} = 1.22$ kcal. mole^{-1}

$\gamma = 10.5 \pm 4.4$

$\underline{V}_{\beta} = 0.36 \pm 0.08$ ml. (S.T.P.) g.$^{-1}$

$\nu = 1.76 \times 10^{12}$ sec.$^{-1}$ (Calculated from the median adsorptive potential)

$2\alpha/\beta$ (Ideal) = 1.002 kcal. mole^{-1}

$\alpha = 47.4 \times 10^{-30}$ erg cm.^{2} molecule^{-2}

$\beta = 13.6$ A.^{2} molecule^{-1}

Thermodynamic Data

$\Delta\underline{S}^{tr} = -0.0104$ kcal. mole^{-1} deg.$^{-1}$

$\Delta\underline{S}^{rot} = 0.0$ kcal. mole^{-1} deg.$^{-1}$

$\Delta\underline{S}^{vib} = 0.0022$ kcal. mole^{-1} deg.$^{-1}$

$\Delta\underline{E}^{kin} = -0.0895$ kcal. mole^{-1}

$\underline{A}^{\circ} = 0.13811 \times 10^{7}$

---

[a] Approximate 95% linear confidence limits.

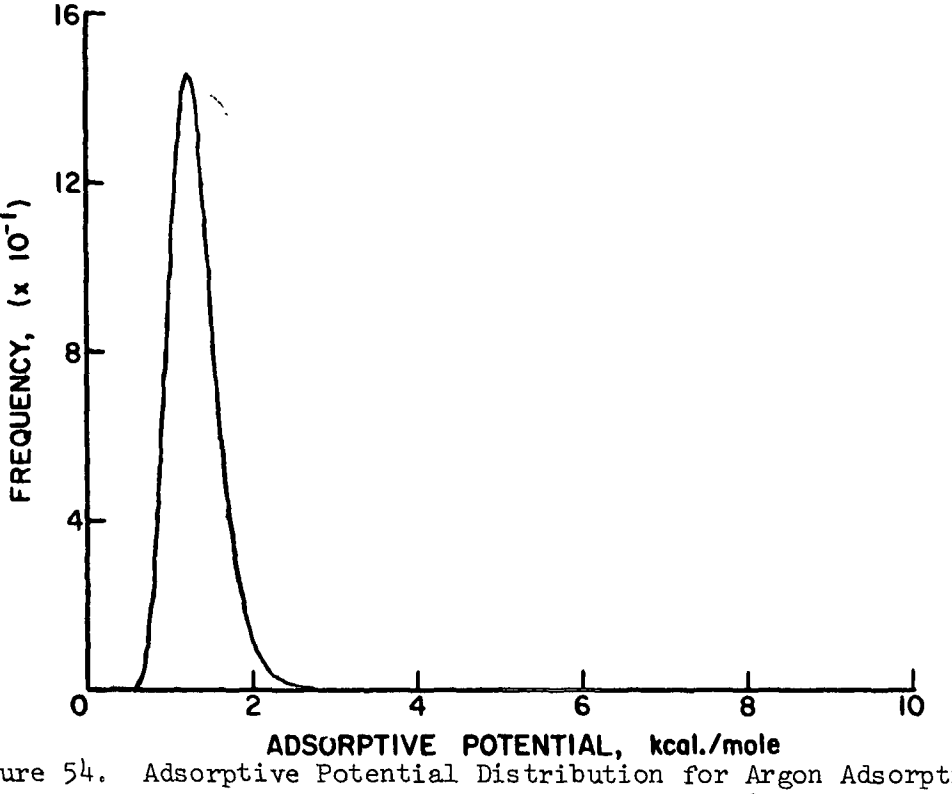

Figure 54. Adsorptive Potential Distribution for Argon Adsorption on Alkali-Extracted Holocellulose at 90.1°K

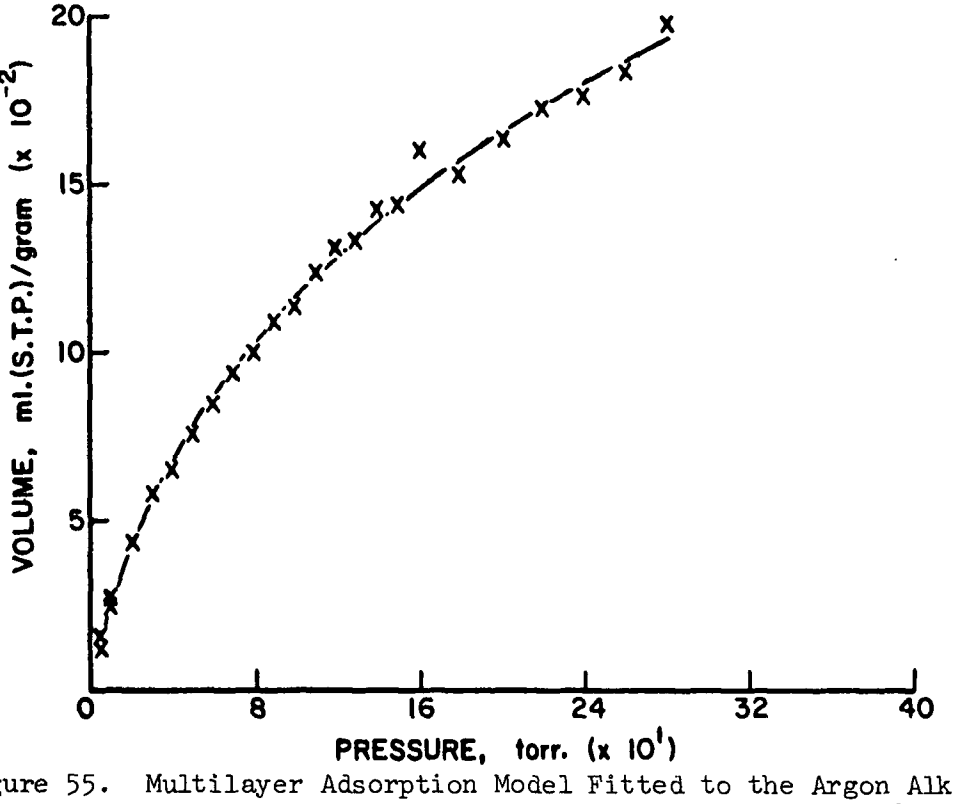

Figure 55. Multilayer Adsorption Model Fitted to the Argon Alkali-Extracted Holocellulose Adsorption Data at 90.1°K with the Vibrational Frequency Eliminated as an Unknown Parameter

TABLE XXXIX

ARGON ADSORPTION DATA

Adsorbent: Acid-Hydrolyzed Holocellulose
Sample Mass: 0.50399 g.
Isotherm Temperature: 77.5°K

Equilibrium[a] Pressure, torr.	Apparent Mass Adsorbed, μg.	Corrected[b] Mass Adsorbed, μg.	Specific[c] Volume Adsorbed, ml. (S.T.P.)/g.
	1st Experimental Run		
0.052	-7.0	33.0	0.0368
0.129	1.0	50.2	0.0559
0.281	16.0	73.2	0.0815
0.529	36.0	99.2	0.1104
1.029	64.0	133.5	0.1486
2.035	106.0	179.6	0.1998
5.120	197.0	281.5	0.3133
10.637	298.5	392.0	0.4362
15.060	350.0	450.2	0.5009
20.186	402.0	509.8	0.5672
25.169	437.0	552.6	0.6148
30.355	467.0	591.5	0.6581
40.022	513.0	652.9	0.7264
49.712	542.0	696.5	0.7750
60.097	567.0	737.7	0.8208
69.988	593.0	782.5	0.8706
79.597	613.0	818.7	0.9109
89.801	640.0	863.2	0.9604
	2nd Experimental Run		
0.042	-2.0	35.1	0.0390
0.078	-1.0	44.8	0.0499
0.151	6.0	56.9	0.0633
0.318	18.0	77.0	0.0857
0.716	49.0	115.3	0.1283
1.514	86.0	157.7	0.1755
3.016	137.0	215.5	0.2397
7.664	250.0	339.0	0.3772
12.949	328.0	425.0	0.4729
17.355	372.0	475.6	0.5292
22.503	415.0	526.3	0.5856
27.673	445.0	564.6	0.6282
35.270	480.0	612.3	0.6813
45.177	516.0	663.8	0.7386
55.119	551.0	713.1	0.7934
65.199	574.0	755.0	0.8401
74.749	595.0	792.3	0.8816
84.442	614.0	828.5	0.9218
94.937	638.0	868.9	0.9668

[a] Pressure corrected for thermal transpiration.
[b] Data corrected for buoyancy and thermomolecular flow effect.
[c] Specific volume adsorbed calculated as volume adsorbed per gram of adsorbent.

TABLE XL

RESULTS OF FITTING MULTILAYER ADSORPTION MODEL TO EXPERIMENTAL DATA

Adsorbent: Acid-Hydrolyzed Holocellulose
Adsorbate: Argon
Temperature: 77.5°K

Model Parameters

$\underline{U}^{Median} = 1.36 \pm 0.02^{a}$ kcal. mole^{-1}

$\underline{U}^{Mean} = 1.40$ kcal. mole^{-1}

$\underline{U}^{Mode} = 1.27$ kcal. mole^{-1}

$\gamma = 7.4 \pm 0.8$

$\underline{V}_{\beta} = 1.39 \pm 0.07$ ml. (S.T.P.) g.$^{-1}$

$\nu = 2.26 \pm 0.58 \times 10^{12}$ sec.$^{-1}$

$2\alpha/\beta$ (Ideal) $= 1.002$ kcal. mole^{-1}

$\alpha = 47.4 \times 10^{-30}$ erg cm.^{2} molecule^{-2}

$\beta = 13.6$ A.^{2} molecule^{-1}

Thermodynamic Data

$\Delta\underline{S}_{s}^{tr} = -0.0103$ kcal. mole^{-1} deg.$^{-1}$

$\Delta\underline{S}^{rot} = 0.0$ kcal. mole^{-1} deg.$^{-1}$

$\Delta\underline{S}^{vib} = 0.0015$ kcal. mole^{-1} deg.$^{-1}$

$\Delta\underline{E}^{kin} = -0.0770$ kcal. mole^{-1}

$\underline{A}^{\circ} = 0.13691 \times 10^{7}$

[a] Approximate 95% linear confidence limits.

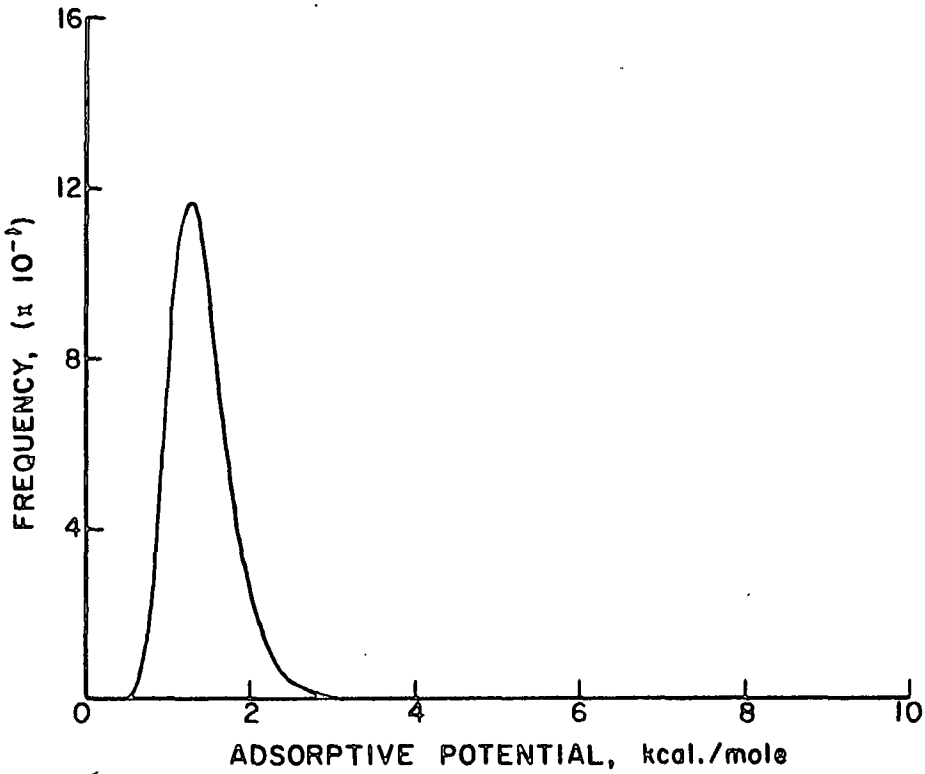

Figure 56. Adsorptive Potential Distribution for Argon Adsorption on Acid-Hydrolyzed Holocellulose at 77.5°K

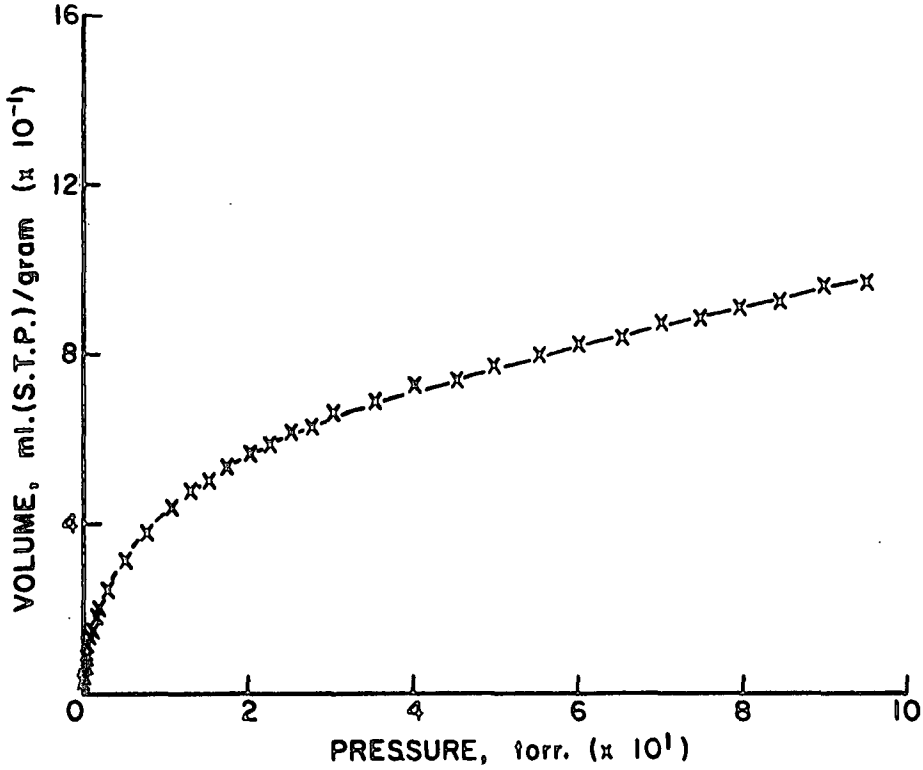

Figure 57. Multilayer Adsorption Model Fitted to the Argon Acid-Hydrolyzed Holocellulose Adsorption Data at 77.5°K

TABLE XLI

ARGON ADSORPTION DATA

Adsorbent: Acid-Hydrolyzed Holocellulose
Sample Mass: 0.50354 g.
Isotherm Temperature: 90.1°K

Equilibrium[a] Pressure, torr.	Apparent Mass Adsorbed, μg.	Corrected[b] Mass Adsorbed, μg.	Specific[c] Volume Adsorbed, ml. (S.T.P.)/g.
	1st Experimental Run		
0.045	-13.0	25.2	0.0280
0.104	-22.5	26.8	0.0298
0.523	-18.0	43.6	0.0485
1.097	-12.0	53.5	0.0595
2.031	-2.0	69.2	0.0770
4.105	15.0	93.3	0.1038
7.463	36.0	117.9	0.1312
12.532	59.0	150.1	0.1670
17.670	80.0	178.6	0.1987
25.654	107.0	216.3	0.2407
35.224	131.5	253.1	0.2816
49.813	159.0	299.1	0.3328
69.839	187.0	355.3	0.3954
89.375	204.0	398.0	0.4428
109.476	211.0	432.3	0.4810
129.573	214.0	462.0	0.5141
149.399	212.5	486.6	0.5414
169.850	207.0	509.4	0.5668
189.571	197.0	527.5	0.5869
222.163	175.0	552.8	0.6151
250.120	151.0	573.4	0.6380
285.349	116.0	603.6	0.6716

[a] Pressure corrected for thermal transpiration.

[b] Data corrected for buoyancy and thermomolecular flow effect.

[c] Specific volume adsorbed calculated as volume adsorbed per gram of adsorbent.

TABLE XLI (Continued)

ARGON ADSORPTION DATA

Adsorbent: Acid-Hydrolyzed Holocellulose
Sample Mass: 0.50354 g.
Isotherm Temperature: 90.1°K

Equilibrium[a] Pressure, torr.	Apparent Mass Adsorbed, μg.	Corrected[b] Mass Adsorbed, μg.	Specific[c] Volume Adsorbed, ml. (S.T.P.)/g.
	2nd Experimental Run		
0.049	-17.0	22.3	0.0248
0.160	-21.0	32.0	0.0356
0.517	-18.0	43.5	0.0484
1.070	-12.0	53.4	0.0594
2.031	-2.0	69.2	0.0770
5.032	21.5	100.7	0.1121
10.097	49.0	135.9	0.1512
15.379	70.0	165.4	0.1841
20.305	87.0	188.8	0.2101
30.204	116.0	231.3	0.2574
39.979	137.0	263.6	0.2933
60.236	169.0	324.4	0.3609
79.889	193.0	374.2	0.4164
99.285	203.0	410.5	0.4568
119.866	209.0	444.2	0.4943
139.370	210.0	470.7	0.5238
159.656	206.0	493.9	0.5495
179.670	201.0	517.9	0.5763
209.332	185.0	542.9	0.6040
240.372	162.0	568.1	0.6322
270.231	134.0	590.7	0.6572

[a] Pressure corrected for thermal transpiration.

[b] Data corrected for buoyancy and thermomolecular flow effect.

[c] Specific volume adsorbed calculated as volume adsorbed per gram of adsorbent.

TABLE XLII

RESULTS OF FITTING MULTILAYER ADSORPTION MODEL TO EXPERIMENTAL DATA

Adsorbent: Acid-Hydrolyzed Holocellulose
Adsorbate: Argon
Temperature: 90.1°K

Model Parameters

$\underline{U}^{Median} = 1.30 \pm 0.10^{a}$ kcal. mole^{-1}

$\underline{U}^{Mean} = 1.36$ kcal. mole^{-1}

$\underline{U}^{Mode} = 1.19$ kcal. mole^{-1}

$\gamma = 5.5 \pm 2.1$

$\underline{V}_{\beta} = 1.30 \pm 0.74$ ml. (S.T.P.) g.$^{-1}$

$\nu = 2.26 \pm 5.48 \times 10^{12}$ sec.$^{-1}$

$2\alpha/\beta$ (Ideal) $= 1.002$ kcal. mole^{-1}

$\alpha = 47.4 \times 10^{-30}$ erg cm.^{2} molecule^{-2}

$\beta = 13.6$ A.^{2} molecule^{-1}

Thermodynamic Data

$\Delta\underline{S}_{s}^{tr} = -0.0104$ kcal. mole^{-1} deg.$^{-1}$

$\Delta\underline{S}^{rot} = 0.0$ kcal. mole^{-1} deg.$^{-1}$

$\Delta\underline{S}^{vib} = 0.0017$ kcal. mole^{-1} deg.$^{-1}$

$\Delta\underline{E}^{kin} = -0.0895$ kcal. mole^{-1}

$\underline{A}^{\circ} = 0.16043 \times 10^{7}$

---

[a] Approximate 95% linear confidence limits.

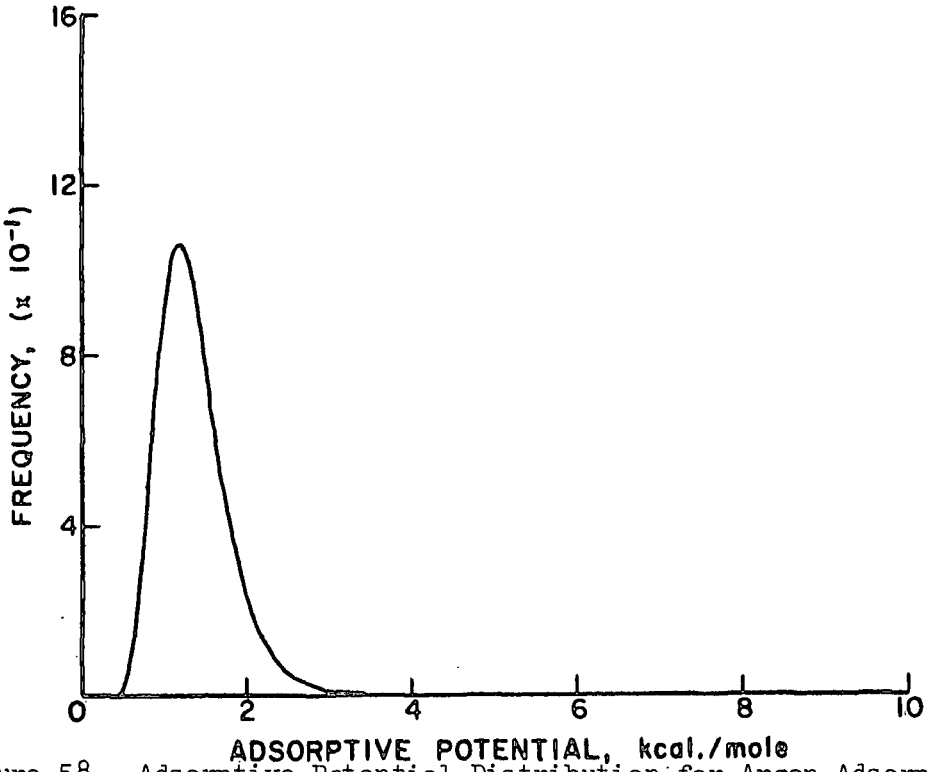

Figure 58. Adsorptive Potential Distribution for Argon Adsorption on Acid-Hydrolyzed Holocellulose at 90.1°K

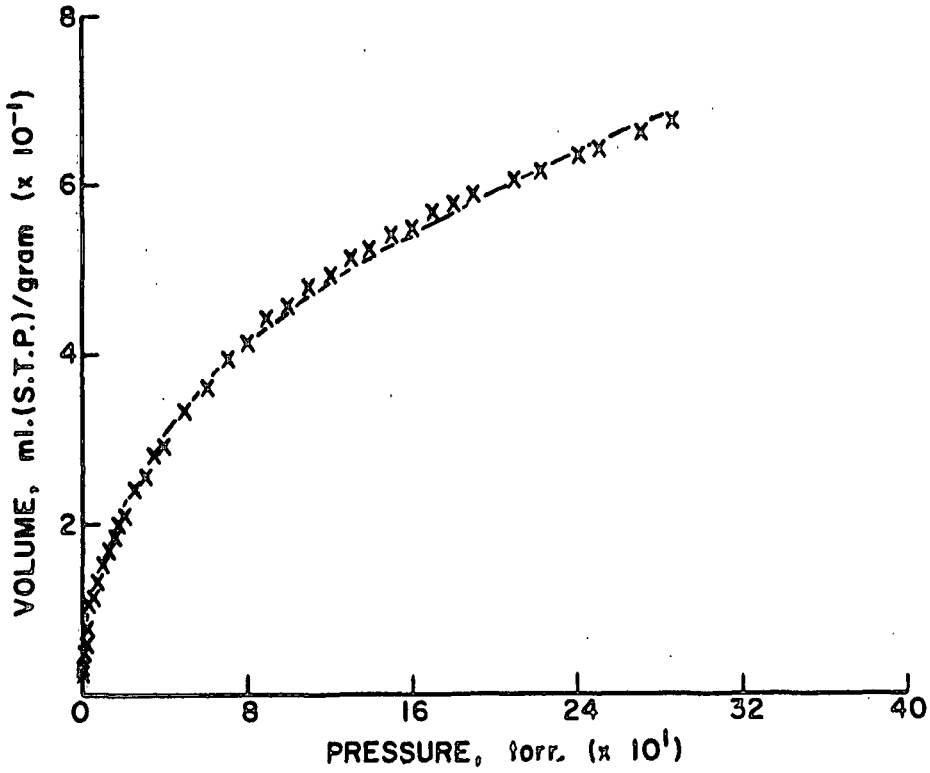

Figure 59. Multilayer Adsorption Model Fitted to the Argon Acid-Hydrolyzed Holocellulose Adsorption Data at 90.1°K

TABLE XLIII

RESULTS OF FITTING MULTILAYER ADSORPTION MODEL TO EXPERIMENTAL DATA WITH VIBRATIONAL FREQUENCY ELIMINATED AS AN UNKNOWN PARAMETER

Adsorbent: Acid-Hydrolyzed Holocellulose
Adsorbate: Argon
Temperature: 90.1°K

Model Parameters

$\underline{U}^{Median} = 1.30 \pm 0.10^{a}$ kcal. mole^{-1}

$\underline{U}^{Mean} = 1.36$ kcal. mole^{-1}

$\underline{U}^{Mode} = 1.19$ kcal. mole^{-1}

$\gamma = 5.6 \pm 1.6$

$\underline{V}_{\beta} = 1.24 \pm 0.22$ ml. (S.T.P.) g.$^{-1}$

$\nu = 1.77 \times 10^{12}$ sec.$^{-1}$ (Calculated from the median adsorptive potential)

$2\alpha/\beta$ (Ideal) $= 1.002$ kcal. mole^{-1}

$\alpha = 47.4 \times 10^{-30}$ erg cm.^{2} molecule^{-2}

$\beta = 13.6$ A.^{2} molecule^{-1}

Thermodynamic Data

$\Delta\underline{S}_{s}^{tr} = -0.0104$ kcal. mole^{-1} deg.$^{-1}$

$\Delta\underline{S}^{rot} = 0.0$ kcal. mole^{-1} deg.$^{-1}$

$\Delta\underline{S}^{vib} = 0.0022$ kcal. mole^{-1} deg.$^{-1}$

$\Delta\underline{E}^{kin} = -0.0895$ kcal. mole^{-1}

$\underline{A}^{o} = 0.13983 \times 10^{7}$

[a] Approximate 95% linear confidence limits.

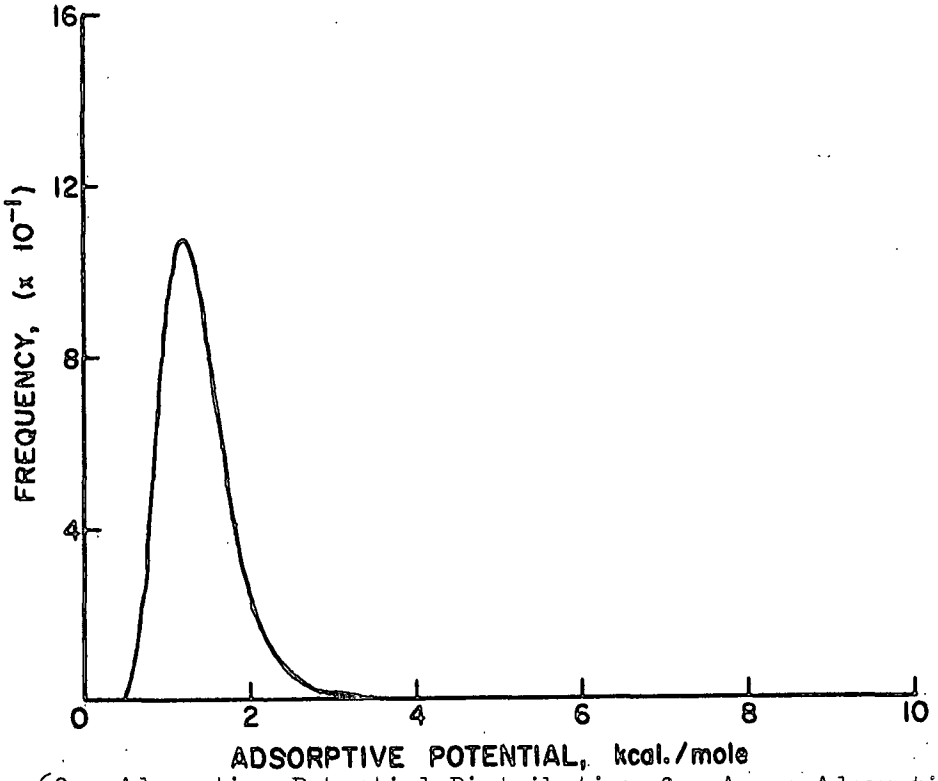

Figure 60. Adsorptive Potential Distribution for Argon Adsorption on Acid-Hydrolyzed Holocellulose at 90.1°K

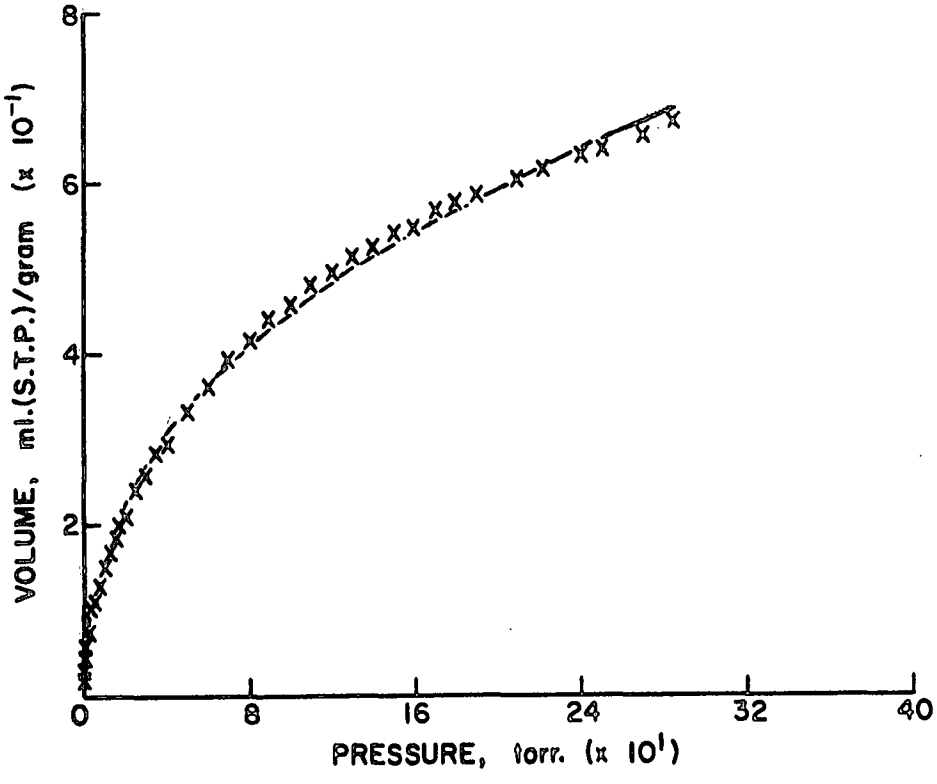

Figure 61. Multilayer Adsorption Model Fitted to the Argon Acid-Hydrolyzed Holocellulose Adsorption Data at 90.1°K with the Vibrational Frequency Eliminated as an Unknown Parameter

TABLE XLIV

RESULTS OF FITTING MULTILAYER ADSORPTION MODEL TO EXPERIMENTAL DATA

Adsorbent: Acid-Hydrolyzed Holocellulose
Adsorbate: Argon
Temperature: 77.5 and 90.1°K

Model Parameters

$\underline{U}^{Median} = 1.34 \pm 0.10$[a] kcal. mole^{-1}

$\underline{U}^{Mean} = 1.38$ kcal. mole^{-1}

$\underline{U}^{Mode} = 1.25$ kcal. mole^{-1}

$\gamma = 7.5 \pm 2.9$

$\underline{V}_{\beta} = 1.37 \pm 0.32$ ml. (S.T.P.) g.$^{-1}$

$\nu = 2.31 \pm 1.89 \times 10^{12}$ sec.$^{-1}$

$2\alpha/\beta$ (Ideal) = 1.002 kcal. mole^{-1}

$\alpha = 47.4 \times 10^{-30}$ erg cm.^{2} molecule^{-2}

$\beta = 13.6$ A.^{2} molecule^{-1}

Thermodynamic Data

$\Delta\underline{S}^{tr} = -0.0104$ kcal. mole^{-1} deg.$^{-1}$

$\Delta\underline{S}^{rot} = 0.0$ kcal. mole^{-1} deg.$^{-1}$

$\Delta\underline{S}^{vib} = 0.0017$ kcal. mole^{-1} deg.$^{-1}$

$\Delta\underline{E}^{kin} = -0.0895$ kcal. mole^{-1}

$\underline{A}$ (77.5°K) = 0.13862×10^7 Å

$\underline{A}$ (90.1°K) = 0.16276×10^7 Å

[a] Approximate 95% linear confidence limits.

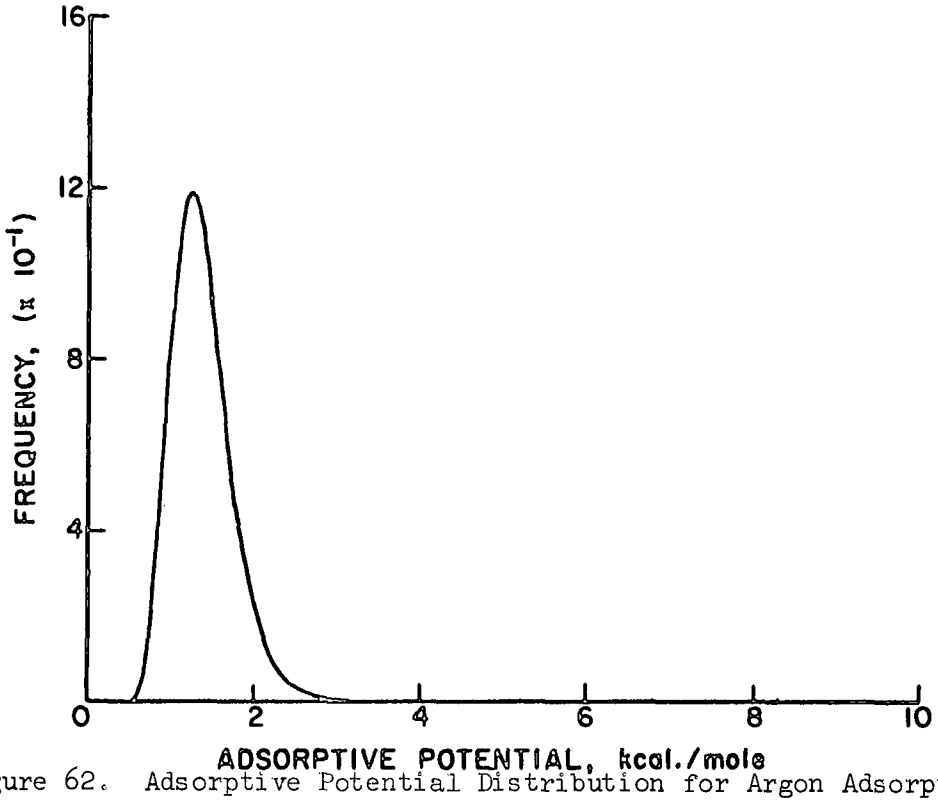

Figure 62. Adsorptive Potential Distribution for Argon Adsorption on Acid-Hydrolyzed Holocellulose at 77.5 and 90.1°K

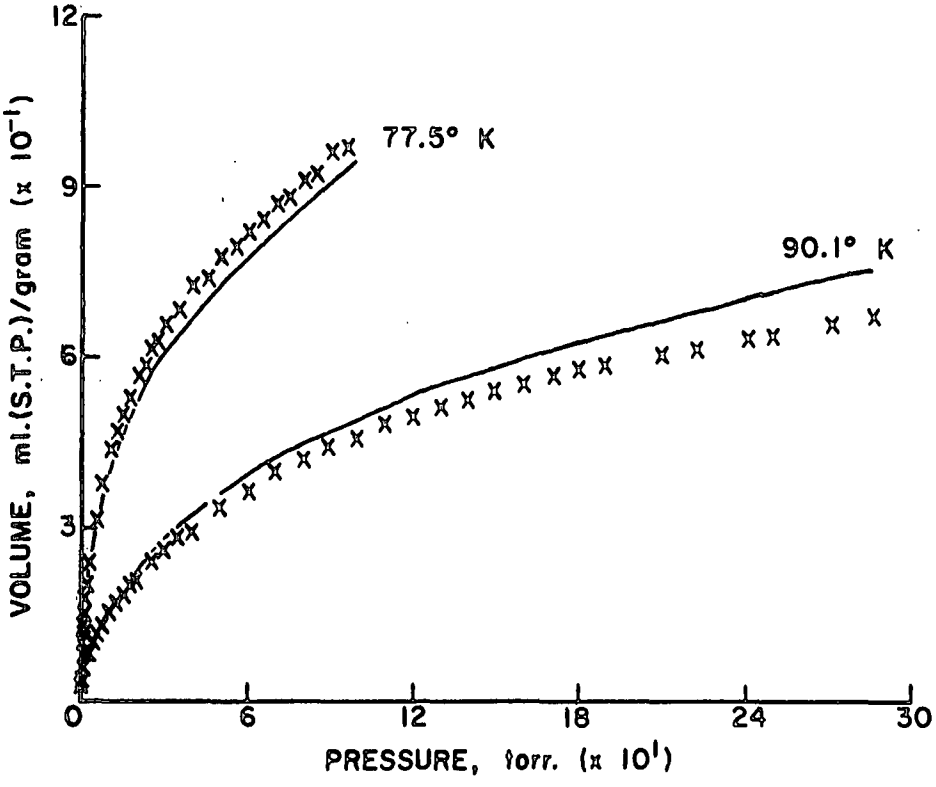

Figure 63. Multilayer Adsorption Model Fitted Simultaneously to the Argon Acid-Hydrolyzed Holocellulose Adsorption Data at 77.5 and 90.1°K

TABLE XLV

NITROGEN ADSORPTION DATA

Adsorbent: Holocellulose
Sample Mass: 0.50429 g.
Isotherm Temperature: 77.5°K

Equilibrium[a] Pressure, torr.	Apparent Mass Adsorbed, μg.	Corrected[b] Mass Adsorbed, μg.	Specific[c] Volume Adsorbed, ml. (S.T.P.)/g.
	1st Experimental Run		
0.125	-32.0	29.6	0.0470
0.521	-30.0	46.3	0.0733
1.033	-29.0	54.6	0.0866
2.496	-30.0	58.9	0.0934
5.021	-26.0	65.3	0.1035
9.999	-23.0	82.6	0.1309
20.090	-29.0	86.5	0.1371
30.070	-36.0	91.7	0.1454
39.961	-45.0	95.5	0.1514
49.824	-56.0	97.8	0.1551
59.821	-70.0	94.9	0.1505
70.999	-82.0	94.0	0.1490
79.661	-89.0	97.9	0.1552
89.784	-103.5	97.4	0.1544
99.450	-119.0	93.2	0.1477
119.486	-137.0	97.8	0.1551
139.320	-162.0	97.2	0.1540
159.378	-188.0	96.9	0.1536
	2nd Experimental Run		
0.110	-32.0	27.1	0.0430
0.645	-32.0	47.2	0.0748
1.529	-33.0	51.5	0.0817
2.983	-30.0	60.4	0.0957
5.980	-24.0	69.8	0.1106
11.992	-26.0	83.1	0.1317
21.972	-28.0	89.3	0.1416
32.004	-33.0	97.8	0.1551
42.146	-44.0	99.4	0.1576
51.878	-58.0	98.2	0.1557
62.184	-73.0	93.0	0.1475
71.770	-81.0	95.9	0.1521
81.603	-91.0	99.6	0.1579
91.530	-104.0	99.0	0.1569
101.581	-118.0	95.8	0.1519
121.383	-138.0	99.5	0.1577
141.513	-168.0	93.1	0.1476
161.597	-195.0	93.8	0.1487

[a] Pressure corrected for thermal transpiration.
[b] Data corrected for buoyancy and thermomolecular flow effect.
[c] Specific volume adsorbed calculated as volume adsorbed per gram of adsorbent.

TABLE XLVI

RESULTS OF FITTING MULTILAYER ADSORPTION MODEL TO EXPERIMENTAL DATA

Adsorbent: Holocellulose
Adsorbate: Nitrogen
Temperature: 77.5°K

Model Parameters

$\underline{U}^{Median} = 1.81 \pm 19.1^{a}$ kcal. mole^{-1}

$\underline{U}^{Mean} = 1.94$ kcal. mole^{-1}

$\underline{U}^{Mode} = 1.57$ kcal. mole^{-1}

$\gamma = 3.5 \pm 54.1$

$\underline{V}_{\beta} = 0.25 \pm 0.37$ ml. (S.T.P.) g.$^{-1}$

$\nu = 1.38 \pm 340.17 \times 10^{12}$ sec.$^{-1}$

$2\alpha/\beta$ (Ideal) $= 0.849$ kcal. mole^{-1}

$\alpha = 45.0 \times 10^{-30}$ erg cm.^{2} molecule^{-2}

$\beta = 17.1$ A.^{2} molecule^{-1}

Fraction of Nitrogen Molecules in Flat Position = 1.0

Thermodynamic Data

$\Delta\underline{S}^{tr} = -0.0099$ kcal. mole^{-1} deg.$^{-1}$

$\Delta\underline{S}^{rot} = -0.0054$ kcal. mole^{-1} deg.$^{-1}$

$\Delta\underline{S}^{vib} = 0.0047$ kcal. mole^{-1} deg.$^{-1}$

$\Delta\underline{E}^{kin} = 0.1540$ kcal. mole^{-1}

$\underline{A} = 0.36171 \times 10^{7}$ A°

---

[a] Approximate 95% linear confidence limits.

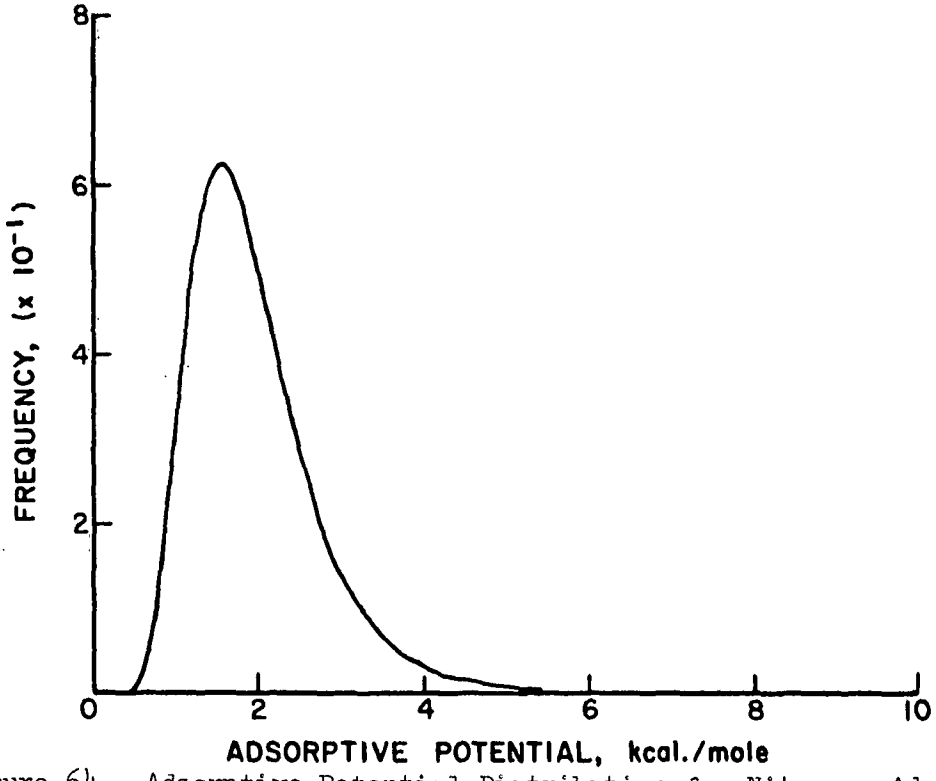

Figure 64. Adsorptive Potential Distribution for Nitrogen Adsorption on Holocellulose at 77.5°K

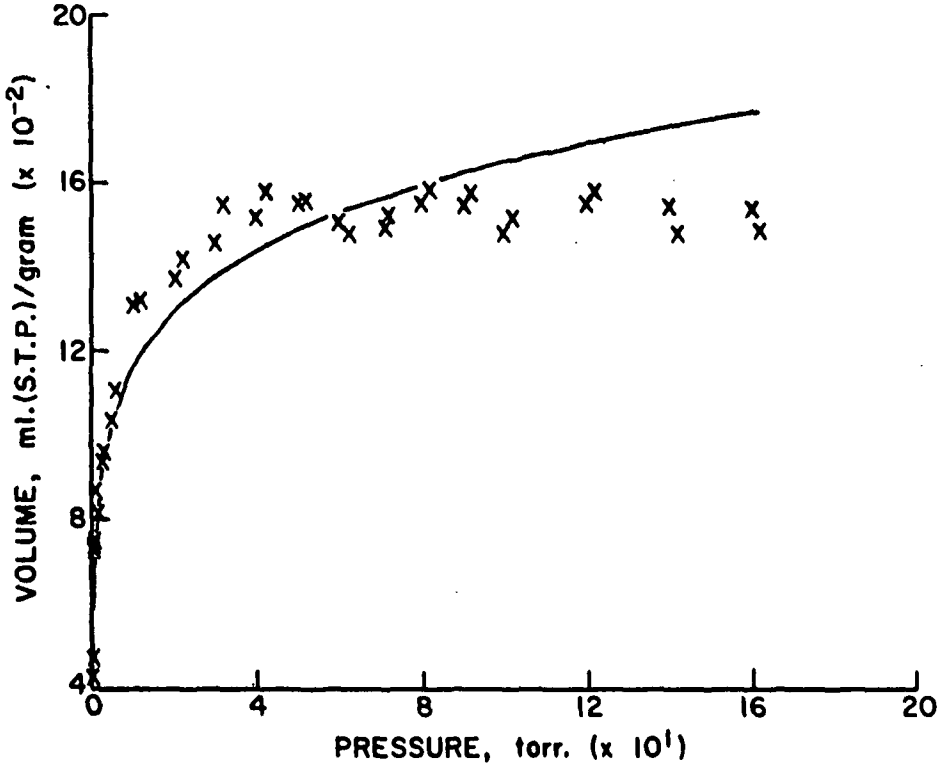

Figure 65. Multilayer Adsorption Model Fitted to the Nitrogen Holocellulose Adsorption Data at 77.5°K

TABLE XLVII

RESULTS OF FITTING MULTILAYER ADSORPTION MODEL TO EXPERIMENTAL DATA WITH VIBRATIONAL FREQUENCY ELIMINATED AS AN UNKNOWN PARAMETER

Adsorbent: Holocellulose
Adsorbate: Nitrogen
Temperature: 77.5°K

Model Parameters

$\underline{U}^{Median} = 1.81 \pm 1.10^{a}$ kcal. mole^{-1}

$\underline{U}^{Mean} = 1.94$ kcal. mole^{-1}

$\underline{U}^{Mode} = 1.57$ kcal. mole^{-1}

$\gamma = 3.5 \pm 8.3$

$\underline{V}_{\beta} = 0.25 \pm 0.88$ ml. (S.T.P.) g.$^{-1}$

$\nu = 2.56 \times 10^{12}$ sec.$^{-1}$ (Calculated from the median adsorptive potential)

$2\alpha/\beta$ (Ideal) $= 0.849$ kcal. mole^{-1}

$\alpha = 45.0 \pm 71.6 \times 10^{-30}$ erg cm.^{2} molecule^{-2}

$\beta = 17.1$ A.^{2} molecule^{-1}

Thermodynamic Data

$\Delta\underline{S}_{\underline{s}}^{tr} = -0.0099$ kcal. mole^{-1} deg.$^{-1}$

$\Delta\underline{S}^{rot} = -0.0054$ kcal. mole^{-1} deg.$^{-1}$

$\Delta\underline{S}^{vib} = 0.0019$ kcal. mole^{-1} deg.$^{-1}$

$\Delta\underline{E}^{kin} = 0.1540$ kcal. mole^{-1}

$\underline{\overset{\circ}{A}} = 0.81468 \times 10^{7}$

---

[a] Approximate 95% linear confidence limits.

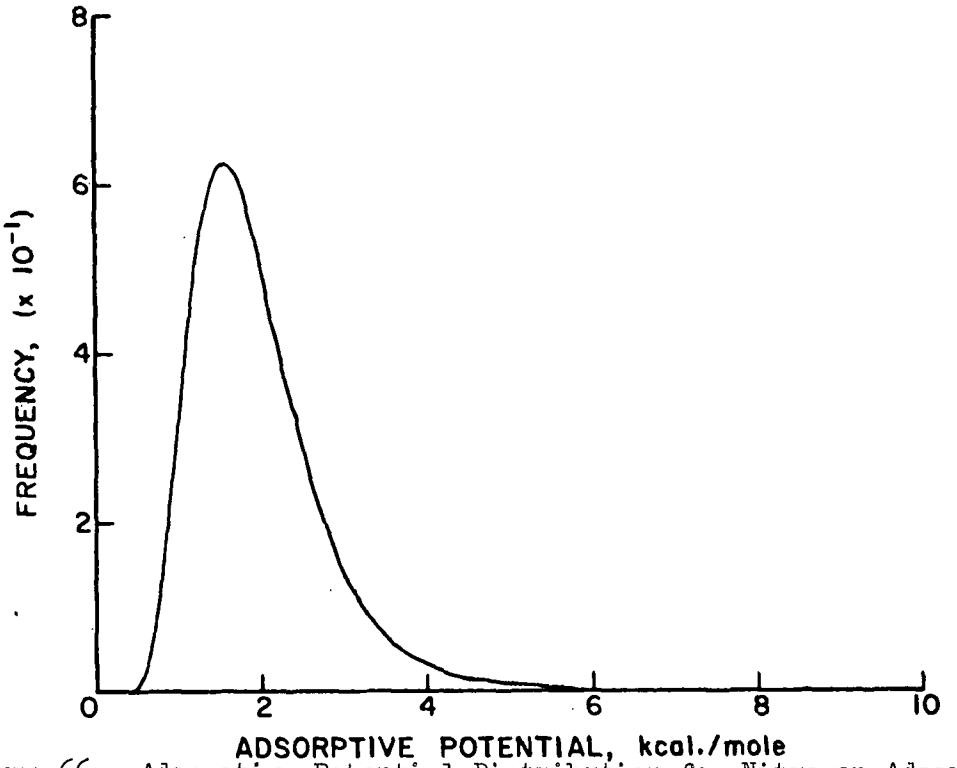

Figure 66. Adsorptive Potential Distribution for Nitrogen Adsorption on Holocellulose at 77.5°K

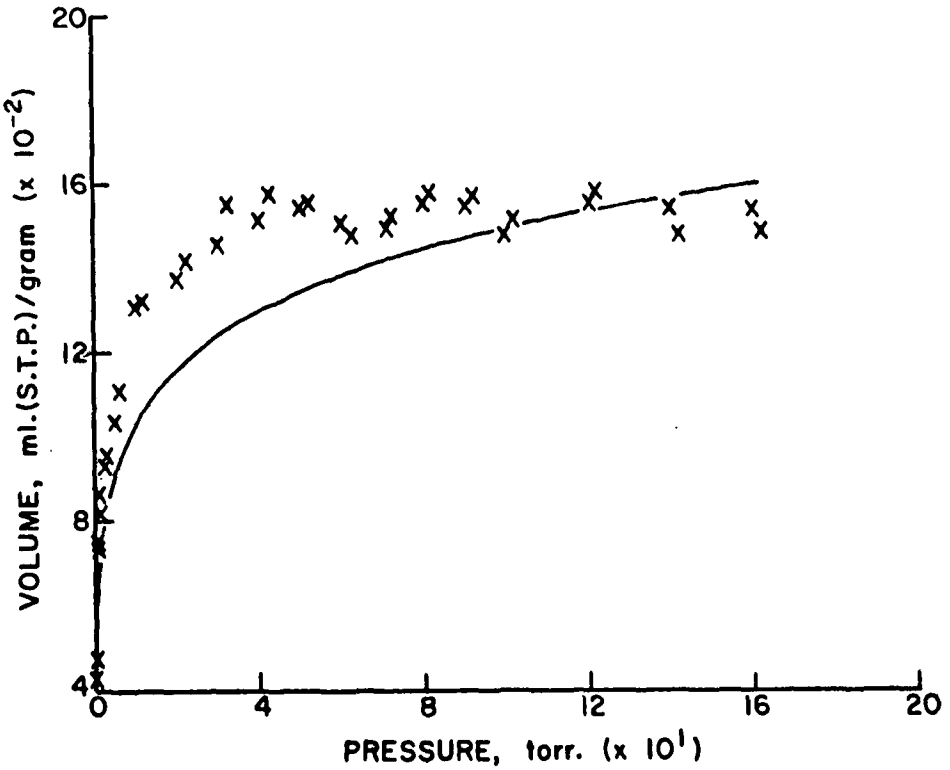

Figure 67. Multilayer Adsorption Model Fitted to the Nitrogen Holocellulose Adsorption Data at 77.5°K with the Vibrational Frequency Eliminated as an Unknown Parameter

TABLE XLVIII

NITROGEN ADSORPTION DATA

Adsorbent: Alkali-Extracted Holocellulose
Sample Mass: 0.50231 g.
Isotherm Temperature: 77.5°K

Equilibrium[a] Pressure, torr.	Apparent Mass Adsorbed, μg.	Corrected[b] Mass Adsorbed, μg.	Specific[c] Volume Adsorbed, ml. (S.T.P.)/g.
		1st Experimental Run	
0.124	-55.0	6.5	0.0103
0.539	-58.0	18.8	0.0299
1.168	-57.0	25.2	0.0402
2.167	-54.0	33.9	0.0539
4.987	-48.0	43.6	0.0694
10.132	-40.0	66.6	0.1060
20.036	-37.0	79.9	0.1272
39.974	-50.0	93.3	0.1486
59.869	-65.0	104.1	0.1658
79.658	-81.0	111.4	0.1774
99.431	-103.0	116.1	0.1848
119.664	-124.0	119.4	0.1901
139.560	-145.0	124.2	0.1977
159.578	-171.0	125.3	0.1994
179.438	-194.0	132.8	0.2115
		2nd Experimental Run	
0.133	-54.0	8.7	0.0139
0.302	-60.5	6.3	0.0100
0.754	-60.0	21.2	0.0338
1.540	-58.0	26.7	0.0425
3.094	-54.0	36.9	0.0587
7.073	-47.5	51.0	0.0812
12.898	-44.0	67.1	0.1069
20.160	-44.0	72.9	0.1161
30.270	-48.5	81.6	0.1299
49.812	-61.0	96.3	0.1532
69.789	-78.0	101.5	0.1615
89.997	-101.0	106.4	0.1694
109.968	-122.0	109.1	0.1737
129.104	-143.0	112.9	0.1797
149.720	-163.0	119.0	0.1894
169.432	-185.0	126.9	0.2020
189.929	-208.0	134.4	0.2139

[a] Pressure corrected for thermal transpiration.
[b] Data corrected for buoyancy and thermomolecular flow effect.
[c] Specific volume adsorbed calculated as volume adsorbed per gram of adsorbent.

TABLE XLIX

RESULTS OF FITTING MULTILAYER ADSORPTION MODEL TO EXPERIMENTAL DATA

Adsorbent: Alkali-Extracted Holocellulose
Adsorbate: Nitrogen
Temperature: 77.5°K

Model Parameters

$\underline{U}^{Median} = 1.40 \pm 0.34^{a}$ kcal. mole^{-1}

$\underline{U}^{Mean} = 1.46$ kcal. mole^{-1}

$\underline{U}^{Mode} = 1.28$ kcal. mole^{-1}

$\gamma = 5.7 \pm 2.6$

$\underline{V}_{\beta} = 0.33 \pm 0.24$ ml. (S.T.P.) g.$^{-1}$

$\nu = 0.78 \pm 2.35 \times 10^{12}$ sec.$^{-1}$

$2\alpha/\beta$ (Ideal) $= 0.849$ kcal. mole^{-1}

$\alpha = 45.245 \times 10^{-30}$ erg cm.^{2} molecule^{-2}

$\beta = 16.943$ A.^{2} molecule^{-1}

Fraction of Nitrogen Molecules in Flat Position = 0.9673

Thermodynamic Data

$\Delta\underline{S}^{tr} = -0.0099$ kcal. mole^{-1} deg.$^{-1}$

$\Delta\underline{S}^{rot} = -0.0052$ kcal. mole^{-1} deg.$^{-1}$

$\Delta\underline{S}^{vib} = 0.0068$ kcal. mole^{-1} deg.$^{-1}$

$\Delta\underline{E}^{kin} = 0.1515$ kcal. mole^{-1}

$\underline{A}^{\circ} = 0.15645 \times 10^{7}$

---

[a] Approximate 95% linear confidence limits.

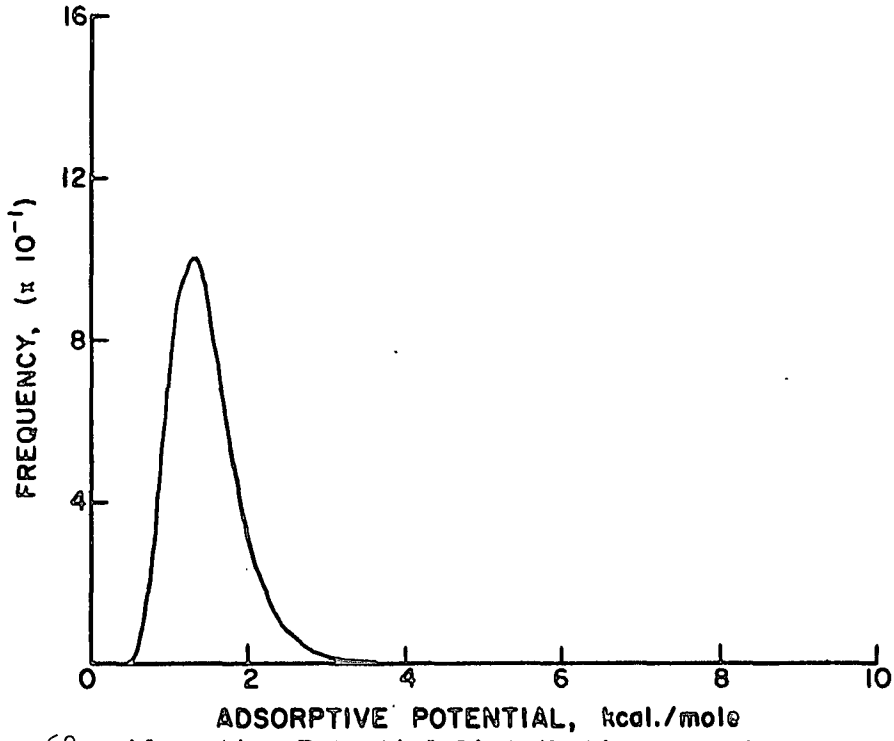

Figure 68. Adsorptive Potential Distribution for Nitrogen Adsorption on Alkali-Extracted Holocellulose at 77.5°K

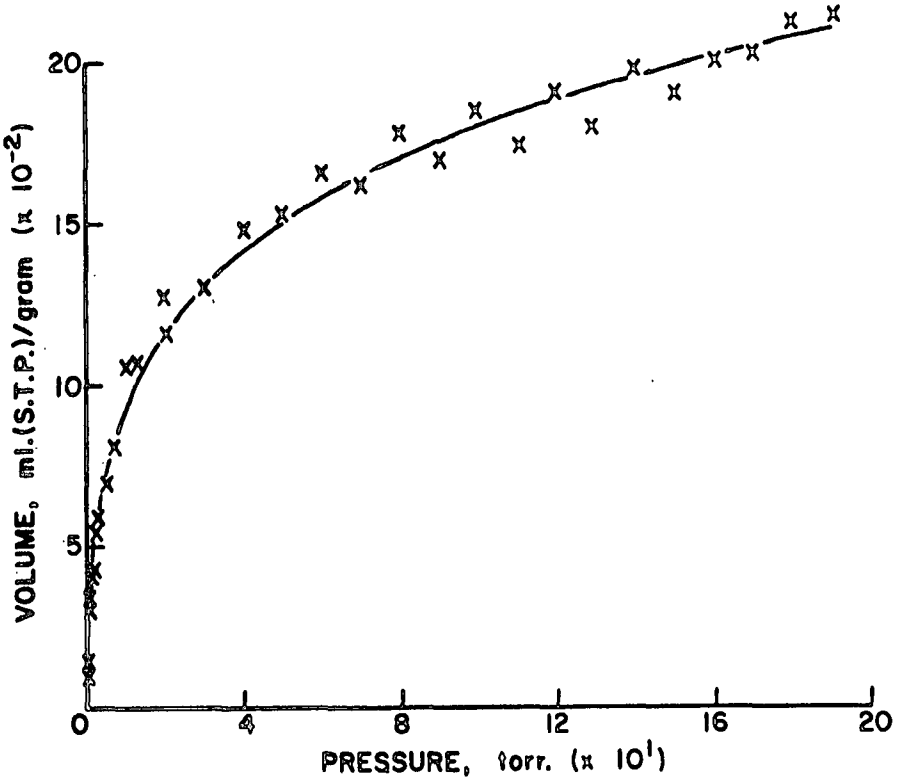

Figure 69. Multilayer Adsorption Model Fitted to the Nitrogen Alkali-Extracted Holocellulose Adsorption Data at 77.5°K

TABLE L

RESULTS OF FITTING MULTILAYER ADSORPTION MODEL TO EXPERIMENTAL DATA WITH VIBRATIONAL FREQUENCY ELIMINATED AS AN UNKNOWN PARAMETER

Adsorbent: Alkali-Extracted Holocellulose
Adsorbate: Nitrogen
Temperature: 77.5°K

Model Parameters

$\underline{U}^{Median} = 1.56 \pm 0.06$[a] kcal. mole^{-1}

$\underline{U}^{Mean} = 1.60$ kcal. mole^{-1}

$\underline{U}^{Mode} = 1.47$ kcal. mole^{-1}

$\gamma = 9.4 \pm 4.0$

$\underline{V}_{\beta} = 0.25 \pm 0.06$ ml. (S.T.P.) g.$^{-1}$

$\nu = 2.38 \times 10^{12}$ sec.$^{-1}$ (Calculated from the median adsorptive potential)

$2\alpha/\beta$ (Ideal) $= 0.849$ kcal. mole^{-1}

$\alpha = 49.3 \pm 1.2 \times 10^{-30}$ erg cm.^{2} molecule^{-2}

$\beta = 14.4$ A.^{2} molecule^{-1}

Thermodynamic Data

$\Delta\underline{S}^{tr} = -0.0099$ kcal. mole^{-1} deg.$^{-1}$

$\Delta\underline{S}^{rot} = -0.0023$ kcal. mole^{-1} deg.$^{-1}$

$\Delta\underline{S}^{vib} = 0.0020$ kcal. mole^{-1} deg.$^{-1}$

$\Delta\underline{E}^{kin} = 0.1100$ kcal. mole^{-1}

$\underline{A} = 0.25617 \times 10^{7}$ A.^{o}

---

[a] Approximate 95% linear confidence limits.

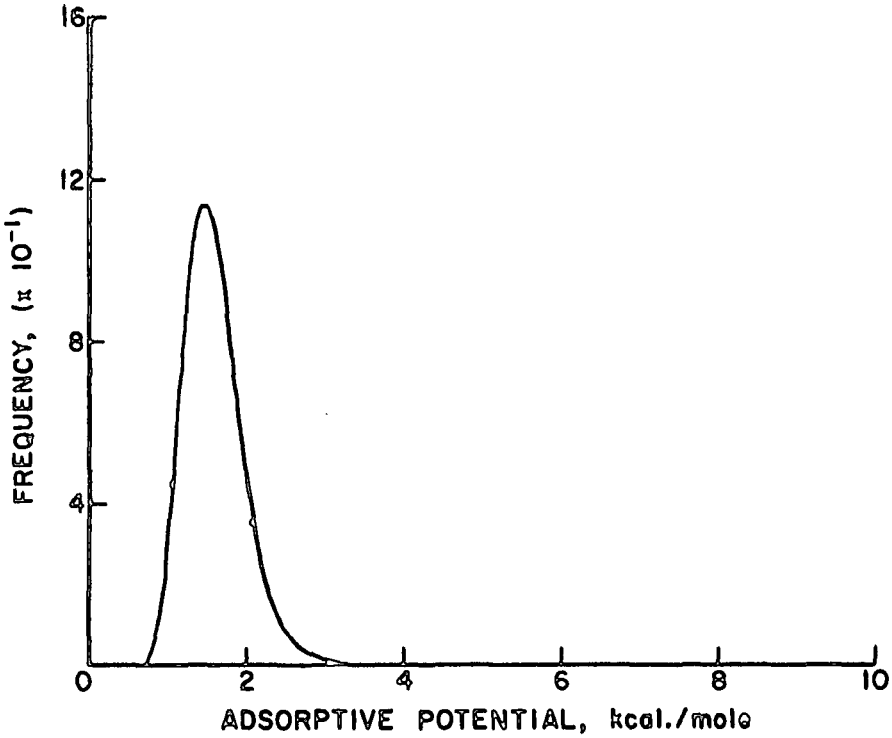

Figure 70. Adsorptive Potential Distribution for Nitrogen Adsorption on Alkali-Extracted Holocellulose at 77.5°K

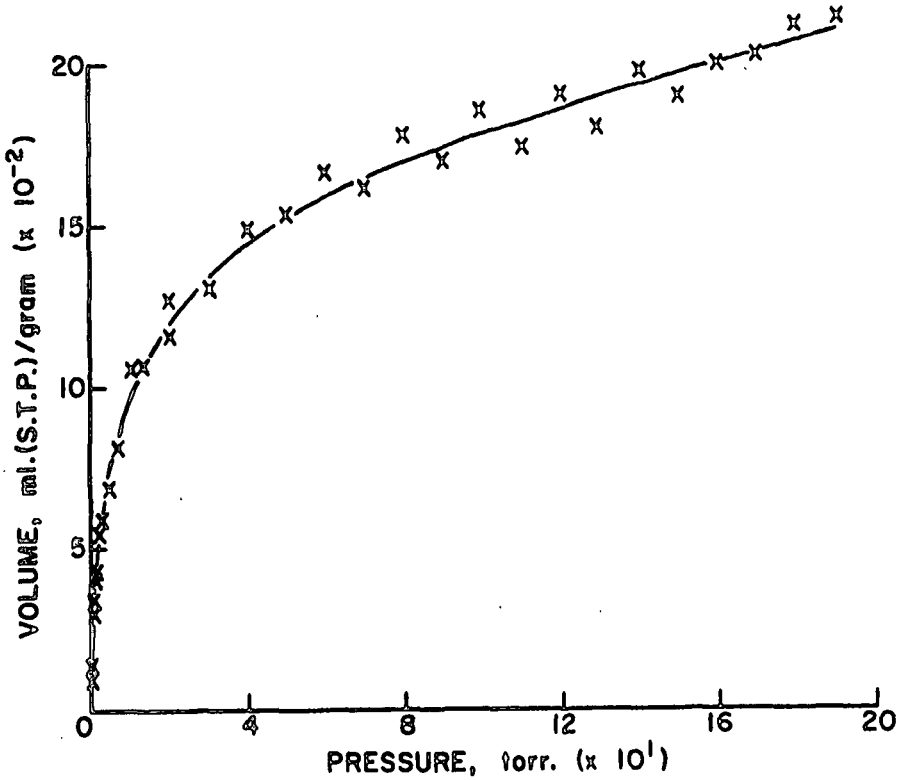

Figure 71. Multilayer Adsorption Model Fitted to the Nitrogen Alkali-Extracted Holocellulose Adsorption Data at 77.5°K with the Vibrational Frequency Eliminated as an Unknown Parameter

TABLE LI

NITROGEN ADSORPTION DATA

Adsorbent: Acid-Hydrolyzed Holocellulose
Sample Mass: 0.50354 g.
Isotherm Temperature: 77.5°K

Equilibrium[a] Pressure, torr.	Apparent Mass Adsorbed, µg.	Corrected[b] Mass Adsorbed, µg.	Specific[c] Volume Adsorbed, ml. (S.T.P.)/g.
	1st Experimental Run		
0.068	-23.0	27.7	0.0440
0.167	-14.5	51.2	0.0812
0.307	-3.0	63.6	0.1009
0.606	14.0	92.3	0.1464
1.014	30.0	113.4	0.1799
1.509	45.0	129.2	0.2050
2.547	67.5	156.2	0.2479
5.000	102.5	193.2	0.3064
10.074	143.5	248.0	0.3934
20.017	182.0	295.0	0.4680
30.178	200.0	324.2	0.5143
40.334	212.0	348.1	0.5522
59.801	220.0	377.6	0.5990
79.633	219.5	396.6	0.6292
100.103	216.0	415.9	0.6598
120.452	208.5	430.1	0.6823
139.614	202.5	444.9	0.7058
160.050	190.0	457.0	0.7250
180.346	176.0	469.6	0.7449
	2nd Experimental Run		
0.060	-27.0	21.8	0.0347
0.103	-22.0	35.9	0.0570
0.254	-7.0	60.7	0.0963
0.626	15.0	93.7	0.1486
1.130	35.0	118.2	0.1875
2.028	57.5	144.4	0.2290
7.000	123.0	220.0	0.3489
12.645	158.0	266.4	0.4226
18.111	179.0	291.2	0.4620
25.125	197.0	314.8	0.4993
34.891	209.0	338.7	0.5373
49.839	221.0	368.7	0.5850
70.014	227.0	393.3	0.6239
89.798	224.5	414.4	0.6575
109.960	221.0	431.0	0.6837
130.919	212.0	445.0	0.7060
149.862	202.0	455.4	0.7225
170.020	191.0	471.1	0.7474
189.242	174.0	479.0	0.7599

[a] Pressure corrected for thermal transpiration.
[b] Data corrected for buoyancy and thermomolecular flow effect.
[c] Specific volume adsorbed calculated as volume adsorbed per gram of adsorbent.

TABLE LII

RESULTS OF FITTING MULTILAYER ADSORPTION MODEL TO EXPERIMENTAL DATA

Adsorbent: Acid-Hydrolyzed Holocellulose
Adsorbate: Nitrogen
Temperature: 77.5°K

Model Parameters

$\underline{U}^{Median} = 1.56 \pm 0.41^{a}$ kcal. mole^{-1}

$\underline{U}^{Mean} = 1.62$ kcal. mole^{-1}

$\underline{U}^{Mode} = 1.43$ kcal. mole^{-1}

$\gamma = 5.8 \pm 1.73$

$\underline{V}_{\beta} = 1.18 \pm 0.38$ ml. (S.T.P.) g.$^{-1}$

$\nu = 1.19 \pm 3.26 \times 10^{12}$ sec.$^{-1}$

$2\alpha/\beta$ (Ideal) $= 0.849$ kcal. mole^{-1}

$\alpha = 45.0 \times 10^{-30}$ erg cm.^{2} molecule^{-2}

$\beta = 17.1$ A.^{2} molecule^{-1}

Fraction of Nitrogen Molecules in Flat Position = 1.0

Thermodynamic Data

$\Delta\underline{S}_{s}^{tr} = -0.0099$ kcal. mole^{-1} deg.$^{-1}$

$\Delta\underline{S}^{rot} = -0.0054$ kcal. mole^{-1} deg.$^{-1}$

$\Delta\underline{S}^{vib} = 0.0053$ kcal. mole^{-1} deg.$^{-1}$

$\Delta\underline{E}^{kin} = 0.1540$ kcal. mole^{-1}

$\underline{A}^{\circ} = 0.29937 \times 10^{7}$

---

[a] Approximate 95% linear confidence limits.

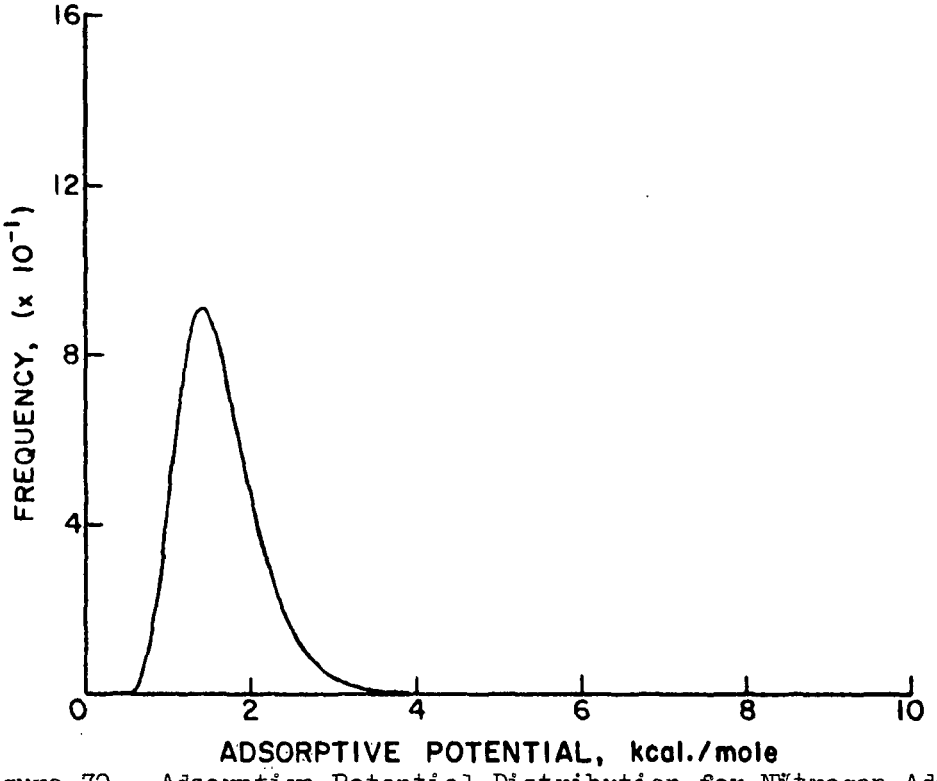

Figure 72. Adsorptive Potential Distribution for Nitrogen Adsorption on Acid-Hydrolyzed Holocellulose at 77.5°K

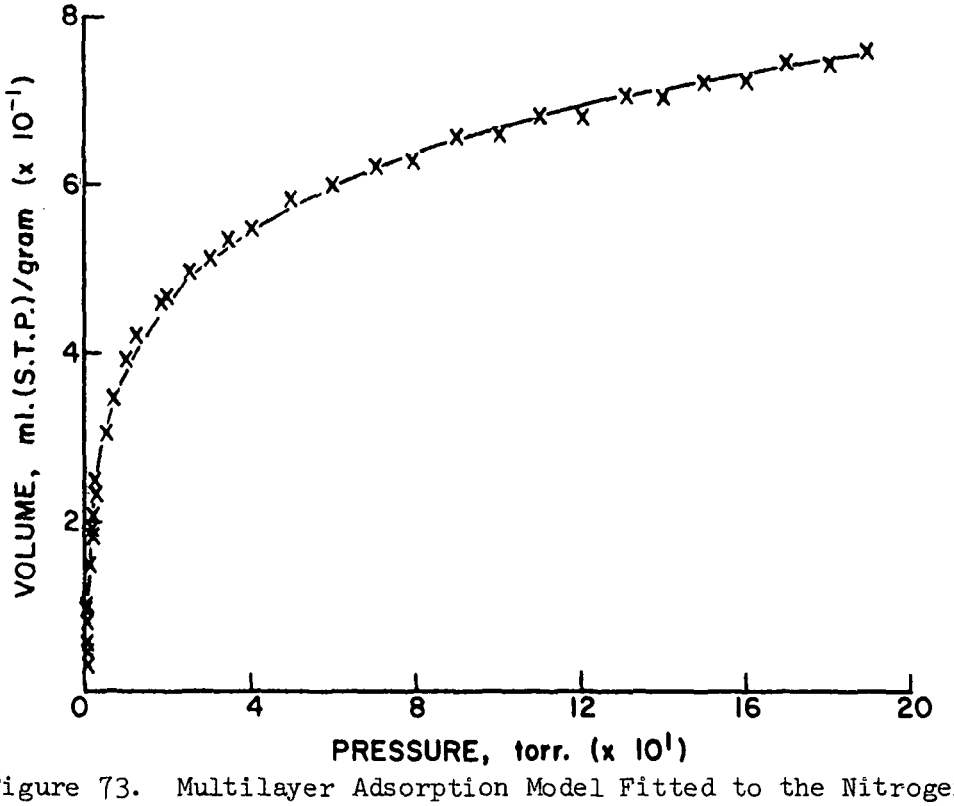

Figure 73. Multilayer Adsorption Model Fitted to the Nitrogen Acid-Hydrolyzed Holocellulose Adsorption Data at 77.5°K

TABLE LIII

RESULTS OF FITTING MULTILAYER ADSORPTION MODEL TO EXPERIMENTAL DATA WITH VIBRATIONAL FREQUENCY ELIMINATED AS AN UNKNOWN PARAMETER

Adsorbent: Acid-Hydrolyzed Holocellulose
Adsorbate: Nitrogen
Temperature: 77.5°K

Model Parameters

$\underline{U}^{Median} = 1.65 \pm 0.05^{a}$ kcal. mole^{-1}

$\underline{U}^{Mean} = 1.71$ kcal. mole^{-1}

$\underline{U}^{Mode} = 1.54$ kcal. mole^{-1}

$\gamma = 7.4 \pm 0.8$

$\underline{V}_{\beta} = 1.02 \pm 0.13$ ml. (S.T.P.) g.$^{-1}$

$\nu = 2.45 \times 10^{12}$ sec.$^{-1}$ (Calculated from the median adsorptive potential)

$2\alpha/\beta$ (Ideal) $= 0.849$ kcal. mole^{-1}

$\alpha = 47.3 \pm 2.2 \times 10^{-30}$ erg cm.^{2} molecule^{-2}

$\beta = 15.6$ A.^{2} molecule^{-1}

Thermodynamic Data

$\Delta\underline{S}^{tr} = -0.0099$ kcal. mole^{-1} deg.$^{-1}$

$\Delta\underline{S}^{rot} = -0.0037$ kcal. mole^{-1} deg.$^{-1}$

$\Delta\underline{S}^{vib} = 0.0023$ kcal. mole^{-1} deg.$^{-1}$

$\Delta\underline{E}^{kin} = 0.1298$ kcal. mole^{-1}

$\underline{A} = 0.39730 \times 10^{7}$ Å

[a] Approximate 95% linear confidence limits.

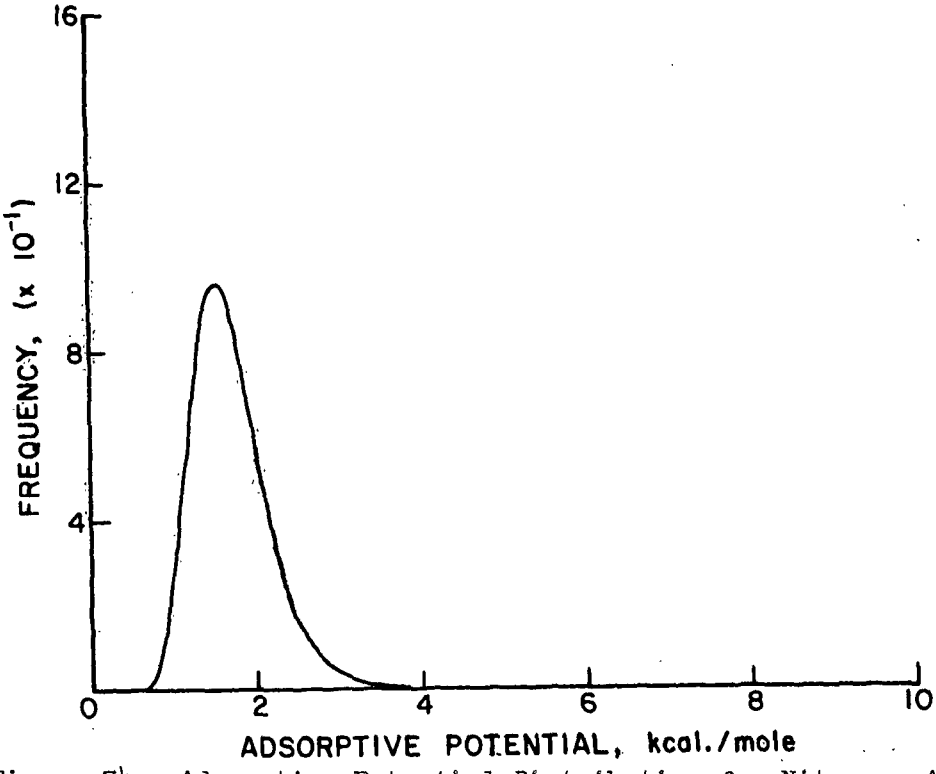

Figure 74. Adsorptive Potential Distribution for Nitrogen Adsorption on Acid-Hydrolyzed Holocellulose at 77.5°K

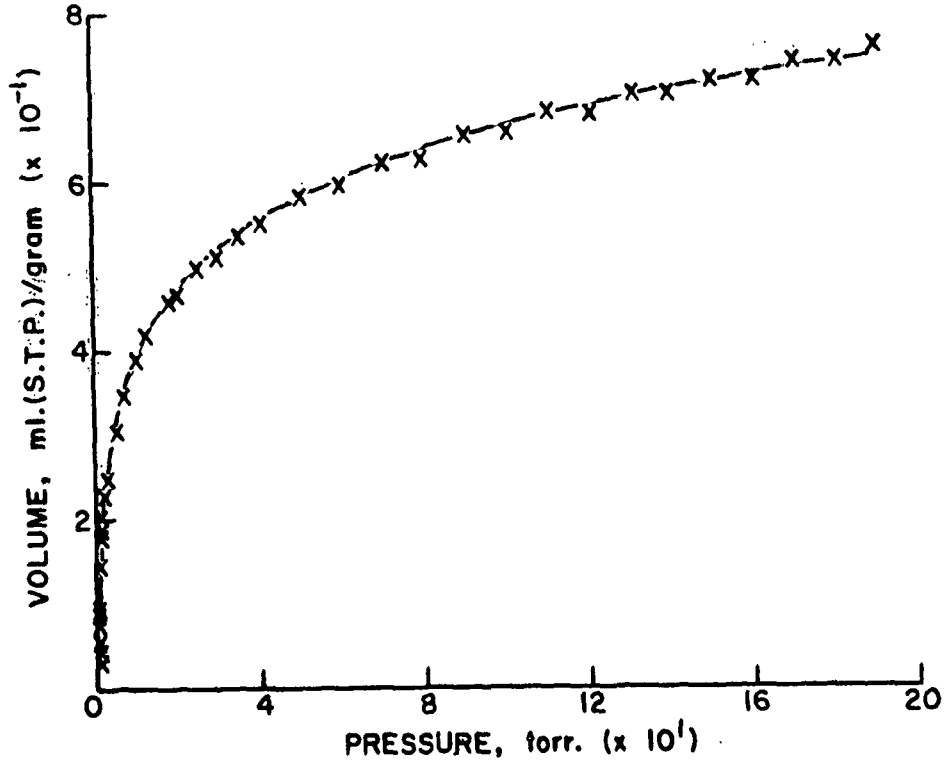

Figure 75. Multilayer Adsorption Model Fitted to the Nitrogen Acid-Hydrolyzed Holocellulose Adsorption Data at 77.5°K with the Vibrational Frequency Eliminated as an Unknown Parameter

TABLE LIV

$CFCl_3$ ADSORPTION DATA

Adsorbent: Holocellulose
Sample Mass: 0.50453 g.
Isotherm Temperature: 258.15°K

Equilibrium[a] Pressure, torr.	Apparent Mass Adsorbed, μg.	Corrected[b] Mass Adsorbed, μg.	Specific[c] Volume Adsorbed, ml. (S.T.P.)/g.
	1st Experimental Run		
0.062	-22.0	8.9	0.0029
0.226	-22.0	18.3	0.0059
0.622	-24.5	21.0	0.0068
1.220	-25.0	24.6	0.0079
2.506	-24.0	28.8	0.0093
5.051	-22.0	37.6	0.0122
7.491	-19.0	45.4	0.0147
12.466	-12.0	59.4	0.0192
17.574	-3.0	78.1	0.0252
22.076	3.0	92.7	0.0300
27.608	9.5	108.1	0.0349
32.030	15.0	120.9	0.0391
37.566	22.0	136.8	0.0442
42.147	22.0	144.4	0.0467
47.248	27.0	157.2	0.0508
54.717	35.0	181.9	0.0588
64.377	46.0	215.0	0.0695
74.513	62.0	257.2	0.0831
	2nd Experimental Run		
0.122	-23.5	12.5	0.0040
0.522	-31.0	13.2	0.0043
1.082	-32.5	16.1	0.0052
2.137	-33.5	18.5	0.0060
5.175	-30.0	30.0	0.0097
9.995	-22.0	45.3	0.0147
15.229	-13.0	63.5	0.0205
20.088	-6.0	80.2	0.0259
25.443	-1.0	94.0	0.0304
30.504	5.0	108.4	0.0350
34.826	11.0	121.4	0.0392
41.005	16.0	136.5	0.0441
44.699	20.0	146.6	0.0474
49.775	27.0	162.1	0.0524
59.665	35.0	193.4	0.0625
69.527	47.0	227.2	0.0734
79.695	60.0	271.0	0.0876
89.264	75.0	315.9	0.1021

[a] Pressure corrected for thermal transpiration.
[b] Data corrected for buoyancy and thermomolecular flow effect.
[c] Specific volume adsorbed calculated as volume adsorbed per gram of adsorbent.

TABLE LV

RESULTS OF FITTING MULTILAYER ADSORPTION MODEL TO EXPERIMENTAL DATA

Adsorbent: Holocellulose
Adsorbate: $CFCl_3$
Temperature: 258.15°K

Model Parameters

$\underline{U}^{Median} = 3.21 \pm 9.71^{a}$ kcal. mole^{-1}

$\underline{U}^{Mean} = 3.33$ kcal. mole^{-1}

$\underline{U}^{Mode} = 2.98$ kcal. mole^{-1}

$\gamma = 6.7 \pm 32.5$

$\underline{V}_{\beta} = 0.82 \pm 3.07$ ml. (S.T.P.) g.$^{-1}$

$\nu = 4.27 \pm 99.81 \times 10^{12}$ sec.$^{-1}$

$2\alpha/\beta$ (Ideal) $= 3.16$ kcal. mole^{-1}

$\alpha = 343.0 \times 10^{-30}$ erg cm.^{2} molecule^{-2}

$\beta = 31.2$ A.^{2} molecule^{-1}

Thermodynamic Data

$\Delta\underline{S}^{tr} = -0.0127$ kcal. mole^{-1} deg.$^{-1}$

$\Delta\underline{S}^{rot} = 0.0$ kcal. mole^{-1} deg.$^{-1}$

$\Delta\underline{S}^{vib} = 0.0025$ kcal. mole^{-1} deg.$^{-1}$

$\Delta\underline{E}^{kin} = -0.2565$ kcal. mole^{-1}

$\underline{A}^{o} = 0.49247 \times 10^{7}$

[a] Approximate 95% linear confidence limits.

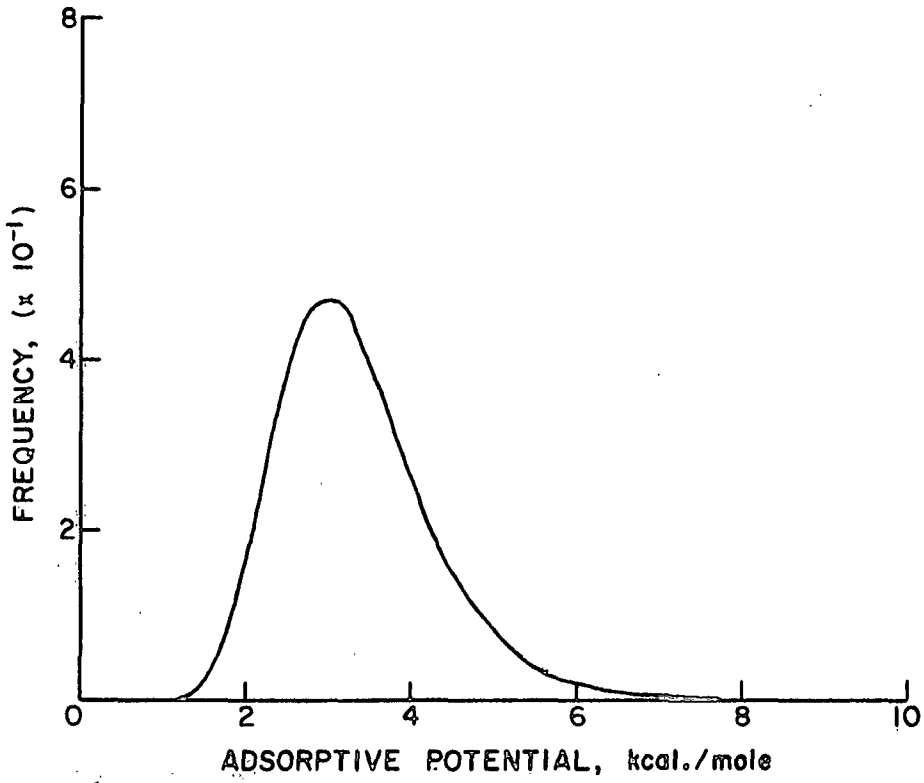

Figure 76. Adsorptive Potential Distribution for $CFCl_3$ Adsorption on Holocellulose at 258.15°K

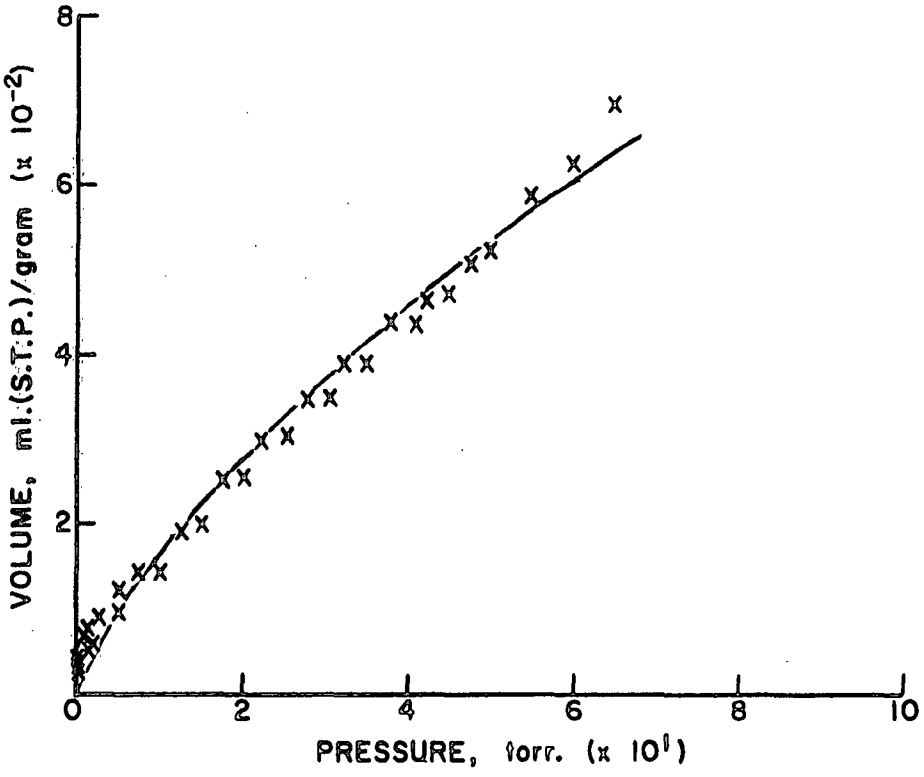

Figure 77. Multilayer Adsorption Model Fitted to the $CFCl_3$ Holocellulose Adsorption Data at 258.15°K

TABLE LVI

$CFCl_3$ ADSORPTION DATA

Adsorbent: Holocellulose
Sample Mass: 0.50442 g.
Isotherm Temperature: 268.15°K

Equilibrium[a] Pressure, torr.	Apparent Mass Adsorbed, μg.	Corrected[b] Mass Adsorbed, μg.	Specific[c] Volume Adsorbed, ml. (S.T.P.)/g.
	1st Experimental Run		
0.113	-18.0	14.3	0.0046
0.521	-22.0	16.2	0.0052
1.047	-22.0	20.3	0.0066
2.006	-21.5	25.1	0.0081
5.033	-21.0	31.6	0.0102
10.149	-20.0	44.6	0.0144
16.246	-19.0	55.5	0.0179
20.063	-21.0	57.8	0.0187
24.934	-20.5	65.0	0.0210
34.791	-16.5	84.5	0.0273
45.883	-15.5	103.9	0.0336
54.667	-16.0	118.1	0.0382
69.578	-18.0	143.8	0.0465
89.746	-22.0	180.6	0.0584
109.270	-24.0	224.0	0.0724
	2nd Experimental Run		
0.131	-22.0	11.4	0.0037
0.528	-24.0	14.1	0.0046
1.040	-25.0	17.3	0.0056
2.024	-23.5	23.1	0.0075
5.073	-22.0	30.6	0.0099
10.048	-19.0	45.4	0.0147
15.009	-18.0	54.7	0.0177
24.862	-13.5	71.9	0.0232
29.871	-15.0	78.2	0.0253
39.830	-14.0	95.5	0.0309
49.824	-11.0	114.8	0.0371
59.804	-16.0	127.3	0.0412
79.627	-21.0	160.6	0.0519
99.305	-25.0	199.1	0.0644
119.272	-32.0	240.4	0.0777
139.403	-35.0	290.3	0.0938

[a] Pressure corrected for thermal transpiration.
[b] Data corrected for buoyancy and thermomolecular flow effect.
[c] Specific volume adsorbed calculated as volume adsorbed per gram of adsorbent.

TABLE LVII

$CFCl_3$ ADSORPTION DATA

Adsorbent: Holocellulose
Sample Mass: 0.50436 g.
Isotherm Temperature: 278.15°K

Equilibrium[a] Pressure, torr.	Apparent Mass Adsorbed, μg.	Corrected[b] Mass Adsorbed, μg.	Specific[c] Volume Adsorbed, ml. (S.T.P.)/g.
	1st Experimental Run		
0.127	-23.0	11.4	0.0037
0.544	-25.0	15.1	0.0049
1.080	-27.5	16.6	0.0054
2.116	-27.0	20.6	0.0066
5.044	-31.0	22.8	0.0074
10.256	-34.0	29.9	0.0097
15.404	-37.0	34.7	0.0112
24.952	-39.0	44.4	0.0144
34.936	-41.5	58.5	0.0189
49.780	-46.5	77.3	0.0250
69.624	-60.0	97.4	0.0315
89.545	-79.0	115.5	0.0374
110.100	-96.5	139.5	0.0451
129.255	-116.0	157.2	0.0508
149.138	-135.0	186.2	0.0602
169.104	-153.0	214.6	0.0694
	2nd Experimental Run		
0.130	-22.0	12.4	0.0040
0.526	-25.0	15.1	0.0049
1.020	-23.0	20.8	0.0067
2.098	-22.0	25.5	0.0083
5.028	-25.0	28.8	0.0093
10.048	-25.0	38.5	0.0125
20.074	-30.0	46.0	0.0149
29.889	-31.0	60.9	0.0197
39.822	-33.0	74.7	0.0242
59.694	-45.0	95.4	0.0308
79.417	-60.0	115.3	0.0373
99.324	-79.0	134.9	0.0436
119.251	-99.0	155.0	0.0501
138.964	-120.0	176.1	0.0569
159.242	-141.0	203.9	0.0659

[a] Pressure corrected for thermal transpiration.
[b] Data corrected for buoyancy and thermomolecular flow effect.
[c] Specific volume adsorbed calculated as volume adsorbed per gram of adsorbent.

TABLE LVIII

$CFCl_3$ ADSORPTION DATA

Adsorbent: Holocellulose
Sample Mass: 0.50423 g.
Isotherm Temperature: 288.15°K

Equilibrium[a] Pressure, torr.	Apparent Mass Adsorbed, μg.	Corrected[b] Mass Adsorbed, μg.	Specific[c] Volume Adsorbed, ml. (S.T.P.)/g.
	1st Experimental Run		
0.116	-17.0	13.4	0.0044
0.518	-21.0	21.1	0.0068
1.023	-20.5	26.7	0.0086
2.059	-23.0	27.0	0.0088
5.087	-26.5	31.5	0.0102
10.006	-31.0	35.1	0.0114
14.951	-34.0	38.3	0.0124
19.937	-33.0	43.8	0.0142
24.914	-35.0	48.8	0.0158
34.804	-39.0	60.2	0.0195
45.082	-49.0	65.7	0.0212
54.759	-56.0	73.2	0.0237
64.485	-65.0	80.2	0.0259
79.404	-84.0	87.9	0.0284
99.467	-108.0	102.3	0.0331
119.337	-131.0	117.3	0.0379
139.494	-158.0	126.7	0.0410
159.523	-184.0	139.5	0.0451
179.252	-211.0	153.3	0.0496
	2nd Experimental Run		
0.126	-21.0	10.0	0.0032
0.530	-26.0	16.3	0.0053
1.103	-18.0	29.1	0.0094
2.129	-24.0	25.9	0.0084
5.187	-29.0	29.2	0.0094
9.977	-32.0	34.1	0.0110
15.182	-34.5	38.0	0.0123
20.065	-34.0	43.0	0.0139
29.922	-39.0	52.8	0.0171
39.868	-47.0	59.9	0.0194
49.872	-53.0	68.6	0.0222
69.470	-74.0	79.9	0.0258
89.654	-96.0	95.5	0.0309
109.220	-118.5	110.6	0.0358
129.184	-140.0	126.6	0.0410
149.236	-168.0	134.9	0.0436
169.314	-194.0	150.5	0.0487

[a] Pressure corrected for thermal transpiration.
[b] Data corrected for buoyancy and thermomolecular flow effect.
[c] Specific volume adsorbed calculated as volume adsorbed per gram of adsorbent.

TABLE LIX

$CFCl_3$ ADSORPTION DATA

Adsorbent: Holocellulose
Sample Mass: 0.50414 g.
Isotherm Temperature: 298.15°K

Equilibrium[a] Pressure, torr.	Apparent Mass Adsorbed, μg.	Corrected[b] Mass Adsorbed, μg.	Specific[c] Volume Adsorbed, ml. (S.T.P.)/g.
	1st Experimental Run		
0.285	-25.0	1.1	0.0003
0.603	-25.0	4.7	0.0015
1.366	-27.0	7.0	0.0023
2.487	-29.0	5.8	0.0019
4.962	-28.0	12.5	0.0040
9.998	-36.0	11.1	0.0036
14.907	-42.0	11.7	0.0038
19.833	-44.0	16.8	0.0054
29.837	-52.0	19.7	0.0064
39.729	-59.0	23.4	0.0076
49.679	-68.0	28.9	0.0094
60.182	-75.0	38.1	0.0123
69.353	-82.0	46.0	0.0149
79.329	-92.0	52.0	0.0168
89.240	-104.0	56.1	0.0181
99.234	-118.0	60.2	0.0195
119.005	-140.0	75.4	0.0244
139.024	-163.0	87.8	0.0284
159.025	-196.0	90.1	0.0292
178.956	-223.0	99.8	0.0323

[a] Pressure corrected for thermal transpiration.
[b] Data corrected for buoyancy and thermomolecular flow effect.
[c] Specific volume adsorbed calculated as volume adsorbed per gram of adsorbent.

TABLE LIX (Continued)

$CFCl_3$ ADSORPTION DATA

Adsorbent: Holocellulose
Sample Mass: 0.50414 g.
Isotherm Temperature: 298.15°K

Equilibrium[a] Pressure, torr.	Apparent Mass Adsorbed, μg.	Corrected[b] Mass Adsorbed, μg.	Specific[c] Volume Adsorbed, ml. (S.T.P.)/g.
		2nd Experimental Run	
0.168	-26.0	0.6	0.0002
0.515	-25.5	3.5	0.0011
1.005	-23.0	9.4	0.0030
2.050	-26.0	9.0	0.0029
5.030	-30.0	10.6	0.0034
10.031	-33.0	14.1	0.0046
14.873	-38.5	15.2	0.0049
19.893	-45.0	15.9	0.0051
25.124	-47.5	19.1	0.0062
34.990	-56.0	20.8	0.0067
44.747	-64.0	25.3	0.0082
54.535	-71.5	32.8	0.0106
67.300	-83.0	41.7	0.0135
74.638	-97.0	39.4	0.0128
84.183	-107.0	44.4	0.0144
94.420	-115.0	54.3	0.0176
113.984	-140.0	66.3	0.0214
134.191	-171.0	71.3	0.0230
154.137	-200.0	77.3	0.0250
174.096	-228.0	85.7	0.0277

[a] Pressure corrected for thermal transpiration.
[b] Data corrected for buoyancy and thermomolecular flow effect.
[c] Specific volume adsorbed calculated as volume adsorbed per gram of adsorbent.

TABLE LX

$CFCl_3$ ADSORPTION DATA

Adsorbent: Alkali-Extracted Holocellulose
Sample Mass: 0.50251 g.
Isotherm Temperature: 258.15°K

Equilibrium[a] Pressure, torr.	Apparent Mass Adsorbed, μg.	Corrected[b] Mass Adsorbed, μg.	Specific[c] Volume Adsorbed, ml.(S.T.P.)/g.
		1st Experimental Run	
0.032	-20.0	6.6	0.0022
0.083	-29.0	4.1	0.0013
0.161	-27.0	11.1	0.0036
0.330	-27.0	15.3	0.0050
0.785	-25.5	21.5	0.0070
1.494	-26.0	24.3	0.0079
3.067	-26.0	28.0	0.0091
7.812	-12.0	53.7	0.0174
12.593	6.0	78.9	0.0256
17.565	25.0	107.9	0.0350
22.824	44.0	137.3	0.0446
27.393	57.5	158.6	0.0514
35.840	81.0	196.7	0.0638
44.798	109.5	240.9	0.0782
54.591	138.0	289.2	0.0938
64.473	174.0	349.8	0.1135
74.519	212.0	414.9	0.1346
79.949	238.0	458.1	0.1486
		2nd Experimental Run	
0.032	-21.0	5.6	0.0018
0.099	-30.0	4.5	0.0015
0.261	-33.0	7.6	0.0025
0.526	-37.0	7.2	0.0024
1.034	-37.0	11.5	0.0037
2.114	-34.5	17.6	0.0057
5.066	-23.0	37.1	0.0120
10.184	-2.0	66.5	0.0216
15.083	16.0	93.7	0.0304
20.164	26.0	114.4	0.0371
29.751	60.5	165.7	0.0538
39.905	91.0	213.8	0.0694
50.077	116.5	257.3	0.0835
59.671	145.0	309.5	0.1004
69.822	179.0	367.2	0.1191

[a] Pressure corrected for thermal transpiration.
[b] Data corrected for buoyancy and thermomolecular flow effect.
[c] Specific volume adsorbed calculated as volume adsorbed per gram of adsorbent.

TABLE LXI

RESULTS OF FITTING MULTILAYER ADSORPTION MODEL TO EXPERIMENTAL DATA

Adsorbent: Alkali-Extracted Holocellulose
Adsorbate: $CFCl_3$
Temperature: 258.15°K

Model Parameters

$\underline{U}^{Median} = 3.03 \pm 9.60^{a}$ kcal. mole^{-1}

$\underline{U}^{Mean} = 3.13$ kcal. mole^{-1}

$\underline{U}^{Mode} = 2.85$ kcal. mole^{-1}

$\gamma = 8.1 \pm 41.6$

$\underline{V}_{\beta} = 1.80 \pm 9.35$ ml. (S.T.P.) g.$^{-1}$

$\nu = 2.49 \pm 45.36 \times 10^{12}$ sec.$^{-1}$

$2\alpha/\beta$ (Ideal) = 3.16 kcal. mole^{-1}

$\alpha = 343.0 \times 10^{-30}$ erg cm.^{2} molecule^{-2}

$\beta = 31.2$ A.^{2} molecule^{-1}

Thermodynamic Data

$\Delta\underline{S}^{tr} = -0.0127$ kcal. mole^{-1} deg.$^{-1}$

$\Delta\underline{S}^{rot} = 0.0$ kcal. mole^{-1} deg.$^{-1}$

$\Delta\underline{S}^{vib} = 0.0035$ kcal. mole^{-1} deg.$^{-1}$

$\Delta\underline{E}^{kin} = -0.2565$ kcal. mole^{-1}

$\underline{A}^{o} = 0.33370 \times 10^{7}$

---

[a] Approximate 95% linear confidence limits.

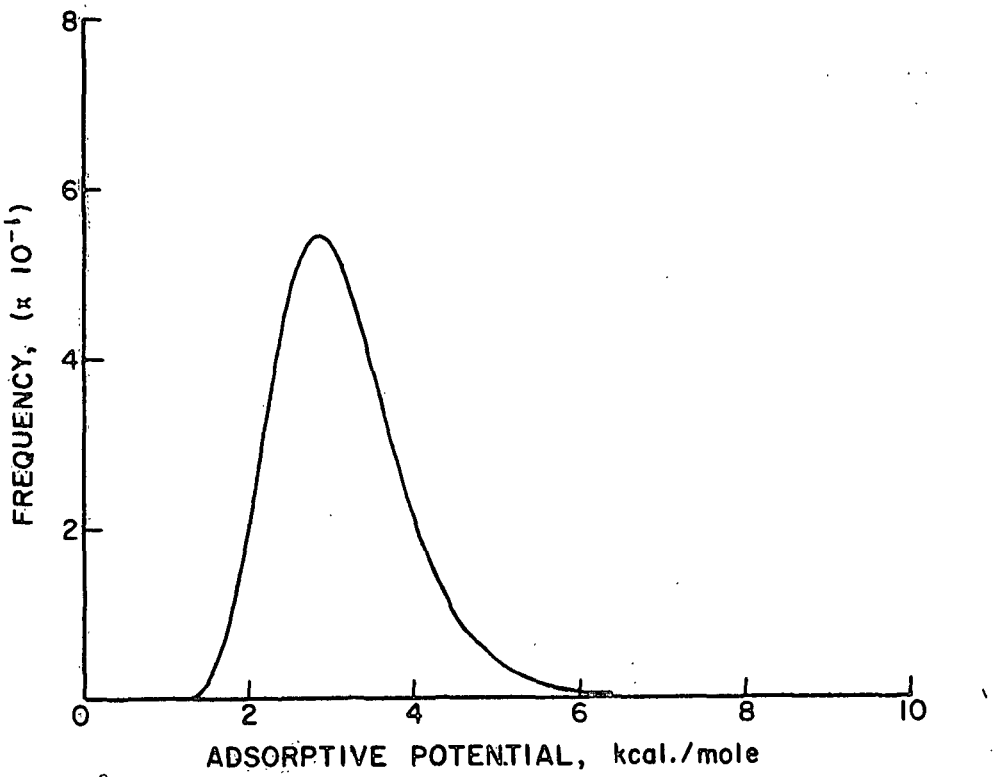

Figure 78. Adsorptive Potential Distribution for $CFCl_3$ Adsorption on Alkali-Extracted Holocellulose at 258.15°K

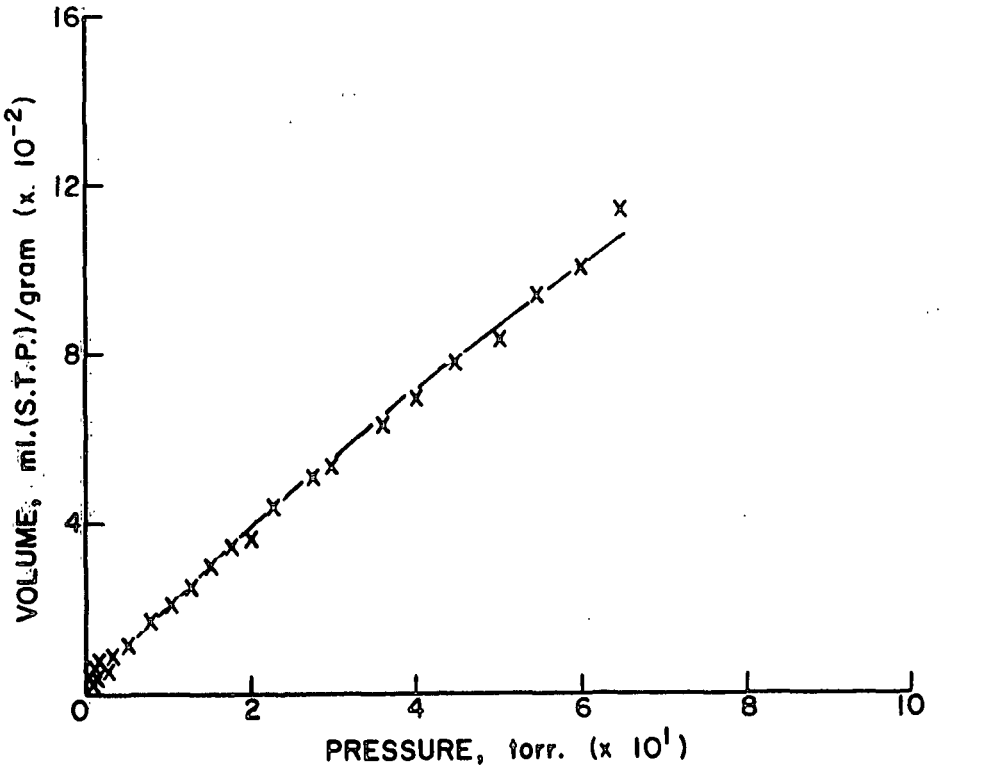

Figure 79. Multilayer Adsorption Model Fitted to the $CFCl_3$ Alkali-Extracted Holocellulose Adsorption Data at 258.15°K

TABLE LXII

$CFCl_3$ ADSORPTION DATA

Adsorbent: Alkali-Extracted Holocellulose
Sample Mass: 0.50261 g.
Isotherm Temperature: 268.15°K

Equilibrium[a] Pressure, torr.	Apparent Mass Adsorbed, μg.	Corrected[b] Mass Adsorbed, μg.	Specific[c] Volume Adsorbed, ml. (S.T.P.)/g.
	1st Experimental Run		
0.046	-20.0	2.3	0.0007
0.115	-23.0	9.4	0.0031
0.285	-25.0	10.5	0.0034
0.581	-26.0	12.0	0.0039
1.149	-27.0	16.3	0.0053
2.068	-26.0	21.0	0.0068
5.331	-20.0	33.4	0.0108
10.025	-11.0	54.6	0.0177
15.047	0.0	74.7	0.0242
19.873	7.5	88.6	0.0288
24.987	15.5	104.2	0.0338
30.087	24.0	121.2	0.0393
40.207	38.5	153.6	0.0498
50.105	50.0	182.5	0.0592
59.567	61.0	211.3	0.0685
79.952	79.0	271.3	0.0880
99.554	98.0	335.5	0.1088
119.655	125.0	412.8	0.1339
139.219	152.0	494.2	0.1603
159.889	218.0	637.1	0.2067

[a] Pressure corrected for thermal transpiration.
[b] Data corrected for buoyancy and thermomolecular flow effect.
[c] Specific volume adsorbed calculated as volume adsorbed per gram of adsorbent.

TABLE LXII (Continued)

$CFCl_3$ ADSORPTION DATA

Adsorbent: Alkali-Extracted Holocellulose
Sample Mass: 0.50261 g.
Isotherm Temperature: 268.15°K

Equilibrium[a] Pressure, torr.	Apparent Mass Adsorbed, μg.	Corrected[b] Mass Adsorbed, μg.	Specific[c] Volume Adsorbed, ml. (S.T.P.)/g.
	2nd Experimental Run		
0.039	-20.0	0.7	0.0002
0.090	-20.5	9.3	0.0030
0.195	-23.0	12.7	0.0041
0.420	-24.5	13.5	0.0044
0.915	-25.5	15.9	0.0052
1.525	-26.0	19.2	0.0062
3.040	-25.0	24.7	0.0080
7.457	-18.0	41.0	0.0133
12.423	-9.0	61.3	0.0199
17.401	0.0	78.1	0.0253
22.464	9.0	93.8	0.0304
27.651	15.5	108.7	0.0353
34.961	25.0	130.6	0.0424
44.953	37.5	161.0	0.0522
55.100	50.0	191.7	0.0622
69.532	65.0	235.4	0.0764
89.196	85.0	297.5	0.0965
109.485	115.0	377.2	0.1224
129.117	137.0	450.2	0.1461
148.972	183.0	554.8	0.1800

[a] Pressure corrected for thermal transpiration.
[b] Data corrected for buoyancy and thermomolecular flow effect.
[c] Specific volume adsorbed calculated as volume adsorbed per gram of adsorbent.

TABLE LXIII

$CFCl_3$ ADSORPTION DATA

Adsorbent: Alkali-Extracted Holocellulose
Sample Mass: 0.50251 g.
Isotherm Temperature: 278.15°K

Equilibrium[a] Pressure, torr.	Apparent Mass Adsorbed, μg.	Corrected[b] Mass Adsorbed, μg.	Specific[c] Volume Adsorbed, ml. (S.T.P.)/g.
	1st Experimental Run		
0.033	-18.5	4.1	0.0013
0.047	-20.0	6.2	0.0020
0.121	-20.0	14.3	0.0046
0.329	-22.0	16.7	0.0054
0.542	-22.0	18.2	0.0059
1.005	-22.0	21.8	0.0071
2.057	-22.0	25.7	0.0083
5.002	-21.0	33.2	0.0108
10.039	-16.0	48.5	0.0157
15.121	-12.0	60.8	0.0197
20.267	-7.0	71.2	0.0231
25.631	-2.0	85.5	0.0278
30.117	3.0	98.2	0.0319
39.924	11.0	122.7	0.0398
49.749	16.0	144.5	0.0469
59.755	19.5	165.7	0.0538
79.419	21.0	203.9	0.0662
99.259	18.0	241.3	0.0783
119.465	16.5	282.3	0.0916
139.281	14.0	324.2	0.1052
159.623	11.0	371.8	0.1206

[a] Pressure corrected for thermal transpiration.
[b] Data corrected for buoyancy and thermomolecular flow effect.
[c] Specific volume adsorbed calculated as volume adsorbed per gram of adsorbent.

TABLE LXIII (Continued)

$CFCl_3$ ADSORPTION DATA

Adsorbent: Alkali-Extracted Holocellulose
Sample Mass: 0.50251 g.
Isotherm Temperature: 278.15°K

Equilibrium[a] Pressure, torr.	Apparent Mass Adsorbed, μg.	Corrected[b] Mass Adsorbed, μg.	Specific[c] Volume Adsorbed, ml. (S.T.P.)/g.
	2nd Experimental Run		
0.056	-21.0	7.0	0.0023
0.120	-24.0	10.3	0.0033
0.238	-22.0	15.0	0.0049
0.523	-23.0	17.2	0.0056
1.081	-24.5	19.7	0.0064
2.049	-24.0	23.7	0.0077
5.052	-21.0	33.3	0.0108
10.264	-17.0	47.9	0.0156
15.079	-10.0	62.7	0.0203
20.015	-5.0	72.8	0.0236
24.940	-0.5	85.3	0.0277
34.833	10.0	113.2	0.0367
44.832	15.0	135.1	0.0438
56.327	18.5	158.6	0.0515
69.491	21.0	184.9	0.0600
89.455	20.0	222.9	0.0723
109.443	18.0	263.2	0.0854
129.303	14.0	299.7	0.0972
149.147	10.0	345.5	0.1121

[a] Pressure corrected for thermal transpiration.
[b] Data corrected for buoyancy and thermomolecular flow effect.
[c] Specific volume adsorbed calculated as volume adsorbed per gram of adsorbent.

TABLE LXIV

$CFCl_3$ ADSORPTION DATA

Adsorbent: Alkali-Extracted Holocellulose
Sample Mass: 0.50238 g.
Isotherm Temperature: 288.15°K

Equilibrium[a] Pressure, torr.	Apparent Mass Adsorbed, μg.	Corrected[b] Mass Adsorbed, μg.	Specific[c] Volume Adsorbed, ml. (S.T.P.)/g.
	1st Experimental Run		
0.061	-18.0	8.8	0.0028
0.117	-18.0	12.5	0.0041
0.258	-17.0	18.6	0.0060
0.528	-17.0	25.3	0.0082
1.042	-18.0	29.2	0.0095
2.031	-18.0	32.3	0.0105
5.019	-19.0	39.3	0.0128
10.044	-18.0	49.1	0.0159
19.960	-13.5	65.2	0.0212
29.903	-9.5	85.0	0.0276
39.781	-9.0	101.5	0.0329
49.832	-7.0	119.1	0.0387
64.401	-9.0	142.0	0.0461
79.835	-14.0	166.1	0.0539
99.285	-21.0	198.1	0.0643
119.200	-33.5	225.5	0.0732
139.056	-47.5	250.0	0.0811
159.134	-63.0	274.4	0.0891
179.759	-81.0	300.9	0.0977
	2nd Experimental Run		
0.050	-18.5	7.4	0.0024
0.172	-19.5	13.6	0.0044
0.345	-21.0	17.1	0.0056
0.755	-21.5	24.1	0.0078
1.502	-24.0	23.4	0.0076
2.998	-25.0	28.3	0.0092
7.019	-24.0	38.5	0.0125
14.938	-21.5	52.1	0.0169
24.932	-20.0	66.1	0.0214
35.068	-17.0	85.8	0.0279
44.804	-17.0	101.4	0.0329
55.028	-17.0	117.7	0.0382
69.347	-22.0	138.1	0.0448
89.312	-30.0	169.2	0.0549
109.329	-40.0	199.4	0.0647
129.043	-54.0	224.3	0.0728
148.949	-70.0	246.1	0.0799
169.318	-84.5	275.6	0.0895

[a] Pressure corrected for thermal transpiration.
[b] Data corrected for buoyancy and thermomolecular flow effect.
[c] Specific volume adsorbed calculated as volume adsorbed per gram of adsorbent.

TABLE LXV

$CFCl_3$ ADSORPTION DATA

Adsorbent: Alkali-Extracted Holocellulose
Sample Mass: 0.50227 g.
Isotherm Temperature: 298.15°K

Equilibrium[a] Pressure, torr.	Apparent Mass Adsorbed, μg.	Corrected[b] Mass Adsorbed, μg.	Specific[c] Volume Adsorbed, ml. (S.T.P.)/g.
	1st Experimental Run		
0.106	-22.0	2.0	0.0006
0.269	-23.5	2.7	0.0009
0.499	-25.0	3.9	0.0013
1.029	-28.0	4.6	0.0015
2.036	-31.0	4.1	0.0014
5.001	-34.5	6.5	0.0021
10.017	-40.0	8.0	0.0026
14.988	-37.0	18.2	0.0059
19.996	-37.0	25.8	0.0084
29.952	-37.0	37.5	0.0122
39.831	-39.5	46.6	0.0151
49.744	-43.0	58.5	0.0190
69.473	-54.0	80.4	0.0261
89.253	-62.0	106.1	0.0344
109.472	-78.0	129.8	0.0422
129.129	-98.0	146.8	0.0477
149.170	-113.0	168.8	0.0548
170.125	-136.0	185.4	0.0602
146.190[d]	-109.0	167.2	0.0543
98.390	-72.0	113.4	0.0368
58.663	-47.5	68.5	0.0222
24.581	-40.0	28.6	0.0093
9.701	-36.0	11.6	0.0038

[a] Pressure corrected for thermal transpiration.
[b] Data corrected for buoyancy and thermomolecular flow effect.
[c] Specific volume adsorbed calculated as volume adsorbed per gram of adsorbent.
[d] Desorption data.

TABLE LXV (Continued)

$CFCl_3$ ADSORPTION DATA

Adsorbent: Alkali-Extracted Holocellulose
Sample Mass: 0.50227 g.
Isotherm Temperature: 298.15°K

Equilibrium[a] Pressure, torr.	Apparent Mass Adsorbed, μg.	Corrected[b] Mass Adsorbed, μg.	Specific[c] Volume Adsorbed, ml. (S.T.P.)/g.
	2nd Experimental Run		
1.016	-32.0	0.6	0.0002
1.991	-35.0	0.2	0.0000
4.966	-37.0	3.9	0.0013
9.982	-37.0	10.9	0.0036
19.869	-43.5	19.1	0.0062
29.788	-47.0	27.3	0.0089
39.775	-50.0	36.0	0.0117
54.479	-55.0	54.1	0.0176
69.481	-62.0	72.4	0.0235
89.109	-73.0	94.8	0.0308
109.211	-87.0	120.3	0.0391
129.240	-103.0	142.1	0.0461
149.431	-124.0	158.3	0.0514
169.238	-144.0	175.7	0.0570
184.233	-161.0	188.4	0.0612

[a] Pressure corrected for thermal transpiration.
[b] Data corrected for buoyancy and thermomolecular flow effect.
[c] Specific volume adsorbed calculated as volume adsorbed per gram of adsorbent.

TABLE LXVI

$CFCl_3$ ADSORPTION DATA

Adsorbent: Acid-Hydrolyzed Holocellulose
Sample Mass: 0.50419 g.
Isotherm Temperature: 258.15°K

Equilibrium[a] Pressure, torr.	Apparent Mass Adsorbed, μg.	Corrected[b] Mass Adsorbed, μg.	Specific[a] Volume Adsorbed, ml.(S.T.P.)/g.
	1st Experimental Run		
0.033	-9.0	17.8	0.0058
0.104	-5.0	29.8	0.0096
0.245	0.5	41.0	0.0133
0.496	6.0	50.1	0.0162
1.083	18.0	66.4	0.0215
2.057	41.0	92.4	0.0299
4.998	93.0	151.5	0.0490
10.186	191.5	257.2	0.0832
15.036	281.0	354.4	0.1146
20.226	376.0	458.8	0.1484
30.169	521.5	618.9	0.2001
40.184	661.0	772.9	0.2500
50.061	790.5	917.2	0.2966
60.132	920.0	1068.6	0.3456
69.965	1065.0	1233.8	0.3990
79.922	1236.0	1433.4	0.4635
	2nd Experimental Run		
0.039	-7.0	20.8	0.0067
0.170	-6.5	32.0	0.0104
0.316	-2.0	40.0	0.0129
0.735	9.0	55.4	0.0179
1.505	22.0	71.9	0.0232
3.048	50.5	103.6	0.0335
6.952	125.0	187.3	0.0606
12.351	226.0	295.0	0.0954
17.387	316.0	393.6	0.1273
22.422	397.0	483.2	0.1563
27.301	478.0	571.2	0.1847
34.769	585.0	690.1	0.2228
45.144	721.0	839.4	0.2715
55.569	862.5	1001.4	0.3238
64.652	984.0	1141.9	0.3693
74.453	1133.0	1314.2	0.4250

[a]Pressure corrected for thermal transpiration.
[b]Data corrected for buoyancy and thermomolecular effect.
[c]Specific volume adsorbed calculated as volume adsorbed per gram of adsorbent.

TABLE LXVII

RESULTS OF FITTING MULTILAYER ADSORPTION MODEL TO EXPERIMENTAL DATA

Adsorbent: Acid-Hydrolyzed Holocellulose
Adsorbate: $CFCl_3$
Temperature: 258.15°K

Model Parameters

$\underline{U}^{Median} = 3.80 \pm 4.10$[a] kcal. mole^{-1}

$\underline{U}^{Mean} = 3.89$ kcal. mole^{-1}

$\underline{U}^{Mode} = 3.64$ kcal. mole^{-1}

$\gamma = 11.2 \pm 20.9$

$\underline{V}_{\beta} = 1.90 \pm 3.38$ ml. (S.T.P.) g.$^{-1}$

$\nu = 2.59 \pm 29.62 \times 10^{12}$ sec.$^{-1}$

$2\alpha/\beta$ (Ideal) = 3.16 kcal. mole^{-1}

$\alpha = 343.0 \times 10^{-30}$ erg cm.^{2} molecule^{-2}

$\beta = 31.2$ A.^{2} molecule^{-1}

Thermodynamic Data

$\Delta\underline{S}^{tr}_{\underline{s}} = -0.0127$ kcal. mole^{-1} deg.$^{-1}$

$\Delta\underline{S}^{rot} = 0.0$ kcal. mole^{-1} deg.$^{-1}$

$\Delta\underline{S}^{vib} = 0.0034$ kcal. mole^{-1} deg.$^{-1}$

$\Delta\underline{E}^{kin} = -0.2565$ kcal. mole^{-1}

$\underline{A}^{\circ} = 0.34708 \times 10^{7}$

[a] Approximate 95% linear confidence limits.

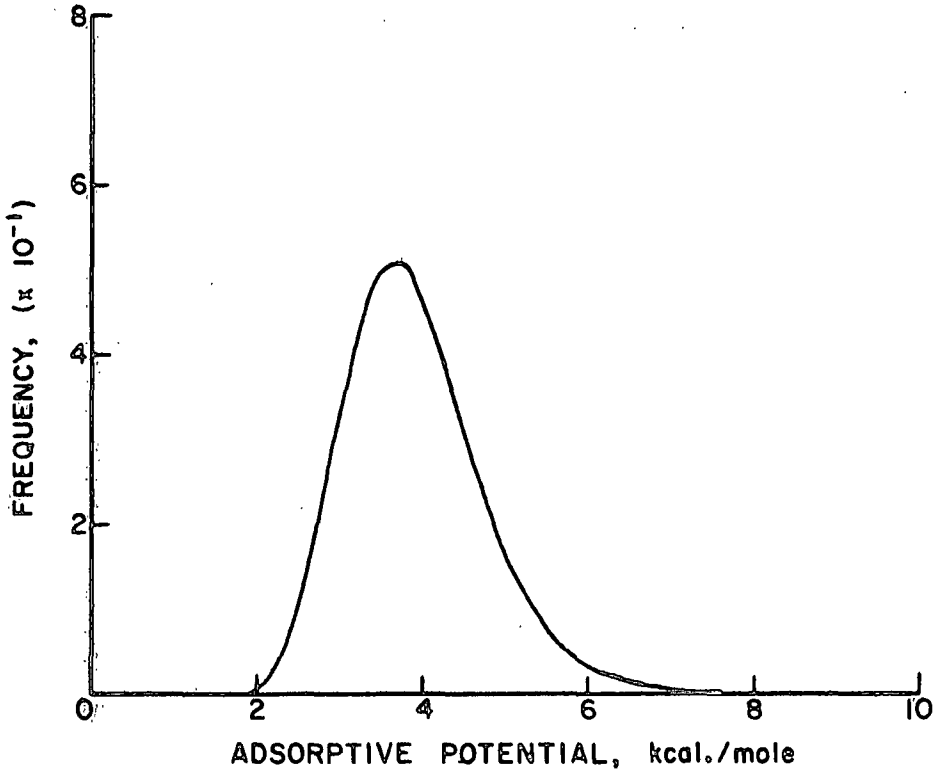

Figure 80. Adsorptive Potential Distribution for $CFCl_3$ Adsorption on Acid-Hydrolyzed Holocellulose at 258.15°K

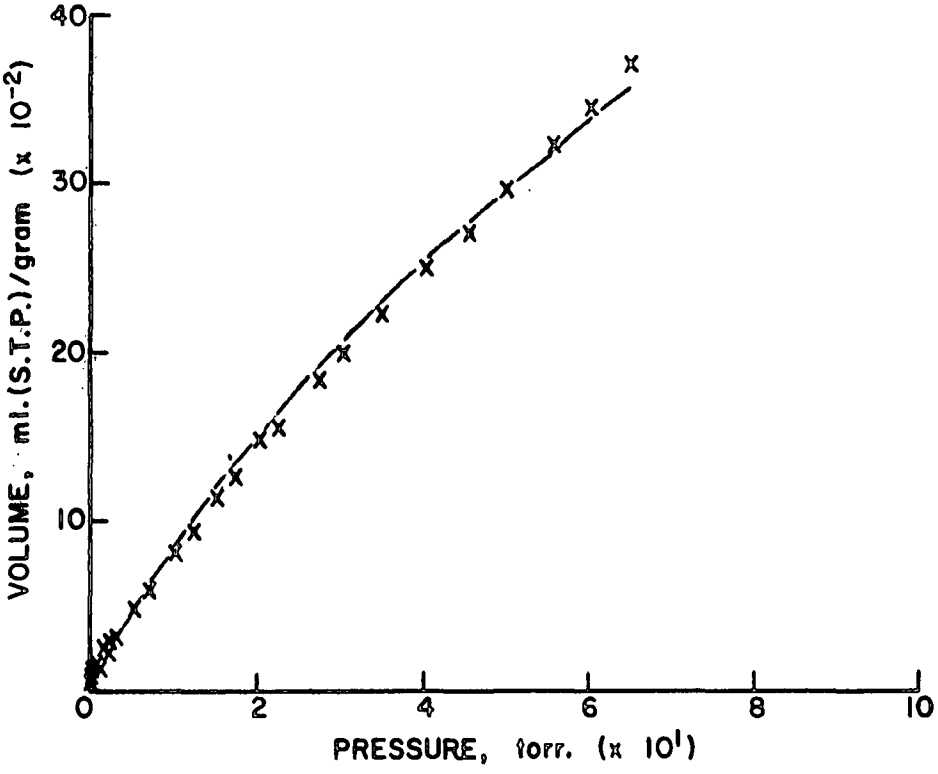

Figure 81. Multilayer Adsorption Model Fitted to the $CFCl_3$ Acid-Hydrolyzed Holocellulose Adsorption Data at 258.15°K

TABLE LXVIII

RESULTS OF FITTING MULTILAYER ADSORPTION MODEL TO EXPERIMENTAL DATA WITH VIBRATIONAL FREQUENCY ELIMINATED AS AN UNKNOWN PARAMETER

Adsorbent: Acid-Hydrolyzed Holocellulose
Adsorbate: $CFCl_3$
Temperature: 258.15°K

Model Parameters

$\underline{U}^{Median} = 3.08 \pm 1.41$[a] kcal. mole^{-1}

$\underline{U}^{Mean} = 3.19$ kcal. mole^{-1}

$\underline{U}^{Mode} = 2.88$ kcal. mole^{-1}

$\gamma = 7.3 \pm 7.4$

$\underline{V}_{\beta} = 3.57 \pm 6.02$ ml. (S.T.P.) g.$^{-1}$

$\nu = 1.48 \times 10^{12}$ sec.$^{-1}$ (Calculated from the median adsorptive potential)

$2\alpha/\beta$ (Ideal) = 3.16 kcal. mole^{-1}

$\alpha = 343.0 \times 10^{-30}$ erg cm.^{2} molecule^{-2}

$\beta = 31.2$ A.^{2} molecule^{-1}

Thermodynamic Data

$\Delta\underline{S}^{tr} = -0.0127$ kcal. mole^{-1} deg.$^{-1}$

$\Delta\underline{S}^{rot} = 0.0$ kcal. mole^{-1} deg.$^{-1}$

$\Delta\underline{S}^{vib} = 0.0046$ kcal. mole^{-1} deg.$^{-1}$

$\Delta\underline{E}^{kin} = -0.2565$ kcal. mole^{-1}

$\underline{A}^{\circ} = 0.21669 \times 10^{7}$

[a] Approximate 95% linear confidence limits.

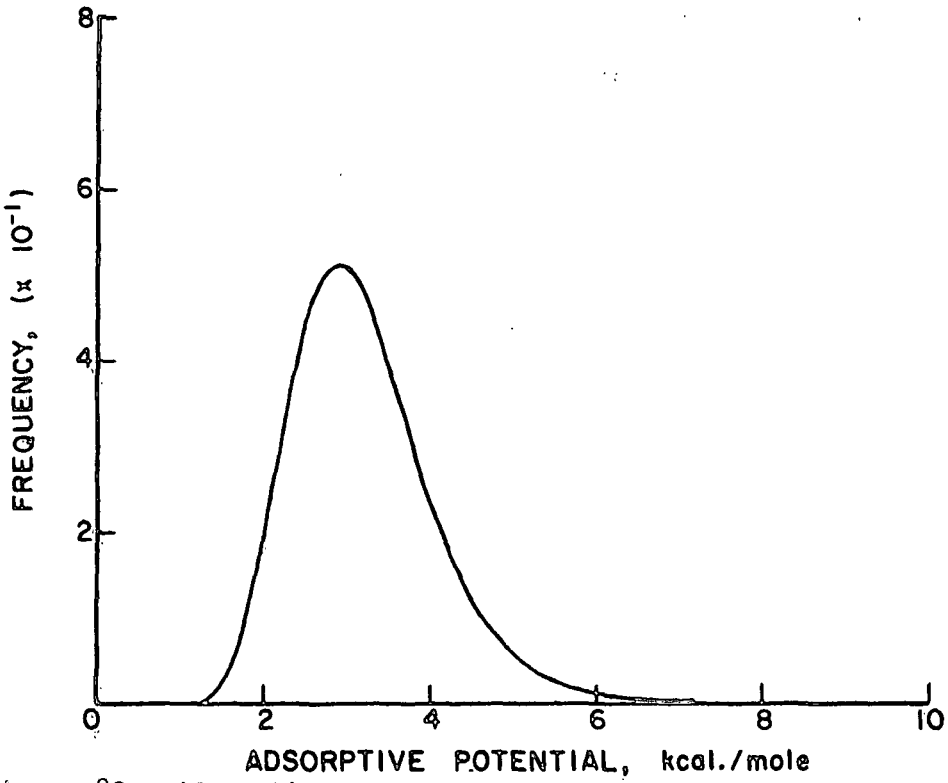

Figure 82. Adsorptive Potential Distribution for $CFCl_3$ Adsorption on Acid-Hydrolyzed Holocellulose at 258.15°K

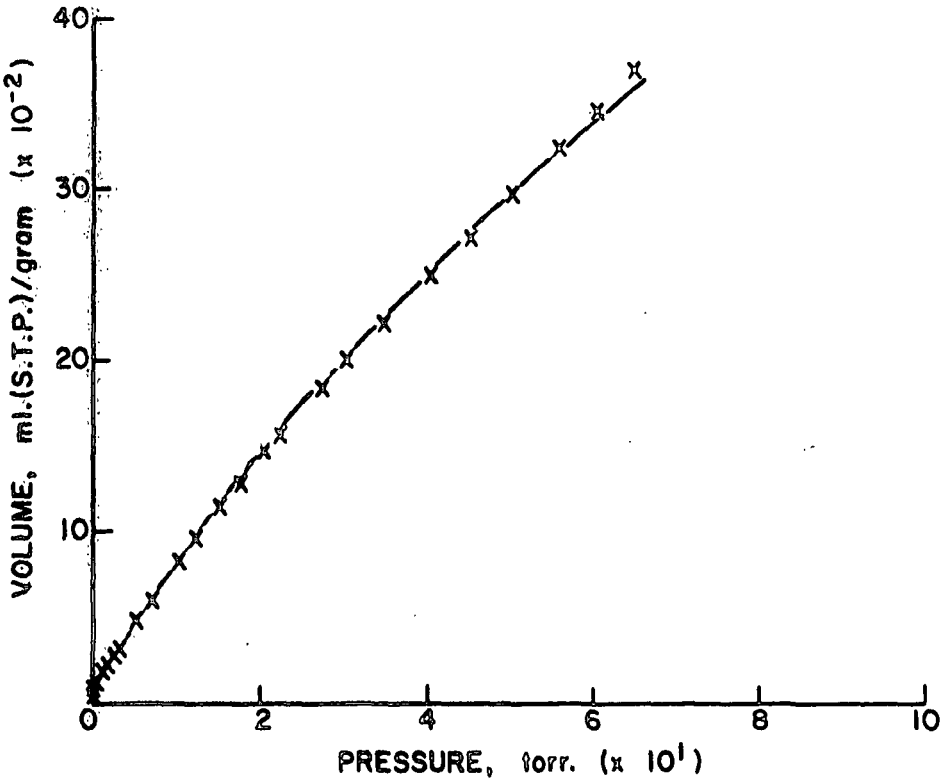

Figure 83. Multilayer Adsorption Model Fitted to the $CFCl_3$ Acid-Hydrolyzed Holocellulose Adsorption Data at 258.15°K with the Vibrational Frequency Eliminated as an Unknown Parameter

TABLE LXIX

RESULTS OF FITTING MULTILAYER ADSORPTION MODEL TO EXPERIMENTAL DATA WITH BOTH VIBRATIONAL FREQUENCY AND MONOLAYER VOLUME ELIMINATED AS UNKNOWN PARAMETERS

Adsorbent: Acid-Hydrolyzed Holocellulose
Adsorbate: $CFCl_3$
Temperature: 258.15°K

Model Parameters

$\underline{U}^{Median} = 4.65 \pm 0.07^{a}$ kcal. mole^{-1}

$\underline{U}^{Mean} = 4.68$ kcal. mole^{-1}

$\underline{U}^{Mode} = 4.60$ kcal. mole^{-1}

$\gamma = 43.3 \pm 22.0$

$\underline{V}_{\beta} = 0.61$ ml. (S.T.P.) g.$^{-1}$

$\nu = 1.82 \times 10^{12}$ sec.$^{-1}$

$2\alpha/\beta$ (Ideal) $= 3.16$ kcal. mole^{-1}

$\alpha = 343.0 \times 10^{-30}$ erg cm.^{2} molecule^{-2}

$\beta = 31.2$ A.^{2} molecule^{-1}

Thermodynamic Data

$\Delta\underline{S}_{\underline{s}}^{tr} = -0.0127$ kcal. mole^{-1} deg.$^{-1}$

$\Delta\underline{S}^{rot} = 0.0$ kcal. mole^{-1} deg.$^{-1}$

$\Delta\underline{S}^{vib} = 0.0042$ kcal. mole^{-1} deg.$^{-1}$

$\Delta\underline{E}^{kin} = -0.2565$ kcal. mole^{-1}

$\underline{A}^{\circ} = 0.25925 \times 10^{7}$

---

[a] Approximate 95% linear confidence limits.

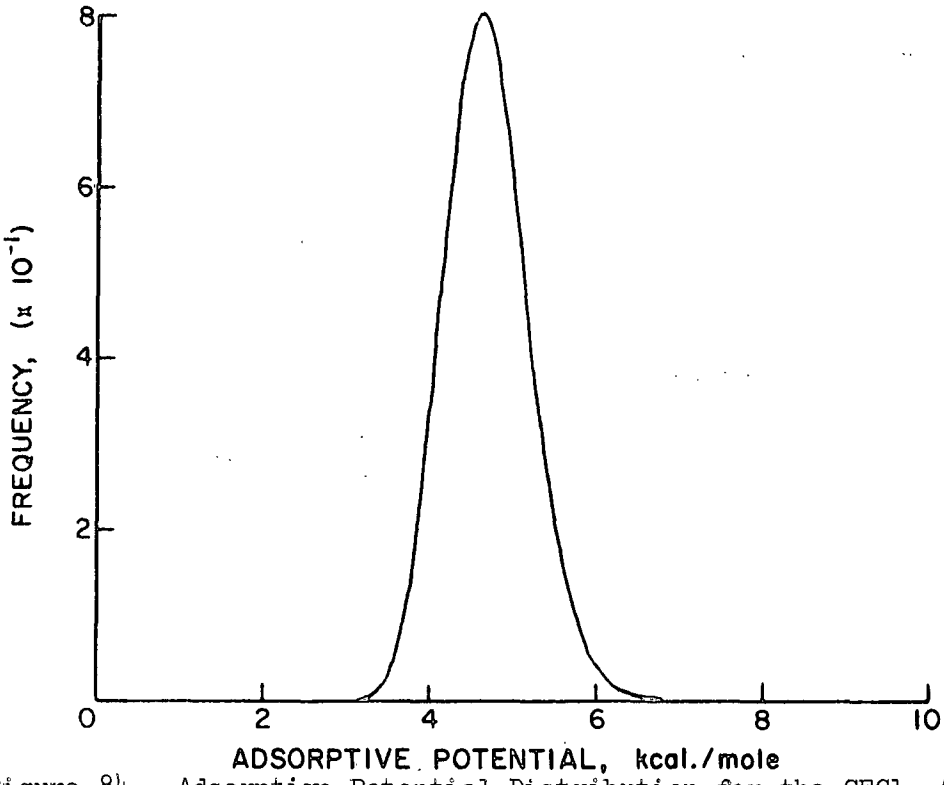

Figure 84. Adsorptive Potential Distribution for the $CFCl_3$ Acid-Hydrolyzed Holocellulose Adsorption Data at 258.15°K

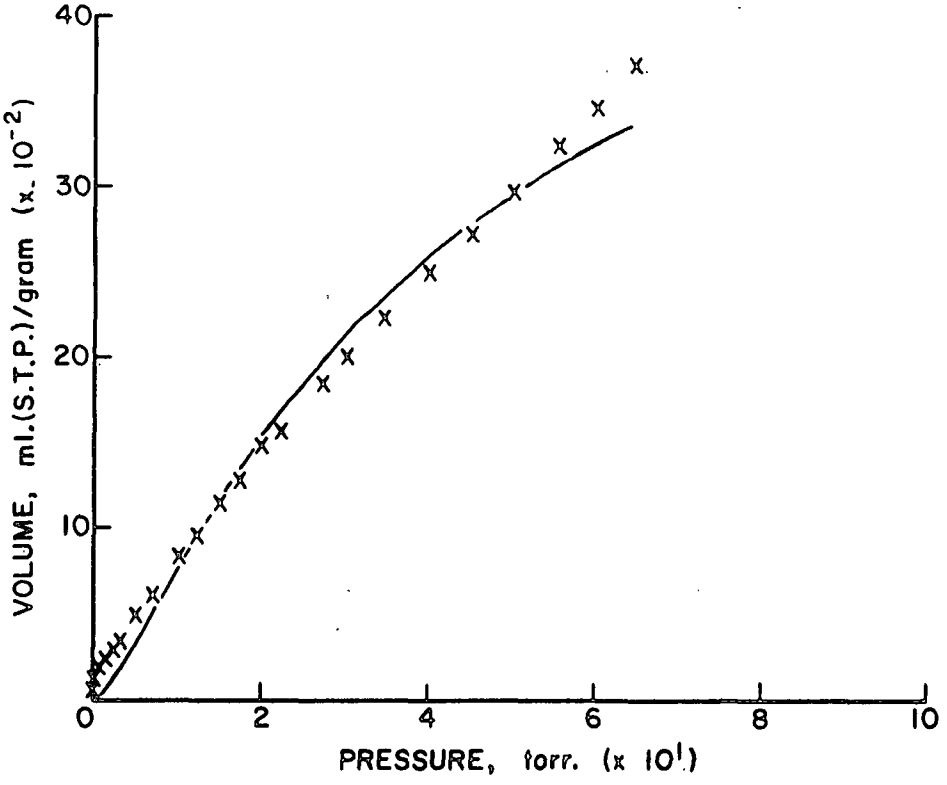

Figure 85. Multilayer Adsorption Model Fitted to the $CFCl_3$ Acid-Hydrolyzed Holocellulose Adsorption Data at 258.15°K with both the Vibrational Frequency and the Monolayer Volume Eliminated as Unknown Parameters

TABLE LXX

$CFCl_3$ ADSORPTION DATA

Adsorbent: Acid-Hydrolyzed Holocellulose
Sample Mass: 0.50304 g.
Isotherm Temperature: 268.15°K

Equilibrium[a] Pressure, torr.	Apparent Mass Adsorbed, μg.	Corrected[b] Mass Adsorbed, μg.	Specific[c] Volume Adsorbed, ml. (S.T.P.)/g.
	1st Experimental Run		
0.156	-30.0	4.6	0.0015
0.317	-32.0	5.0	0.0016
0.753	-24.0	15.9	0.0051
1.503	-17.0	27.6	0.0090
2.999	1.0	49.7	0.0161
7.437	52.0	108.8	0.0352
12.450	105.0	171.7	0.0556
17.659	167.0	240.2	0.0779
22.585	219.0	297.2	0.0964
27.502	271.0	355.6	0.1153
34.902	351.0	446.1	0.1446
45.093	438.0	548.3	0.1777
54.827	521.0	645.9	0.2094
69.693	637.0	787.0	0.2551
89.374	771.0	957.4	0.3103
109.586	934.0	1163.8	0.3773
129.019	1118.0	1392.6	0.4514
149.462	1375.0	1703.8	0.5523
	2nd Experimental Run		
0.264	-33.0	2.6	0.0009
0.517	-33.0	5.1	0.0016
1.040	-30.0	12.1	0.0039
2.314	-19.0	27.6	0.0090
5.089	13.0	64.7	0.0210
9.933	68.0	130.4	0.0423
15.354	126.0	196.6	0.0637
19.927	180.0	255.2	0.0827
25.026	235.0	316.3	0.1025
29.974	291.5	379.6	0.1231
39.904	389.0	491.7	0.1594
50.017	484.0	601.5	0.1950
59.726	562.0	694.8	0.2252
79.648	710.0	877.9	0.2846
99.297	857.0	1063.9	0.3449
119.255	1035.0	1286.7	0.4171
140.793	1273.0	1577.9	0.5115
159.904	1562.0	1933.6	0.6268

[a] Pressure corrected for thermal transpiration.
[b] Data corrected for buoyancy and thermomolecular flow effect.
[c] Specific volume adsorbed calculated as volume adsorbed per gram of adsorbent.

TABLE LXXI

$CFCl_3$ ADSORPTION DATA

Adsorbent: Acid-Hydrolyzed Holocellulose
Sample Mass: 0.50280 g.
Isotherm Temperature: 278.15°K

Equilibrium[a] Pressure, torr.	Apparent Mass Adsorbed, μg.	Corrected[b] Mass Adsorbed, μg.	Specific[c] Volume Adsorbed, ml. (S.T.P.)/g.
	1st Experimental Run		
0.052	-24.0	3.2	0.0010
0.105	-27.0	6.7	0.0022
0.275	-28.0	9.6	0.0031
0.543	-29.0	11.0	0.0036
1.048	-28.0	15.7	0.0051
2.057	-23.5	23.7	0.0077
5.184	-5.0	48.1	0.0156
10.006	24.0	85.8	0.0278
15.677	57.0	126.4	0.0410
20.034	90.0	162.6	0.0527
30.335	158.0	245.6	0.0796
39.959	218.0	319.3	0.1035
50.390	276.0	392.4	0.1272
60.161	330.0	461.1	0.1495
79.518	435.0	597.2	0.1936
99.297	521.0	718.3	0.2329
119.465	609.0	843.5	0.2735
139.122	689.5	962.8	0.3122
159.143	774.0	1092.1	0.3541
	2nd Experimental Run		
0.030	-20.5	1.3	0.0004
0.174	-30.0	5.1	0.0016
0.341	-32.0	6.8	0.0022
0.776	-33.0	9.0	0.0029
1.540	-32.0	14.1	0.0046
3.250	-24.0	26.1	0.0085
7.830	6.0	64.1	0.0208
12.610	35.0	100.5	0.0326
17.848	70.0	139.9	0.0454
25.542	125.0	205.7	0.0667
35.245	185.0	279.6	0.0906
44.688	248.0	356.1	0.1155
54.962	312.5	435.7	0.1413
69.947	393.0	539.4	0.1749
89.655	481.5	661.3	0.2144
110.107	584.0	801.7	0.2600
129.180	655.0	906.5	0.2939
149.767	741.0	1038.7	0.3368

[a] Pressure corrected for thermal transpiration.
[b] Data corrected for buoyancy and thermomolecular flow effect.
[c] Specific volume adsorbed calculated as volume adsorbed per gram of adsorbent.

TABLE LXXII

$CFCl_3$ ADSORPTION DATA

Adsorbent: Acid-Hydrolyzed Holocellulose
Sample Mass: 0.50279 g.
Isotherm Temperature: 288.15°K

Equilibrium[a] Pressure, torr.	Apparent Mass Adsorbed, μg.	Corrected[b] Mass Adsorbed, μg.	Specific[c] Volume Adsorbed, ml. (S.T.P.)/g.
	1st Experimental Run		
0.035	-13.0	11.6	0.0038
0.099	-13.0	16.4	0.0053
0.314	-13.0	24.2	0.0078
0.767	-13.0	32.5	0.0105
1.523	-9.0	38.0	0.0123
3.026	-4.0	48.6	0.0158
7.020	10.0	70.7	0.0229
12.585	29.0	96.4	0.0313
17.991	50.0	121.5	0.0394
25.171	82.0	162.1	0.0526
34.668	118.0	211.4	0.0686
49.901	179.0	292.6	0.0949
69.410	251.0	393.7	0.1276
89.481	321.0	497.8	0.1614
109.036	381.5	592.7	0.1922
128.998	435.0	680.5	0.2207
149.390	484.0	763.2	0.2475
169.004	529.0	845.7	0.2742
188.988	573.0	925.8	0.3002
	2nd Experimental Run		
0.049	-14.0	11.8	0.0038
0.105	-12.0	17.8	0.0058
0.250	-12.0	23.4	0.0076
0.510	-10.5	31.3	0.0102
1.046	-9.0	38.0	0.0123
2.047	-3.0	46.7	0.0152
5.060	7.0	64.2	0.0208
10.371	25.0	89.9	0.0291
15.626	45.0	115.5	0.0374
20.578	64.5	138.8	0.0450
30.203	105.5	192.9	0.0626
40.506	150.0	251.4	0.0815
50.379	190.0	304.2	0.0987
59.508	225.0	352.3	0.1142
79.546	296.0	455.4	0.1477
99.019	361.0	554.5	0.1798
119.085	421.5	650.1	0.2108
138.990	473.0	735.2	0.2384
159.016	519.0	815.9	0.2646
178.924	565.0	899.9	0.2918

[a] Pressure corrected for thermal transpiration.
[b] Data corrected for buoyancy and thermomolecular flow effect.
[c] Specific volume adsorbed calculated as volume adsorbed per gram of adsorbent.

TABLE LXXIII

$CFCl_3$ ADSORPTION DATA

Adsorbent: Acid-Hydrolyzed Holocellulose
Sample Mass: 0.50276 g.
Isotherm Temperature: 298.15°K

Equilibrium[a] Pressure, torr.	Apparent Mass Adsorbed, μg.	Corrected[b] Mass Adsorbed, μg.	Specific[c] Volume Adsorbed, ml(S.T.P.)/g.
	1st Experimental Run		
0.108	-18.0	6.1	0.0020
0.258	-17.0	9.6	0.0031
0.508	-17.0	11.9	0.0038
1.018	-15.0	17.3	0.0056
2.022	-12.5	22.2	0.0072
5.019	-6.5	33.3	0.0108
10.074	4.0	49.6	0.0161
15.450	15.0	67.1	0.0218
20.060	27.0	85.0	0.0276
30.045	50.0	117.3	0.0380
39.831	72.5	148.9	0.0483
50.187	97.0	186.9	0.0606
59.667	118.0	221.0	0.0717
79.178	159.0	290.4	0.0942
98.931	199.0	361.2	0.1171
119.269	239.0	436.3	0.1415
138.995	274.5	503.6	0.1633
159.102	301.0	562.5	0.1824
179.082	328.0	623.2	0.2021
137.925[d]	272.0	499.4	0.1620
98.551	201.0	362.5	0.1176
59.251	120.5	223.0	0.0723
19.783	34.0	91.7	0.0297

[a] Pressure corrected for thermal transpiration.
[b] Data corrected for buoyancy and thermomolecular flow effect.
[c] Specific volume adsorbed calculated as volume adsorbed per gram of adsorbent.
[d] Desorption data.

TABLE LXXIII (Continued)

$CFCl_3$ ADSORPTION DATA

Adsorbent: Acid-Hydrolyzed Holocellulose
Sample Mass: 0.50276 g.
Isotherm Temperature: 298.15°K

Equilibrium[a] Pressure, torr.	Apparent Mass Adsorbed, μg.	Corrected[b] Mass Adsorbed, μg.	Specific[c] Volume Adsorbed, ml(S.T.P.)/g.
	2nd Experimental Run		
0.046	-13.5	4.4	0.0014
0.100	-14.5	9.0	0.0029
0.271	-12.0	14.0	0.0046
0.762	-13.0	17.8	0.0058
1.533	-12.5	21.7	0.0070
3.051	-10.0	26.8	0.0087
7.166	-2.0	40.6	0.0132
12.610	8.5	57.1	0.0185
17.624	20.5	75.7	0.0246
25.176	35.0	97.8	0.0317
34.813	56.0	127.7	0.0414
44.702	80.0	162.3	0.0526
54.637	98.5	194.5	0.0631
69.443	132.0	249.3	0.0808
89.149	169.0	315.1	0.1022
108.994	214.0	394.2	0.1278
128.959	250.0	463.0	0.1501
149.534	281.0	526.9	0.1709
169.194	310.0	588.2	0.1908
189.568	336.5	650.3	0.2109

[a] Pressure corrected for thermal transpiration.
[b] Data corrected for buoyancy and thermomolecular flow effect.
[c] Specific volume adsorbed calculated as volume adsorbed per gram of adsorbent.